Commissioning of a Modular Steiner Tunnel

by

Njegoš Bijelić

A thesis
presented to the University of Waterloo
in fulfillment of the
thesis requirement for the degree of
Master of Applied Science
in
Mechanical Engineering

Waterloo, Ontario, Canada, 2015

I hereby declare that I am the sole author of this thesis. This is a true copy of the thesis, including any required final revisions, as accepted by my examiners.

I understand that my thesis may be made electronically available to the public.

Abstract

This thesis presents methods used for, and results from, tests conducted during the final installation and commissioning of a modular Steiner tunnel delivered to the UWFRL. The overall aim of the present research is to design the support systems for this new Steiner tunnel, to commission the tunnel for operation and to characterize the final tunnel operation against a series of materials with known fire performance characteristics. The first stage of commissioning is to design and implement the safety controls system for the Steiner tunnel, fulfilling all the requirements of the safety regulations and provide additional safety calculations needed for approval of the system. Following this, the overall tunnel operation is tested with the tunnel installed at its full 25 foot length. In the first phase of testing, a series of 'pre- calibration' experiments is conducted using various off-the-shelf wood product samples. These tests are designed to examine the behaviour of the tunnel prior to the much more costly, formal red oak calibration test, since it has been reported that red oak calibration criteria can be fairly difficult to meet, especially for newly constructed tunnels. Tests are conducted on various wood products including red oak, OSB, particle board, and plywood to evaluate the tunnel performance. The three specific parameters that are found to have significant influence on tunnel operation are gas flow to the burner, draft pressure within the main tunnel section, and the exhaust damper position. During calibration tests, it is found that of the three parameters that are studied (gas flow, tunnel draft, and damper position), the damper position has the most influence on FSI. The far damper should be utilized to control tunnel air flow. If this is not possible, the damper position should be kept 18 pipe diameters from the end of the tunnel. Gas flow effects are found to be largely dependent on outside temperatures, and most likely is outside of lab facilities control. For gas flow, flame spread results are most affected for flow rates below 7.0 m^3/hr which corresponded to maintaining inlet gas temperature above 18^oC. Therefore, it is determined that the tunnel should only be operated when the lab temperature is above 18^oC. Airflow through the tunnel as indicated by tunnel draft pressure is found to greatly impact measured flame spread characteristics for most samples tested. The appropriate range for the tunnel draft pressure is determined to be between 0.090 - 0.110 in-WC (22.4 - 27.4 Pa) so that it would not have a significant effect on flame spread results. Since sudden changes in draft pressure are found to essentially obstruct flame progression, FSI results are improved when fan control measures are implemented to stabilize the draft pressure within the main tunnel enclosure.

Acknowledgements

I have received a lot of help on this project, and I would first like to thank the almighty God for giving me the strength and courage to finish this work in good health. Most importantly I would like to thank my supervisor, Dr. Elizabeth Weckman, for making this project experience possible and for her great advice, wisdom and patience throughout.

My special thanks goes to our lab technician Gord Hitchman, for the countless hours we have spent in the lab in trying to configure the tunnel, and for his technical expertise and guidance. I would also like to thank Andy Barber and Neil Griffett for their expertise in troubleshooting electronics and for their great contributions in setting up the LabVIEW software.

I would like to acknowledge the contributions of ECR and OCE, for all of their financial contributions to this project. I would like to thank Jonathan Adair from ECR for the time taken to prepare and ship samples for testing, as well as with the help received for the design and construction of the damper system. Also, the opportunity provided from Emmanuel Sopeju to visit the ULC fire testing lab and to observe live Steiner tunnel tests was a very helpful experience.

I would like to thank my friends and colleagues from the University of Waterloo Fire Research Lab; Patrick Mulherin and Matt DiDomizio for their great expertise in fire testing, Sergio Suarez with his early involvement in the design stage of the project, and the rest of the group who helped with the lifting of the lids and running the tests including Kevin Gordon and Alen Topic.

Finally, I want to thank my family and friends who have fully supported me throughout this period, especially my girlfriend Sanja who was there with me through the hard times.

Table of Contents

List of Tables

List of Figures

Chapter 1

Introduction

Throughout history, the flammability characteristics of interior finish materials within buildings have played a major role in building fires. These caused massive destruction and took countless lives [1]. In the mid 1940's, a number of disastrous fires occurred in hotels and nightclubs in Boston, Chicago and Atlanta resulting in 670 deaths from only three fire incidents [1, 2]. The high number of fatalities from these fires was directly related to the high rate of flame spread and heavy smoke development due to interior finish materials. This demonstrated the need to regulate the burning characteristics of materials used for finishing the interiors of buildings. To accomplish this task, Albert J. Steiner developed the original Steiner tunnel in the early 1920's. This tunnel emerged as the basis for a predominant test method used for regulating surface burning characteristics of interior finish materials [2]. The tunnel is a long furnace chamber (25 foot or 7.6 m), that is 17.625±0.375 in (450±9.5 mm) wide and 12.0±0.5 in (320±13 mm) deep, and in which flame spread and smoke development can be measured. Realistic fire exposures are produced using direct flame impingement on large specimens (36 square-foot or 3.25 m^2) [1]; however, because the Steiner tunnel requires such large specimens, repetitive testing can become costly. To add to this, Steiner tunnel test samples are specified to be 24 foot (7.32 m) long, and for repetitive screening of new products, preparing and shipping 24 foot long specimens adds substantially to the costs outlined above [3, 4]. Finally, the test apparatus requires monthly calibration using red oak lumber[1], so additional material cost for testing can also be very high the cost for a single red oak test may be as high as $800 depending on location [5]. Nonetheless, Steiner tunnel testing is extremely useful for industries screening new products, since small scale fire tests such as the cone calorimeter may not always represent the actual fire performance of a material at the large scale.

To this end, University of Waterloo (UW) together with Algonquin College and an

[1]The ASTM E84 procedure dictates the use of red oak lumber and inorganic reinforced cement board as calibrating materials [1].

industry partner, Elevator Cab Renovations (ECR) in Ottawa, Ontario, have collaborated to design and construct a unique, modular Steiner tunnel at the UW Fire Research Laboratory (UWFRL) with the goal of carrying out fire safety research related to flame spread over single-layer and laminated composite materials. The overall tunnel design is similar to that specified in the American Society for Testing and Materials (ASTM) E84 Steiner Tunnel [1] test standard with several modifications made to suit its intended use for fire safety research. One significant difference from the tunnel design specified in ASTM E84 is that the UW Steiner tunnel is built in six modular sections to facilitate testing of samples with lengths anywhere between 8, 12, 16, 20 and 24 feet. In addition, extra monitoring systems have been installed, including an array of thermocouples located to better monitor temperatures throughout the tunnel during testing.

The overall aim of the present research is to design the support systems for this new Steiner tunnel, to commission the tunnel for operation and to characterize the final tunnel operation against a series of materials with known fire performance characteristics. As such, the first step in commissioning the Steiner tunnel after installation is to design and install an automated ignition and control system and obtain field approval for operation of the system from Technical Standards and Safety Authority (TSSA) of Ontario. Following this, the overall tunnel operation is tested with the tunnel installed at its full 25 foot length. In the first phase of testing, a series of 'pre- calibration' experiments is conducted using various off-the-shelf wood product samples. These tests are designed to examine the behaviour of the tunnel prior to the much more costly, formal red oak calibration test, since it has been reported that red oak calibration criteria can be fairly difficult to meet, especially for newly constructed tunnels [6]. In addition, examination of these other wood products provided a cost-effective way to systematically characterize overall tunnel operation as well as to investigate the many operational parameters that affect the determination of flame spread in a Steiner tunnel. The results of these experiments are then applied to refine the methods used to interpret the data and to determine the appropriate range of control parameters to be used for the red oak calibration test.

As such, the overall objectives of the present research are as follows:

- To fully commission the new modular Steiner tunnel at the UWFRL,
- To evaluate the overall performance of the tunnel, and
- To use the measured evaluation data to improve understanding of the parameters that affect the tunnel results and to determine a consistent methodology by which to calibrate the tunnel.

Specific objectives of the research are as follows:

- To design and implement the safety controls system for the Steiner tunnel, fulfilling all the requirements of the safety regulations and provide additional safety calculations needed for approval of the system,
- To evaluate the operation of the tunnel using commercially available wood products and the calibration procedures specified in ASTM E84,
- To study the effect of gas flow, draft pressure and damper position on flame spread in order to define an appropriate range of operating conditions for each of the parameters that will minimize calibration costs, and
- To provide recommendations for conducting scaling tests for tunnel operation at shorter tunnel lengths in the future

The overall layout and operational characteristics of the tunnel, details of commissioning of the tunnel, performance characterization test results and calibration test results are reported in the present thesis. In Chapter 2, the literature on the Steiner tunnel test method is reviewed. This chapter describes the history and development of the Steiner tunnel test method and associated test system. Previous attempts to reduce the overall scale of the tunnel as outlined in the 8-ft (2.44 m) tunnel test methods are also discussed. Additionally, since assessment of individual tunnel parameters is one of the objectives listed above, variables influencing tunnel performance are reviewed to provide background for this portion of the research.

The remainder of the thesis describes the design of the tunnel, followed by operational methods and characterization tests conducted to commission and calibrate the tunnel. The overall apparatus, controls design, and a description of the test methods used to evaluate the tunnel operation are described first (Chapter 3), followed by the results of the various characterization and calibration tests conducted in the tunnel (Chapter 4). The tunnel performance will be analyzed and discussed in each chapter as appropriate as well. Finally, conclusions and recommendations for future testing are presented in Chapter 5.

Chapter 2

Background

The current understanding of the Steiner tunnel test method is reviewed in this chapter. Only those variables that influence flame spread and smoke development in the Steiner tunnel are discussed; correlations of Steiner tunnel results with other heat release rate measurements and comparison of Steiner tunnel data to other large scale test results are outside the scope of the present work. With those restrictions, the first section of this chapter provides introductory information on the tunnel and standards applicable to fire performance testing in the Steiner tunnel. This is followed by a detailed outline of the ASTM E84 Steiner tunnel [1] test method, including: history and development, the test apparatus and procedures employed, and the derivation of test results. Finally, the parameters that have been found to influence Steiner tunnel test results are reviewed as a guide for development of experimental methods and calibration procedures needed for this research, as well as for final evaluation of the operational characteristics of the UW Steiner tunnel.

2.1 ASTM E84 Steiner Tunnel Test

The Steiner tunnel test is named Test for Surface Burning Characteristics of Building Materials [1]. It is commonly employed to measure the burning characteristics of interior finish materials used in buildings. Several organizations in Canada and United States (US) incorporated the Steiner tunnel test method as their standard method for evaluation of fire performance of interior materials, including: American Society for Testing and Materials (ASTM) E84 [1], National Fire Protection Association (NFPA) 255 [7], Underwriters Laboratories (UL) 723 [8], and the Underwriters Laboratories of Canada (ULC) S102. All four standards stipulate similar methodologies where the sample is mounted into the tunnel on the ceiling and the exposed surface of the specimen is facing down [1, 7, 8, 9].

The Canadian standard (ULC S102) has a slight difference in the apparatus and calculation methodology [10]. These differences will be outlined in Sections 2.3 and 2.4. In this study, the ASTM E84 standard test method is applied since the UW Steiner tunnel was designed and constructed according to the specifications in that standard.

The Steiner tunnel itself is a long furnace chamber into which a specimen that is 24 ft (7.32 m) long and 1.5 ft (0.46 m) wide is inserted and tested for flame spread when exposed to direct flame impingement from a large gas burner. Materials are classified for their fire performance according to flame spread index (FSI) and smoke developed index (SDI). The test procedure dictates calibration of the unit using inorganic reinforced cement board to represent zero flame spread and red oak lumber for a higher reference flame spread [2]. It is reported that red oak propagates flames to the end of the tunnel in 5.5 minutes (± 0.25 min) [1] for an assigned FSI of 90 and SDI of 100 [1]. In contrast, cement board is assigned both FSI and SDI values of 0 [2]. Building codes or other documents then define and regulate the values of FSI and SDI necessary for a material to be adopted for use in a particular application. Currently in North America, interior wall and ceiling finish materials are classified into one of the three categories as defined in Chapter 8 of the International Building Code [11], or similar classifications in Appendix D3 of the National Building Code of Canada (NBCC) [12]:

Table 2.1: Material classifications for interior finish in accordance with ASTM E84

Material Classification	Flame Spread Index	Smoke Developed Index
Class A	0-25	0-450
Class B	26-75	0-450
Class C	76-200	0-450

Class A materials are usually required in enclosed vertical exits. Class B materials are permitted in exit access corridors, while Class C products can be used in all other areas [13]. Materials falling outside the ranges classified above would not normally be permitted for use as interior finish in buildings. The only exception to this requirement would be if the material passes an entirely different fire performance test the room corner test for interior wall or ceiling finish [11]. In US building codes, there is also a separate classification for materials installed in a plenum or air-handling space. These materials are required to have a FSI of 0-25 and a SDI of 0-50 [14]. This is also known as '25/50 rating' when tested in accordance with ASTM E84 [15]; however, this does not apply in Canada [15]. Although plenum spaces have specific requirements, it is of particular interest to this work

[1]The calculation methodologies for flame spread and smoke developed indices will be discussed in Section 2.4

that there are no special ASTM E84 requirements for materials installed in elevators in the US. Canada, on the other hand, has more stringent requirements for elevators used in high rise buildings. NBCC requires elevator walls and ceiling finish to be restricted to 0-25 FSI, and SDI to be limited at 0-100 [16, 17] although the codes may also vary depending on the requirements of the local jurisdiction.

Canada has an additional standard named ULC S102.2 Surface Burning Characteristics of Flooring, Floor Covering, and Miscellaneous Materials [18]. This test can also be used to generate values for flame spread and smoke developed indices for materials, although the sample mounting procedures are different and therefore the results will not be the same as for an ASTM E84 test. The ULC S102.2 standard utilizes the same basic Steiner tunnel apparatus (Section 2.3); however, the sample is mounted on the floor instead of the ceiling [15]. This is mainly done for testing of thermoplastic foams which tend to melt and drip during fire testing [18]. Materials used in this study are mainly wood products so although they are mounted on the ceiling, the orientation of the specimen is not expected to have a significant impact on results.

2.2 History and Development of the Steiner Tunnel

Major fires that occurred in the early 20^{th} century were distinguished by rapid flame spread of interior finish in buildings [1, 2]. This was determined to be a significant potential cause for death or injury in these fires, and therefore aroused public concern and demonstrated the need for regulating burning characteristics of these materials. The specific concerns identified were the spread of flame and smoke development from the lining materials which subsequently led to research and development of various testing protocols at Underwriters Laboratories (UL) [1].

An engineer from UL's fire protection department, Albert J. Steiner, developed the initial version of the tunnel furnace in 1922. The first prototype consisted of a long wooden bench that was 16-ft (4.9 m) long, and 1.5 ft (0.46 m) wide with a non-combustible top [2]. Initially the tunnel was used for testing paint products. The interior of the tunnel was coated with the paint that was under investigation and it would be ignited with a certain quantity of wood at one end. The extent of flame spread distance was compared with an unpainted replica of the tunnel, thus the flame retardancy of the coating was evaluated [2].

By the late 1920's, further research at UL led to modifications to the original tunnel design when evaluating the fire performance of chemically impregnated wood. Instead of the 1922 version of a long wooden bench, the test samples would form the top of a 3.0 ft (0.914 m) wide by 1.1 ft (0.33 m) deep and 23-ft (7.0 m) long chamber [1]. At this time, also, red oak flooring was introduced as the first method for calibrating the

tunnel, where the fuel and draft were also controlled. During the 1930's, Albert Steiner and Simon Ingberg from the National Bureau Standards took on the challenge to develop a standardized tunnel test for flame spread ratings of building materials [19, 10].

In the mid 1940's, a number of disastrous fires occurred in hotels and nightclubs of Boston, Chicago, and Atlanta [2]. There were a total of 670 casualties from only 3 fire incidents [1, 2]. The high number of fatalities was directly related to rapid flame spread and smoke development across interior finish materials, leading to the definition of a classification index for materials using the Steiner tunnel test method. The surface burning characteristics classification scale was introduced by measuring three burning characteristics: flame spread, fuel contribution, and smoke development. A comparative scaling method was required in order to classify materials with respect to their relative hazard levels. Combustible red oak lumber was defined as having an arbitrary index value of 100 and non-combustible cement board was assigned an index of 0 [2].

The current version of the Steiner tunnel test apparatus design was virtually completed in the late 1940's. Additional controls were added to improve repeatability and reproducibility of test results. The current version of the test method then started to gradually develop over the years, with refinements made as the method gained acceptance from surrounding communities. The first standard Steiner tunnel test method was published in 1950 at the Underwriters Laboratories as standard UL 723 [8]. NFPA and ASTM soon followed by publishing their own versions of the standard using the same parameters, NFPA 255 and ASTM E84 respectively, in 1955 and 1961 [1]. However, the classification scale for the Steiner tunnel of the time, based on flame spread index, smoke developed index and flame contribution index, was still not part of the building codes [2]. This scale also evolved over time, with incorporation into the codes in 1976, leading to the modern day classification scale which was outlined in Section 2.1.

Flame spread index (FSI) and smoke developed index (SDI) are the two most important results obtained from the Steiner tunnel test. Before 1978, fuel contribution index (FCI) was also reported as a measure of surface burning characteristics in the Steiner tunnel [2]. It was based on exhaust gas temperatures measured at the end of the tunnel furnace during testing. This index was removed from the testing method, however, since it was reported as an invalid measure of the contribution of the fuel to the flame spread [1, 2].

While the method for calculating SDI has remained virtually the same since it was originally proposed, the calculation method for FSI has undergone some modifications over the years. It was first calculated as the ratio of the time taken for the flame to travel some distance along the tunnel length relative to that of red oak. In 1976, this calculation method was criticized because no account was taken for flame front recession in situations where the flame first advanced along the sample surface and then receded after a period

of time [1, 2]. Therefore, the FSI calculation method was changed to a time-flame spread distance-area basis. The current method is still based on the time-flame spread distance-area, but it also incorporates the rate of flame travel [1]. Calculation methods for both SDI and FSI will be further explained in Section 2.4.

2.3 Present Day Steiner Tunnel

Cross-sectional and side views of a present day Steiner tunnel apparatus are shown in Figures 2.1 and 2.2. The Steiner tunnel consists of a 25-foot (7.6 m) long steel furnace duct with a chamber that is 17.625 ±0.375-in (450 ±9.5 mm) wide and 12.0 ±0.5-in (320 ±13 mm) high. The test specimen is 24-feet (7.32 m) long and may be up to 2.0 ft (0.61 m) wide. As illustrated in Figure 2.1, the walls and floors of the tunnel are insulated with fire brick. The thickness of the specimen is limited to 4-in (100 mm). The standard requires that the first 14-in (356 mm) of the specimen be covered with a piece of sheet metal [1]. Therefore, only 24-feet (7.32 m) of the sample is potentially involved in the flame spread testing. The specimen is mounted as the ceiling of the chamber, supported by the side ledges; this leaves 17.75 ±0.25-in (450 ±6.35 mm) of the sample width directly involved in the fire testing. The top of the specimen is covered with a lid assembly that contains 1/4-in (6.4 mm) thick asbestos cement board insulated with a minimum of 2-in (51 mm) thick calcium silicate. To prevent air leakage into the fire testing chamber, the lid is water sealed as indicated in Figure 2.1.

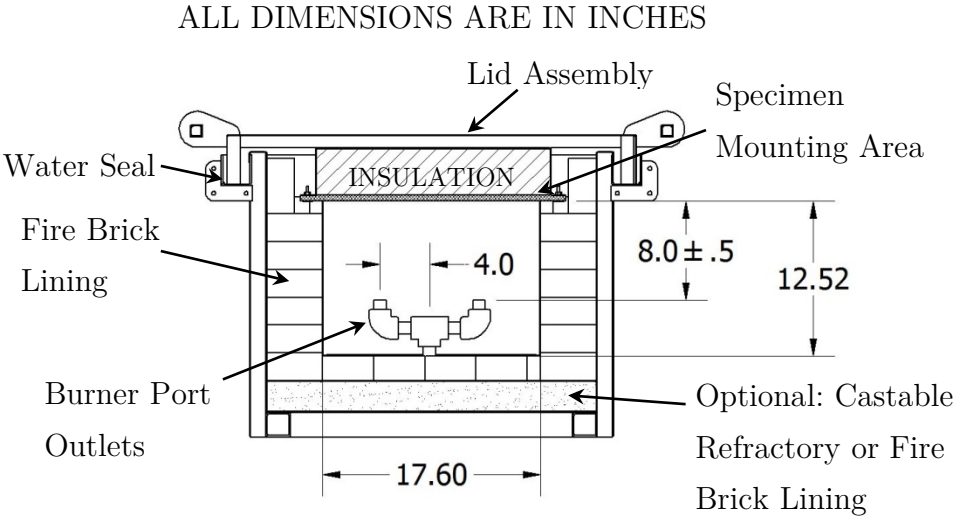

Figure 2.1: Cross-sectional view at the burner location for a representative Steiner tunnel

Two nominal one-inch pipe burner ports are used to create diffusion flames using methane gas. The diffusion flames output an intensity of 5000 BTU/min (88 kW) [1, 20].

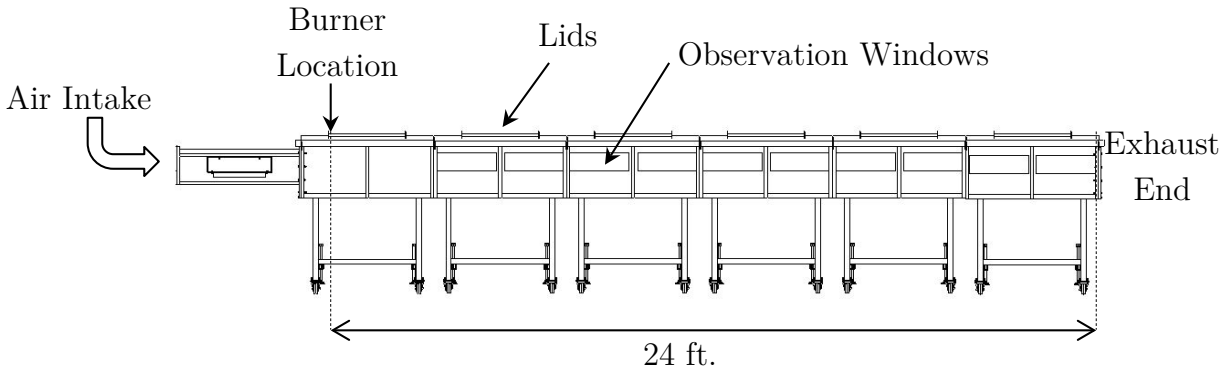

Figure 2.2: Full side-view of a representative Steiner tunnel

The burner ports are symmetric (4-in from centre) pointed upwards and aligned with the inlet air flow. The tip of the burner ports are 7.5 ±0.5-in (190 ±13 mm) below the specimen and generate a test flame extending downstream to a distance of 4.5-feet (1.37 m) over the specimen surface. The burner is located 24-feet (7.3 m) from the end of the tunnel as indicated in Figure 2.2 [1].

Openings are provided at each end of the tunnel to facilitate flow through the system; one is for the air intake and the other is for exhaust. The air intake constantly provides air to mix with the fuel supplied to the burner outlets. Air turbulence for proper mixing and combustion is established by positioning six refractory firebricks at set positions along the side walls of the chamber.[1] Fumes and smoke are constantly extracted from the tunnel through the exhaust end. The exhaust end is fitted with a transition piece that leads into a circular exhaust duct 16-in (410 mm) in diameter [1]. A constant draft between 0.055 - 0.100 in-WC (1.44 - 2.54 mm-WC) is induced through the two openings using a controlled fan and damper system [1, 20, 21].

An automatically controlled damper is used to regulate the draft pressure in the tunnel according to the draft gage reading. The draft pressure tap connection is placed 15-in (380 mm) from the air-intake opening, while the damper is installed downstream of the smoke measurement device [1]. The smoke measurement device is mounted within the exhaust duct, a minimum of 16-ft (4.88 m) away from exhaust end [1]. The device is a photometer system consisting of a white lamp and photoelectric cell aligned to determine the obscuration of the lamp beam by smoke collecting in the tunnel during a test. There is a thermocouple located 23-ft (7.0 m) from the burner that is exposed directly to the hot gases in the tunnel, as well as the flames if the burning front proceeds to the far end of

[1]On the window side 7, 12 and 20 ±0.5-ft (2.1, 3.7 and 6.1 $\pm 0.2m$), on the brick side 4.5, 9.5 and 16 ±0.5-ft (1.3, 2.9 and 4.9 ±0.2 m) from the centre of the burner distance [1].

the tunnel. This thermocouple also provides data for the time-temperature curve during the calibration process. Another thermocouple is located 13-ft (3.96 m) from the burner, buried 1/8-in (3.2 mm) below the surface of the floor of the tunnel. This thermocouple establishes a starting temperature for each test [1].

The front wall of the tunnel contains a series of observation windows such as those shown in Figure 2.2. The ASTM E84 tunnel has windows that are double glazed which tend to reduce the turbulence in the tunnel, leading to the use of refractory fire bricks to generate turbulence along the side walls of the testing chamber described above [1]. The Canadian ULC S102.1 test apparatus contains windows that are single glazed and mounted on the exterior walls so that they are inset from the inside wall of the tunnel chamber and themselves promote turbulent mixing down the tunnel length. Consequently, the Canadian standard does not specify the use of turbulence-creating bricks on the tunnel floor [10].

Prior to testing, a prescribed average air velocity of 240 ft/min (1.2 m/s) is established at the exhaust end of the tunnel. The tunnel is preheated to 41^oC (105^oF) as indicated by the buried thermocouple at 13-ft (3.96 m) from the burner exit [1, 20]. The air draft pressure is regulated between 0.055 and 0.1-in (1.40 and 2.54 mm) of water column. Draft pressure within this range is maintained throughout the test by an automatically controlled damper [1].

During testing, the burner flames act as the ignition source for flame spread over the test specimen since the specimen is directly exposed to these flames for an interval of 10 minutes. A controlled inlet air draft of 240 ft/min (1.2 m/s) will result in flames that extend 4.5 ft (1.4 m) down the tunnel [2]. This leaves 19.5-ft (5.94 m) of length of the original 24-ft (7.32 m) specimen past the end of the 'pilot' flames. Once the specimen is ignited, windows located on the side of the tunnel allow the operator to observe flame front propagation. Corresponding values of flame spread distance and time are recorded, preferably by a trained Steiner tunnel operator [20]. This is because at times the flames are visible only as brief flashes, while in other tests smoke may obscure the windows and cause viewing problems as well [20]. Nonetheless, time is reported at intervals of 15 seconds and the flame travel distance to the nearest 0.5-ft (0.15 m). The output from the photoelectric cell is also recorded at least every 15 seconds for smoke measurements. At the end of the 10 minute exposure, the gas to the burners is shut off, thus ending the test. The specimen is then carefully removed for further examination [1]. Recorded values of flame spread distance and time are used to determine the FSI. The photoelectric cell voltage over time is used to determine the SDI.

Calibration of the Steiner tunnel is usually performed once a month depending on the number of tests performed in the tunnel [20]. For this, the tunnel is preheated to 66^oC (150^oF) and then cooled to 43^oC (110^oF) before a specimen is inserted. Any air leaks in the

tunnel and other operational concerns are fixed during this calibration process. In the first calibration run, fiber-cement board is used and the fuel supply is adjusted to the burners to meet the standard time-temperature curve specified in the ASTM E84 standard. In the final calibration run, the red oak sample is used and the air velocity is adjusted such that the flame front passes over the sample and reaches the end of the tunnel in approximately 5.5 minutes. These results are then used in calculations for FSI (and SDI) discussed in the next section.

2.4 Flame Spread Index and Smoke Developed Index Calculation

FSI and SDI are the two most important parameters used to characterize the fire performance of a sample tested in the Steiner tunnel. The FSI is determined based on two factors: the rate, and the total distance, of the flame front propagation. SDI on the other hand is a time integrated measurement of the obscuration of a visible light beam by smoke generated during testing of the sample [22].

To determine the FSI of a material, recorded values of the flame front position are plotted as a function of measured time. An illustrative plot of flame front position versus time is shown in Figure 2.4. The total area (A_T) under the flame spread versus time curve is used for calculating FSI. This is the sum of areas A_1 (dark grey) and A_2 (light grey) in the figure and can be calculated using trapezoidal integration of the area under the curve [23], resulting in units of $ft \cdot min$ ($m \cdot min$). The FSI is then computed using this area, A_T, according to Equations 2.1a and 2.1b [1, 24].

$$FSI = 0.515 \cdot A_T \; for A_T \leq 97.5 \text{ ft} \cdot \text{min} \tag{2.1a}$$

$$FSI = \frac{4900}{195 - A_T} \; for A_T > 97.5 \text{ ft} \cdot \text{min} \tag{2.1b}$$

The old method of calculating FSI was derived using a specified value of 100 for red oak lumber combined with a time of 5.5 min for the flames to reach the end of the tunnel in a red oak calibration test [25]. Prior to 1976, FSI was determined based on one of the four formulas presented below; depending on how soon the flames reached the end of the tunnel or the position where the flames stopped within the tunnel [25]:

1. If the flames reached the end of the tunnel before 5.5 minutes, the FSI = 550/t, where t is in minutes. This explained an FSI of 100 being assigned to red oak.

2. If the flames reached the end of the tunnel before the 10 min test period, and longer than 5.5 minutes, the FSI = 50 + 275/t.

3. If the flames stopped at a distance past 18.5 ft (5.5 m), or before the end of the tunnel (24.0 ft or 7.3 m), the FSI = 50 + 4.62(d_{max} - d_0) where d_{max} is the maximum distance from the burner (in meters) and d_0 is the length of the burner flames (in meters).

4. If the flames stopped before 18.5 ft (5.5 m), the FSI = 16.7(d_{max} - d_0).

The discrepancy found within this method was that if the flames were to spread to a point just short of the end of the tunnel in 0.55 minutes, the FSI = 77.5; however, if they passed over to the end of the tunnel in the same time, the FSI = 1000; meaning both values can be achieved if conducting multiple tests on the same product [25]. However, as discussed in Section 2.2, the method to calculate FSI has undergone some changes over the years. Since 1976, FSI was calculated based on the area under the flame spread distance versus time plot. This method is also called the GWL method after George Williams-Leir of the National Research Council of Canada (NRCC) who proposed it [25]. The method was established by essentially considering the maximum possible area under the flame spread distance versus time plot (19.5 ft x 10 min = 195 ft·min) and dividing the area into two equal triangular areas as shown in Figure 2.3. Figure 2.3 from ASTM E84 [1] shows an idealized flame spread distance-time plot (no flame regression) and a steady progression of flame front to a maximum distance at the end of the 10 min test to produce a maximum possible area (ORB) of 97.5 ft·min (FSI = 50). The hatched out portion with the idealized straight lines OI, OI', and OI" that produce a family of trapezoidal areas ranging from 97.5 ft·min to 195 ft·min (ORBI) represent flame front progression to the end of the specimen before the end of the 10 min test.

For area less than 97.5 ft·min, the current formula is equated with the previous formula using a proportionality constant K and the area (A) under the curve (ORB in Figure 2.3) with the following equation [1]:

$$FSI = \frac{550}{t} = KA \tag{2.2}$$

Substituting the maximum possible area A = 97.5 ft·min, and t = 10 min into Equation 2.2 simplifies to:

$$K = \frac{550}{10 \cdot \ 97.5} = 0.564 \tag{2.3}$$

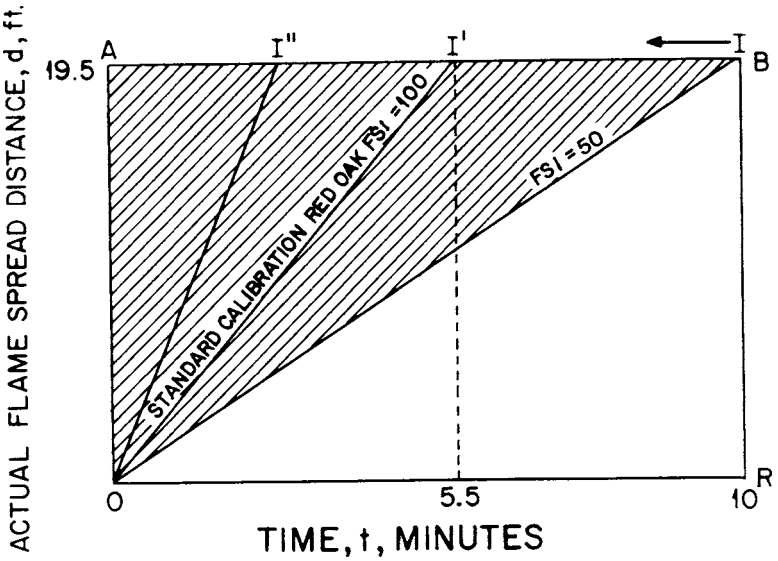

Figure 2.3: Idealized straight-line flame spread distance versus time curve [1]

Similarly, for area greater than 97.5 ft·min (ORBI in Figure 2.3), can be expressed as A_T:

$$A_T = \left(\frac{1}{2} \cdot \ 19.5 \cdot \ OR\right) \ + \ \left(\frac{1}{2} \cdot \ 19.5 \cdot \ (10 \ - \ AI)\right) \tag{2.4}$$

The remaining triangular area OIA (195 - ORBI) is divided into a proportionality constant K which determines the relationship between flame spread indices and the rate and distance of flame propagation, and hence for the following Equation [1]:

$$FSI = \frac{K}{OIA} \ = \ \frac{K}{195 \ - \ A_T} \tag{2.5}$$

K is once again established by relating the current and the previous formulas [1]:

$$FSI = \frac{550}{t} \ = \ \frac{K}{195 \ - \ A_T} \tag{2.6}$$

Equation 2.6 is fully established at the red oak calibration point of 19.5 ft and 5.5 min [1], therefore, substituting AI = 5.5 min into Equation 2.4, where OR in Equation 2.4 is always equal to 10 min, simplifies Equation 2.6 to:

$$K = \frac{550 \cdot \ (53.63)}{5.5} \ = \ 5363 \tag{2.7}$$

Therefore, Equations 2.1a and 2.1b were initially expressed as [1, 25]:

$$FSI = 0.564 \cdot A_T \ for A_T \leq 97.5 \text{ ft} \cdot \text{min} \tag{2.8a}$$

$$FSI = \frac{5363}{195 - A_T} \ for A_T > 97.5 \text{ ft} \cdot \text{min} \tag{2.8b}$$

Before being further reduced to compensate for the disproportionate increase that can occur in FSI values on products being classified as having an FSI no more than 25, rather than being classified as having an FSI above 25 [1, 25]. As a result, the GWL formulas above were modified to reduce all indices by a factor of 8.7 % to the current set of equations [1, 25].

In the current Equations 2.1a and 2.1b, the FSI for red oak is approximately 90 [2]. In general, the faster the flame propagates to the end of the tunnel, the larger the value of A_T, and hence the value of FSI will be higher [26].

For some materials, the flame will progress forward, and then it might stall and recede backwards with continued exposure time [27]. For example, the flame front travel distance-versus-time curve for 1/2-in thick (12.7 mm) structural polyvinyl chloride (PVC) is shown in Figure 2.4. After 0.5 minutes of testing, the flame had advanced to 1.5-ft (0.457 m), and then it receded. In this case, the area under the curve is calculated as if the flame regression did not occur. The flame front may recede for a period of time and then advance again. For example, at 2.75 min into the test shown in Figure 2.4 the flame spread to 2-ft (0.61 m), then receded and subsequently advanced again. The area is calculated as if the flame had spread to 2-ft in 2.75 minutes and then remained at 2-ft until the flame front passed the 2-ft mark again (at 3.5 min). Similar observations can be made throughout the remainder of the test in which the maximum flame spread distance is 5.0-ft (1.52 m). Using the test results shown in Figure 2.4 for structural PVC, the FSI is calculated to be 20, using Equation 2.1a since $A_T = A_1 + A_2 = 36.87$ ft $\cdot$ min.

The ASTM E84 test procedure also involves determining smoke obscuration over the duration of the test. The light absorption versus time curve of smoke generated from the sample is denoted as SDI. The light obscuration, which is related to the smoke density in the tunnel, is measured using a photoelectric cell that detects changes in the incident intensity of a beam of visible light due to obscuration of the beam by smoke particles in the tunnel [28]. The smoke obscuration percentage, $SO\%$, is calculated using Equation 2.9, where E_t is the voltage output from the photoelectric cell at a given time, and E_{max} is

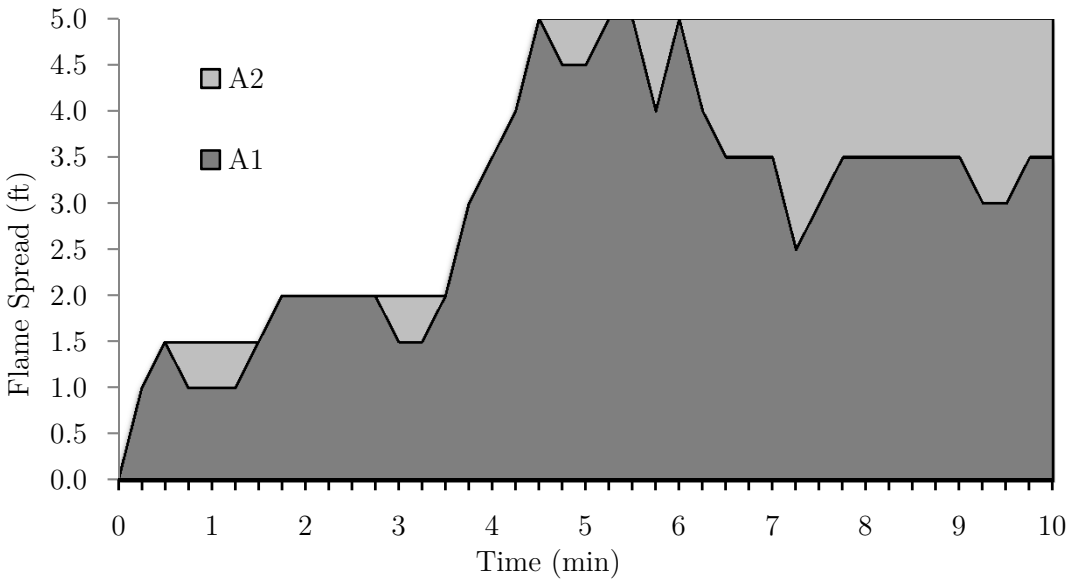

Figure 2.4: Illustrative flame spread distance-time plot for structural PVC

the maximum voltage that the photocell generates when exposed to the full (unobscured) intensity of the light beam [23, 28].

$$SO\% = \left(1 - \frac{E_t}{E_{max}}\right) \cdot 100\% \tag{2.9}$$

Using the measured values of voltage output from the photocell, the smoke obscuration ($SO\%$) is calculated and recorded at least every 15 seconds for the entire 10 minutes of the test [1]. The resulting values are then plotted against time and the calculated area under the curve provides the value of the total smoke obscuration, TSO, in $SO\%\cdot$ min for the specimen. DiDomizio [23] demonstrates the derivation of TSO in his thesis. Basically the area under the curve is determined using trapezoidal integration, which simplifies to Equation 2.10, assuming that the sampling frequency of $SO\%$ is 1 s, and the duration of the test is 600 s (10 min). For a given test, the sampling frequency will depend on the data acquisition system and Equation 2.10 would have to be modified accordingly.

$$TSO = \frac{1}{1200} \sum_{t=0}^{N-1} (SO_{i+1} + SO_i) \tag{2.10}$$

A typical smoke obscuration-time curve of a specimen is presented in Figure 2.5. As can be seen in the figure, the $SO\%$ starts off at a low, relatively constant value due to

early flame establishment, and after flaming is established it is characterized by a period of high obscuration, after which it gradually declines.

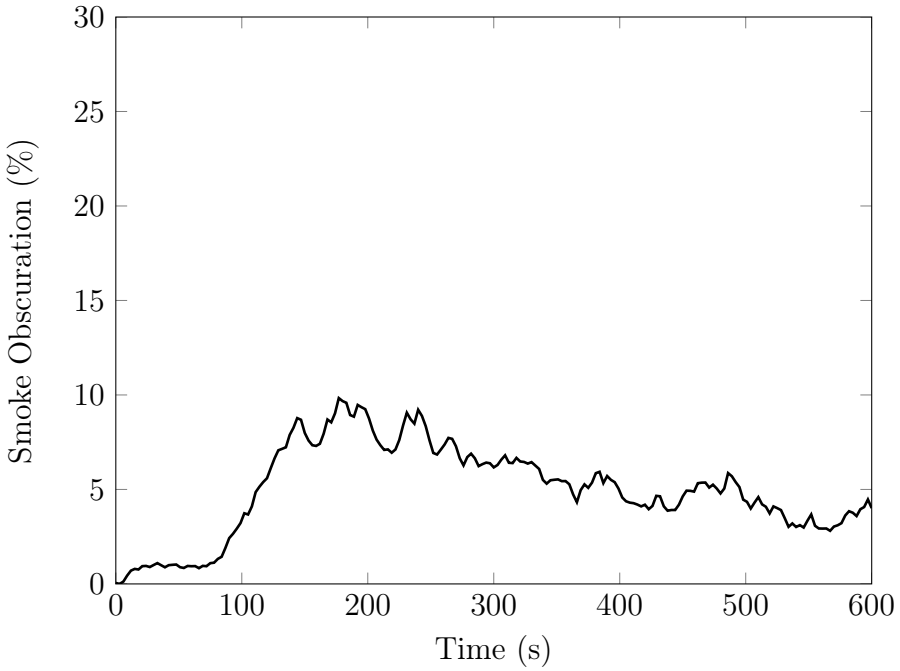

Figure 2.5: Representative smoke obscuration-time curve for Red Oak

The SDI is then determined by comparing total smoke obscuration of the test sample (TSO) to that of red oak (TSO_R) [23, 26]. TSO_R is computed with a running average of a single tunnel for at least 5 red oak calibration tests [1]. SDI for red oak was established to be 100 [1, 13, 26], and therefore the SDI for a sample of a material is calculated according to Equation 2.11 [24].

$$SDI = \left(\frac{TSO}{TSO_R}\right) \cdot 100 \tag{2.11}$$

The upper limit on SDI of 450 shown in Table 2.1 was originally developed at the UL research facility [29]. They conducted research where they burnt various samples in the tunnel and sent smoke into rooms illuminated with exit signs. The time it took for the exit signs to be totally obscured by the smoke was compared with the SDI values of the materials determined in the Steiner tunnel test. For a material with an SDI value of 325, there was still 'good to marginal' visibility of the signs, while other materials produced conditions of 'marginal' visibility to full 'obscuration' within the 6 minute period of the room test [29]. The range of SDI values between 0 and 450 has now been used for many years in classification of potential smoke obscuration by materials and it seems to provide

a 'reasonable' limit on acceptable SDI values for materials to be used for interior finish in rooms [29]. The SDI limit of 450 takes into account both the time required to produce the smoke and the effect of the smoke on distance of visibility within the space [29].

As expected, for a given material, the FSI and SDI are not necessarily related to each other since many different parameters influence flame spread in contrast to smoke generation in fires. For example, traditional building products such as wood will generally have higher FSI values than polyurethane foams with fire retardants (FR) [27]. FR polyurethane foam, on the other hand, will have a significantly higher SDI than wood due to both the base material composition, as well as the impact of the FR additives on smoke production from the foam [23]. To be used in building construction, however, both materials would have to satisfy both FSI and SDI requirements per the classifications outlined in Section 2.1 and Table 2.1 in order to be used for certain applications, so a balance of characteristics generally leads to optimal fire performance for any given material.

Despite having been developed into a standard test method for determination of the relative fire performance of materials, variability still exists in tunnel test data even for repeat tests of a given material. In reality, however, small differences in measured values of SDI (e.g., 10-20 points) are not considered to represent a significant difference in actual fire behaviour, and as a result, measured SDI values are rounded to the nearest multiple of 50 points [29]. FSI values, on the other hand, are generally somewhat more repeatable and are rounded to the nearest multiple of 5 points [29]. To elucidate the potential variability further, some of the limitations and parameters which affect the operation of the Steiner tunnel will be further addressed in the following section.

2.5 Limitations and Parameters Affecting the Operation of the Steiner Tunnel

This section describes the limitations and parameters which affect the operation of the Steiner tunnel. The affecting parameters which were studied in a shorter, 8-ft [30], tunnel method are first discussed, followed by the limitations and affecting parameters of the full 25-ft tunnel. A potentially major limitation in the 25-ft Steiner tunnel test relates to the overall cost of testing, particularly when a product is in the research and development phase, requiring iterative testing to optimize its fire performance. Since the Steiner tunnel test requires 24-ft (7.32 m) long product samples, preparing, shipping and testing such large specimens is burdensome and costly. From an operational point of view, the calibration tests with red oak which have to be performed each month are also expensive as each of these can also cost up to $882 [5] for the materials for a single burn. As a result, early

studies attempted to reduce the overall tunnel length; these are discussed in the following section.

2.5.1 Development of the 8-ft Tunnel Method

Over the years, various users of the Steiner tunnel were concerned with the costs of sample fabrication and material testing in the Steiner tunnel [19]. As a result, the U.S. Department of Agriculture, Forest Products Laboratory (FPL) developed a significantly smaller tunnel test in 1951 [19]. This test, named the FPL 8-ft Tunnel Method [19], was intended to imitate tests that were conducted on acoustical materials, Douglas fir plywood, gypsum, mineral wool and hardboard. While tests were conducted to characterize the performance of the new apparatus relative to the original ASTM E84 test, the 8-ft tunnel was intended mainly for purposes of product research and development. A complete investigation of the 8-ft tunnel method was completed by considering the following variables [3, 31]:

- Heat energy release in the combustion chamber
- Initial partitioning plate temperature
- Specimen distance from hot plate
- Burner position
- Depth and slope of the tunnel
- Specimen moisture content
- Density of red oak

There were three models that were developed over a four year investigation period as discussed below [31].

First Model

The first model was designed by scaling down the large tunnel furnace to 8-ft (2.44 m) in length and 15-in (0.381 m) in width [31]. The burner intensity was also scaled down to 970 BTU/min (17.1 kW) from 5000 BTU/min (88 kW) to compensate for the scaled geometry [31]. The inside dimensions of the tunnel were 12-in (0.305 m) wide and could vary from 7 to 12-in (0.178 to 0.305 m) in depth [31]. A series of investigation tests were conducted

to determine the impact of modifications to the contour and depth of the tunnel, burner design and placement, and air flow conditions on the measured flame spread characteristics of representative materials. The flame was only applied to the first 2-ft (0.61 m) of the specimen, while keeping the same air velocity conditions as in the original 25-ft tunnel [31]. It was noticed that the exact position of the flame front was difficult to observe in the small tunnel because of the high air velocity conditions. The tips of the flame were irregular and flickered between 12 to 18-in (0.305 to 0.457 m) which induced substantial test to test differences in measured flame spread results [31].

Second Model

A second model of the 8-ft tunnel was introduced, with the test specimen tilted at 30 degrees across its short axis. It was thought that tilting the sample would force the irregular flame tips to travel along the upper side of the specimen and form a flaming area that was more easily located [31]. Instead of an exhaust duct located at the end of the tunnel distant from the burner, in this new design a duct that instantaneously removed the products of combustion extended over the entire length of the specimen and the exhaust gases were channeled to a central stack where smoke measurements were taken [31]. Following all the investigations, the model was established with the furnace oriented at a 4 degree upward slope along the length of the furnace [31]. A perforated steel plate was placed lengthwise along the furnace dividing the tunnel into two sections; the lower combustion chamber and the upper test specimen chamber. The combustion chamber was heated with a separate 4000 BTU/min gas burner which radiated heat through the partitioning plate and onto the specimen [31]. The initial ignition source was a small igniting burner located at the lower end of the specimen. Holes were provided along the lower edge of the specimen chamber to introduce the necessary air for the possible burning of the specimen [31]. This is in contrast to ignition in the large tunnel test, where the sample is directly exposed to the flames from the burner. Nonetheless, measured flame spread indices were fairly well approximated as compared to results obtained in the 25-ft tunnel for untreated wood products. However, poor correlation of flame spread indices was obtained for fire retardant materials with weak flaming tendencies [31]. It was believed that in a rather severe exposure in the small tunnel, small progressive flaming would occur for these materials, while in large tunnel it was believed that the flames were extinguished due to a combination of the extinguishing actions of the combustion gases and high draft conditions [31]. The size of the holes in the partitioning plate in the small tunnel were graduated to compensate for observed discrepancies in flame spread until flames were extinguished in the same manner as in the large tunnel furnace [31].

Third Model

After further investigation of the small tunnel performance, the lengthwise slope of the tunnel was changed to 6 degrees and the energy output of the burner in the combustion chamber was reduced from 4000 to 3400 BTU/min (70.3 to 59.8 kW) [31]. The partition plate was replaced with a stainless steel plate and named as the 'radiant panel' [31]. A more efficient smoke duct was incorporated into the design and the specimen width was reduced to 14-in (0.356 m) [31].

Development of ASTM E286

In studies undertaken in 1960 and 1961, three test methods for flame spread over materials, i.e. the 8-ft tunnel, the 25-ft ASTM E84 tunnel and the ASTM E162 radiant panel [32], were evaluated by NFPA with cooperation from Los Angeles Fire Department [33]. Several full-scale fire tests were conducted in school buildings in Los Angeles in which ceiling tile materials were tested by using them to cover the ceiling of a corridor that was 8-ft (2.44 m) wide, 12-ft (3.66 m) high and 64-ft (19.5 m) long. The tiles were ignited at one end using wood cribs varying in weight, which were burned to reach a maximum intensity of approximately 18 000 BTU/min (317 kW) in 2.5 to 3 min [31]. The distance of flame travel along the ceiling of the corridor with time was compared to the flame spread indices as evaluated using the 8-ft tunnel, the 25-ft tunnel, and the radiant panel methods. The 8-ft tunnel FSI value correlated to the performance of the ceiling tiles in the corridor fire with a correlation coefficient of 0.96, followed by the radiant panel at 0.90 and the large tunnel at 0.86 [31]. Based on this investigation, the 8-ft tunnel method started to gain a reputation, leading ASTM to develop the standard ASTM E286-69 Method of Test for Surface Flammability of Building Materials Using an 8-ft (2.44 m) Tunnel Furnace in 1965 [34].

ASTM E286 Test Standard

In the ASTM E286 method, the sample is conditioned to 80^oF (26.7^oC) and 30 percent relative humidity and positioned in the tunnel with asbestos and metal covering the back [31]. The radiant panel in the tunnel is adjusted to 85^oF (29.4^oC), and the pressure and temperature of the gas are adjusted to obtain a burner intensity of 3400 BTU/min (59.8 kW) in the combustion chamber [31]. The small ignition burner is set to 85 BTU/min (1.5 kW) and positioned to impinge on the first 4-in (0.1 m) of the specimen as the ignition source [31]. Once the sample is ignited, the operator observes the progression of flames

through the side windows in a fashion similar to that used in the full Steiner tunnel test. The flame front position and time are recorded at every observation window. The maximum length of flame travel is 87-in (2.21 m) and for red oak the travel time is approximately 18.4 min [31]. The FSI for flames reaching the end of the tunnel faster than red oak is computed using Equation 2.12 [31, 35]. To calculate the FSI for flames travelling slower than those over red oak, Equation 2.13 is used [31].

$$FSI = \left(\frac{Time\ to\ reach\ end\ of\ red\ oak\ specimen}{Time\ to\ reach\ end\ of\ test\ specimen} \right) \cdot 100 \tag{2.12}$$

$$FSI = \left(\frac{Distance\ reached\ on\ test\ specimen\ in\ 18.4\ min}{Distance\ reached\ on\ red\ oak\ in\ 18.4\ min} \right) \cdot 100 \tag{2.13}$$

The standardized FPL 8-ft tunnel method proved to be a fairly useful tool for research and for providing information on various aspects of flame travel over materials. Flame spread indices for untreated wood products continued to agree well with values obtained in the full Steiner tunnel test. Those for some fire retardant products were improved to the point that they were only slightly higher than those determined in the large tunnel [3]. Measured FSI for a few materials, such as fire retardant-coated fibreboard and gypsum wall board, were still inconsistent; the flame spread index for FR coated fibreboard was significantly smaller in the large tunnel and gypsum wall board behaved somewhat erratically and therefore exhibited large variations in flame spread in the small tunnel [3]. The fire performance of materials in several large scale tests, including the corner wall test, ASTM E84 and radiant panel tests, were also compared to flame spread results obtained using the 8-ft tunnel [31] with encouraging results. In one comparison study conducted at FPL, the fire performance of a variety of test materials, including lumber, plywood, hardboard, and particle board, were compared in the wall-corner test and the 8-ft tunnel test. Flame spread results for all materials were well correlated between the two methods [3].

In contrast, the ability of the 8 ft tunnel test method to identify highly effective treatments or highly flammable materials was fairly limited as compared to the ASTM E84 tunnel test [34]. In 1981, R.H. White and E.L. Schaffer evaluated flame spread performance of red oak structural flake-board and softwood plywood using both the 8-ft and the 25-ft tunnel [36]; however, no correlations could be found between the two sets of results. ASTM E84 indicated a higher flame spread for flake-board and lower flame spread for plywood, while the opposite was the case for the 8-ft tunnel tests. In 1985, an exploratory study by S.L. Le Van involved four wood composite panels and evaluated flame spread using ASTM E286 [37]. In this case, the 8-ft tunnel failed to distinguish the effects of density,

moisture content, and heating rate of similar wood products, effects which had been noted in previous flame spread tests using other methods.

In the limited studies available, correlations of SDI obtained in the 8 ft tunnel demonstrate poor correlation with those measured during large tunnel tests of the same materials, although SDI values obtained from the 8 ft tunnel test are computed in the same fashion as in ASTM E84 method, using the area under the curve of measured light obscuration versus time [35]. Total obscuration for red oak and for the test specimen are likewise compared using Equation 2.11. Again, the comparison of results was particularly poor for the case of fire-retardant treated or coated materials, which had extremely high values of SDI (six times greater than red oak), while in the ASTM E84 test, the same material exhibits an SDI value that is one-fourth that of red oak [31, 38]. Such discrepancies are perhaps understandable since smoke development is highly dependent on variables such as the rate of heating of the sample, air flow, oxygen consumption, chemical composition and moisture content of the material and these are not directly scaled between the E286 and E84 test tunnels [31, 38]. Due to its inherent limitations and the overall enhanced utility of the ASTM E84 test over time, the ASTM E286 method was withdrawn as a standard test method in 1991 [34]. Nonetheless, many of the above factors that were observed to impact the operation of the 8 ft tunnel to a certain extent also affect results from the full length Steiner tunnel as discussed further in the next section.

2.5.2 Limitations of the Steiner Tunnel

The function and the intent of the Steiner test is to rank a series of materials based on a relative measure of their propensity for supporting flame spread and contributing to smoke development during a fire. Therefore, even when values of FSI and SDI are obtained for a given material, these values provide, at best, a relative ranking of the tested material in comparison to other materials tested in the Steiner tunnel. As such, the results do not provide a quantitative measure of fire performance and there is no real connection between ASTM E84 results and actual fire performance [4]. Since the test was developed for ranking the fire performance of wood products, results from these tests demonstrate fairly good predictability [39]. Correlations of results for other materials with their real fire performance characteristics are much less clear.

The Steiner tunnel was developed in the late 1940's for testing flame spread over interior finish materials. At this time, the major construction materials were traditional wood products [4]. Its use for fire testing continued through the 1970's when plastics began to emerge as more commonly used materials in construction [4, 40]. This change in finish materials led UL to conduct a study to assess the utility of the Steiner tunnel test for determining relative flame spread and smoke developed characteristics of other materials

in relation to their performance in room fire tests, specifically plastics, composites and laminated products. They found that tunnel testing did not necessarily provide accurate relative performance indices for lightweight materials with low thermal inertia, such as thermoplastics, since these materials often melt and drip to the floor of the tunnel during testing. This restricts flame spread in contrast to wood based materials that are self-supported throughout the duration of the test. By 1973, it was found that there were potential issues with Steiner tunnel test results for a range of materials including [4]:

- Foam Plastics
- Floor Coverings
- Loose-Fill Insulation
- Thin Laminates and Single-Layer Membranes
- Textile Wall Coverings

To address these issues, variations on the Steiner tunnel test method were adopted by different jurisdictions. For example, in Canada, the problem of testing foam plastic materials was already addressed in 1978 through design of a special variant of the Steiner tunnel, ULC S102.2 [10, 18, 27] (as discussed in Section 2.1), which utilized a downward facing burner with the material under test (i.e., foam) positioned on the floor [10]. Under the National Building Code of Canada (NBCC), materials that are used on building floors, or materials that tend to melt or drip when exposed to fire are to be tested according to this standard [27]. Observations at the National Research Council of Canada (NRCC) revealed that, once ignited, flames could spread over a foam plastic insulation with a low measured value of FSI much more quickly than expected, which means that the level of hazard from use of that material could be under-predicted using the standard ASTM E84 configuration for Steiner tunnel testing [27]. Therefore, for foam plastic insulation, a new equation for flame spread index, FSI_2 was developed as given in Equation 2.14,

$$FSI_2 = 92.3 \cdot \frac{d}{t} \tag{2.14}$$

where t is the time in minutes, and d is the flame front propagation distance in meters. This method was introduced to emphasize initial flame spread and speed of flame propagation and is used to determine the classification indices listed in Table 2.1 for foamed plastics [27]. For instance, in tunnel tests on polyurethane foam conducted by NRCC, the FSI calculated using Equation 2.14 was 427, while that determined using the traditional FSI equation (Equation 2.1b) was only 74. By current convention for lightweight materials,

therefore, the higher value of FSI between these two calculation methods is always selected as the rating for that material. In addition, alternative large scale tests are to be conducted when there are significant differences in the values of FSI found using Equation 2.14 in comparison to the traditional FSI equations, Equations 2.1a and 2.1b [27].

The FSI for thermoplastic foams continues to be rated using the standard version of the Steiner tunnel in the U.S., although some building codes have recognized the issue in a general way by suggesting that fire performance indices should be supplied from a more realistic test [18]. Factory Mutual (FM) [18], NRCC [27], and U.S. Federal Trade Commission [41] concluded that the ASTM E84 tunnel test is inadequate for providing satisfactory ratings for certain cellular foam commercial products; specifically low density materials that melt or drip. The Uniform Building Code (UBC) stipulates specific testing requirements for assemblies containing plastic foams through UBC Standard 26-3 [10]. This standard incorporates a room fire test that measures the actual fire performance of the material in a full scale configuration with more detailed test requirements than the U.S. model building codes [4, 10].

The applicability of the Steiner tunnel test for ranking fire performance of floor coverings and other non-standard materials has also been the subject of debate. An extensive test program at National Institute of Standards Technology (NIST), indicated that the Steiner tunnel was not an appropriate test method for ranking fire performance of floor coverings because results did not indicate the same rankings for fire performance as were determined using the flooring radiant panel test (ASTM E648, NFPA 253) [4]. As a result, fire performance of interior floor finishes is now mostly regulated via the flooring radiant panel test [40]. In other modifications to extend the utility of the Steiner tunnel test method for fire performance ranking of additional materials, wire-screen sample holders were utilized in attempts to test loose-fill insulation in the ceiling of the Steiner tunnel. 'Screen factors' were developed to account for the red oak flooring that was placed on top of the screens to assist the progress of flame [21]. Eventually the use of this testing method diminished due to its limitations, and ASTM instead established an independent test method, the Standard Test for Attic Floor Covering (ASTM E970). Similarly, in 1987, researchers at the University of California [4] conducted a test program where they established that wall coverings were improperly rated in the Steiner tunnel for the same reason as already mentioned; the fire performance level of certain materials did not correlate well with their relative performance rankings determined using the standard [4]. As a result, the International Conference of Building Officials (ICBO) developed a full-scale room fire test for wall coverings, UBC Standard 8-2, which has been adopted for use in many countries [4]. Other materials, such as thin laminates and single-layer membranes, are still tested according to ASTM E84, even though it is well known that the methods of mounting these materials can influence the measured values of FSI [4].

2.5.3 Parameters Affecting the Operation of the Steiner Tunnel

Despite the demonstrated utility of the Steiner tunnel test method for ranking the fire performance of a wide range of materials, certain levels of test-to-test variability and uncertainty are inherent in the test results. In commissioning a new tunnel for operation, then, it is important to understand how these parameters might affect the overall operation of the tunnel. The key parameters, and their effect on tunnel operation, will be discussed in this section.

Poor reproducibility of Steiner tunnel test results was reported as early as 1962. In correlating test results across a range of acoustical materials tested in different labs, Yuill [42] concluded that improper construction of Steiner tunnel test apparatus was the critical factor that drove poor correlation of results. It was not until 1975, however, that the first attempt to quantify precision of Steiner tunnel test results was made when Lee and Huggett [43] did a survey on the key physical attributes of 11 different tunnels that existed in various laboratories. Key areas leading to variability in test results were assessed and it was determined that most of the tunnels did not comply with the ASTM E84 standard, probably because the standard was not sufficiently detailed in its specifications of the tunnel design and operation. The main differences noted related to tunnel construction details and measurement techniques. To determine the impact of these differences, tests were conducted on 9 different materials across labs [25]. The coefficient of variation between the labs was in the range from 7 to 43% for FSI and 35 to 85% for SDI [25]. The exact differences and parameters causing these significant variations were difficult to assess due to the number of differences and variations in parameters that were reported. Some, however, were fairly obvious, such as where one of the labs did not follow air-leak test procedures completely, and as a result it contributed to low SDI [25]. Several labs consistently reported low and high smoke results for certain materials due to differences in smoke measuring systems [43]. The smoke photometer was improperly specified in the standard and the reproducibility of smoke results was less than satisfactory. In more recent reports, measured values of FSI have been shown to vary by up to 50 depending on the type of wood species being tested [44]. Such variations arise due to inhomogeneity in the test samples, but also because of the difficulty of operating a large scale test system such as the Steiner tunnel [14]. In the paragraphs below, therefore, the many variables that influence tunnel performance are presented and discussed.

To address issues of uncertainty and variability in Steiner tunnel testing, Resing [14] recently applied a statistical process analysis to the Steiner tunnel tests using the Define, Measure, Analyse, Improve, Control (DMAIC) method to identify and improve key processes that could cause variation in measured values of FSI and SDI for a given material. Since airflow through the tunnel has a significant influence on the measured values

of flame spread, all of the subsystems related to control of inlet air flow were considered as potential causes for variations in the results. A Statistical Process Control (SPC) tool was used to review a set of average test results for standard calibration runs and regular routine checks of a tunnel. Parameters such as cold duct air velocity, temperature of the tunnel prior to test, inlet temperature, and inlet humidity were plotted over time on a SPC chart to identify possible causes of variation. Once the sources of variations were identified, such as tunnel temperatures and air flow velocity, process control monitoring was implemented on all of the tunnel parameters, and they were controlled within their limits. As a result, the standard deviation of FSI and SDI results was reduced for heptane tests[1] and red oak tests [14]. No specific averages on the results were identified in this study; however, the authors claimed that the DMAIC method enabled a reduction in the number of calibration tests required by the tunnel of approximately 40 % [14]. UL [8] recently completed a study to measure repeatability and reproducibility of FSI and SDI results. Two variables were considered, one being the variation in results between materials with different fire performance characteristics (e.g., Class A versus Class B materials as defined in Table 2.1) and the other being the variation between tunnel operators. Six different building materials were tested by two different operators. The variability in results proved to be less than 10% across the 6 materials for both FSI and SDI. Such consistency was also noted in earlier work by Groah [45], where FSI had been determined by a fairly experienced operator and compared to values determined by an operator who had observed only 12 tests and had never read flame spread. The difference of only 4% between the FSI values obtained by the two operators indicates that when well calibrated, maintained and operated, the Steiner tunnel test method is a good measurement system.

Despite the possible level of consistency that can be achieved in test results as outlined above, the reality is that there are many test parameters in the Steiner tunnel methodology that can significantly influence the measured results. Each of these is related to one or several of the control mechanisms that govern operation of the tunnel and through careful calibration and attention to detail during testing, they may be altered to obtain acceptable precision of the results. In terms of commissioning a new tunnel, it is important to document and understand the impact of these parameters on the overall operation of the tunnel. Therefore, the key parameters that are likely to influence the performance of a Steiner tunnel and the precision of measured value of FSI and SDI are listed in Table 2.2 [25], and will be discussed below. As can be seen from the Table, these parameters can be broadly divided into three categories: parameters related to the apparatus, parameters related to the specific specimen under test and finally, parameters related to overall operation of the tunnel. Most of the parameters specified in Table 2.2 affect measured

[1]Heptane test was conducted by placing 310 g of laboratory grade heptane in a round metal pan placed near the burner, and the heptane was ignited using an electronic igniter.

values of FSI and SDI because they either influence the heat loss to the surroundings or the heat transfer to the specimen [25]. In addition, these values may be influenced by parameters affecting airflow and local mixing within the tunnel [25]. In general, impacts of the various parameters associated with design and layout of the apparatus would often be outside the control of a given laboratory or tunnel operator. Variation of parameters associated with test specimens is minimized through sample conditioning and consistency and standardization of methods used in mounting the specimens in the tunnel [46]. In contrast, the parameters associated with operation of a given tunnel are likely to relate directly to the conditions in a given laboratory, as well as to the operating procedures specified for, and care taken by, operators running a particular tunnel test apparatus [25]. For that reason it is studies related to these latter parameters that are emphasized in the discussions below.

Table 2.2: Parameters that influence ASTM E84 tunnel performance

Apparatus Parameters	Specimen Parameters	Operational Parameters
Gas inlet and burner design	Thickness	Inlet Air
Thermal properties of the lining brick	Moisture content	-velocity
Window design and location	Method of retention	-flow
Turbulence bricks		-temperature
Duct/Tunnel cross-sectional area		-moisture
Specimen mounting		Fuel
Exhaust/Damper design		-flow
		-heating value
		-temperature and pressure
		Other
		-specimen preheat
		-brick temperature
		-operator

Because of the importance of each of these sets of parameters to the values of FSI and SDI obtained in a Steiner tunnel test, various studies have been conducted to investigate the impacts of one or more parameters on the test results. For example, Endicott and Bowhay [46] reported that FSI for Douglas fir plywood and particle board are significantly affected by specimen moisture content, thickness, preheat time, and the brick lining temperature at the start of each test. Small variations in the air draft velocity did not have a significant effect on measured values of FSI, although the SDI was strongly influenced. Similar observations were made in a UL study that employed a wider range of draft velocities [25].

The Hardwood Plywood Manufacturers Association (HPMA) expanded the above study of the impact of various operating variables on results from the 25-ft tunnel method [45]. Seven variables were investigated including draft velocity, air intake opening, material weight, gas flow, brick temperature, operators, and method of joints. Each variable was tested under two conditions; a high condition and a low condition. The material selected for this study was particle board with a 3/4-in (19.1 mm) thickness. These results indicated that gas flow through the tunnel was by far the most important parameter studied, as changes in gas flow conditions had the most significant effect on both FSI and SDI results. Other variables that were found to have a substantial influence on FSI results were sample weight, brick temperature and draft velocity [45].

Some testing facilities operate on city methane gas, and in order for the city to provide a test lab with sufficient fuel during cold winters when gas demand is high, they will infrequently place diluted propane gas into the mixture at one part propane to one part air in the line [45]. With this mixture, effectively only 47-48 ft^3 of gas would be available to be burned instead of the regular 52 ft^3 when the flow rate is set the same [45]; since there would be less 'gas' in the mixture due to the addition of diluted propane, and, hence, less total energy in the gas mixture, potentially the burner energy output would decrease and as a result influence the FSI. Groah of HPMA [45] conducted a set of tests using 3/4 in (19 mm) particleboard by setting the gas flow rate to a high and a low condition; high condition averaged across tests was 52.22 ft^3 total volume of gas burned, whereas the low condition averaged 47.63 ft^3. The FSI obtained for particleboard using 52 ft^3 of gas to the burner was 159, while for 47 ft^3 of the same gas it was 136 [45], a reduction of 17 %. Another major work by FPL concluded that variations in burner fuel input required attention. Quintiere and Raines [47] determined that about half of the energy lost from the burner is due to radiation and convection to surrounding surfaces. Tests performed on fibre board specimens at NRC of Canada have shown that the burner accounts for the majority of the total heat release into the tunnel [25]. In fact, flame propagation along the fibre board specimen only accounted for 17% of the total heat release [25]. Since the burner is the major source for promoting pyrolysis and preheating the specimen, particularly in the early stages of a test, it is essential that the burner characteristics are well defined. The characteristics of the burner can be defined in terms of energy release and flame length [25]. It is generally recommended that the accuracy of the burner output is controlled within 1% of its calibrated value [25]. The calibrated value, as mentioned in Section 2.3, is the required amount of energy release for flames to propagate to the end of the tunnel in 5.5 minutes for red oak specimen. It should be noted that larger cross-sectional areas in the tunnel or the duct will require higher burner fuel flow rates. This is to compensate for the higher volume flow rate of air through the tunnel since the air velocity is constant and the area increases.

Specimen thickness and mounting methods cannot be completely standardized since these will vary across products. Since they may have some impact on consistency of results from test to test, they are recorded in the test report to facilitate later interpretation of the results if required. More significant parameters related to the test specimens are moisture content and density of the products. Variation of weight in wood products of the same base density can occur because of variations in the moisture content of a given sample. In general, such effects should be minimized by consistent conditioning of the samples before they are tested, however, a higher moisture content of one wood sample over another will decrease the value of FSI since the additional moisture will act as a heat sink and effectively increase the time taken for the sample surface to reach the pyrolysis temperature. Other tests have been conducted to compare the effect of product density on FSI values [45]. In one such study, a heavier weight (more dense) particle board resulted in decreased values of FSI (on the order of 12) in comparison to a lighter version of the same product. Based on experience from HPMA testing of a variety of different products, however, flame spread versus material density relationships were not always clear [45]. In more recent studies, White [48] concluded investigations correlating the FSI with densities for sawn lumber of various hardwood species, and determined that FSI is inversely related to the density of the wood ($R^2 = 0.56$), meaning the higher the density the lower the FSI. The same relationship could not be drawn for softwood species due to a number of reasons including the chemical composition, and both the lignin content and extractives of each specie [48]. Higher lignin content of softwoods would likely decrease the FSI due to higher residual char layer, while the presence of flammable extractives would increase the FSI [48].

As far as tunnel brick temperature is concerned, a longer preheat time of the tunnel has been shown to result in higher measured values of FSI [25]. This is due to the fact that mounting a sample into tunnel environment that is at a higher temperature will effectively reduce the time taken for the sample surface to reach pyrolysis temperature [25]. The importance of this parameter is acknowledged in the ASTM E84 standard, but according to Abrams et. al [25] it is inadequately handled. The standard focuses on the surface temperature of the brick as an indicator of the brick lining temperature rather than monitoring the temperature gradient through the tunnel wall [1, 25]. As such, it fails to recognize that the time required to mount the specimen will vary from test to test, resulting in a temperature gradient through the fire bricks that may also vary. It was also discovered that the surface condition of the lining brick was not a significant parameter for surface emissivity and thus would not likely have a large impact on wall radiant heat transfer or the FSI results [45]. Therefore, the standard only requires that the bricks are kept in good physical condition to prevent any influence on turbulence within the tunnel, while the influence of lining materials on FSI has not been studied [45].

A study conducted by Quintiere and Raines [47] in 1975 indicated that the inlet air mass

flow rate in the Steiner tunnel drops substantially during the course of a test. Velocity measurements and calculations have shown a drop in air supply rate which was found to be dependent on the density of gases in the tunnel and the duct [25, 47]. From the results, it was not clear whether the drop in airflow was associated with the temperature rise in the duct, change in mass transfer as the specimen burned, or if it was related to a particular tunnel facility. Moreover, it was not known what effect this reduction of oxygen supply to the tunnel had on measured values of FSI and SDI [47]. Such observations led to a modification of the standard to include a tunnel draft regulating device, where draft pressure was measured at the air inlet of the tunnel [1]. Since the air coming through the inlet is at ambient temperature and pressure, this usually requires increasing air draft pressure during testing to maintain the air flow within the required range.

Parameters Affecting Smoke Measurements Only

The SDI value from the Steiner tunnel test is intended as a relative measure of smoke generation from one product in comparison to another; however, it has been argued that the smoke measurement methodology in the ASTM E84 is technically not correct for this purpose [4]. From a physical perspective, smoke generation is directly related to flame spread, particularly through the quantity of material that is burning at any point in time. For products such as Douglas fir plywood, particleboard, polystyrene and polyurethane foams, a poor representation of the flame spread will affect the measurements of smoke obscuration [49]. In addition, the ASTM E84 test methodology involves calculation of SDI using only the percent of light transmitted across the tunnel section and therefore, is not a quantification of the 'amount' of smoke being generated per mass of material involved in the fire. Further, Babrauskas [50] concluded that smoke generation should be quantified by the logarithm of the photometer signal rather than a linear percentage of the maximum signal intensity, because the present calculation procedure has been shown to result in values of SDI for some products to be equal to red oak when, in reality, the smoke generated from that product can be as much as five times greater (or less) than that actually generated during the red oak test.

In addition to the above discussions, parameters affecting SDI results were studied by Abrams et. al [25]. His work indicates that the distance between the tunnel exit and the photometer was another cause for concern due to heat transfer characteristics of the exhaust duct. Smoke generated from wood products consists mainly of condensed liquids that are temperature dependent, while smoke generated from synthetic polymers contains mostly carbon particulates which are time dependent due to coagulation [25]. Therefore the heat transfer characteristics of the exhaust duct was mostly a concern for synthetic products [25]. The standard was then revised to insulate the exhaust duct with a 2-in (51

mm) high temperature mineral composite up to the point of photometer location[1].

Turbulence level in the exhaust duct is also an important variable for smoke measurement. Gas concentration profiles obtained by Abrams et al. [25] indicated appreciable stratification of gases at the photometer location, and this can be reduced or eliminated by introducing a damper at a short distance from the tunnel exit which will essentially inject a counterflow of air in the exhaust duct and provide swirling motion. A damper used for mixing exhaust gas in the study improved smoke data reproducibility, and reduced SDI standard deviation by more than 20% [25].

2.6 Summary

Even though the Steiner tunnel test method suffers from limitations such as those discussed above, no other single test method is capable of providing a comparable evaluation of the potential for fire development over a material in a building [2]. Therefore, results obtained from the Steiner tunnel test will continue to form one basis by which to regulate fire performance of materials and to provide a classification system for enforcement authorities. Despite the emergence of other complementary test methods, the Steiner tunnel remains the most common test method for evaluating fire performance of interior finish materials in buildings [2]. With the critical parameters from the Steiner tunnel tests (gas flow, air flow and the influence of the apparatus parameters) identified, variations of these parameters will be used to properly calibrate, and further understand the behaviour of, the modular Steiner tunnel that forms the basis of the present research. In the following chapter, therefore, details of the UW Steiner tunnel design and testing methods are provided, leading up to testing and calibration in the tunnel in Chapter 4.

Chapter 3

Experimental Apparatus and Methods

The experiments undertaken in this research are aimed towards the characterization of a unique modular Steiner tunnel system that was built as a collaborative final year design project between Elevator Cab Renovations (ECR) and Algonquin College, Ottawa [51], then delivered to the University of Waterloo Fire Research Lab (UWFRL). The tunnel is installed in the UWFRL and key ancillary systems are then designed during this work such that it met operational requirements, as well as safety regulations. These included the tunnel exhaust and damper design, gas supply train, safety controls system, and any additional instrumentation. As a final stage of the work, the tunnel is commissioned for operation and a parameter study is conducted to determine the impact of key tunnel controls on ASTM E84 rankings of a range of test materials. This chapter outlines the overall (as supplied) design and installation of the tunnel including final safety systems, as well as the experimental methods undertaken to evaluate the tunnel performance. In the following chapter, the commissioning for operation and initial evaluation of the tunnel performance is discussed, with conclusions and recommendations in Chapter 5.

3.1 Overall Steiner Tunnel Design

The overall design and layout of the Steiner tunnel apparatus is shown in Figures 3.1 and 3.2, with top and side views in Figure 3.1 and the overall layout in the UWFRL in Figure 3.2. The main test section consists of 4 modules, as well as air intake and exhaust sections. Each module is approximately 4.17-ft (1.27 m) long and they are assembled in sections, from Modules A to F, to form the full length of the tunnel. As shown in Figure 3.1, the tunnel test section has an overall length of 359.2 in (9.1 m) from the air intake shutter to the exhaust end, and a width of 33.9 in (0.861 m). Due to gas supply, intake and exhaust requirements, the entire tunnel testing apparatus is spread across two labs as illustrated

in Figure 3.2. The main gas supply, test section and exhaust duct transition piece are housed in the large scale testing lab. The test section is then attached to an exhaust duct transition section, with damper, through the furniture calorimeter fume hood to the 16-in (0.41 m) diameter laboratory exhaust ducting which passes into the small cone calorimeter lab through an insulated hole near the top of the fire rated wall. The fan controls, smoke analysis system, and 'far' exhaust duct damper are located in the small cone lab.

The tunnel is situated approximately 8ft (2.44 m) away from the outside wall of the large scale testing lab. This wall contains a 26-ft by 26-ft (7.93 m) overhead door that can be opened and closed with a chain drive system. During the experiments, this door is opened sufficiently to allow fresh air to enter the lab. Similarly, the exit door shown on the bottom left hand side of Figure 3.2 is kept open during each test to allow circulation of fresh air, and maintain constant atmospheric pressure in the lab. The exit door is situated 20 ft (6.10 m) behind the air intake module on the left hand corner of the lab facility.

In the following sections, more detailed descriptions of each element of the full Steiner tunnel test apparatus will be presented as follows:

- Modules
- Exhaust duct transition piece and the near damper assembly
- Exhaust fan, duct and far damper sssembly

The sections following the description of the tunnel apparatus will discuss the design of the safety controls system and an overall comparison of the present tunnel apparatus with the ASTM E84 tunnel.

3.1.1 Modules

The main tunnel test apparatus is comprised of six separate modular sections which can be configured to provide tunnel lengths ranging from three to six modules long. The tunnel apparatus is built in this fashion to allow research into the impact of tunnel length on fire test results, but also because the UWFRL is a multi-use lab facility, so the tunnel has to be mobile and relatively easy to disassemble and store as required. While this design allowed significant flexibility for research and use of the tunnel, it also posed certain design challenges as discussed below.

Each module comprising the main test section consists of a square, steel-walled outer duct, that is nominally 4.17-ft (1.27 m) long and 2.83-ft (0.86 m) wide and 5.32 ft (1.62 m) high. Each duct is open on the top, whilst the floors and walls of the duct are lined with

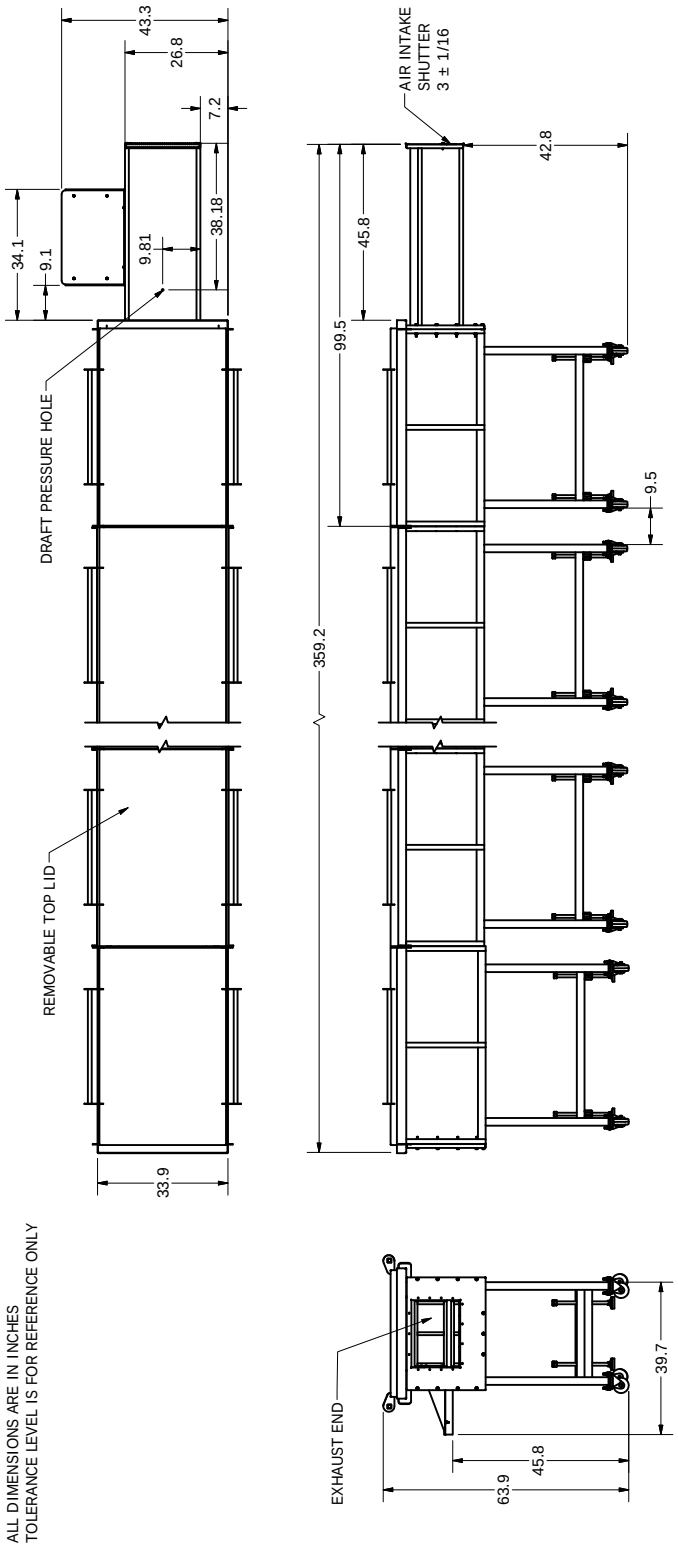

Figure 3.1: Top and side views of the full tunnel assembly

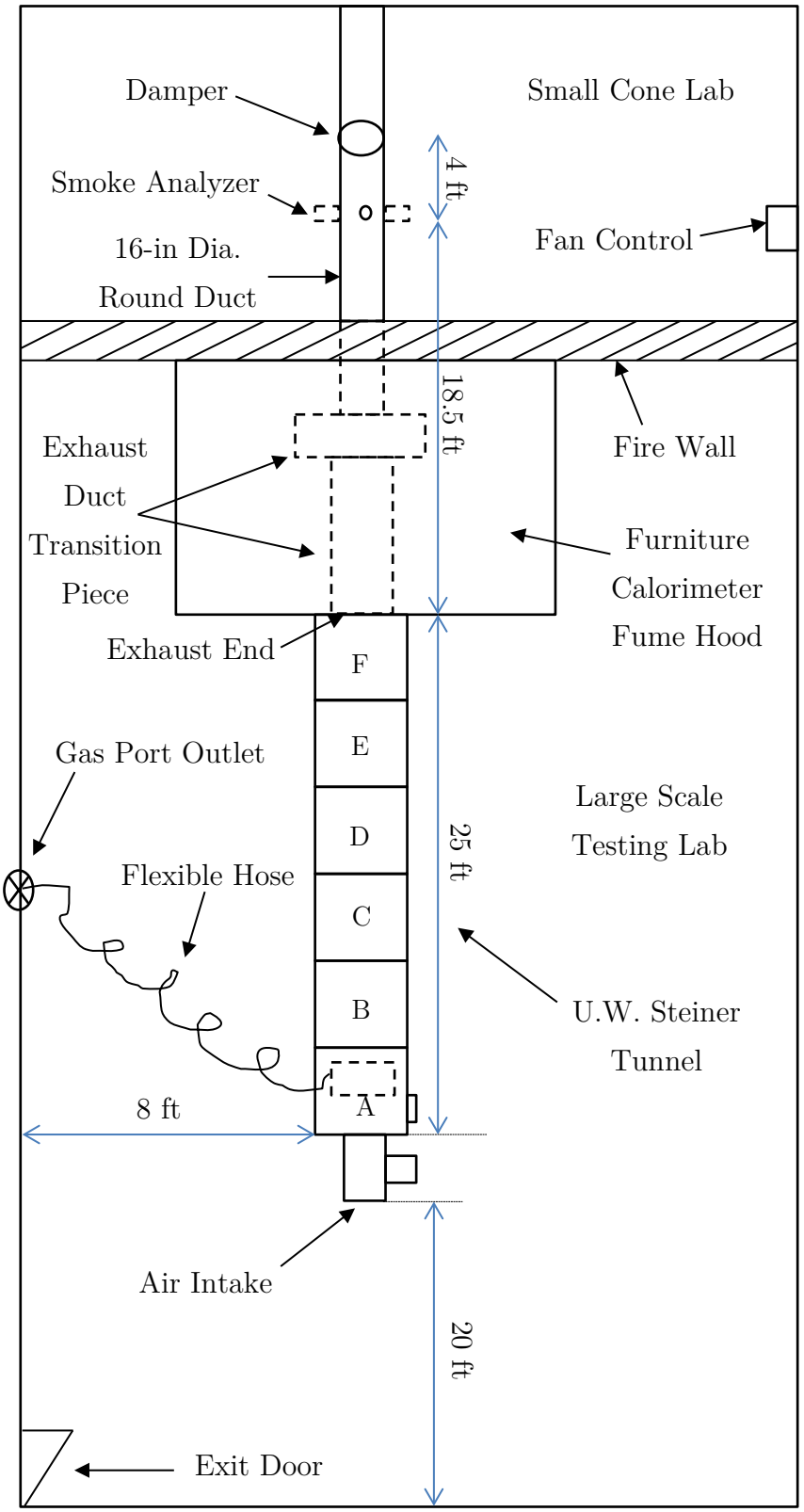

Figure 3.2: Steiner tunnel floor layout

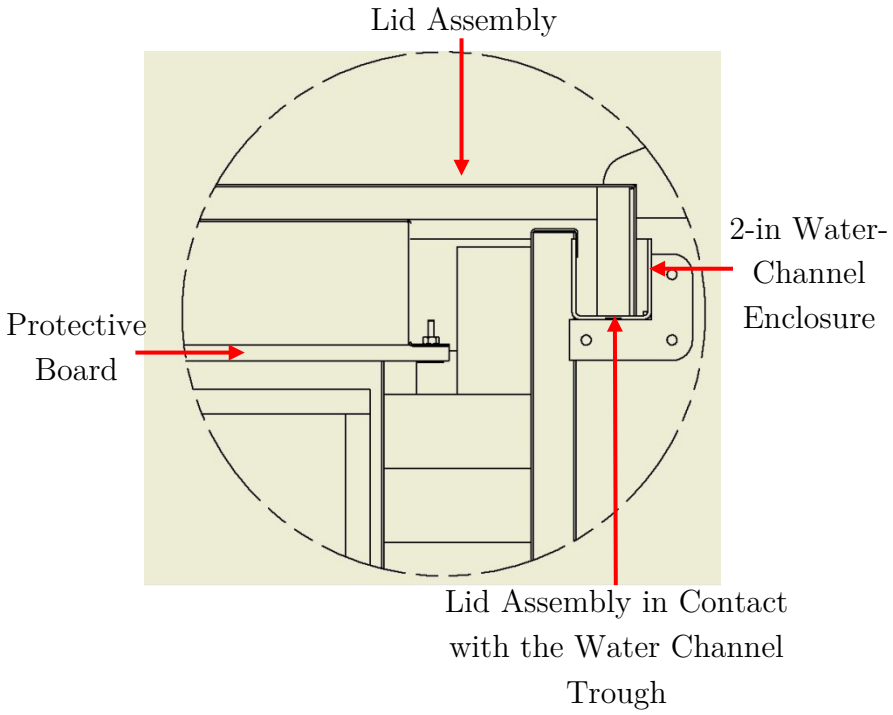

Figure 3.3: Contact between the water channel trough and the lid assembly

fire brick to protect them from thermal exposure during testing. The resulting interior tunnel cross-section is 17.6-in (0.45 m) wide and 12.5-in (0.32 m) high. During testing, the test sample is placed on top of the duct and covered with a protective board. Each module is then capped with a steel lid assembly which fits into a 2 in (51 mm) high water channel trough which is welded to the top of the exterior duct as shown in Figure 3.3. The water channel serves to provide an airtight seal between the tunnel duct and lid, as well as affording cooling to the joint over the duration of each test. The depth of the water channel trough, however, places a limitation on the maximum thickness of specimen that can be tested in the tunnel. Because of the protective board that is placed on top of the specimen, the maximum thickness of test sample is limited to 2.5-in (63.5 mm). For testing of more volatile materials, a 1/4-in (6.35 mm) thick hardy frame panel is placed on top of the test specimen to further protect the lid assembly. In this case, the thickness of sample is reduced to 2.25 in (57 mm).

Each module is supported with four struts that are welded to the bottom of the exterior tunnel duct as shown in Figure 3.4. Each strut is supported on a lockable, 4-in (101 mm) caster secured with four bolts. The casters facilitate the necessary maneuverability for set-up, storage and reconfiguration of the modules between tests. Further details of the frame support designed for each module is shown in Appendix A.1, Figure A.13.

During set up of the tunnel, the modules are aligned and then assembled with a 1/4-in

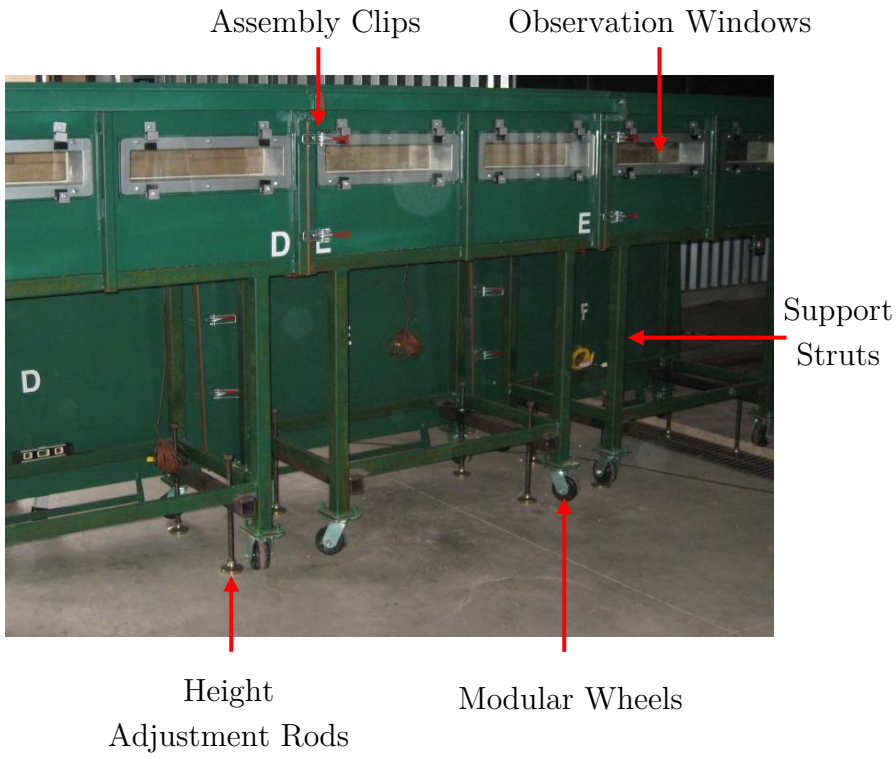

Figure 3.4: Sub-modular assembly of the Steiner tunnel

(6.35 mm) thick high temperature gasket placed between each module to seal the joints against air leaks (Figure 3.5b). Neighbouring modules are then connected using six self-locking, adjustable grip assembly clamps (Figure 3.5a), two on each side of the main assembly frame and four additional clamps for each lid. Additionally, joints at the water channel trough are tightened with four 3/16-in (5 mm) bolts.

(a) Assembly clamps

(b) Tight-seal joints

(c) Height adjustment rods

Figure 3.5: Assembly features of the Steiner tunnel

The front wall of the fully assembled tunnel test section contains 10 viewing windows, with two in each of modules B through F (refer to Figure 3.4) designed for observing flame spread along the tunnel section. Each window is double-paned, with the inside pane flush mounted with the wall and therefore directly exposed to the fire. The exposed window is 21.25-in (540 mm) wide and 4-in (102 mm) high made from silica heat resistant glass. The exterior window is 23-in (58 mm) wide and 7-in (0.18 mm) high, fabricated using non-heat resistant glass. A more detailed view of the window assembly is shown in Appendix A.1, Figure A.16.

The Canadian version of the Steiner tunnel test standard (ULC S102) does not require the use of turbulence bricks (refer to Section 2.3). However, since the UW Steiner tunnel does not contain any recessed windows and the windows are constructed according to the specifications prescribed in ASTM E84, refractory bricks are placed to provide the necessary air flow turbulence. Six refractory firebricks are positioned along the side walls of the chamber. Three firebricks are placed along the window side at 7, 12, and 20 ft (2.1, 3.7, and 6.1 m), and three on the opposite side at 4.5, 9.5, and 16 ft (1.3, 2.9, and 4.9 m), as indicated in the ASTM E84 standard.

Since the floor of the large scale test lab is fairly uneven, each module is further equipped with four height adjustment rods (Figure 3.5c). These are used to lift the casters off the ground in order to compensate for both the uneven surface of the floor, and to provide fine adjustment of the height between the exhaust end of the tunnel and the entrance of the transition duct piece (Section 3.1.3). For more detailed assembly drawings and a step by step assembly procedure for the full Steiner tunnel apparatus, refer to Appendix A, and Appendix Section A.1.

One of the six main modules for the tunnel is the air intake module, shown in Figure 3.6. While the main section of this module is constructed as described above, a 4-ft (1.22 m) long, 17.5-in (440 mm) by 12.75-in (320 mm) rectangular steel air inlet duct is attached to one end. The duct section is fitted with a hinged, manually adjusted inlet air shutter that can be positioned to restrict the size of the inlet to a 3-in (76 mm) high opening across the width of the duct. The air shutter can also be opened fully (Figure 3.6) for cooling and ventilating the tunnel after a test.

Detailed drawings of the individual module assemblies are illustrated in Appendix A.1.

The modules are usually assembled in an order starting from the exhaust end module (Module F) and working back towards the air intake module (Module A). This particular order is more convenient when trying to align the exhaust end of the tunnel with the exhaust duct transition piece which is described in the next section.

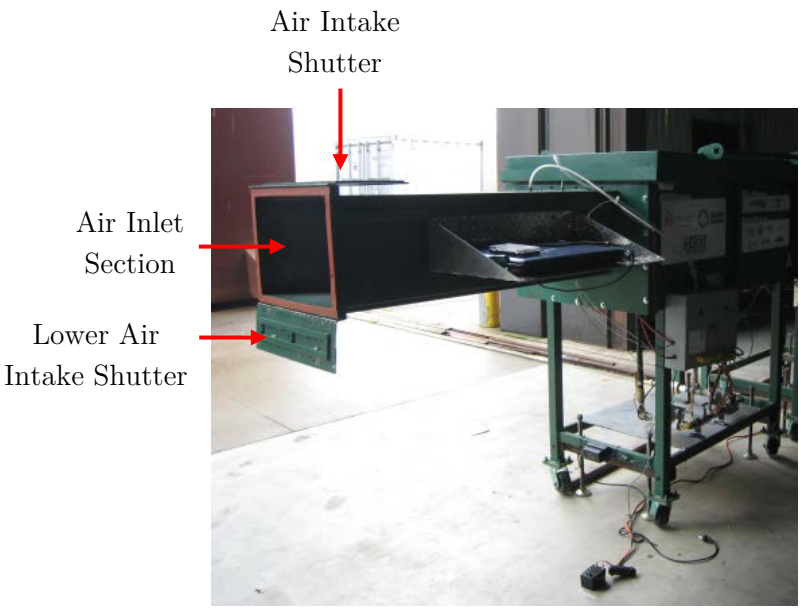

Figure 3.6: Air intake module of the Steiner tunnel (Module A)

3.1.2 Near Damper and Exhaust Duct Transition Piece

The exhaust end of the tunnel is directly integrated into the existing large furniture calorimeter fume hood, duct work and fan system (Figure 3.2). For this, a four section exhaust duct transition assembly is designed, including: a duct, a damper assembly, a 90^o elbow, and the main transition piece (Figure 3.7). All four pieces are made of 16 gauge stainless steel since stainless steel has adequate resistance to heat and corrosive fire exhaust gases, making it a feasible material for the tunnel exhaust.

The duct, damper assembly and 90^o elbow are rectangular, each with cross-sections of 17.5-in (0.44 m) by 12.75-in (0.32 m. They are connected together, as well as to the bottom portion of the main transition piece, via duct flanges that are welded to each section and drilled with 3/8-in (9.5 mm) holes.

During assembly, 1/4-in (6 mm) high temperature ECS-T gaskets (orange in Figure 3.7) manufactured by Chesterton of Burlington, ON are used to seal the exhaust end of the last tunnel module to the exhaust duct entrance, while smooth 1/8-in (3 mm) thick gaskets are used for the connections between the rectangular duct, 90^o elbow and the lower portion of the main transition piece, which often stay assembled in one piece. All sections are then bolted together using 3/8-in (9.5 mm) hex head bolts with additional 1/2-in (13 mm) hex head bolts added to the connection between the exhaust end of the tunnel and the exhaust duct entrance to minimize stress from thermal expansion.

The exhaust duct transition section is configured to connect the outlet of the 90^o elbow

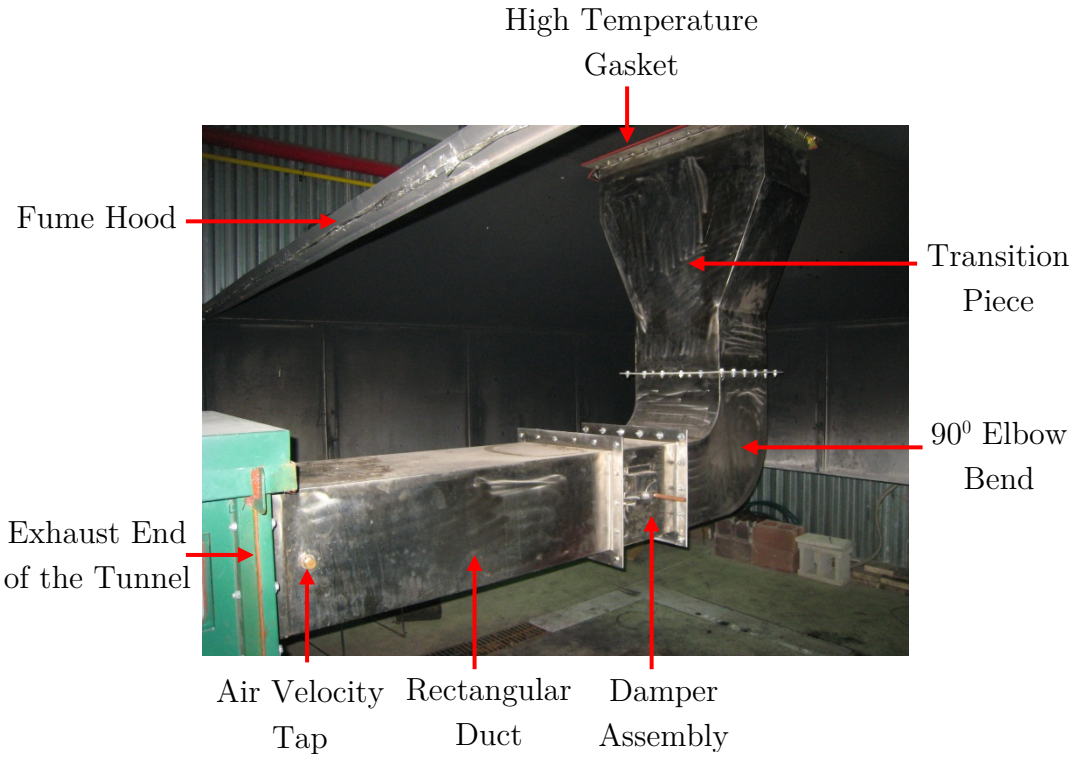

Figure 3.7: Exhaust duct transition piece connecting the exhaust end of the Steiner tunnel to the exhaust fan system below the fume hood.

to the 34.5-in (0.88 m) by 15.0-in (0.38m) opening of the furniture calorimeter fume hood. The top opening of the transition section is welded with thicker flanges (10 gauge), one flange is flat and bolted to the fume hood baffle (Figure 3.8a) with 12 hexagonal bolts (3/8-in), while the other three flanges are slanted 35^o and bolted to the fume hood roof using a total of 18 - 3/8-in hex head bolts (Figure 3.8b). Refer to Figures A.19 - A.24 in the appendix for more details on the exhaust duct transition section.

Downstream of the transition piece, the entrance to the fume hood contains stainless steel baffles that promote mixing of exhaust gases before they enter the main circular exhaust duct.

The damper assembly is installed to adjust the air draft pressure in the tunnel at the transition piece. [1] For detailed drawings of the transition piece damper assembly (Near Damper), and the other transition piece components, refer to Appendix A, FiguresA.19 - A.24.

(a) Flat flange-baffle connection

(b) Slanted flange-fume hood connection

Figure 3.8: Main transition piece bolt connection to the fume hood entrance

The transition piece connects into the 16-in (400 mm) diameter main fume hood exhaust ducting that passes through the wall from the large scale testing lab into the small cone calorimeter lab. Partway into that laboratory an additional damper is installed into the system to facilitate further adjustment and fine tuning of the tunnel exhaust flow rates as required during each test. The fan and additional damper, called the 'far' damper since they are further from the exit of the tunnel than the 'near' damper discussed above, form the subject of the next two sections.

3.1.3 Exhaust Duct, Exhaust Fan and Far Damper System

The ducting from the transition piece is connected into the existing furniture calorimeter variable speed controlled exhaust fan system in the small cone calorimeter lab. A detailed

[1] For the purpose of this thesis, the transition piece damper will hereafter be referred to by its position relative to the tunnel end, 'near damper'.

drawing of this system is contained in Appendix A, Figure A.24, with a brief summary of the main features outlined here. It consists of a 1.0 m length of 16 in (400 mm) diameter stainless steel ductwork from the exit of the fume hood through the wall into the small cone calorimeter lab and an additional 5.0 m length of 16 in diameter stainless steel ductwork to the fan which is mounted on the roof of the testing facility (Figure A.24). Interior to the exhaust ductwork, at 1.0 and 6.0 m downstream from the fume hood exit, are two 0.4 m long steel guide vanes which split the cross-sectional area (flow) into 8 eight equal sections to enhance mixing of the gases in the duct.

The roof-mounted extraction fan system is constructed according to Fire Testing Technology (FTT) guidelines for the large cone calorimeter operation. It can generate flow rates up to 2 m^3/s through the exhaust duct system. A variable frequency drive [Danfoss (Nordberg, Denmark) Model VLT FC 102] on the fan motor permits operation at flow rates to a minimum of 0.7 m^3/s. To further reduce the exhaust flow rates during Steiner tunnel operation, the 'far' Damper system is required in the exhaust duct such that the fan speed and the damper position can be adjusted to regulate the flow and establish the necessary flow rate through the exhaust.

The 'far' Damper system consists of two circular 10 gauge stainless steel perforated plates that are mounted in a custom designed frame such that the damper can be placed in the main exhaust duct through a 1 x 1 ft (0.305 x 0.305 m) square access opening that is located 2.0-ft (0.61 m) downstream of the Smoke Analyzer instrumentation. In addition, the frame is adjustable such that the damper plates can be centered in the exhaust duct, but also so that the damper can be inserted into the duct far enough downstream of the smoke analyzers that it does not create any flow interference at the analyzers. Each of the damper plates contains 41 x 3/4-in (19.1 mm) holes that are aligned symmetrically from the centre of the plate as shown in Figure 3.9.

The entire 'far' Damper assembly consists of two circular perforated steel plates (front plate and a back plate), a nut and a bolt assembly, suspension rods and threaded turnbuckles as shown in Figure 3.10. The front and the back plate are held by a nut and bolt assembly and are loose enough to allow rotation of the plates along their centre axis. The two plates can be rotated above a 1/2-in nut and bolt assembly if more flow area reduction is required. The end of the back plate is threaded to and held by four 1/4-in (6.35 mm) suspension rods that are each 2.5-ft (0.762 m) long. The other end of the suspension rods are threaded to a pair of turnbuckles which are tightly fitted along the edges of the duct, keeping the suspension rods and the plates centered. The suspension rods are used to push the damper assembly downstream to a nominal distance of 4-ft (1.22 m) from the Smoke Analyzer. As such, the damper assembly is nominally centered in the exhaust duct, at a longitudinal distance of 22.5-ft (6.86 m) from the exhaust end of the tunnel (refer back to Figure 3.2).

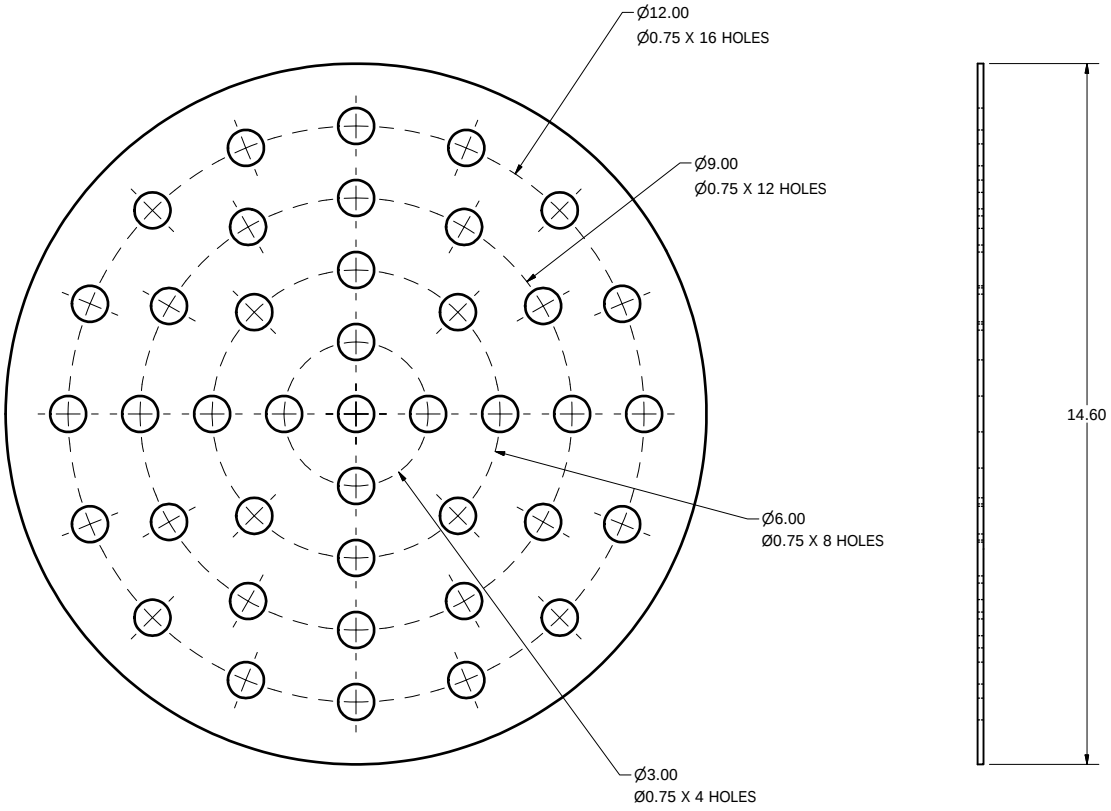

Figure 3.9: Perforated plate used for the far damper assembly

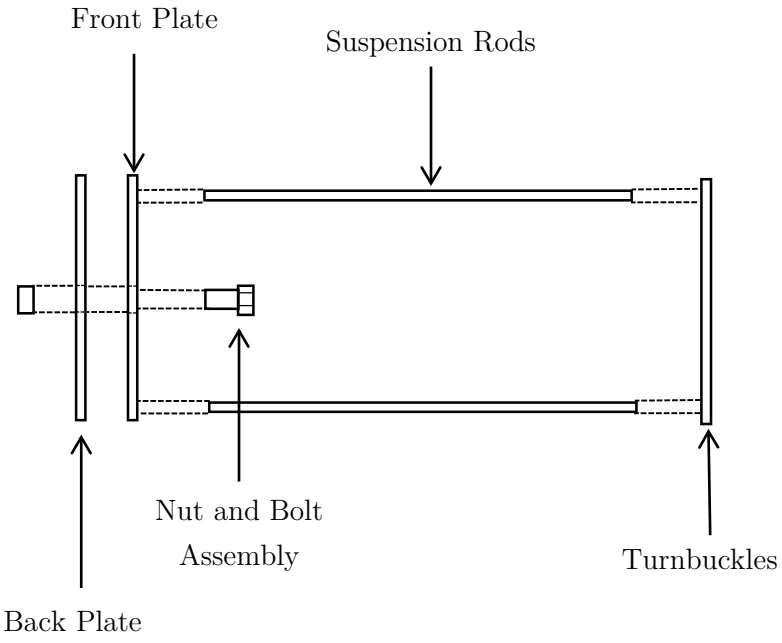

Figure 3.10: Side view of the Far Damper assembly inside the duct.

Based on calculating the pressure loss through a perforated plate, the damper is designed to have a flow area of 19% of the total area of the duct section. This is the flow restriction required to obtain the minimum required air draft pressure in the tunnel at the lowest speed of the lab exhaust fan.

3.1.4 Safety Calculations

In addition to design of exhaust ductwork, fan interface and the far damper system installation, the tunnel is required to satisfy safety calculations for fan extraction rates and explosion relief area. The Steiner tunnel was classified as a Class A appliance during a technical review by Technical Standards and Safety Authority (TSSA). Therefore, it is necessary to ensure that the exhaust fan is capable of extracting all of the fumes from the tunnel chamber. Calculations and discussions related to these requirements are outlined in this section.

The safety ventilation rate is calculated in accordance with sections 11.6.6 of NFPA 86 - 2011 [52], to confirm that the exhaust fan is capable of extracting all the products of combustion contained within the Steiner tunnel. For explosion relief calculations, NFPA 86 mainly contains provisions that serve to prevent explosions in the first place. However, the purpose of explosion venting is to relieve any internally generated combustion pressure

in a safe manner should there be excessive combustion within the tunnel itself.

For the ventilation calculations, the temperature correction factor (K_T) is first calculated using the following equation [52]:

$$K_T = \frac{T_{Ex} + 273}{21 + 273} \tag{3.1}$$

Where T_{Ex} is the exhaust temperature in ^{o}C. Determining the products of combustion value, V_{CT}, is then derived from the following ratio [52]:

$$\frac{V_C}{Q_A} = \frac{5.18\ m^3/min}{293.1\ KW} \tag{3.2}$$

Where V_C is the required flow (uncorrected for temperature), and Q_A is the actual energy input. The full calculation details are outlined in Appendix B, Section B.5. From the calculations, it is determined that the minimum required flow to be generated by the fan is 29.9 m^3/min to extract the combustion products. Based on the exhaust fan specifications outlined in Section 3.1.3, the exhaust fan can exhaust at rates up to 2.0 m^3/s or 120 m^3/min, which is more than enough to extract the gases at the required flow of 29.9 m^3/min.

For the explosion relief requirements, the Steiner tunnel is designed to have two open ends. The inlet section is the air intake area of the tunnel, as described in Section 3.1.1, and the exhaust end of the tunnel is connected to the exhaust fan via the exhaust transition piece (described in Section 3.1.2). In the event of an explosion, the two open ends would act as the safety relief areas, illustrated in Figure B.15.

NFPA 86 - 2011 presents a fairly simple formula for explosion relief in an oven or furnace. The explosion relief is designed as a ratio of relief area to oven volume [52]. Detailed calculations are outlined in Appendix B, Section B.5. The overall relief area to the volume of tunnel ratio is calculated to be 3/44, which satisfies the minimum requirement of 1/15.

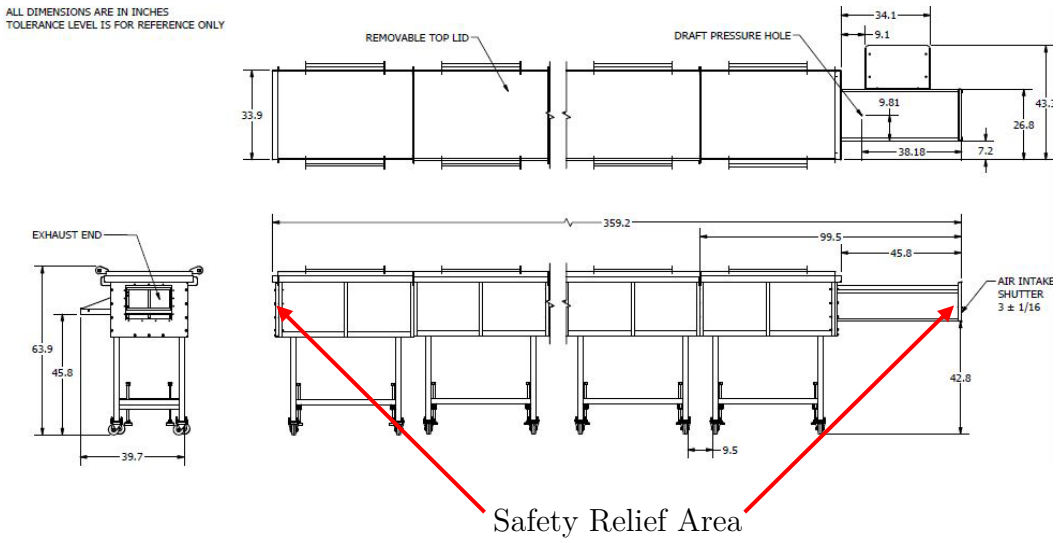

Figure 3.11: Safety relief area for the UW Steiner tunnel

3.2 Safety Controls System

Once the overall Steiner tunnel apparatus is installed and assembled, the next step is to design the controls system for the gas burner. For Ontario, any custom made equipment with components that use fuel or vent combustion products need to obtain field approval for code compliance and safety; TSSA-FA-2012 [53]. However, TSSA-FA-2012 adopts the CSA B149.1-10 Natural Gas and Propane Installation Code and NFPA 86-2011 Standard for Ovens and Furnaces [54]. The TSSA-FA-2012 requirements are generally constructed around heating appliances such as furnace and ovens, and most of those requirements adopt the NFPA 86 standard. In accordance with the TSSA-FA-2012, the tunnel most closely falls under the category of Class A - Oven and Furnace Appliance. Since the Steiner tunnel burner at the UWFRL is supplied with natural gas, the tunnel safety controls system is to be designed according to the NFPA 86-2011 and CSA B149.1-10 requirements.

The control systems of the Steiner tunnel are essentially divided into two segments; the fan safety controls and the gas burner safety system which are both regulated by the S8702D Ignition Control.

3.2.1 S8702D Ignition Control

In the centre of Figure 3.12, is the S8702D ignition control module. The S8702D is the main component within the controls system. The S8702D ignition module enables and disables gas flow to the burners, and it also generates spark ignition and acts as a bypass

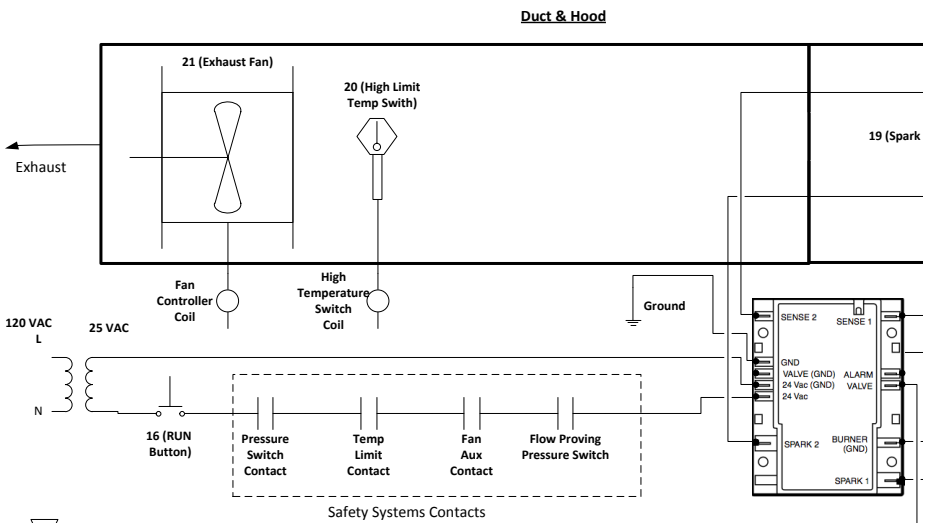

Figure 3.12: Safety system contacts interlocked with S8702D control module

controller that detects flames at the burner nozzles. NFPA 86 recommends that a bypass controller is a flame supervision device that detects flame presence at the burners (to be discussed in the Gas Burner Safety Section 3.2.3). The S8702D ignition control module is powered with a 24 VAC electrical power supply, wired in series with the safety contacts (illustrated in Figure 3.12). The safety system contacts shown in Figure 3.12 have to be satisfied for the S8702D module to enable gas flow to the burners.

From Figure 3.12, the safety contacts interlocked with the S8702D Ignition Control includes both the fan safety controls such as the exhaust fan auxillary contact (Fan Aux Contact), the airflow proving switch, and the high temperature limit control (Temp Limit Contact) which are discussed in the next section, as well as gas burner safety contacts such as the low gas pressure switch (Pressure Switch Contact), and the two quick safety shut-off valves (not shown in Figure 3.12).

3.2.2 Fan Safety and Temperature Limit Control

Both the fan safety and temperature limit controls are incorporated into the safety controls system; the following is a list of TSSA required items/components:

- The tunnel purge period
- Exhaust fan auxillary contact
- Air-flow proving switch

Table 3.1: Total volume of air required for purging

Component Section	Total Volume
Steiner Tunnel	34.8 ft^3
Transition Piece	21.2 ft^3
Fume Hood Baffle	25.7 ft^3
Straight Duct	31.0 ft^3
Roof Exhaust	6.7 ft^3
Motor and Roof Stack	13.0 ft^3
Total Volume	132.4 ft^3

- High temperature limit device
- Bypass controller

As part of the TSSA and NFPA 86 requirement, equipment that employs direct transform spark igniters to light the main burners are required to have a proven purge period prior to the ignition cycle [53]. Thus, the controls system of the Steiner tunnel is required to be provided with a proven purge period that operates in conjunction with the combustion air supply (exhaust fan). The purge is required to provide at least four air changes within the combustion zone of the chamber at an airflow rate of no less than 60% of the maximum fan input [53]. This accounts for cycling four times the total volume of air from burner port, including the exhaust duct transition piece, the tunnel volume and the exhaust duct leading to the outside vent situated on the roof. The total volume of air is summarized in Table 3.1, and the purge time calculated using Equation 3.3, where V is the total volume tabulated in Table 3.1 in ft^3, and Q is the total flow rate of the fan in ft^3/min (cfm). Therefore the total purge time is set at 7.48 seconds.

$$t = \frac{V}{Q} \cdot 4 \tag{3.3}$$

The fan control panel is further hard wired to the safety control system via an electrical relay signal, so that after the fan is powered on, there is usually a 10 second delay before the signal is received at the controls system. In addition, the fan control is operated manually, and therefore tunnel purge is part of the standard operating procedure for a test.

Exhaust fan operation is considered to be an essential component of the tunnel safety control system, so in addition to the exhaust fan electrical interlock as discussed above; an air-flow proving switch is required to prove airflow in the tunnel.

TSSA-FA-2012 [53] indicates that in the event of failure of the flow producing device (exhaust fan), the fuel supply to the burners should be immediately disabled. For this, a static air pressure switch is installed upstream of the burner ports and hard wired into the Steiner tunnel controls system. Additionally, the control panel of the exhaust fan is interlocked with the safety and controls system to prevent start-up of the gas burners when the fan controls are disabled. A Dwyer (ADPS-08020N) static air pressure switch is selected for the air-flow proving switch. It is mounted on top of the control panel box and wired as shown in (Figure 3.17b). The switch is interlocked with the S8702D control module and is set to maintain a minimum static air pressure of 0.05 in-WC (12.5 Pa).[1] The draft hose for the air pressure switch is also installed through a 1/4-in (6.35 mm) tap, 38.2-in (0.97 m) downstream of the air inlet section. Detailed dimensions of the air draft pressure hole at the air inlet section are shown in Appendix A, Figure A.17.

In the event the temperature in the tunnel apparatus exceeds the safe limit during testing, an approved manual reset high temperature limit controller is included in the tunnel controls system [53]. This is intended to prevent any damage to the equipment in the tunnel system during testing. For this an OMEGA - CN3261 high temperature limit controller is used with a J type thermocouple, which is wired directly to the limit controller. The thermocouple is installed inside the exhaust duct where the smoke analyzer is located, 18.5-ft (5.64 m) from the exhaust end of the tunnel, at a position that would indicate if the safe operating temperature limit is exceeded. Based on previous tests conducted on wood cribs [55] in the large cone calorimeter at the UWFRL, it was discovered that damage to the duct and instrumentation could occur at exhaust duct temperatures of 288^0C (550.4^0F) measured approximately at the smoke analyzer. Therefore, the high temperature limit device is interlocked to the controls system with a temperature limit of 250^0C (482^0F) in the exhaust duct. This is deemed appropriate since it limits operating temperatures to levels below those for which damage could be imposed on the duct instrumentation, while not causing disturbances to, or extinction of, the burner flames during testing.

3.2.3 Gas Burner Safety

Natural gas is supplied to the UWFRL facilities gas outlet at residential pressure of 7 in-WC (178 mm-WC). To establish a connection with the burners within the mobile Steiner tunnel, the main line is terminated with a flex hose and quick disconnect coupling at an accessible location adjacent to the Steiner tunnel (Figure 3.2). Both the hose and the coupling are appropriately rated by the Canadian Standards Association (CSA) for use with natural gas. Figure 3.13 shows the gas outlet station and its components.

[1] According to ASTM E84 procedure, the tunnel draft is operated between 0.055 - 0.1 in-WC (12.5 - 25 Pa), hence for the 0.05 in-WC adjustment.

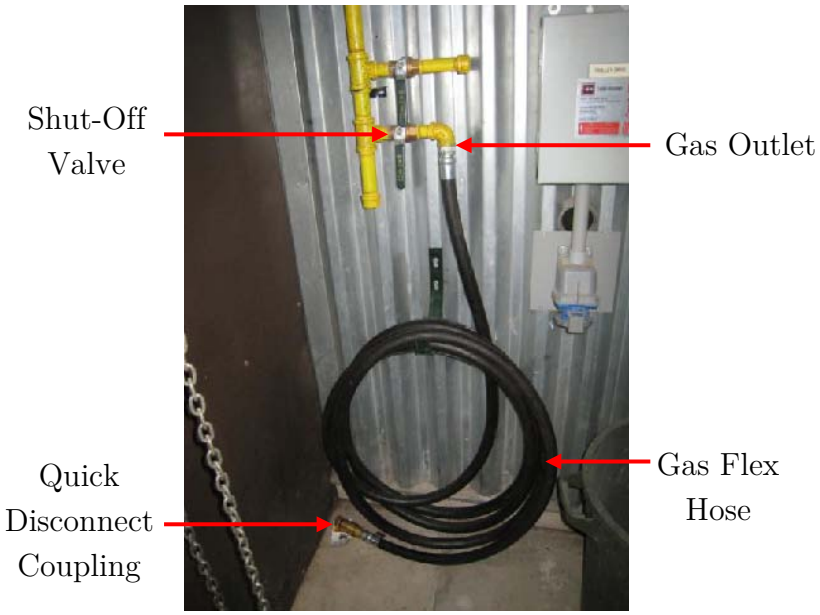

Figure 3.13: Natural gas line flex hose and quick disconnect

The natural gas at the UWFRL is supplied by Union Gas, a mass distributor for Ontario and Manitoba regions [56]. Table 3.2 outlines the typical composition of natural gas delivered from the Union Gas system [56]. However, Union Gas does not guarantee the average composition stated in Table 3.2, and therefore provided a range of mole percentages that may depend upon the region and time of year.

Since there is already an existing gas outlet installed within the UWFRL's large scale testing lab, the next step is to proceed with the design and installation of the gas supply train.

The final approved design from TSSA for the gas supply train is illustrated in

Table 3.2: Chemical composition of natural gas supplied from Union Gas Co.

Composition	Average (mole %)	Range (mole %)
Methane	95.0	87.0 - 97.0
Ethane	3.2	1.5 - 7.0
Nitrogen	1.0	0.2 - 5.5
Carbon Dioxide	0.5	0.1 - 1.0
Propane	0.2	0.1 - 1.5
Specific Gravity	0.58	0.57 - 0.62
Gross Heating Value (MJ/m^3)	38.0	36.0 - 40.2

Figure 3.14. The gas supply train includes 10 components and a gas burner, starting from the existing gas outlet, and ending at the exit of the burner nozzles inside the tunnel. The components consist of those required by TSSA and those included as part of the instrumentation of the tunnel. They are connected with 3/4-in (19.1 mm) NPT pipe, arranged with three 90^0 elbows to reduce the overall length of the system. Once connected, the threads at each joint are sealed with pipe compound.

All components are installed at the bottom of Module A, supported by a 1/4-in (6 mm) thick steel plate that is fastened to the bottom struts (shown in Figure 3.15), as illustrated in Figure 3.15. They are all wired into the main control panel box.

The main components of the gas train are shown in Figure 3.14 and listed below.

- Shut-off valve
- Non-return valve (Check Valve)
- Low gas pressure switch (Pressure Switch)
- Two-quick acting safety shut-off valves (Solenoid Valve 1 and 2)
- Pressure regulator
- Gas burner outlets (Nozzles)

These will be discussed in turn in this section, while the remaining components will be discussed in the Instrumentation section of this Chapter.

Past the gas inlet, a certified manual safety shut-off valve was already installed to safely enable and disable gas flow to the gas train via manual control.

The TSSA required non-return valve (check valve) is included with the quick disconnect attachment on the flex hose. This would act as pressure relief in the event of explosion or any major back pressure within the gas line.

For appliances with an input up to 12 500 000 BTUH (3663 kW), either a high or a low gas pressure switch is required [53]. Since natural gas is supplied at residential pressure of 7 in-WC to the UWFRL, and the gas pressure entering the facility is regulated by the city, gas pressure exceeding safe burner operating pressures is not of concern and a high pressure limit switch is not required. Thus, a Honeywell C6097 low pressure switch is interlocked to the tunnel controls, to detect any sudden drop in gas pressure that might arise due to a non-controlled testing environment. The switch, which is hard wired into the S8702D ignition control (shown previously in Figure 3.12), is deactivated after a 50% drop in pressure, disabling gas flow to the burners.

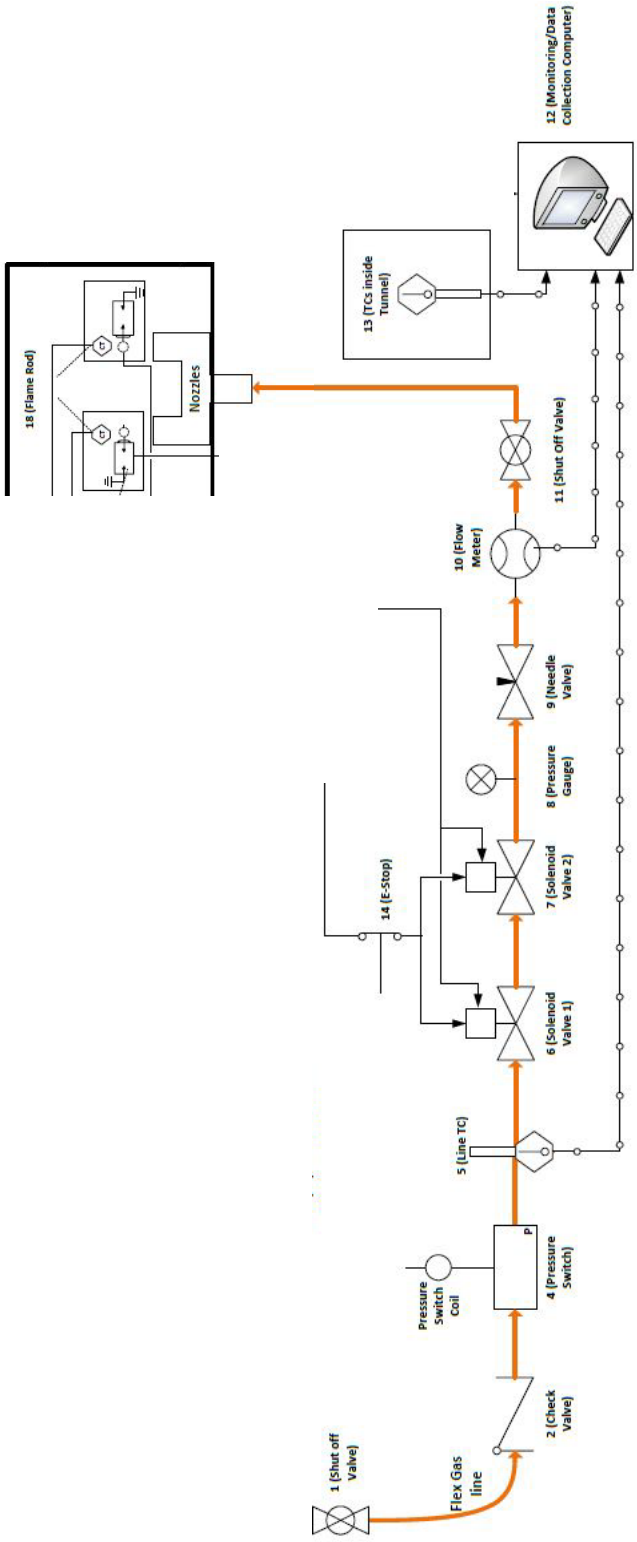

Figure 3.14: Approved design for the gas train

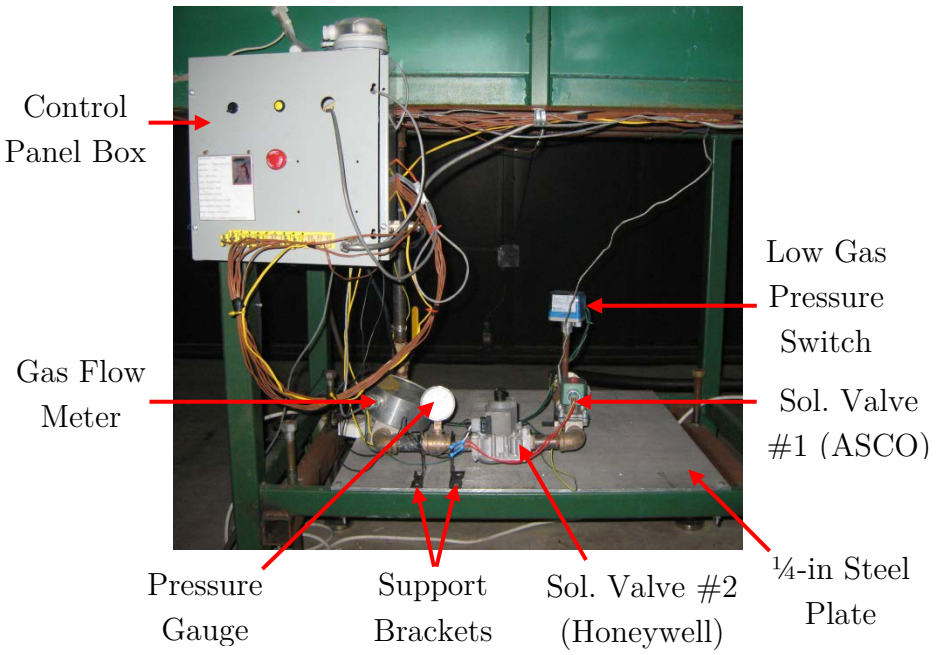

Figure 3.15: Gas train installation for the UW Steiner tunnel

Following the low pressure switch are two solenoid shut-off valves, one model ASCO 8030 and the other Honeywell VR8345M. The intermediate relays used to control these automated safety shut-off valves are wired and installed in series with both controlled by the same ignition control module (S8702D). Therefore, both contacts must be triggered in order to enable gas flow to the burners. In case one of the shut-off valves mechanically fails in the open position, the other shut-off valve will still disable gas flow to the burners. Proof of closure switches are not needed for the tunnel under TSSA regulations since the burners operate at only 5000 BTUH (88 kW), well below the 12 500 000 BTUH (3663 kW) for which such a safety system is needed.

In addition to automated shut off values, pressure regulators or pressure controllers are required in the gas supply train to regulate the fuel supply to the burner ports shown in Figure 3.14 schematic. Excessive fuel supplied to the burner may elicit safety concerns within the furnace such as explosions or excessive flame lengths that would potentially damage the instrumentation in the duct. On the other hand, insufficient fuel supply may cause complications with tunnel operation, such as burner ports not igniting or lack of sufficient flame length with which to properly calibrate the tunnel. Therefore a pressure regulator or a pressure controller is utilized to control the pressure to the burner to within $\pm$ 10% of its set point [53]. For this purpose, the second solenoid shut-off valve contains a pressure regulator which can be adjusted to operate in the range between 3 - 5 in-WC (0.75 - 1.25 KPa).This regulates the gas pressure to the burner ports such that a flame

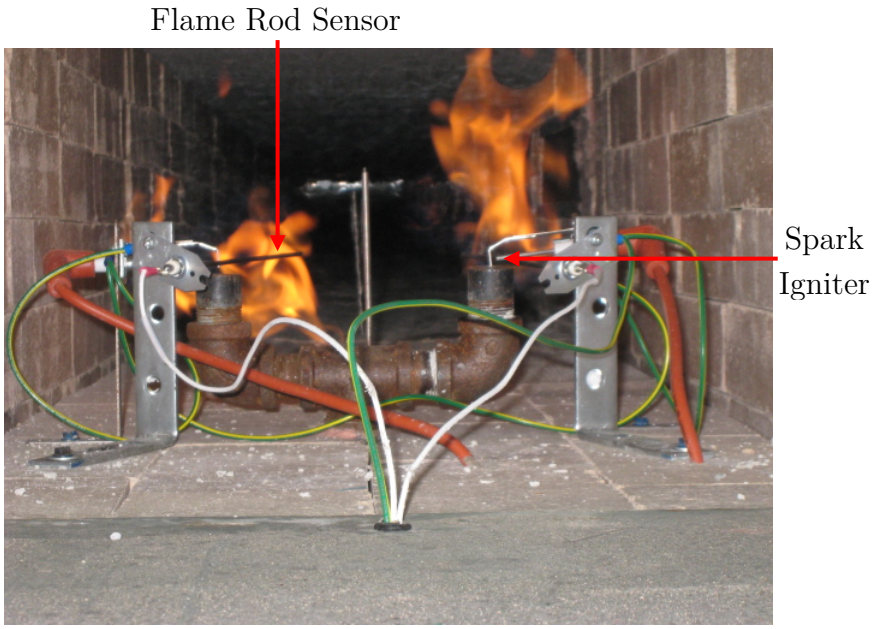

Figure 3.16: Burner nozzle equipped with spark igniters and flame rod sensors

energy output of 5000 BTU/min (88 kW) is obtained.

The dual burner outlet ports are constructed using a 3/4-in (19 mm) size -steel pipe, T-junction fitted with two elbows, each terminated with a pipe fitting. The burner is located 1-ft from the inlet end of the tunnel. Flame rod sensors (Honeywell Model Q354) and spark igniters (Model Q347) are mounted directly at the tip of the burner nozzles (shown in Figure 3.16) such that the burner flames impinged directly on the flame rod sensors. Separate taps underneath the tunnel section are provided for the Q347 spark igniter cables (orange in Figure 3.16), and flame rod sensor (Q354) wires (white in Figure 3.16) are fed through the bottom of the air inlet section tap. Both systems are wired directly to the S8702D ignition package inside the control panel box (shown in Appendix B, Figure B.10) with the internal control logic diagram as shown in Appendix B, Figure B.6.[1]

The ignition control package (S8702D), in conjunction with flame detectors and a temperature sensor, are utilized to detect flames at the burner ports and respond via collaboration with the two quick acting safety gas shut-off valves. For example the S8702D module is preset for the spark igniters to generate electrical sparks for a maximum of 5 seconds. If no flames are detected within those 5 seconds, the S8702D module enters lockout mode and the fuel supply to the burners is disabled by the solenoid safety shut-off valves. The operator is then required to start-reset the system before tunnel operation

[1]The Q354 flame rod sensors and Q347 spark igniters are included with the S8702D ignition control package.

can continue. Under a different scenario, a bypass controller integrated within S8702D is equipped with a temperature sensor carefully placed to monitor whether there are continuous flames issuing from the burners. In this case, if temperatures of less than 760^oC (1400^oF) are detected at the burner outlet, it is assumed the burner flame has extinguished and the shut-off valves stops the gas flow and thereby disables operation of the burners. In combination, the elements of the control system provide various levels of safety during both start-up and on-going operation of the Steiner tunnel.

3.2.4 Gas Flow Calculations

After design of the gas supply train, calculations are necessary to determine whether there is enough gas flow to generate the required energy at the burners (88 kW). For these, the components that might restrict the gas flow are identified. These include the non-return valve (check valve), the metering valve (needle valve), the solenoid shut-off valves and the gas flow meter.

The ASTM E84 standard suggests that the gas supply should initially be adjusted such that a value of 37.3 MJ/m^3 (1000 BTU/ft^3) energy is available from the burners [1]. This suggests a supply requirement of 5.3 MJ/min (5000 BTU/min). Since the Armor-Flo 3600 gas flow meter measures volume flow of gas in m^3/hr, to achieve the two values provided in the ASTM E84 standard, it is necessary to determine the necessary volume flow rate of gas using Equation 3.4. The calculated flow rate to the burners is 8.53 m^3/hr (301.2 ft^3/hr), via application of the Bernoulli principle from the gas train to the burner ports. Detailed calculations and descriptions are shown in Appendix B, Section B.1, while the summary of results are outlined in this section.

$$Gas\ Flow\ Rate\ \left(\frac{m^3}{hr}\right) = \frac{Gas\ Supply\ Rate\ \left(\frac{MJ}{hr}\right)}{Heating\ Value\ \left(\frac{MJ}{m^3}\right)} \tag{3.4}$$

The pressure at the burner nozzles induced by the air draft in the tunnel is determined first by assuming atmospheric pressure at the air inlet section of the tunnel (Point 1 in Figure B.13) and 1.2 m/s for the air velocity at the burner nozzles (Point 3 in Figure B.13). The pressure at the burner nozzles (Point 3) is then calculated to be 101 317 Pa. This pressure is used in the Bernoulli equations used in the gas flow calculations.

The gas flow at the burner nozzle is initially calculated to be 3.78 m^3/hr, a value much too low to supply the required energy to the burner. It is then determined that some of the gas train components result in very large flow losses and therefore have to be removed

to obtain a gas flow closer to the required range of 8.53 m^3/hr. Both the adjustable needle valve used for additional adjustments of gas flow to the burners and the non-return valve are removed since the same functionality is obtained using the gas shut off valve, which is used to regulate the gas flow to the burners, and the quick disconnect hose coupling, which already contains a certified non-return valve mechanism. After removing those two components from the gas train, the calculated gas flow is improved to 7.66 m^3/hr which is significantly closer to the required flowrate of 8.53 m^3/hr. It is deemed as an appropriate flowrate with which to start the operation of the gas burner.

As previously noted, however, the energy content of gas supplied to the Steiner tunnel facilities will change from time to time. Since the burners operate solely on the street supply of natural gas, it should be understood that the heating value of gas may be influenced by cold winter conditions, as indicated previously in Section 2.5.3. Groah [45] confirmed that the energy content of the gas tends to change with seasons as the mixture is diluted with added propane. This is consistent with the range of propane compositions indicated in Table 3.2 [56], where the limits on propane concentration range from 0.1% and 1.5%, with the average mole percentage for propane in the supply gas expected to be on the low end of the stated range at 0.2 %.

With both the fan safety and gas burner components described in the sections above, the next section discusses the electrical hardware installed in the control panel box pertaining to these components.

3.2.5 Electrical Hardware

Most of the wiring for the control systems for both the fan safety and the gas burner safety components is contained. The S8702D ignition control module, high temperature limit controller, exhaust fan relay contact, and the E-Stop are housed inside a control panel box to protect them from water damage. The box is supplied with 24 VAC and is situated underneath the air intake module. Also in the box is the run-switch that is wired in series with the rest of the safety system contacts (Figure 3.12) as shown in Figure 3.17b. In addition there are two draft pressure hoses coming from the air inlet section; one leading to the air flow proving switch (TSSA required component) and one leading to the pressure transducer that monitors air draft pressure (to be discussed in Instrumentation Section 3.3).

The two gas shut-off solenoid valves are interlocked with 6 emergency push buttons (E-Stops). In Modules B to F, the E-Stops are right below the windows (Figure 3.17a), and the final E-Stop is located on the main control panel box (Figure 3.17b). This provides easy access for the tunnel operator to reach an E-Stop at any stage of a tunnel test. The E-stops are supplied with 24 VAC power to interlock them with the control system (shown

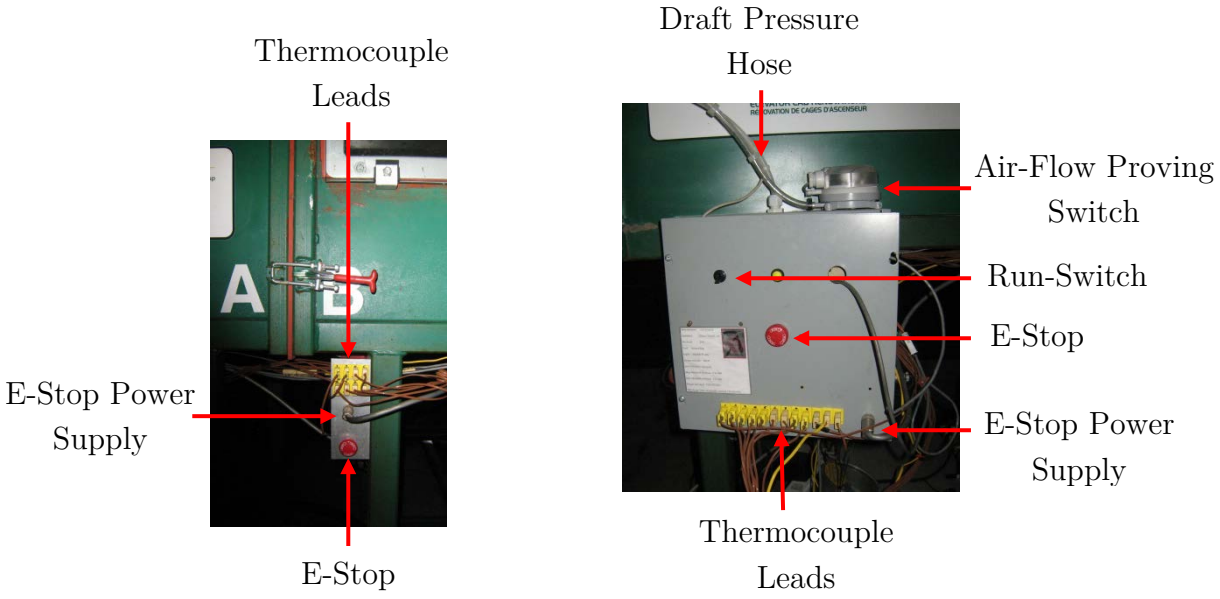

(a) Modular E-Stops

(b) Control panel box

Figure 3.17: E-Stop locations and control panel box wiring

in Figure 3.17a). Appendix B, Figures B.3-B.5 include electrical diagrams showing this wiring, as well as the wiring for the control panel box hardware including relay contacts for fan, air flow proving switch, and high temperature limit control.

Now that the Steiner tunnel safety controls system has been described, the overall logic and function of the system is described in more detail in the next section.

3.2.6 Overall Logic Diagram of the Controls System

The overall logic and function of the system is presented in the flow chart in Figure 3.18.

The logic of the control system is largely dictated by the requirements of the safety system outlined in Figure 3.12. The proper status of all four safety components (fan relay, air flow, low gas pressure switch, high temperature limit controller) have to be satisfied before enabling gas flow to the burners. Further, the status of the fan relay and the air flow proving switch have to be satisfied prior to the start of a Steiner tunnel test. Sudden decrease in gas pressure, or rise in temperature of the exhaust above the set limit of 250^0C (482^0F), are expected to occur during a test, so these two conditions are placed into the control logic after the S8702D ignition control in the flow chart. The S8702D ignition control logic is identified with a blue star in Figure 3.18, because that unit contains its own internal logic as shown in Appendix B, Figure B.6. The S8702D internal logic determines

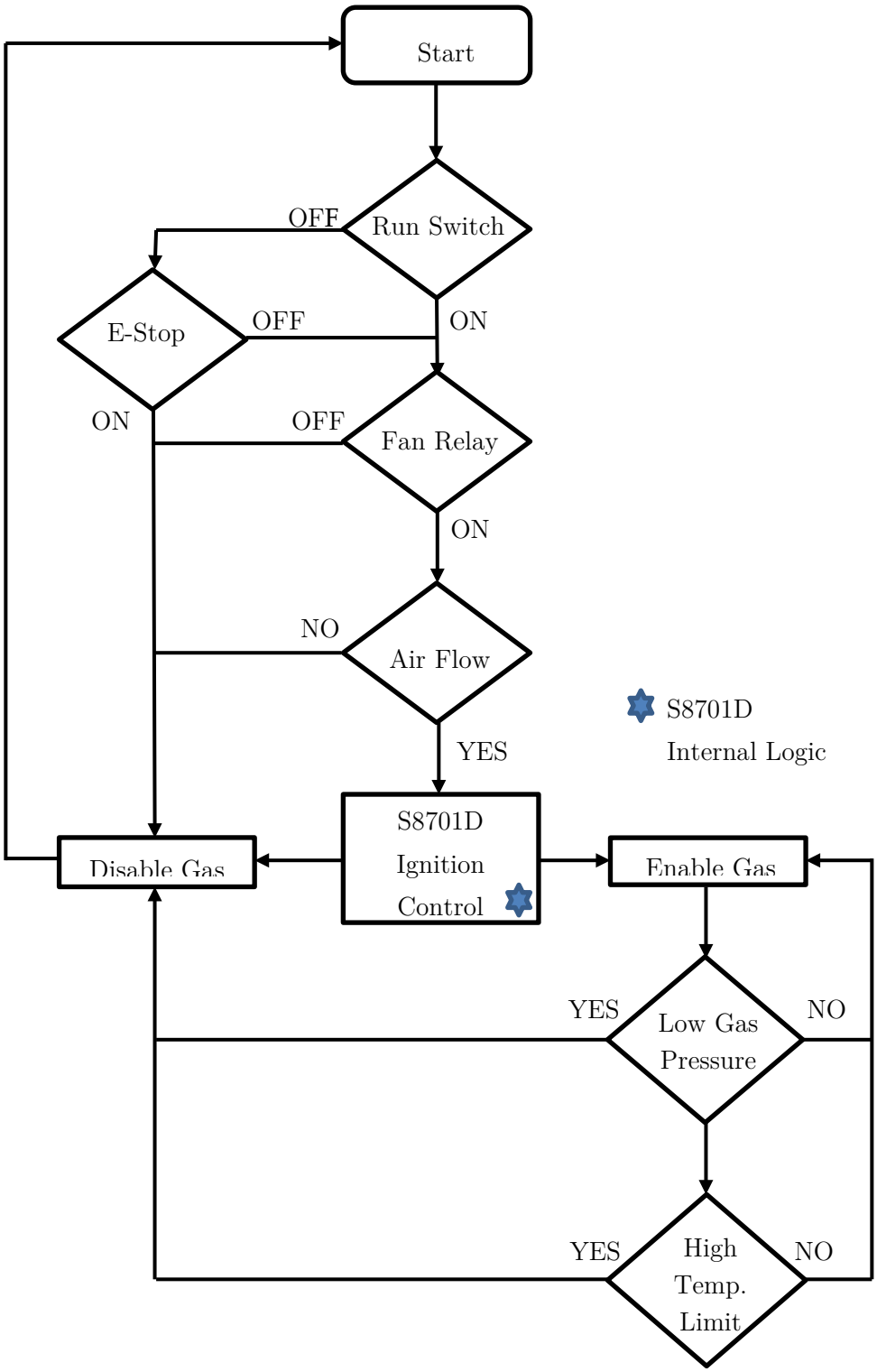

Figure 3.18: Control Systems logic diagram for the Steiner tunnel

whether there is a flame at the burner nozzles. If not, gas flow to the burners is enabled for a maximum of 5 seconds, and the Q347 igniters are enabled. If the flame rod sensors do not detect presence of a flame (ignition) within the 5 seconds, the S8702D ignition module will lockout and automatically disable the gas flow, causing the ignition cycle to stop until it is reset by an operator. Similarly, if the tunnel run switch is off when the ignition cycle is attempted, or if any of the E-Stops are pushed at any time during operation, the S8702D controller will override all other components and disable gas flow to the tunnel.

As a final note, it should be mentioned that the final control system design described above was developed in an iterative fashion in conjunction with the TSSA engineering staff. For completeness of record, the initial design proposals for the control system, electrical diagrams, S8702D flow chart, and gas train figures are all included in Appendix B. Once the final control system was approved through technical review by the TSSA committee, on-site verification and testing of the system was arranged and the approval tag was obtained (Figure B.11).

With the overall tunnel apparatus and controls system laid out, the next section describes additional instrumentation that is installed in the Steiner tunnel apparatus for monitoring tunnel condition and collecting data during calibration and testing.

3.3 Instrumentation

Instrumentation in the Steiner tunnel includes a series of Type K thermocouples for temperature measurement in the test sections and exhaust, 1/4-in (6.35 mm) pressure taps to monitor draft pressure and flow through the system and a smoke analysis system. A gas flow meter, pressure gauge and gas thermocouple are included to monitor the gas supply to the tunnel during testing as well.

Data acquisition is conducted using an NI-USB 9162, hi-speed USB carrier, distributed system manufactured by National Instruments of Austin, Texas.[1] This system is linked through a USB cable to a laptop computer running LabVIEW software. A custom program is written for control and monitoring of the tunnel operation, as well as to acquire data from the instrumentation described in this Section. A screen shot of the LabVIEW interface from this program is shown in Figure 3.19. The program is configured to sample all data from the instrumentation system at a rate of approximately 1.0 Hz, with the acquisition mode set to 1 sample on demand, running continuously.

To facilitate connection of the sensor leads to the DAQ and subsequently to the computer system, a 1/8-in (3 mm) thick holding plate is mounted on the right hand

[1]From here on, will be referred to as the DAQ module.

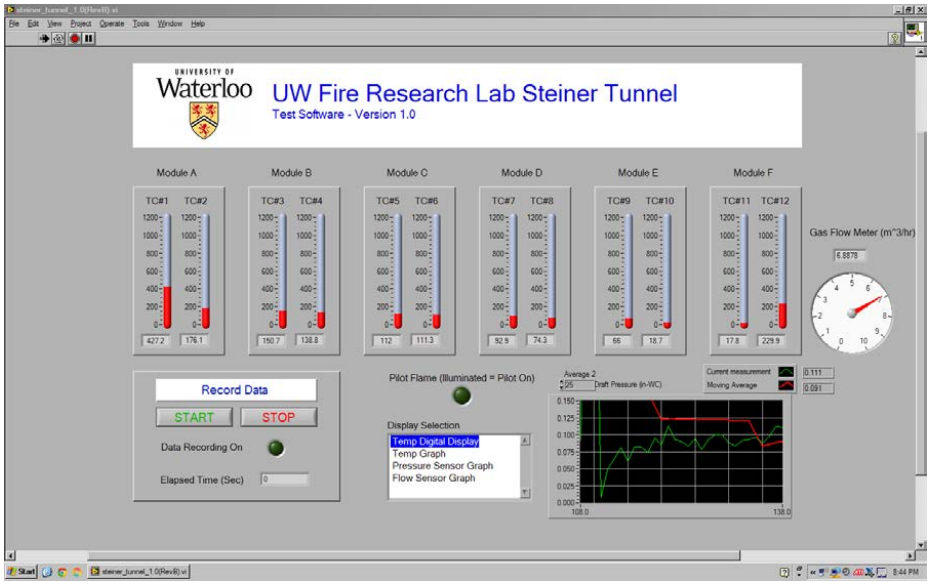

Figure 3.19: Screen shot of the LabView program

side of the inlet section of the tunnel. Also on the right hand side is a steel 12-in (0.30 m) by 12-in (0.30 m) by 4-in (0.10 m) control panel box which contains all the electrical hardware, as illustrated in Figure 3.20. The connections for the 13 thermocouples and the gas flow meter are wired to the DAQ module inside this control panel box, with the main terminal for the thermocouple leads installed at the bottom of the box (Figure 3.17b). Each module is equipped with its own thermocouple terminal (Figure 3.17a) as well and the wires leading from the thermocouples and gas train components are run underneath the tunnel and along the support struts in order to minimize the exposure of the cables to heat.

An overview of the layout of instrumentation is shown in Figures 3.20 and 3.21.[1] The coordinate system used for describing the location of all the instrumentation is defined with its origin located at the floor of the tunnel test section on the centre plane of the burner ports. As depicted in Figures 3.20 and 3.21, the positive x direction is in the same direction as air-flow, and positive y direction is vertically upward from the tunnel floor.

A full list of the instrumentation installed in the Steiner tunnel and monitored by the DAQ module is presented in Table 3.3. Each component is discussed in more detail in the subsequent paragraphs.

[1]For the purpose of visual comparison between top and side view, the smoke analyzer is not shown in the top view since it is located at a substantially further distance from the end of the tunnel, in the small cone calorimeter lab.

Table 3.3: List of UW Steiner tunnel instruments and their locations in reference to the burner

Instrument	x (ft)	y (ft)
DPT	-4.08	11.0
Gas Meter	0	-2.5
Gas TC	1.08	-2.5
TC # 1	1.00	0.52
TC # 2	4.17	0.52
TC # 3	6.33	0.52
TC # 4	8.50	0.52
TC # 5	10.58	0.52
TC # 6	12.75	0.52
TC # 7	14.92	0.52
TC # 8	18.08	0.52
TC # 9	22.42	0.52
TC # 10	13.00	0.01
TC # 11	23.25	0.01
TC # 12	23.00	0.92
Smoke Analyzer	42.5	7.0

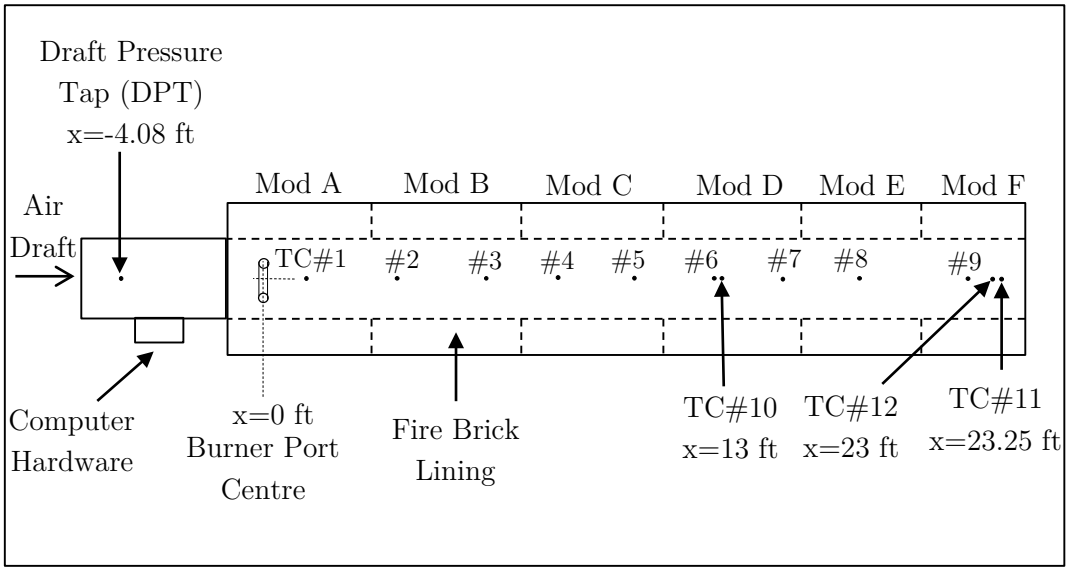

Figure 3.20: Sketch of instrument layout, top view (distances from burner shown)

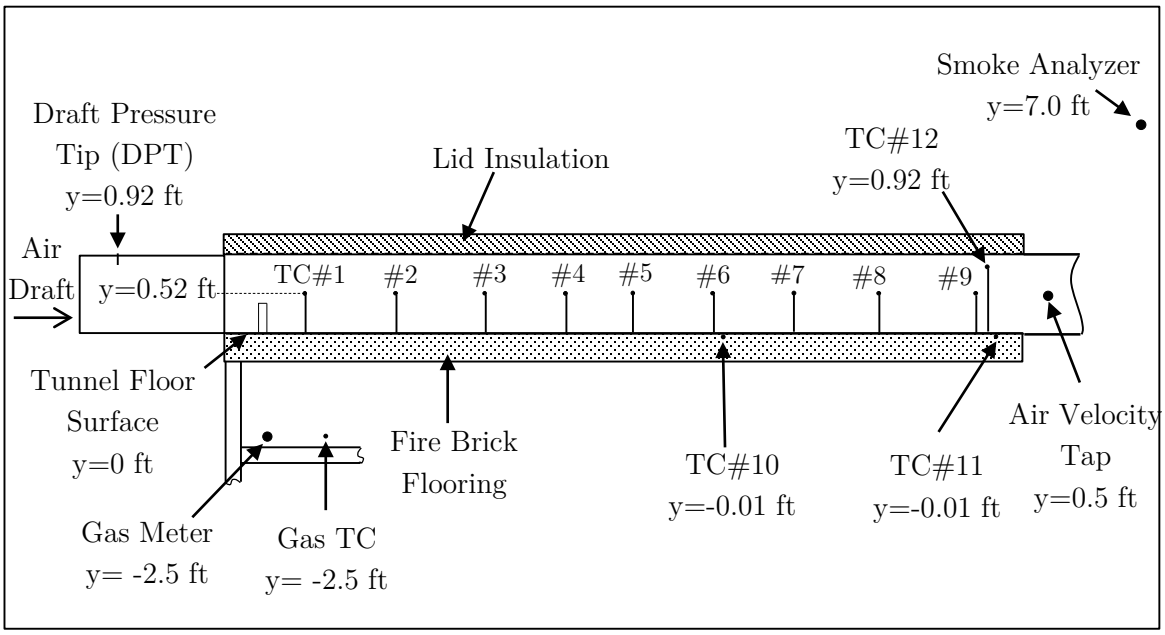

Figure 3.21: Sketch of instrument layout, side view (distances from tunnel floor shown)

The Draft Pressure Tap (DPT) used for measuring draft pressure at the air-inlet section is located at a distance of x = -4.08 ft (1.24 m) upstream of the burner port (Figure 3.20). A 1/4-in (6.35 mm) diameter plastic tube is inserted through the top of the tunnel at the mid-width, 1-in (25.4 mm) below the ceiling, and 15-in (381 mm) downstream of the air-inlet shutter. The other end of the tube is connected to an OMEGA PX655 low pressure transmitter which is located inside the control panel box. This produces a 4-20 mA output signal that is sent directly to the DAQ module. Due to the unsteady nature of the draft pressure reading, a moving average is applied to the data in the LabVIEW program. In Figure 3.19, the time resolved draft pressure is plotted in green, and the moving average is plotted simultaneously as the red line. The number of data points used in calculating the moving average is adjustable from test to test depending on the stability of the draft readings.

The Armor-flo 3600 gas flow meter is positioned underneath the burner ports as the second last component in the gas train. It measures the volume flow of gas to the burners in m^3/hr and outputs an electrical signal in the range of 4 - 20 mA which is sent to the DAQ module. The internal electrical components of the meter are encased in a cylindrical housing to protect them from moisture (Figure B.12, in Appendix B). In the LabVIEW program, the gas volume flow is indicated with a red needle valve on the right hand side of Figure 3.19. In addition, a gas thermocouple (Gas TC) is included in the gas train to

[1]For practicality purposes, it is deemed as the most appropriate location

measure the local gas temperature.[1] It is positioned (perpendicular to gas flow) between the gas inlet and the first solenoid valve. The thermocouple sensor locations throughout the tunnel are sketched in Figure 3.20 and 3.21, and their coordinates are listed in Table 3.3. The total number of thermocouples inside the tunnel is 12, distributed over the 6 tunnel modules. Type K (chromel-alumel), Inconel-sheathed, 1/8-in (3 mm) thermocouple probes are installed at each modular section to monitor temperature profiles along the mid-height of the tunnel. As illustrated in Figure 3.21, these thermocouples are aligned along the centre of the tunnel width, located at distances of 1-ft (0.305 m), 4.17-ft (1.27 m), 6.33-ft (1.93 m), 8.50-ft (2.59 m), 10.58-ft (3.23 m), 12.75-ft(3.89 m), 14.92-ft (4.55 m), 18.08-ft (5.51 m), and 22.42-ft (6.83 m) downstream from the burner port centre. They are mounted through the bottom bricking with the tip of the probe situated 0.52-ft (0.159 m) from the floor surface. In addition, the temperatures inside the brick floor (TC # 10 and TC # 11) are measured using 18 gauge (1.02 mm diameter), Type K thermocouples, insulated with Nextel ceramic fibre and covered with protective Inconel braiding. These thermocouples are formed with exposed junctions and mounted through the bottom bricking layer of the tunnel at 13-ft (3.96 m), and 23.25-ft (7.09 m) from the burner port centre. They are embedded 0.01-ft (3.2 mm) below the floor surface of the testing chamber and covered with refractory cement as specified in ASTM E84 standard [1]. The exposed thermocouple (TC # 12) located at 23-ft (7.0 m) downstream of the burner centerline, is also installed according to standard (1-in (25.4 mm) below the test sample). In the LabVIEW program, the thermocouple values for each module are represented with a red bar graph (Figure 3.19.

The last instrument required for operation of the Steiner tunnel is the smoke analyzer, which is physically situated in the small cone calorimeter lab. The smoke analyzer laser beam is located x = 42.5 ft (12.9 m) downstream of the burner, and approximately 18.5-ft (5.64 m) from the exhaust end of the tunnel. Smoke measurements are made using the FTT smoke analyzer that is supplied with the UWFRL furniture calorimeter and shown in Figure 3.22.

The smoke analyzer consists of a 1.0 mW helium-neon laser, detector, alignment cradle and power supply. The 1.0 mW helium-neon laser (Melles Griot Model: 05-LHR-494) produces a 632 nm wavelength beam of light, 2-ft (0.61 m) long, 0.054-in (1.36 mm) diameter. This beam is transmitted through a clear lens across the diameter of the duct and intercepted by a laser detector on the left. The alignment cradle is mounted onto the tunnel exhaust duct with the laser beam aligned in the horizontal direction. The power supply for the laser and detector are attached to the bottom of the alignment cradle, as illustrated in Figure 3.22.

Before each test, the laser transmission characteristics for the smoke analysis system are calibrated using the LSHRCalc software provided by FTT. Transmission data is not directly saved to the data files, but instead the direct outputs from the photometric circuit,

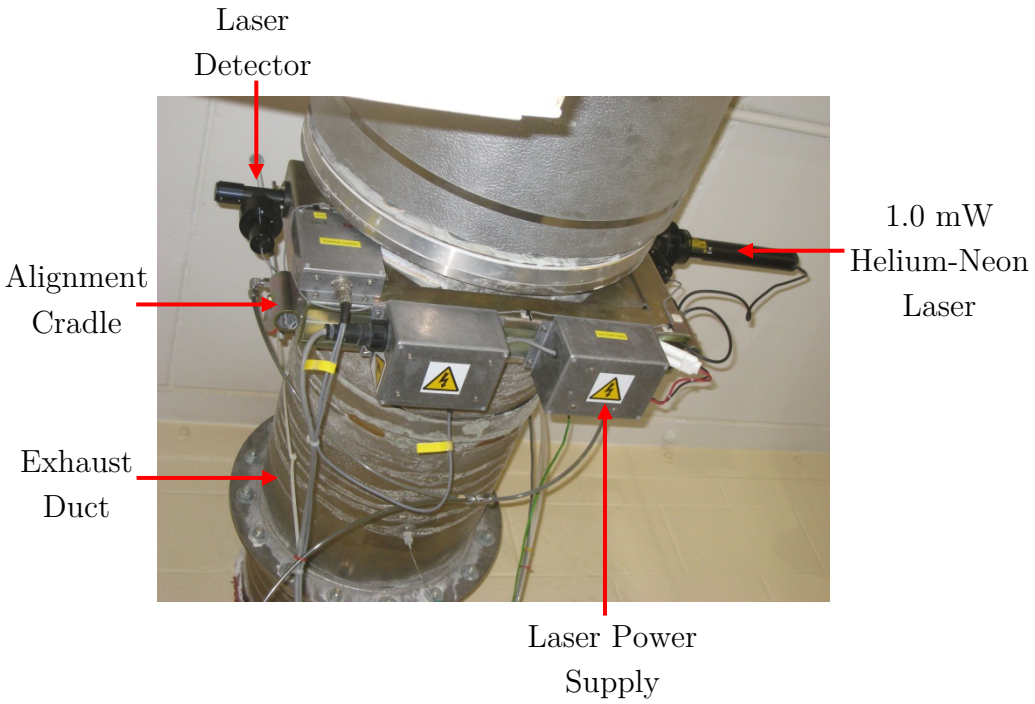

Figure 3.22: Smoke analyzer used for the furniture calorimeter at the UW Fire Lab

PDM and PDC, are combined to calculate the transmission, E_t, using Equation 3.5:

$$E_t = (PDM - PDC) + 1 \tag{3.5}$$

where PDM is the main photodiode and PDC is the compensating photodiode of the system. E_t, is then used to calculate the smoke obscuration, $SO\%$, as discussed in Chapter 2.

3.3.1 Ancillary Instrumentation Systems

An additional set of ancillary instrumentation systems are used to monitor the tunnel air velocity, as well as the environmental conditions within the UWFRL large scale lab during each test.

Measurement of air velocity at the end of the tunnel ensure that the proper air flow through the tunnel is established prior to testing. A heated wire anemometer, VelociCheck (Model 8330), manufactured by TSI of Shoreview, Minnesota is inserted through the air velocity tap and used to measure the air velocity across the width of the tunnel. The tap is a 1/2-in opening drilled at mid height of the exhaust transition piece (refer back to

Figure 3.7) and situated 25 ft (7.62 m) downstream of the burners. The hole is capped off when the probe is not being used.

The outside wind velocity near the roof stack, as well as the ambient temperature and relative humidity within the large scale testing lab is monitored using LA Crosse Technology sensors since Steiner tunnel test results have been shown to be dependent on ambient conditions in the test area [43]. The outside wind velocity can be measured during select tests using a hand held anemometer to determine its effect on tunnel results. The interior sensors are located in an open area on the right hand side of the tunnel, at a distance of approximately 16-ft (4.88 m) from the air-intake module and 3.5 ft (1.07 m) above the ground. This location is selected to minimize disruption to the measurements by the outside air draft coming from the open exit door which is left open during the entire duration of the test to allow new air circulation and to maintain the atmospheric pressure inside the lab.

3.4 Comparison to ASTM E84

The Steiner tunnel apparatus utilized in this study follows most of the specifications laid out in the ASTM E84 standard; however, there are several differences in the design and instrumentation which will be discussed in this section. It was not known a priori if these effects would influence the test results so they are noted here and their effects will be further discussed using the calibration results that are outlined in Chapter 4. The following list identifies all of the variations in design between the standard ASTM E84 Steiner tunnel and the UW Steiner tunnel. They are ordered according to each of the main elements of the tunnel system and discussed in further detail below.

- Observation windows
  - Interior window panes
  - Exterior window panes
- Lid assembly
  - Fiber-cement board thickness
- Exhaust duct design
- Gas volume measurement
- Photometer system

  - Light source
  - Light beam direction
  - Distance between the light source and photocell lens
- Air velocity measurements

ASTM E84 specifies dimensional constraints on the glass in the tunnel windows in order to keep the heat loss through the windows consistent for every tunnel [25]. In the case of the UW Steiner tunnel, the observations windows are modified to be compatible with the modular nature of the tunnel. Each window is larger than the one specified in the standard to allow close video monitoring of the flame spread. The inside window pane that is flush mounted with the tunnel wall is significantly wider at 20-in (508 mm), compared to the specified requirement of 11 in (279 mm). However, the UW tunnel only contains 10 windows, whereas an ASTM E84 tunnel has a total of 16 windows. In addition, the ASTM E84 tunnel also has an additional window to view the burner ports, while, the air intake module of the UW Steiner tunnel does not contain any windows (refer back to Figures 2.1 and 3.6). The last window beside the exhaust end of the UW tunnel is slightly shorter than the rest of the windows (17.5-in (444 mm) wide). The inside panes of the UW Steiner tunnel windows are also slightly taller (4-in (101 mm) high) than the ones specified in the standard.[1] Since the exposed glass surface of the UW tunnel is larger than required, but with less number of windows, the surface area of the glass can be compared. Based on the given dimensions for the inside pane of the present Steiner tunnel and the total number of windows (10 windows of 20 x 4 in, and 17.5 x 4 in), the total surface area of the exposed glass is 790 in^2 (0.510 m^2). For the ASTM E84 tunnel (17 windows of 11 x 2.75 in), the total surface area of the exposed glass is 514.25 in^2 (0.332 m^2). Therefore the total surface area of exposed glass inside the UW Steiner tunnel is 35 % larger than that in the standard design.

A cross-sectional view of the window assembly in the current tunnel is shown in Appendix A, Figure A.15. The exterior panes of the windows also vary from the design prescribed in the standard. 3/8-in (9.5 mm) thick laminated float glass comprised of 2 glass sheets is used for the exterior pane in the present Steiner tunnel while the ASTM E84 standard tunnel windows are Borosilicate glass with a 1/4-in (6.35 mm) thickness for the exterior pane due to their great resistance to thermal shock. Unlike those in a standard tunnel, the present exterior pane of the window is not pressure tight and it does not provide a seal to the outer layer of the tunnel. Instead, the panes are clamped to the outside frame of the window as illustrated in Figure 3.23a leaving a 1/4-in (6.35 mm) gap between the

[1] ASTM E84 requires the height of the exposed inside glass to be 2.75-in (± 0.375 *in*) (70 mm ± 9.5 mm).

glass and the frame, which allows free flow of air between the panes. The interior panes, however, are installed according to standard; mounted flush with the wall (Figure 3.23b). This protects the outer window from direct heat exposure. Nonetheless, certain issues are encountered with the exterior window panes, as will be discussed in Section 4.2.

(a) Exterior window pane

(b) Interior window pane

Figure 3.23: UW Steiner tunnel observation window

The lid assembly of the UW Steiner tunnel follows most of the specifications outlined in ASTM E84 except for the design of the water channel which limits the maximum thickness of the test specimen to 2.5-in (63.5 mm) as discussed in Section 3.1.1. The testing apparatus in the ASTM E84 standard allows maximum thickness of the test specimen to be 4-in (101 mm)[1]. To provide more insulation for the lid cover in the present tunnel, the fiber cement board used as protection for the furnace lid is also 1/4-in (6.35 mm) thicker than what is advised in the standard.

The exhaust duct design of the UW Steiner tunnel is outlined in Section 3.1.1, and it varies significantly from the one suggested in ASTM E84. A typical duct in the ASTM E84 tunnel contains two 90^o elbows situated in a horizontal plane. These reverse the direction of the duct to run back along the side of the fire test chamber. The UW tunnel utilizes only one 90^o elbow that is directed vertically upwards away from the fire test chamber (refer back to Figures 3.2 and 3.7). The UW exhaust duct transition piece is not insulated (Figure 3.7) unlike the insulated duct which is specified to run from the exhaust end up to the photometer location in a standard tunnel configuration. Insulation is used in the standard tunnel to minimize heat losses from the duct and thus reduce any effect of the temperature dependence of the smoke particulate. Since this has been shown to only present a concern during testing of synthetic products [25], and synthetic products are not used in the present research, the uninsulated exhaust duct is not considered to affect the tunnel results.

For instrumentation of the tunnel, ASTM E84 suggests using a gas meter that only reads total volume of gas; however, the UW Steiner tunnel safety control system incorporates a gas flow meter that measures volume gas flow to better monitor gas flow variations throughout testing. Total volume of gas can be integrated from the volume gas flow-time curve, and it is determined that the difference in calculating the volume of gas would have no impact on the final tunnel measurements.

A study conducted by Lee and Hagget [43] involving 11 Steiner tunnel laboratories indicates that all of the photometers are oriented along a vertical axis, as indicated in the ASTM E84 standard. The UW Steiner tunnel deploys a photometer system aligned in a horizontal orientation because it is already installed in the duct as part of the FTT furniture calorimeter apparatus. A laser based system driven by a 1.0 mW helium-neon laser beam is used instead of a white light system as well.[1] This is not considered a major drawback to the present tunnel since past studies have shown that systems based on white light and those based on laser light obtain similar smoke density results in tests conducted using the ASTM E1537 furniture calorimeter [57]. There are also differences in the distance between the light source lens and the photocell lens in the present system: whereas in an ASTM system these are required to be 3-ft (0.91 m) apart, and the diameter of the cylindrical light beam to be usually 2-in (51 mm), the Melles Griot laser employed in the UW smoke analyzer has a significantly smaller diameter of 0.054-in (1.36 mm), and the light to photocell distance is only 2-ft (0.61 m).

For the air velocity measurements at the end of the tunnel, ASTM E84 requires that the measurements be conducted at a location 23-ft (7.01 m) downstream from the burner across the centre of the tunnel width. In addition, the calibration procedure in ASTM E84 requires removing any refractory turbulence bricks and positioning 2-ft (0.61 m) straightening vanes, positioned 16 and 18-ft (4.88 and 5.49 m) from the burner, to divide the furnace cross section into 9 uniform sections [1]. This is most likely suggested in an attempt to generate a smooth uniform air velocity profile at the end of the tunnel during the velocity measurements. As discussed in Section 3.3.1, the velocity measurements in the UW Steiner Tunnel are taken at a distance slightly longer; 25 ft (7.62 m) from the burner. During the measurements, the refractory bricks are removed but placement of straightening vanes in the tunnel is impractical since it would require removing the thermocouples. Therefore this requirement is disregarded during measurements of velocity at the outlet end of the tunnel.

[1]The light source suggested by ASTM E84 is a 12-V sealed beam with clear lens, auto spot lamp (General Electric No. 4405). The photocell is a Huygen Corp. No. 856RRV photronic cell [1].

3.5 Experimental Uncertainties and Sources of Error

Now that difference between the present tunnel and its instrumentation with the ASTM E84 tunnel have been described, this section is devoted to summarizing the principal sources of uncertainty in the present data and discussing their impact on measured values obtained from the instrumentation in the Steiner tunnel test results outlined in the next several sections. Due to the large variety of relevant parameters, an estimation of measurement uncertainty in a global value derived from a large scale test such as the Steiner tunnel is not straightforward. Previous works on uncertainty in values of FSI and SDI [43], provide background information on an inter-laboratory test study that examined the consistency of test results from lab to lab, and indicated poor reproducibility of the test data. The high variability in measurements between labs are hypothesized to be due to variations in tunnel construction, instrumentation, and operation in different laboratories. A more recent study [14], shows that with proper statistical process control of the most important tunnel parameters, the major contributor to uncertainty in measured values of FSI and SDI is primarily due to differences in the materials used for repeat test samples, and less influenced by the measurement device used to monitor and control the tunnel or the person conducting the test. The study done by Rensing[14], however, was only conducted on a single tunnel, suggesting that internal laboratory repeatability of tests is reasonable, but poor reproducibility between laboratories may still exist [1].

Estimation of experimental uncertainty is intended to provide an estimate of the error in the measurement, usually defined as the difference between the true value and a measured value [58]. The overall uncertainty in measured values of FSI and SDI from the present Steiner tunnel apparatus therefore arises from a combination of potential sources, extending from instrumentation error through to uncertainty arising from test-to-test variations in the relatively uncontrolled environment in the lab that houses the Steiner tunnel test apparatus.

The total error or the experimental uncertainty is usually expressed as a function of the bias error, B, and a random or precision error, S, [58, 59]:

$$\epsilon_t = \pm\sqrt{B^2 + (t_{95}S)^2} \tag{3.6}$$

where t_{95} is a multiplier of 95 % confidence and a sample number greater than 30. The multiplier t accounts for the number of degrees of freedom represented by a 95 % confidence limit.

Bias or fixed errors are errors that remain constant during an experiment. They are also known as systematic errors and they usually arise from tolerances of instrumentation,

calibration and data acquisition. The bias limit of a certain measurement can be expressed as a root sum-square of all of the component bias errors [58]:

$$B = \sqrt{\sum_{i=1}^{n} B_i^2} \tag{3.7}$$

S, also known as the precision index of a measurement [59], represents the random error. This error is usually estimated based on a set of measured data and, assuming a normal distribution in the data, it is equal to the standard deviation of the data set. The precision index is calculated as:

$$S = \sqrt{\sum_{i=1}^{n} S_i^2} \tag{3.8}$$

Errors can arise at all stages of data acquisition, instrument calibration and data reduction. These are reflected as variations in the final measured values for repeat tests under nominally the same experimental conditions. Average values and standard deviations are calculated to assess the variation, and can be simply calculated using Equations 3.9 and 3.10 [60]:

$$\bar{x} = \sum_{1}^{n} \frac{x}{n} \tag{3.9}$$

$$s = \sqrt{\sum_{1}^{n} \frac{x - \bar{x}}{n - 1}} \tag{3.10}$$

where x represents the individual sample, and n is the total number of samples. The variance percentage, Var%, or the relative standard deviation, is then calculated using Equation 3.11.

$$Var\% = \frac{s}{\bar{x}} \cdot 100\% \tag{3.11}$$

As discussed in Section 3.3, the Steiner tunnel instrumentation includes a pressure transducer (DPT), gas flow meter, anemometers, thermocouples TC # 1-12, and the smoke analyzer system. The following sub-sections focus on uncertainties related to the bias errors obtained from these instruments, as well as their calibration curves, and data transmission, acquisition system and precision errors where applicable.

3.5.1 DPT, Gas Flow Meter and Anemometers

As discussed in Section 3.3, the DPT is connected to the differential pressure transmitter reader via plastic hose tube. The accuracy of calibration error of the differential pressure transmitter, as supplied by the manufacturer, is minimal at 0.35%.

The transmitter signal linearity error on the ERDCO Gas Flow Meter reported by the manufacturer is no more than 5%. The current output signal used for measuring gas flow has a repeatability of 0.5 %. A hard copy of the calibration curve is provided by the manufacturer, where the mA signal output is correlated with the actual gas flow. The calibration curve is reproduced using a web plot digitizer before being incorporated into LabVIEW. The measured gas flow is also indicated on the meter by a change in the needle position on the gauge proportional to the flow, and the current output signal is directly linked relative to needle's position. To provide an ongoing record of the gas flow, a video camera is installed above the meter and the movement of the needle is recorded throughout trial tests. The needle position is then compared to the calibration curve provided by the manufacturer. This experiment is repeated for several tests until a conclusive agreement is made that the difference between the actual gas flow needle position and the manufacturer's calibrated curve is 3.2%. Using Equation 3.7, the total bias error associated with the gas flow measurements is estimated at 6%.

The average air velocity at the end of the tunnel is calibrated to 1.2 m/s ($\pm$0.025 m/s). As mentioned in Section 3.3, the air velocity for the Steiner tunnel is measured 25-ft (7.62 m) from the burner port centre with a heated wire anemometer. Average velocity is measured across 7 equal widths at the geometrical centre of the tunnel cross section. The anemometer is positioned with the guidance of camera tripods such that the tip of the probe is held in a relatively steady position. The calibration error for the VelociCheck heated wire anemometer is within $\pm$5% of the reading, or $\pm$0.025 m/s as reported by the manufacturer. The total precision error is determined by calculating the standard deviation of the 10 selected trials at standard ambient temperature and adjusting the air velocity at the end of the tunnel to 1.2 m/s. In this way, it is determined to be no more than 1 %. The total measurement uncertainty for the air velocity measurements is then determined using Equation 3.6 to be 5 %.

The handheld anemometer has a manufacturer specified resolution of $\pm$0.1 m/s, as listed by LA Crosse Technology.

3.5.2 Thermocouples

The K-type thermocouples utilized in the Steiner tunnel are subject to measurement error compromising the greater of $\pm 2.2^{o}$C or $\pm$0.75% for temperatures measured above 0^{o}C

[61]. For a maximum temperature of 749^{o}C measured near the burner during the tests, the corresponding calibration uncertainty is $\pm$5.6^{o}C. The thermocouples inside the tunnel are connected to extension-grade thermocouple wires outside the tunnel via thermocouple terminals explained in Section 3.3. These extension wires, which are connected to the DAQ board have their own calibration uncertainty of $\pm$2.2^{o}C. The input modules of the DAQ have a manufacturer-specified uncertainty which included errors to gain, offset, nonlinearity, linearization, quantization, noise, and measurement of cold-junction temperature, which is stated to be no more than $\pm$2.2^{o}C [61]. Table 3.4 illustrates the total bias error associated with the thermocouple measurements. The total bias error is estimated to be less than 2%, which is most likely outweighed by the overall operational uncertainty of the tunnel discussed in the next chapter.

Table 3.4: Estimated bias (B) thermocouple uncertainties

Temperature (^{o}C)	B_{TC} ($\pm^o$C)	B_{Wire} ($\pm^o$C)	B_{DAQ} ($\pm^o$C)	B_{Tot} ($\pm^o$C)
300	2.2	2.2	1.3	5.7
500	3.8	2.2	2.2	8.2
800	6.0	2.2	2.2	10.4

3.5.3 Smoke Analyzer

Smoke measurements are conducted using the smoke analyzer discussed previously in Section 3.3. The 1 mW (632.8 nm) Helium Neon laser utilized in the furniture calorimeter has a beam point stability that is within 3 % after its initial 15 minute warm-up period, as specified by the manufacturer. There is also a drift value associated with the measurements after the calibration of the instrument.

After the zero calibration and balancing of 100 % transmission of the laser light through the PDM and PDC outputs, there is a slight deviation prior to, and after the tunnel test. The 100 % light transmission should ideally remain at 100 % prior to the test (or SO% = 0) before the burners are ignited, and it should also return to its baseline of 100 % after the sample has been removed from the tunnel and there is no further evidence of smoke in the duct. However, slight deviations are noticed in the SO% prior to and after the test (shown in Figure 3.24), most likely because there is still some smoke particulate remaining inside the duct after a test.

To examine this further, raw data is collected after several tests to determine the amount of time it takes for SO % to return to its zero baseline. The total time across 3 red oak tests is averaged to be 756 seconds. The deviation prior to the test is noise recorded from

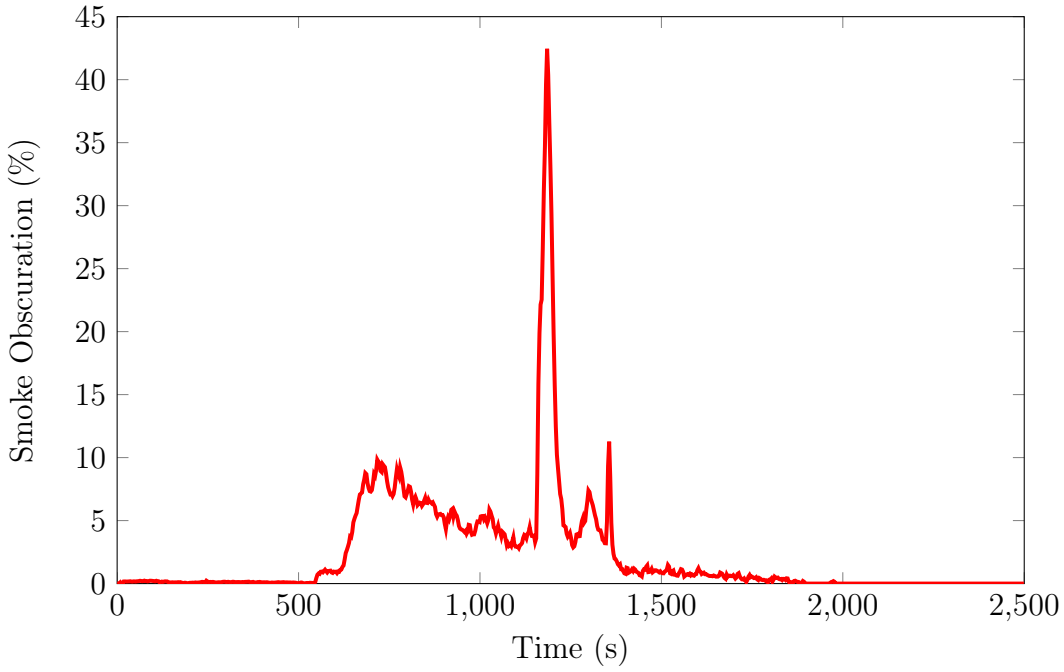

Figure 3.24: Representative smoke obscuration curve shown for red oak calibration

the photometric circuit. The average standard deviation in SO% calculated across 21 tests is 0.5 %. With the 3 % error on the laser beam point stability, and 0.5 % from the data noise, the total uncertainty for smoke measurements is estimated at 3.5 %.

3.6 Methods

The present section describes the experimental procedures and the samples selected for use in commissioning and evaluating the overall performance of the fully installed Steiner tunnel described in the sections above.

3.6.1 Experimental Procedure

The overall experimental protocol for operation of the Steiner tunnel apparatus consists of the following 4 key steps:

1. Tunnel Preheat phase
   (a) Verification of Ambient Condition, Water and Air Flow
   (b) Establish Gas Flow to Burner

(c) Preheat sample loading

(d) Burner shut-off and removal of lids

2. Test Sample Loading

3. Test

(a) Verification of Ambient Condition, Water and Air Flow

(b) Establish Gas Flow to Burner

(c) Burner shut-off and removal of lids

4. Shutdown and purge

Before the preheat phase is started, the temperature and relative humidity in the lab are checked to ensure that they are within the ranges of 18.6 - 26.0^{o}C, and 45 - 60 %, respectively, as stipulated in the ASTM E84 test method. It is found that, in the mornings and evenings, the relative humidity of the air is higher than the standard requirement. As such, the tunnel pre-heat is conducted in the mornings to provide enough time to run actual tests when the relative humidity settles to within its required range in the afternoon.

Next, the water level around the lids of the tunnel is verified and topped up as necessary. The fan in the small cone calorimeter lab is turned on and the air velocity is measured by inserting the heated wire anemometer through the air velocity tap. The airflow is then adjusted to meet specifications in E84 by adjusting the draft in the tunnel using the manual damper assembly in the Exhaust Duct Transition Piece, or by adjusting the fan speed using the fan control. Because tunnel operation is found to be very sensitive to the airflow setting, a study is conducted into the effect of damper setting on the test data. Results will be discussed in the following Chapter.

To establish gas flow to the tunnel burner, the solenoid valve in the electrical panel room (breaker # B59) has to be enabled first. Since the breaker for this solenoid is switched off at the end of the day for safety purposes, this procedure is performed first. The main gas shut-off valve in Figure 3.13 is then opened and it is verified that all the E-Stops are disabled. Following this, the run-switch on the control panel box is switched on and the main control system takes over and ignites the burners. Under normal operation, the burners generate a flame length of approximately 4.5 ft (1.37 m) on the cement board during preheating of the tunnel.

The first phase in operation of the tunnel is to preheat the tunnel as per the ASTM E84 standard such that the brick temperature at TC #11 is 66^0C (150^0F). This is done with cement board installed in place of a test sample. The preheat consists of 3 steps

as itemized above. Very similar steps are also involved in each of the sample tests. It is found that the preheat takes considerable time, so to maximize efficiency in scheduling of tests, two sample tests are run after preheating the tunnel on a given day whenever possible. Depending on ambient conditions, it usually takes between 25 and 35 minutes to preheat the tunnel to the temperatures required in ASTM E84. At this point, the E-stop is pressed, the shut-off valve is switched off, and the tunnel is cooled down by increasing the fan speed until the temperature measured by the floor thermocouple, TC # 10, approaches 40.5^oC (105^oF).[1] This second (cooling) process usually lasts between 45-70 minutes, also depending on ambient conditions.

After the tunnel is preheated and cooled down to its appropriate temperature, all 6 lids are removed one by one with a modular gantry crane so that a conditioned test sample can be placed in the tunnel. As the lids are removed from Lids A to F, they are stacked on top of each other on the laboratory floor in two stacks each 3 lids high. Fire bricks are placed between each lid to provide enough clearance so that the assembly clamps do not interfere with one another (Figure 3.25). Once the testing chamber has been cleaned, and the gaskets on the chamber ledges checked for integrity and placed and changed as required, the test samples are placed on the ledges that run along the top of the tunnel and the lids are placed back one by one onto their corresponding modules in the reverse order from Lids F to A. The Steiner tunnel test is then conducted on the sample.

At the end of the test, the E-Stop is pressed and the run switch is turned off on the control panel box. The manual shut-off valve in Figure 3.13 is also switched off for safety purposes. The air intake shutter is fully opened and the exhaust fan turned up to full speed to cool down the tunnel. This lasts between 30 and 70 minutes, depending on the material being tested. Once the tunnel is cooled down, and the brick temperatures are in the safe range (usually aim for TC # 10 to be below 50^oC), the lids are removed and the sample is disposed of safely. The tunnel chamber, including the observation windows, is then cleaned and the next sample is mounted if running consecutive tests. Differences in initial air temperature between consecutive tests are within 5 ^oC. After the last test of the day, the cement board is placed back into the tunnel so that the tunnel is ready for pre-heat on the next testing day.

Two people are generally required to operate the Steiner tunnel during a test. One person is responsible for operating the tunnel and recording the flame spread readings, while a second monitors the tunnel draft pressure and temperature levels during the test, and initiates the smoke measurement data logger at the beginning of the test.

[1] It is found that aiming for a floor temperature of 48^oC provides enough time to take off the lids and place the test sample into the tunnel.

Figure 3.25: Two lids placed on top of each other on the laboratory floor.

3.6.2 Samples Tested

Samples used in the present research include those that would normally be utilized during regular calibration of a Steiner tunnel, as well as many additional samples that are tested to systematically evaluate the impact of fan control, gas flow and damper position on the operation of the as-installed tunnel apparatus. Based on a preliminary set of results, some minor modifications are implemented to both the design and operational procedures for the tunnel and a second set of tests is conducted, culminating in a full calibration of the tunnel per ASTM E84 standard test protocols.

The materials used in the full suite of testing conducted in this research are described below, followed by the methods used for conditioning and preparing the samples before they are installed in the tunnel for testing.

There are two main materials that are specified for use in calibration of a Steiner tunnel. These are cement board and red oak lumber as previously discussed in Section 2.1. Cement board is a non-combustible material that is structurally robust with 1 and 2-hour fire resistance ratings [62] and therefore is used to calibrate for an FSI value of 0. On the other hand, red oak is used as the material by which to set the upper end of the calibration for an FSI of 90.

In this research, 1/2-in (13 mm) Durock cement board is used, manufactured by United

States Gypsum Company of Chicago, Illinois. While this cement board is thicker than the 1/4-in (6.35 mm) specified in the standard, it is used consistently for tunnel pre-heat and cement board calibration tests. The sheet has to be replaced when it could no longer support its own weight when installed on the tunnel ledges therefore, use of the thicker material serves to minimize replacement of the boards.

Kiln dried, sanded red oak boards manufactured in Metrie, Virginia are purchased from a local lumber store (Lowes, Waterloo, ON) to manufacture the test samples used for upper end calibration runs. Both 96 x 2 in (2.44 x 0.051 m) and 96 x 3 in (2.44 x 0.076) planks are ordered, each 3/4-in (19 mm) thick. As discussed in Section 2.5; however, red oak lumber is found to be a relatively expensive material for repetitive commissioning and calibration of the tunnel. Due to its' expense, a series of other wood products, that are significantly less expensive, are used in most of the commissioning and tunnel 'pre-calibration' tests. Various wood products [2, 44, 63, 64, 65, 66, 67] with reported flame spread indices that are determined by approved fire testing facilities are considered and the following materials are selected as test materials for evaluation and commissioning of the tunnel.

Table 3.5: Summary of samples tested in the Steiner tunnel

Material	Thickness	FSI - Literature	SDI - Literature
Cement Board	1/2-in (13 mm)	0	0
Red Oak	3/4-in (19 mm)	90	100
Oriented Strand Board (OSB)	7/16-in (11 mm)	86-150	-
Particle Board (PB)	3/4-in (19 mm)	145	-
Douglas-Fir (DF) Plywood (Sanded)	1/4-in (6.35 mm)	150	100
Douglas-Fir Plywood (DF)	3/8-in (9.5 mm)	110-150	-
Luan Plywood	13/64-in (5.2 mm)	108-158	

Most of the pre-calibration tests are conducted using 7/16-in (11 mm) Blue Ribbon OSB, manufactured by Georgia Specific. This is the least expensive material from the 7 listed above. The local manufacturer for Ontario is located in Englehart, ON. The board is manufactured of various wood species such as aspen and southern yellow pine [63]. FSI results reported in the literature for OSB are in fairly wide range, FSI results anywhere between 86 - 150 are observed [63]. Several testing facilities report averages of 148, 138, and 131 [64, 65, 66]. This is to be expected since OSB can be manufactured using a wide range of different wood species and adhesives.

Particle-board (PB) is also selected since it has been suggested as a possible reference material for the tunnel [1, 45]. The board remains intact and does not collapse during the 10 minute interval of the test. It generates well-controlled burning with relatively uniform char patterns [45]. The particle board used here is 3/4-in (19 mm) thick Flakeboard product from a local manufacturer located in Sault Ste. Marie, ON. Flame spread indices

recorded by the UL test labs are in the range of 145 [44]; however, exact values will again depend on the wood specie, and the type of adhesives used.

Douglas fir plywood (DFP-CANPLY) samples are manufactured by Tolko industries of North Vancouver, BC. The 1/4-in (6.35 mm) thick pieces are sanded on one side and the 3/8-in (9.5 mm) are rough on both surfaces. No surface coatings are applied to any of the samples tested. Flame spread for DFP-CANPLY will depend on the surface of the board (sanded versus non-sanded, coated versus non-coated). The SDI for un-coated DFP-CANPLY reported in literature is the same as red oak (SDI = 100) [67].

Finally, Luan plywood samples are 13/64-in (5.2 mm) thick and manufactured by McCorry Group out of Sabah, Malaysia. The flame spread reported for this specific product is 120 [63].

The samples listed in Table 3.5 are purchased, then prepared and conditioned before testing, as described in the following section.

3.6.3 Materials Preparation and Conditioning

All the materials listed above, except for the red oak, are purchased in 96 in x 48 in (2.44 m x 1.22 m) sheets. A single sheet is cut into 2 samples that are 96 in x 21 in (2.44 x 0.533 m), illustrated in Figure 3.26, leaving a piece 96 in long x 6 in wide (2.44 m x 0.152 m). Since the total length of a tunnel test sample is 288 in x 21 in (7.32 x 0.533 m), 1.5 sheets are required for a single test. The remaining 96 x 6 in (2.44 x 0.152 m) piece is used to cut three 6 in x 4 in (0.152 m x 0.102 m) samples, which are used for measuring moisture content.

All of the test materials are cut to size and then conditioned for at least 3 days prior to testing in a humidifying chamber at the UWFRL facility. The chamber temperature is maintained at 23 $\pm$2.8^{o}C, and a relative humidity of 50 $\pm$5%.

Moisture content, $MC\%$, is measured using the oven dry method according to ASTM D4442, Standard Test Method for Direct Moisture Content Measurement of Wood and Wood Based Materials [68]. Moisture content is calculated according to Equation 3.12, where OM is the original mass of the sample, and ODM is the oven-dry mass.

$$MC\% = \left(\frac{OM - ODM}{ODM}\right) \cdot 100\% \tag{3.12}$$

The following table lists the range of moisture content measured for the samples tested in this study.

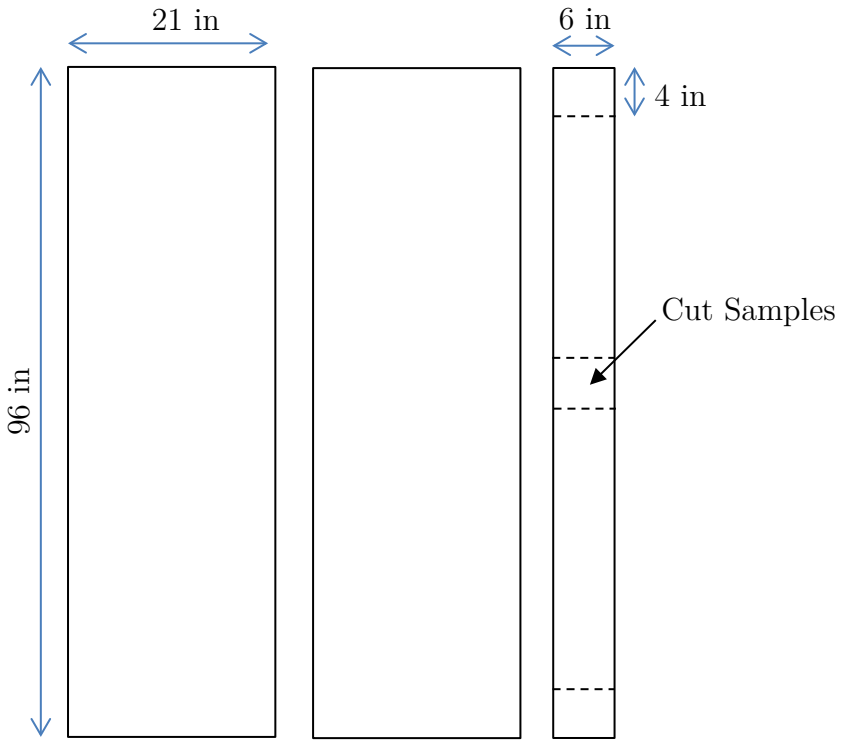

Figure 3.26: Typical samples cut from a 96 x 48 in (2.44 x 1.22 m) sheet

Table 3.6: Measured moisture content for samples tested

Material	MC % Range	Average (MC %)	Std. Deviation (MC %)
Cement Board	0	0	0
Red Oak	6.55 - 7.48	7.00	0.40
Oriented Strand Board (OSB)	3.59 - 5.91	4.81	0.84
Particle Board (PB)	7.98 - 8.44	7.50	1.01
Douglas-Fir Plywood (Sanded)	-	-	-
Douglas-Fir Plywood	-	-	-
Luan Plywood	-	-	-

Since the number of tests conducted on the plywood products is small in sample size, the moisture content (MC %) is not measured for these products as part of the varying parameters.

The apparatus description and the tunnel test methods outlined in the sections above are followed during commissioning and calibration of the Steiner tunnel, as well as in tests designed to gain insight into the primary parameters which affect the tunnel results.

Chapter 4

Tunnel Commissioning and Operation

Using the samples outlined above, the operation of the tunnel is characterized through a series of tests conducted in a manner similar to that outlined in the ASTM E84 standard. The list of calibration procedures specified in the standard include an air leak test, as well as flame spread tests using cement board and red oak. In addition to the calibration procedures, experiments are conducted to determine a measure of the repeatability of the tests conducted in the tunnel, as well as to identify key operational parameters and any issues encountered during calibration. From the results, three key parameters that affect flame spread measurements in the tunnel are identified. The sensitivity of tunnel test results to each of these parameters is evaluated to provide guidance as to an appropriate range of operating conditions within which calibration and test runs will essentially be minimized.

4.1 Air Leak Test

An overall test to determine air leakage from the tunnel constitutes the first step in characterization of the Steiner tunnel. This test is conducted with the removable lids in place and with the cement board inserted on top of the tunnel ledges as the test specimen. The air inlet shutter is kept open at the required 3.0-in (76 mm) and an air draft pressure of 0.15 in-WC (37.4 Pa) is established through fan control. For the test, the air shutter is closed and sealed off without making any adjustments to the damper position. According to guidance in the ASTM E84 standard [1], when the tunnel is sealed, the draft pressure reading should increase to at least 0.375 in-WC (93.4 Pa).

In an initial set of tests, the draft pressure reading after closing the shutters is quite low, 0.103 in-WC (25.7 Pa) on average (Figure 4.1), suggesting that the tunnel has excessive

air leakage. A supplemental leakage test is then performed to determine the location of these. For this test, the air intake and the exhaust ends of the tunnel are sealed off and a 20 000 cfm (566 m^3) smoke generating machine is placed inside the air intake module as shown in the photographs in Figures 4.2 and 4.3.

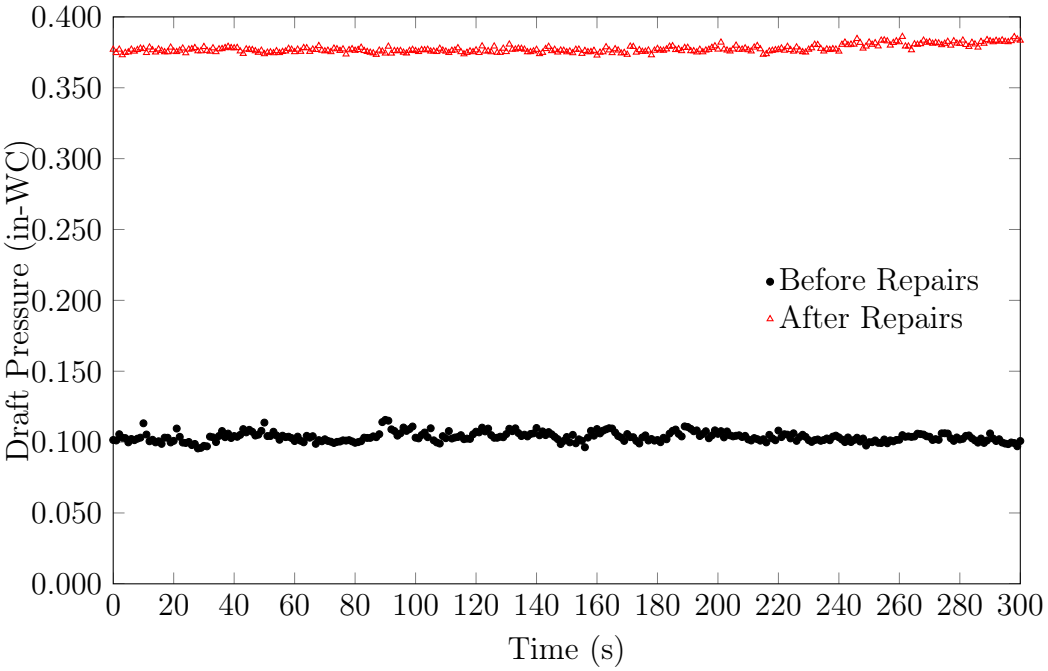

Figure 4.1: Air Leak Test - draft pressure reading before and after repairs on the tunnel

As can be seen from the photographs, there is excessive leakage around the windows of the tunnel and at the joint sections of the modules (shown in Figure 4.2) as well as underneath the water channel trough (Figure 4.3). Leaks at the joint sections and the window viewing area are because the joining gaskets are too thin to ensure pressure tight seals in those areas and for the water channel, the leaks come from gaps at the lap joints that form the structure of the water trough.

To address these leaks, several changes are made to the Steiner tunnel. Each window is disassembled and sealed around the mid-section connecting the interior and exterior panes with 1/4-in (6.35 mm) fire blanket to fill up any air gaps. The interior and exterior pane mounts are then also sealed around the edges with caulking. Along the lid joints and along the modular joining sections, the existing 1/8-in (3 mm) thick gaskets are replaced with 1/4-in (6.35 mm) thick gaskets. Finally, all of the sheet metal gaps around the water channel trough and the windows are sealed with high temperature silicon caulking.

The smoke generating machine is again placed in the air intake module and it is found that the air leaks are far less significant (Figure 4.4) with only minor air leaks remaining

Figure 4.2: Photograph of the air leak test, window view of the tunnel

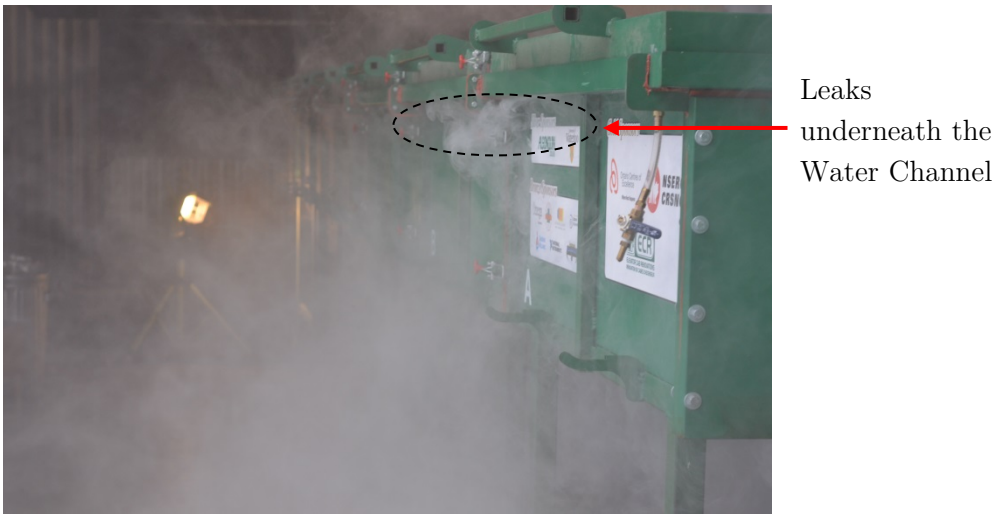

Figure 4.3: Photograph of the air leak test, back view of the tunnel

Figure 4.4: Air leak test after the tunnel repairs

underneath the water channel trough and the window viewing area. These are sealed with caulking and the test conducted a final time with the draft adjusted to 0.15 in-WC (37.4 Pa), and the air shutter closed. In contrast to the initial value of 0.103 in-WC (25.7 Pa), the draft pressure reading now averaged 0.380 in-WC (94.7 Pa), as shown in Figure 4.1. The tunnel repairs demonstrated to be effective in reducing air leaks such that the minimum requirement of 0.375 in-WC listed in the ASTM E84 standard is satisfied.

4.2 Issues Encountered During Calibration

After the tunnel draft pressure is within range, the next step in the tunnel characterization procedure is to pre-heat the tunnel until TC # 11 reached 66^{o}C (150^{o}F) as per ASTM E84 [1]. During the initial pre-heat run, however, when TC # 11 measured only 40^{o}C (104^{o}F), the exterior pane on the glass window closest to the burner started to crack due to radiation from the 5000 BTU/min (88 kW) burner inside the tunnel. The interior pane did not show any signs of cracking since it is high temperature silica glass; however, the exterior pane is constructed of laminated float glass, which has a fairly low resistance to thermal stress [69]. Although the exterior pane does not provide an air seal for the tunnel, cracking of this window merits further investigation since preheating of the tunnel is required before every test.

Theoretical and experimental studies of glass cracking in fires have been conducted in the past. Skelly [70], for example, conducted a series of experiments where windows

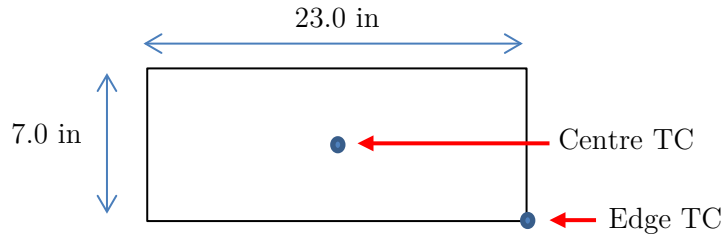

Figure 4.5: Thermocouple locations taped on the inside surface of the glass window

were directly exposed to the fire environment in a small-scale fire test room. Temperature differences between 60 and 80^{o}C were found to cause the entire window to break in less than 200 s into the test. Some of the first extensive theoretical analysis of glass cracking in fires was done by Keski-Rahkonen [71]. He was able to predict that the temperature difference of 80^{o}C (176^{o}F) between the centre and the edge of the glass was needed to initiate cracking. Other studies conducted, assuming different thermal and mechanical properties of glass, have predicted initiation of cracking with temperature differences of 58^{o}C (136^{o}F) [71]. Moreover, these latter studies concluded that the temperature difference between the exposed glass surface and that of the glass surface that was shielded by an edge mounting frame was the major contributing factor to cracking of the glass.

To further investigate the reason for cracking of the exterior pane, therefore, two 18 gauge (1.02 mm diameter), chromel-alumel (Type K) thermocouples are taped on the inside surface of the laminated glass window, at the center and at a bottom corner, as shown in Figure 4.5. The thermocouples are positioned to measure the highest temperature difference across the pane; the bottom corner of the window would be cooler than the upper corner because the tunnel burner flame is closest to the top of the window.

For this test, the gas burners are ignited to pre-heat the tunnel from a cold start (ambient temperature 21.4^{o}C), the thermocouples are connected to a hand held digital thermometer (OMEGA CL3512A), and temperatures on the glass are recorded at intervals of 40 seconds. Cracks are observed to initiate in the pane after 1387 s (23.1 min) when the temperature difference between the two thermocouples is 60.3^{o}C, as shown in Figure 4.6. This temperature difference aligns closely to other values reported in literature [71], although the time to cracking of the pane is longer in the present study. This is likely because the configuration of the tunnel windows is significantly different than those used in the previous studies. First, the Steiner tunnel exterior window pane is not directly exposed to the fire so cracking will be delayed. Additionally, as discussed in Section 3.4, there is a 1/4-in (6.35 mm) gap that allows free movement of cold ambient air in between the window panes which further delays the heat transfer by radiation from the burner flame to the window.

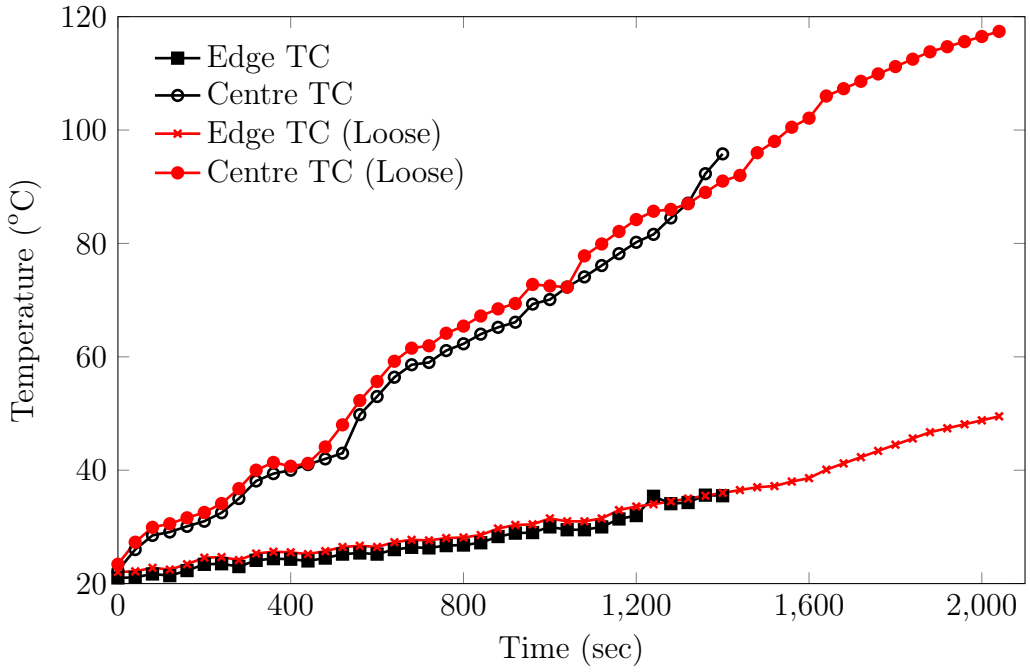

Figure 4.6: Time temperature history for loose and tightened panel

Further investigation indicated that the cracks in the exterior window panes propagate mainly from sections where the clamps are tightly screwed on to the window panes (Figure 4.7). It is thought that the additional stress induced by the clamps likely led to the initiation of crack propagation as well. Therefore, the clamps on the panes are loosened, and the experiment is again repeated from cold start. In this case, an additional 10.7 min (see Figure 4.6) is needed before new cracks are initiated at the centre of the window pane.

Using the current exterior window panes, the results of these tests suggest that the tunnel pre-heat should not be conducted longer than 34 minutes (2040 sec). If longer periods are required due to ambient conditions, the preheat should be performed at intervals, allowing sufficient time for the window panes nearest to the burner to cool down between heating stages. This is possible since the fire bricks have higher thermal conductivity than the window panes, so that the window panes cool down faster than the bricks between heating cycles. Another solution, not pursued in the present work, would be to replace the exterior panes with borosilicate glass which has a much higher resistance to thermal stress than float glass.

Figure 4.7: Locations of window crack initiation

4.3 Cement Board Test

After the issues of glass cracking is investigated and addressed, the first calibration test for characterizing tunnel operation in more detail are conducted using a cement board sample. This follows the ASTM E84 procedure which outlines that cement board is one reference material for calibration of a tunnel (Section 2.1). The requirement is that cement board has a measured FSI of 0 which suggests that no flames should spread further than the 4.5 ft (1.37 m) from the burner position (x = 0 ft). Additional to this requirement, the time-temperature curve at the end of the tunnel (TC # 12) needs to match a standard time temperature curve specified in ASTM E84 [1] since this reflects the contribution of energy into the tunnel and test samples that comes from the burner and fuel [1]. As a result, matching the standard tunnel time-temperature curve suggests that the intensity of the burner (88 kW) specified in [1] is matched as well. ASTM E84 [1] suggests that if appreciable variation exists with the representative time-temperature curve, then suitable adjustments in the fuel supply can be made based on the red oak calibration test.

Figure 4.8 contains plots of two measured time-temperature curves recorded at TC # 12 with two different gas flows to the burner, as well as comparison curves from results reported in ULC [6] and in the ASTM E84 standard [1]. In the plot, data from the present study has been smoothed using an arbitrary value of 25 point moving average in order to damp out high-frequency fluctuations in the individual values.

For the same gas flow rates, temperatures at the end of the test are higher for the ULC

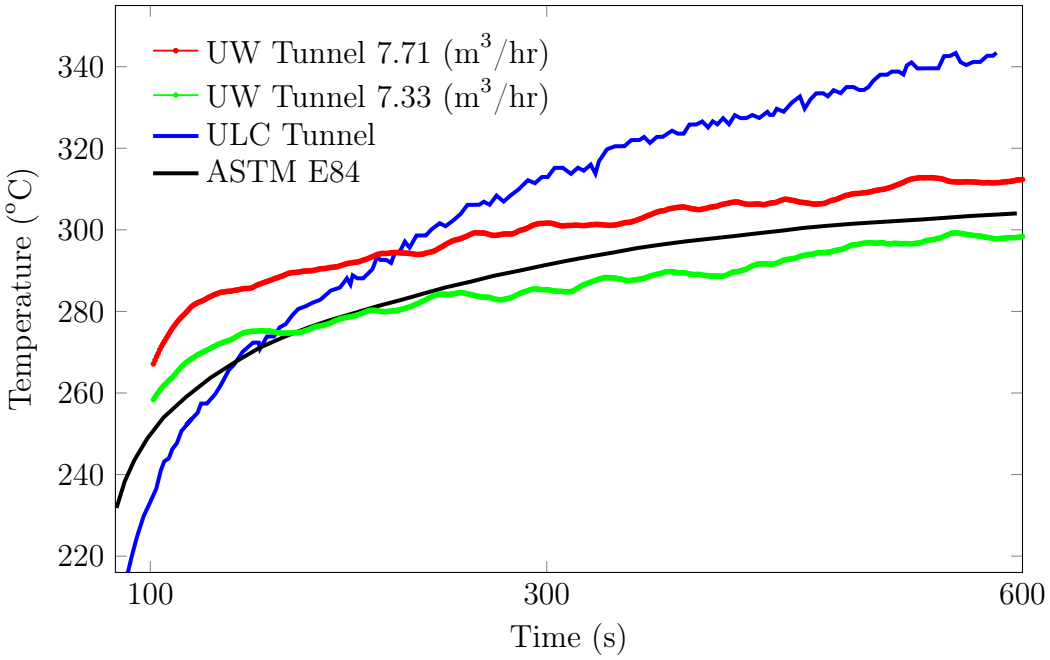

Figure 4.8: Comparison of time-temperature curves for the cement board calibration test

and present tunnel than that specified in the ASTM standard. The standard indicates, however, that adjustments to the fuel supply can be made to meet the red-oak calibration curve, provided that the flame length does not extend beyond 4.5 ft (1.37 m). This is the case for the ULC curve from Figure 4.8, where additional fuel is supplied in order to meet the red oak calibration curve [6]. For the UW Steiner tunnel, the red oak curve represented in Figure 4.8 is tested at maximum fuel supply; the average gas flow recorded for the test in Figure 4.8 is 7.71 m^3/hr, and the temperature at the end of the 10 minute test is 312.8^{o}C, while the flames are flickering slightly past the 4.5 ft (1.37 m) mark. The temperatures recorded are higher than in the ASTM E84 curve which indicates that the burner has sufficient energy input to satisfy tunnel requirements. However, since gas flow can vary from day-to-day, especially at colder outside conditions where the gas flow tends to drop, the temperatures may not always reach the ASTM E84 representative curve. The green curve in Figure 4.8 represents the lower gas flow at 7.33 m^3/hr where the temperature recorded by TC #12 at the end of the 10 minute test is only 298^{o}C, slightly lower than the ASTM E84 curve (304.1^{o}C). These results suggest that the gas flow to the burners should be closely monitored described in Section 4.5.1.

4.4 Test Repeatability

Following all of the preheat and characterization tests discussed above, the next to final phase of tunnel characterization involves assessment of the repeatability of test results obtained using the same material under nominally the same operational conditions. In general, repeatability is defined as the precision determined from multiple test results conducted under the same conditions [72]. In fire testing, such tests are generally run by a single operator using the same set of equipment over a relatively short period of time so that the lab environment does not change appreciably. Repeatability can then be estimated as the standard deviation of results. For a good approximation of test to test standard deviation in fire testing, at least 30 test results are recommended [72]. The repeatability, as given by that standard deviation, s, is calculated according to Equation 3.10.

In large scale fire testing, test-to-test repeatability is often an area of significant concern; however, it can be quite difficult to assess. While it is usually feasible to conduct large numbers of replicate measurements in bench-scale tests to obtain valid repeatability and variance numbers, this is usually not cost effective for large scale tests. Additional to the cost, in an uncontrolled test environment usually inherent in large scale tests, it is also difficult to keep ambient conditions relatively the same.

To assess repeatability of the Steiner tunnel, therefore, three tests are conducted under 'repeatable' conditions using 7/16-in (11 mm) OSB samples. Table 4.1 lists the tunnel operating parameters as recorded during each of the tests. All of the parameters except moisture content (MC%), are kept within 10 % variance. There are slight variations in ambient conditions because Test 36 was conducted on June 10, 2014 while Test 37 and Test 38 were conducted on the following day. For the moisture content (MC %), samples are purchased from the same location and are kept in the humidifying chamber for equal periods of time prior to testing, however, since OSB is manufactured and assembled from various wood species, some variance in MC% is expected. The average wind velocity measured at the exhaust stack is very similar across the two days of testing, so it should not result in any significant effects on the test results.

Figures 4.9 and 4.10 show the FSI and smoke measurements over time for the three repeatability tests conducted in the characterized Steiner tunnel. In Figure 4.9, only the first 300 seconds (5 min) of the test are shown since the flame reaches the end of the tunnel in 255 seconds for all three tests. The flame spread indices for the three tests, shown in Table 4.2, match well with average values of 148, 138 and 139 and the range of 85-150 reported in the literature [64, 65, 66]. Since the SDI is generally determined from comparison to a minimum of 5 red oak calibrations tests, only the total smoke obscuration (TSO) values are compared in Figure 4.10.

Based on results shown in Figures 4.9 and 4.10, the standard deviation for the FSI

Table 4.1: Recorded parameters for the three OSB repeat tests

Parameter	Test 1	Test 2	Test 3
DPT (in-WC)	0.109	0.105	0.102
Gas Flow Average (m^3/hr)	6.26	6.36	6.38
MC %	5.07	3.59	3.95
Ambient Temperature (^{0}C)	20.0	22.7	24.0
Relative Humidity (%)	65	76	69
Outside Wind (m/s)	1.0	1.05	0.92

Table 4.2: Results for the three OSB repeat tests

Test Number	FSI	TSO (%)
1	150.5	11.1
2	137.8	9.52
3	147.7	13.5

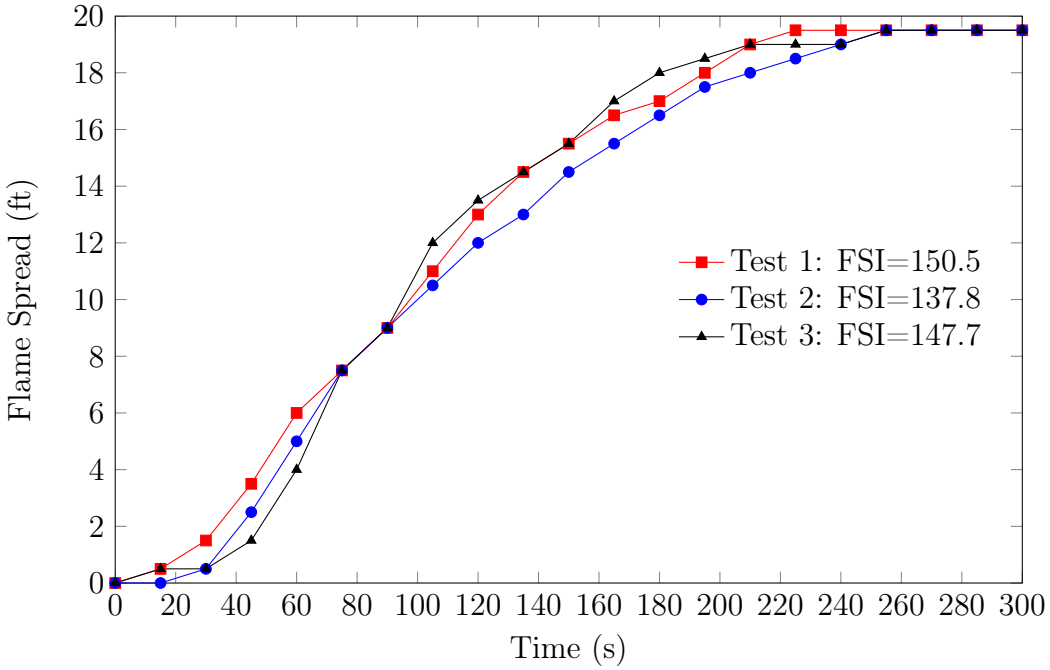

Figure 4.9: Comparison of flame spread results for three repeat OSB tests

results is calculated to be 6.7 or 4 %, and 2 % for the TSO measurements. In comparison to the standard deviation for FSI of 15.0 reported in ASTM E84 for Douglas fir plywood [1], the repeatability of the UW Steiner tunnel could be considered excellent. However, the

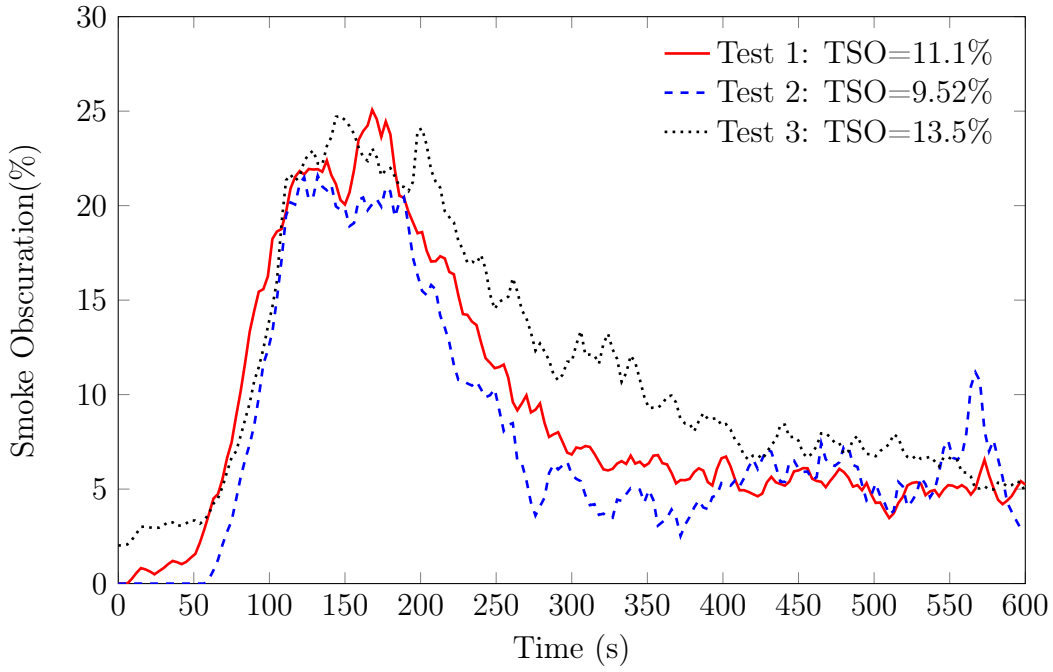

Figure 4.10: Comparison of smoke measurements for three repeat OSB tests

number of repeated tests conducted in this study is fairly low and therefore, sufficient tests may not have been conducted to draw any major conclusions. In future, then, additional repeatability tests should be conducted with different materials as well.

It should be noted that for the OSB repeatability tests, the gas flow has to be significantly reduced to an average of 6.04 - 6.38 m^3/hr (Table 4.1) in order to obtain repeatable results with comparable values to those reported in the literature. For a fully open shut-off valve, the measured FSI is as high as 223, much higher than any value in the literature. While this indicates that lower gas flows might be most appropriate for the present tunnel, it should be noted that the OSB results are also affected by other parameters. These combined influences on FSI will be discussed further in the pre-calibration test results in the following section.

4.5 Pre-Calibration Test Results

This section contains results from a set of 78 'pre-calibration' tests which are run prior to final calibration of the tunnel using red oak per [1]. In these, each of the parameters affecting flame spread results is studied systematically. For the most part OSB samples are used because OSB is much cheaper than red oak and it is thought that comparing

the FSI results determined using OSB with results reported in literature would be a good initial indicator of the performance of the tunnel. Other products such as particle board (PB), Douglas-Fir plywood (sanded and non-sanded), and Luan plywood that are also relatively cheaper than red oak are used to further validate and compare FSI results with those reported in literature.

Table 4.3 shows the overall test matrix which summarizes the calibration tests conducted in the Steiner tunnel. The listed inlet draft and gas flow ranges are representative average values based on measurements recorded by the instrumentation for each test. Averages are recorded for the first 5.5 minutes duration of the test, since that is the most critical time for red oak calibration curve (discussed previously in Chapter 2). The conducted tests are analyzed in this section. Further details of the conducted tests are provided in Appendix C, where the recorded test parameters are summarized in tables.

Table 4.3: Overall test matrix for the Steiner tunnel calibration tests

	Cement Board	Red Oak	OSB	PB	DF Plywood	Luan Plywood
# of Tests	19	4	28	20	8	3
DPT Range (in-WC)	0.099 - 0.110	0.096 - 0.110	0.064 - 0.180	0.067 - 0.160	0.068 - 0.153	0.091 - 0.114
Gas Range (m^o3/hr)	6.91 - 8.05	6.04 - 7.64	5.71 - 7.86	7.53 - 8.14	7.52 - 8.10	8.0 - 8.02
Amb. Temp. (^{o}C)	22.4 - 25.6	19.9 - 26.0	6.0 - 26.0	19.3 - 27.2	18.0 - 26.0	21.9 - 23.9
FSI Range	0	59.0 - 96.7	62.5 - 223.4	75.0 - 140.3	32.8 - 116.5	65.3 - 89.2

From a review of the literature Section 2.5.3, as well as the preliminary tunnel tests outlined above, 21 parameters that affect both flame spread and smoke measurements in the tunnel are identified. These include parameters that relate to the tunnel control and operation, as well as to the condition of the test sample itself. Of these, values of 6 parameters – average draft, average gas flow rate, sample moisture content, ambient temperature and relative humidity and the outside wind speed – are varied across different ranges in the pre-calibration test series. In addition, fan control and damper position are included in the characterization study since they are also anticipated to have a significant impact on tunnel measurements. Before outlining the results for any one parameter in detail, it is of interest to compare the relative standard deviation (% Var) in measured flame spread values across all of the tests as these six parameters are varied through their specified ranges shown in Table 4.3. Results are plotted in Figure 4.11.[1] It can be seen

[1]The FSI for the 78 calibration tests is compared for each of the parameters, while keeping other relevant parameters within 10 % variance.

that the four parameters related to the tunnel operation and apparatus listed below have a more significant impact on measured value of FSI than did those related to the properties of the test sample or the ambient conditions.

- Gas Flow
- Fan Control
- Draft Pressure
- Damper Position/Design

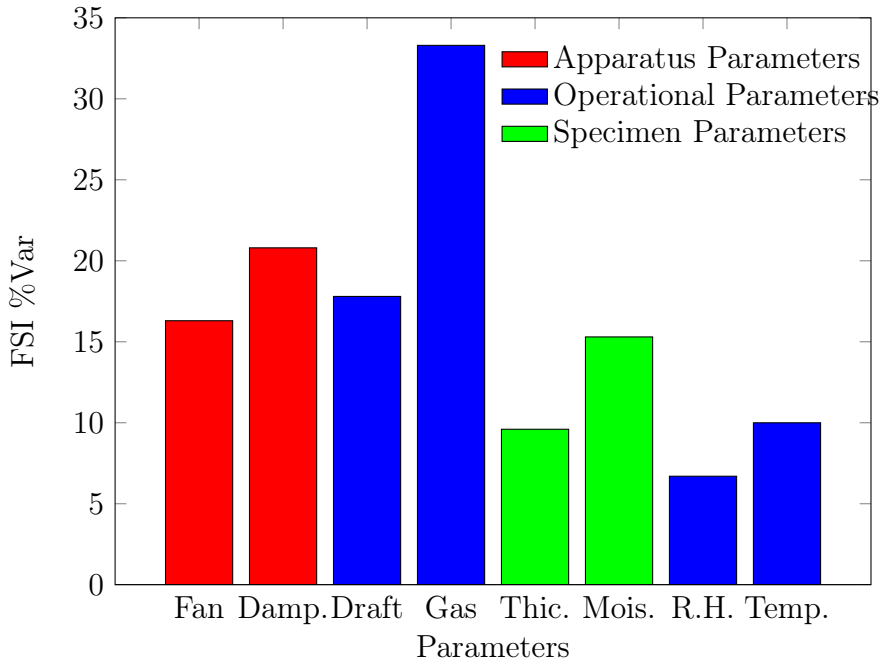

Figure 4.11: Comparison of flame spread variance for a set of affecting parameters

Since fan control, as an apparatus parameter, is mainly used to regulate the draft pressure in the tunnel, these two parameters will be discussed as a single parameter under 'Tunnel Draft'. Therefore, details of the impact of three main parameters on tunnel results, are outlined in Sections 4.5.1 through 4.5.4.

4.5.1 Effect of Gas Flow on FSI

Based on earlier discussions in Chapter 2, individual Steiner tunnel facilities will operate on natural gas from street supply, while others may operate on bottled gas. Since the UW

Steiner tunnel operates on street supply, gas flow variations which influence the FSI results are noticed throughout the measurements.

The operational uncertainty associated with the gas flow measurements is determined using the average gas flows recorded during the calibration tests under identical conditions. There are a total of 20 pre-calibration tests (Test # 41-61) conducted under the same conditions described in Table 4.4, where the shut-off valve is kept fully open, allowing maximum gas supply from the city and the safety controls system.

Table 4.4 illustrates some of the average values of gas flow recorded on different test days. Each value is an average taken over the first 5.5 minutes of the calibration tests. When gas flow is measured during a period when ambient temperatures lay within the range specified by the ASTM E84 Standard Test Method [1], the average gas flow is considered independent of the ambient temperature. Averages range anywhere between 7.57 m^3/hr and 8.10 m^3/hr (Table 4.4) and the standard deviation in gas flow is calculated to be $\pm$0.20 m^3/hr, or 2.5 %. For instance, from Table 4.4, on a given test day, the ambient temperature recorded would be 24^{o}C and the gas flow measured is 7.94 m^3/hr, while on another day the ambient temperature is 21.6^{o}C and the measured gas flow is higher at 8.02 m^3/hr, and vice-versa on other testing days. These day-to-day variations in average gas flows from the city supply could not be explained, other than the fact that neighbouring facilities might be using the same gas line.

Table 4.4: Average gas flows reported for various tests at fully open shut-off valve

Test Day	Test Number	Average Gas Flow	Ambient Temperature
21 Jun 2014	42	7.94 m^3/hr	24.0^{0}C
23 Jun 2014	43	8.02 m^3/hr	21.6^{0}C
24 Jun 2014	45	8.10 m^3/hr	24.3^{0}C
03 Jul 2014	53	7.57 m^3/hr	19.3^{0}C
10 Jul 2014	56	7.86 m^3/hr	22.6^{0}C

It is then decided to monitor the measured gas flow across a wider range of ambient temperature conditions. Figure 4.12 contains measured average values of gas flow and gas temperature for all the 'pre-calibration' tests conducted on OSB as listed in Table 4.3. For all of the tests, the gas flow shut-off valve is kept fully open and the average gas temperature is recorded at the gas thermocouple (Gas TC) located in the gas train (see Figure 3.21). The trend in average gas flow with gas temperature shown in Figure 4.12 can be approximated with a linear fit, although more tests are suggested in order to more accurately represent

[1] Between 18.6 - 26.0^{0}C

the relationship between the average gas flow and average gas temperature. For gas temperatures lower than 18^{o}C, the gas flow starts to decrease significantly (more than 10%). For gas temperatures higher than 23^{o}C, higher gas flows are recorded with less variation in the flow.

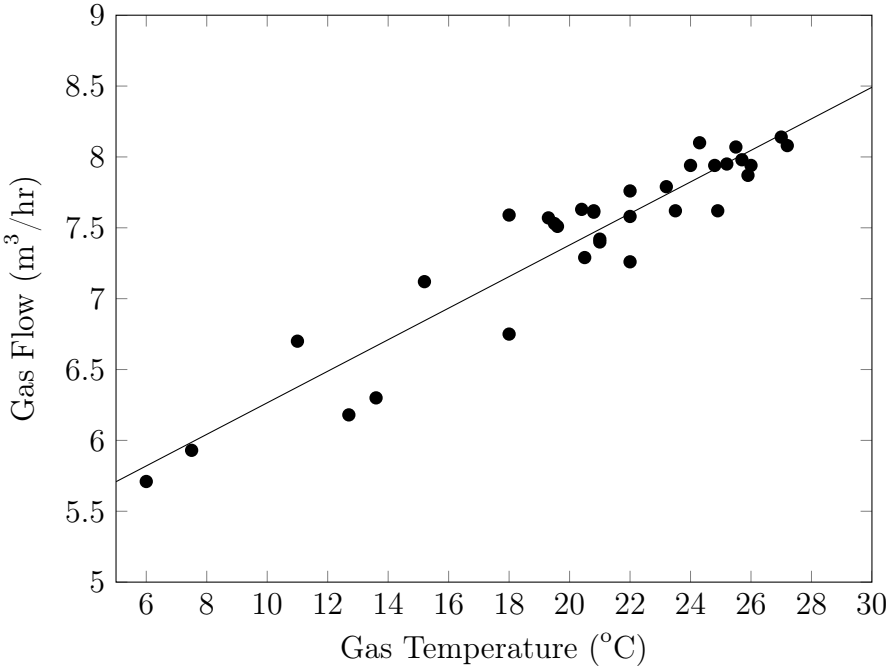

Figure 4.12: Average gas flow and temperature relationship for the UW Steiner tunnel

In contrast to the results shown in Figure 4.12, studies experimented with measured values of volumetric flow of common gases across temperature ranges between -40 and 100^{o}C concluded that temperature only affects the flow within ±11-12% [73]. This further leads one to believe that the most valid explanation for the drop in gas flow to UWFRL when ambient temperature is colder (Figure 4.12) would be a higher gas demand in the local region, thus restricting the flow of gas to the facility.

Groah [45] conducted Steiner tunnel experiments on particle board where he varied the gas flow by 9 % and determined that the difference between average FSI values was 15 %. For the present study, Figure 4.13 shows measured values of FSI as a function of inlet gas flow rate. The results can be represented with a quadratic fit, where the slope of the curve approaches zero past 7.2 m^3/hr. The value of FSI starts to be affected when the gas flow rate to the burner drops below about 7.0 m^3/hr. Overall, for average gas flow rates that vary between 5.5 - 7.76 m^3/hr (30% variation), the FSI results vary between 100 and

[1]These tests are selected comparisons where the operational and specimen parameters are kept within 10 % variance.

225 for OSB, where the FSI is reduced on average in value by almost 40% from highest to lowest gas flow rate used.[1] In general, a 10% decrease in average gas flow rate results in a decrease in measured FSI of more than 15%. It should also be noted that the FSI results are not consistent across different classes of materials with respect to their variation as the inlet gas flow is changed so results from similar series of tests would have to be compared to determine the impact of gas flow on FSI results for other products. This is beyond the scope of the present study.

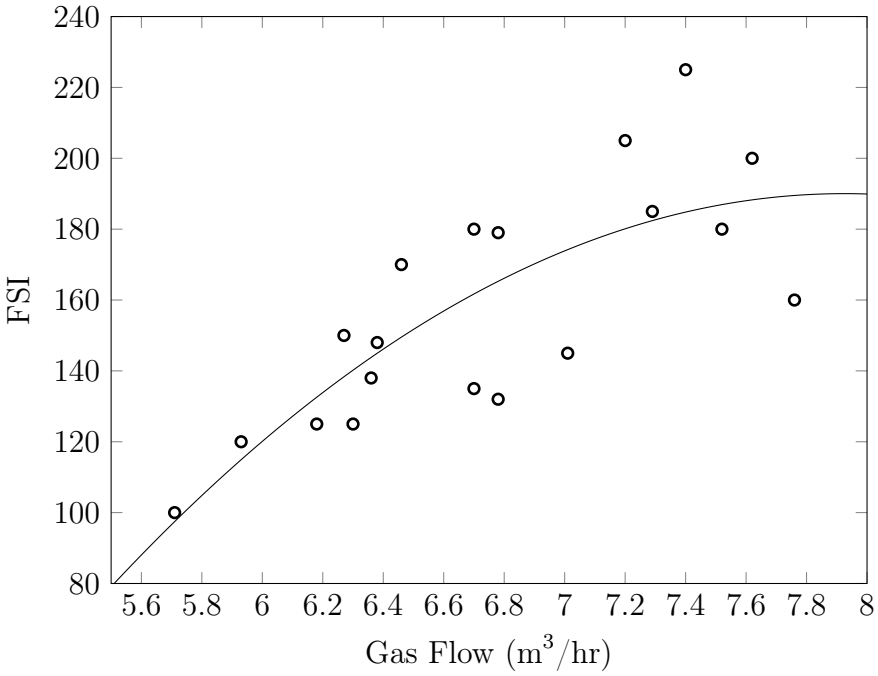

Figure 4.13: Gas flow effect on FSI for OSB tests

Based on the results discussed above, the effect of gas flow on Steiner tunnel FSI values can be controlled to some degree since it is dependent on the ambient temperature conditions of the large scale testing lab. Figure 4.13 suggests that FSI results for OSB are only affected when gas flow starts to drop below 7.0 m^3/hr which occurs when the ambient temperature falls to less than 18^{o}C. For average gas flow rates greater than 7.0 m^3/hr, FSI are less affected by the ambient temperature so variations in results seen in Figure 4.13 for the higher gas flows are most likely caused by other parameters, as discussed in the following sections.

4.5.2 Effect of Tunnel Draft

Control of the exhaust fan during a Steiner tunnel test is required to provide constant draft pressure in the tunnel for the duration of the test. Through this, enough oxygen should be provided to the burners to sustain constant progression of flame spread down the length

of the sample. On the other hand, sudden changes in draft pressure may instantaneously retard progression of the flame either because not enough air is supplied to the specimen to sustain flame spread, or because an excessive amount of air is supplied, simultaneously cooling down the hot gases to the point where heat transfer to the unburnt sample is affected and the flame progression is also delayed. Due to the importance of maintaining a constant draft pressure in the tunnel, then, a series of characterization tests are undertaken to characterize the flow through the tunnel, and hence define the impact of variations in draft pressure on values of FSI measured in the new UW Steiner tunnel. An additional series of tests is conducted to further understand operation of the tunnel under different conditions of ambient wind as well. The initial results led to further studies to characterize draft pressure in the tunnel when the speed of the main tunnel exhaust fan is manually controlled throughout a test. In this section, results of various sets of pre-calibration tests are used to illustrate the impact of draft pressure on FSI results in the present tunnel, and thus help to understand the implications of changing tunnel draft pressure in terms of ongoing operation of the apparatus.

Four tests are conducted using approximately the same average gas flow rates to the burner (within 5%) but under different conditions of tunnel draft pressure to determine the impact of draft pressure on measured FSI for samples of 3/4-in (19 mm) particle board. The average values of draft pressure and corresponding measured values of FSI are shown in Table 4.5. Usually, the average draft pressure in the Steiner tunnel prior to conducting a test is adjusted to 0.099 in-WC. During the test, the tunnel draft is then adjusted manually, either through manually controlling the fan speed or physically adjusting the near damper plate position. Two of the tests are conducted for average draft pressures lower than the pre-set average value of 0.099 in-WC; lower values of FSI are recorded in both cases. For the extremely high draft pressure (0.16 in-WC), the recorded flame spread is again reduced, in this case to a value low enough that the material would be classified into 'Class B' instead of the expected rating of 'Class C' that is known for particle board.

Table 4.5: The tunnel draft effect on FSI results for Particle Board

Test Number	DPT	FSI
58	0.081 in-WC	98.6
56	0.090 in-WC	115.2
59	0.101 in-WC	123.9
13	0.160 in-WC	75.0

Temperature-time profiles measured at the end of the tunnel (TC # 12) during several tests are shown in Figure 4.14. These help to explain the trends in measured FSI for the various values of draft pressure. In Test 58, where the draft pressure is lower than the

target value, the temperature rise and flame progression are similar to those recorded in Tests 56 and 59 for the first 300 seconds of the test. However, due to the low draft in the tunnel during Test 58, a lack of air reaching the burner and flaming sample eventually retards the progress of the flames, resulting in decreasing temperatures at the end of the tunnel for the period 300 s <t <600 s. As a result, the final measured value of FSI is also low. In Test 13, on the other hand, low temperatures are measured at the exit of the tunnel from the beginning of the test because of the high rates of airflow through the tunnel. These kept the tunnel from heating up and also cooled any exhaust gases significantly. The resultant changes in heat transfer local to the burning flame front, and the continual cooling of the sample, the ability of the flames to burn through the depth of the specimen is greatly reduced. Instead, once the flames are established on the specimen, at approximately t = 200 s, they propagate quickly down the surface to the end of the tunnel. The time taken for the flames to reach the end of tunnel, 350 s, results in a FSI of only 75, largely as a result of the slow flame progression during the first 200 seconds of the test. After the flames reach the end of the sample, the tunnel exit plane temperatures continue to grow progressively through the remainder of the test because the established burning is now accelerated due to the availability of air under the high draft conditions.

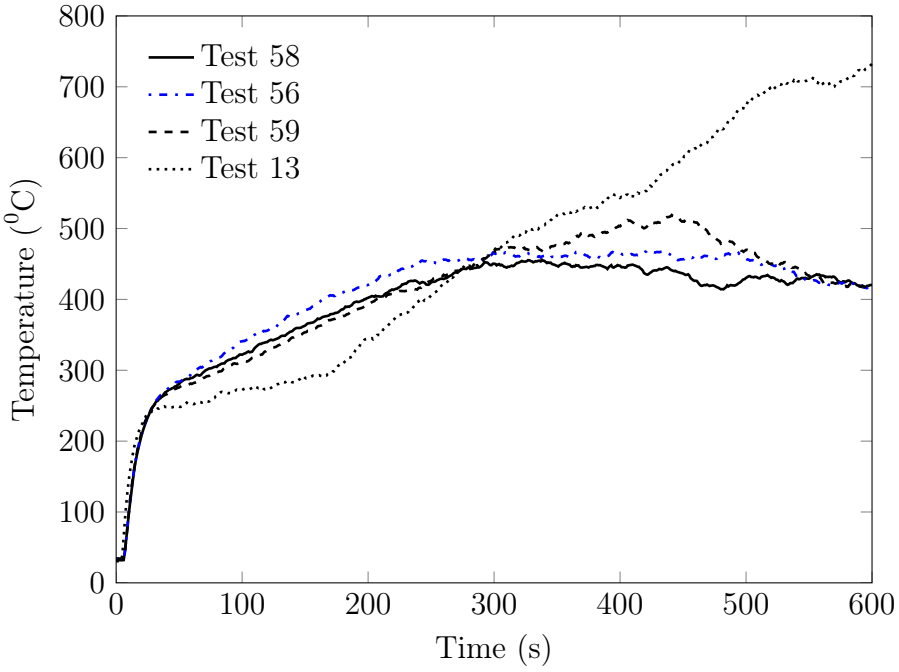

Figure 4.14: Measured temperatures at TC # 12 for tests conducted under various draft pressures for particle board

It should be noted that the tests summarized in Table 4.5 are conducted without fan

control, and that the draft pressure is adjusted intentionally higher or lower than the pre-set average value of 0.099 in-WC in order to demonstrate the effect of draft pressure on FSI. Since the Steiner tunnel is situated in the large scale testing lab, in which the ambient temperature and atmospheric pressure vary according to outside ambient conditions, the tunnel draft may also be affected by changes in the ambient wind conditions outside the tunnel. In particular, a wind generation system, composed of six large fans and a connecting plenum, is located on the right hand side of the Steiner tunnel. An exhaust duct connecting to the roof stack of the small cone lab is connected to the exhaust end of the tunnel. For a number of reasons, these fans and ducts do not have flow dampers or louvres so the outside wind does affect conditions within the large scale testing lab. Very early in this research, these are observed to have an impact on the tunnel draft, and thus the flow and temperature profiles along the length of the tunnel, because the tunnel itself has not been fitted with an automatic inlet air damper system. To better characterize these potential effects, a study is undertaken to look at the effect of wind on the tunnel draft (DPT), temperatures, and air velocity measurements through examination of time resolved measurements collected during the initial pre-heat of the tunnel with a cement board sample in place.

In order to determine the effect of outside wind, the outside wind velocity is measured at the roof stack using an LA Crosse Technology hand held anemometer. Three separate testing days are selected whith average values of wind velocity measured at the roof stack of 1.2 m /s, 2.5 m /s and 3.0 m /s. The tunnel draft and gas flow are adjusted to relatively the same conditions (within 5%) and the impact of the wind on tunnel draft and exit temperature are analyzed. High winds near the exhaust fans in the roof stack are essentially expected to act as if there is a larger area inlet since the overall air pressure would increase.

First, it is important to understand the phenomena of draft pressure changes within the tunnel before and during a Steiner tunnel test, prior to analyzing the impact of outside wind on draft pressure measurements. For this, air inlet draft pressure is recorded at the draft pressure tap (DPT). A typical time trace of draft pressure measurements prior to and during pre-heat of the tunnel is shown in Figure 4.15, with the average air velocity at the end of the tunnel set to 1.2 m/s. This test is conducted on the day when outside wind speeds are recorded to be 2.5 m/s. The corresponding average draft pressure for Figure 4.15 across the measurements is 0.099 in-WC (24.9 Pa). It can be seen that the draft pressure is relatively stable before flame ignition at the burners, but that the pressure decreases sharply as the fuel is ignited (79 s), then levels off to a steadier value within 10 seconds of ignition. These trends indicate that the volume of expanding fire plume gases which is initially formed at the burners, acts somewhat like a physical obstruction to the air flow causing the air draft pressure to momentarily drop until it can restore back to its original operating range. The opposite occurs when the gas burners are shut-off at the end

of the test. The fluctuations in draft pressure in the heated tunnel are significantly higher compared to those in the 'cold' tunnel.[1] This is expected, since the nature and extent of the turbulent burner flames vary greatly with time.

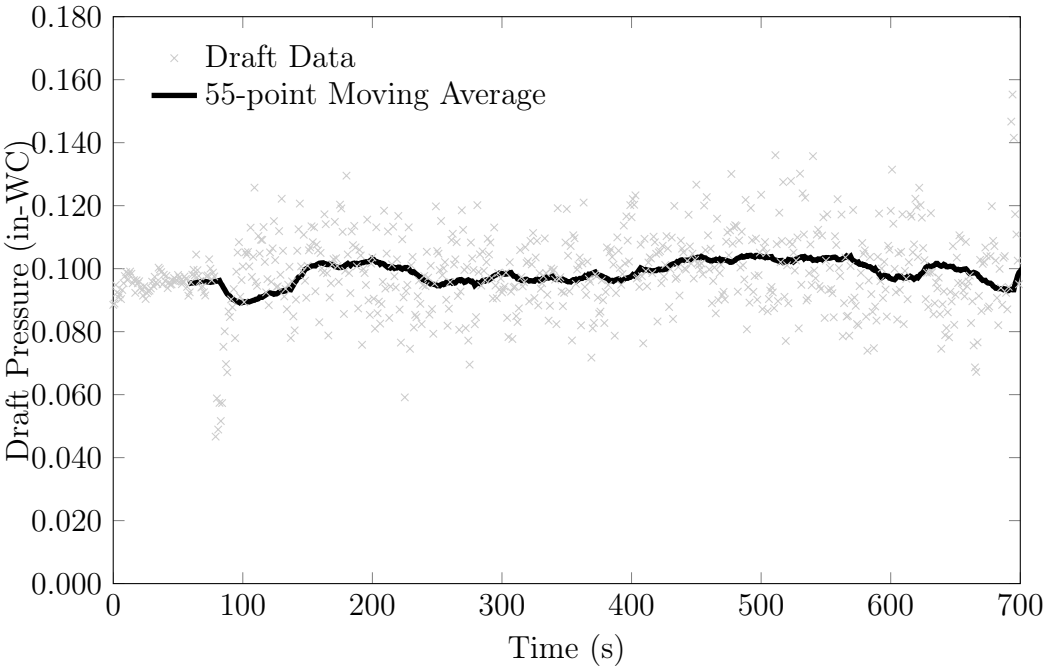

Figure 4.15: Hot-Draft pressure measurements at the air-inlet section of the tunnel

With the above information in hand, the sensitivity of draft pressure readings to changes in ambient wind conditions outside of the lab are also examined, since these will impose an additional level of uncertainty in the overall results. Using the calculation methods from Section 3.5, uncertainty in measured draft pressure due to the impacts of ambient wind is estimated for both 'hot' and 'cold' draft pressure readings. The total uncertainty, ϵ_t, estimated for the 'cold' readings is 15 %, 12 %, and 10 % for outside wind speeds of 3.2 m/s, 2.5 m/s and 1.2 m/s, respectively. For the 'hot' readings, total uncertainty is estimated to be slightly higher at 16 %, 13 %, and 11 %. These results suggest that the outside wind speed does have a marked effect on draft pressure but there is no significant difference in impact on draft pressure between the 'hot' and the 'cold' tunnel conditions. Due to high level of uncertainty among the draft pressure measurements noted above, a method for establishing the time extent over which there is a steady draft pressure in the tunnel is developed with the intent to provide a quantitative measure for 'draft stability' during any given test. For each of the wind speed days listed above (3.2 m/s, 2.5 m/s and

[1] 'Cold' draft refers to those times when the tunnel operates without flames. 'Hot' draft refers to draft pressure during an actual test once the flames are ignited.

1.2 m/s), raw data for 'cold' readings is collected for 2200 s (43.3 min) at the initial tunnel air velocity of 1.2 m/s and an average draft pressure of 0.099 in-WC. A 55-point moving average is then applied to each draft pressure versus time trace (shown in Figure 4.16) in order to damp out high frequency fluctuations in the data. A period of steady draft is then determined, based on examining the slope of the 55 point averaged pressure-time trace curve. The limits on changes in slope are set to 0.002 in-WC/s and -0.002 in-WC (±0.5 Pa/s), selected based on the standard allowance of 2 % variations in air velocity measured at the end of the tunnel [1]. The periods of steady draft for the 3 tests are summarized in Table 4.6.

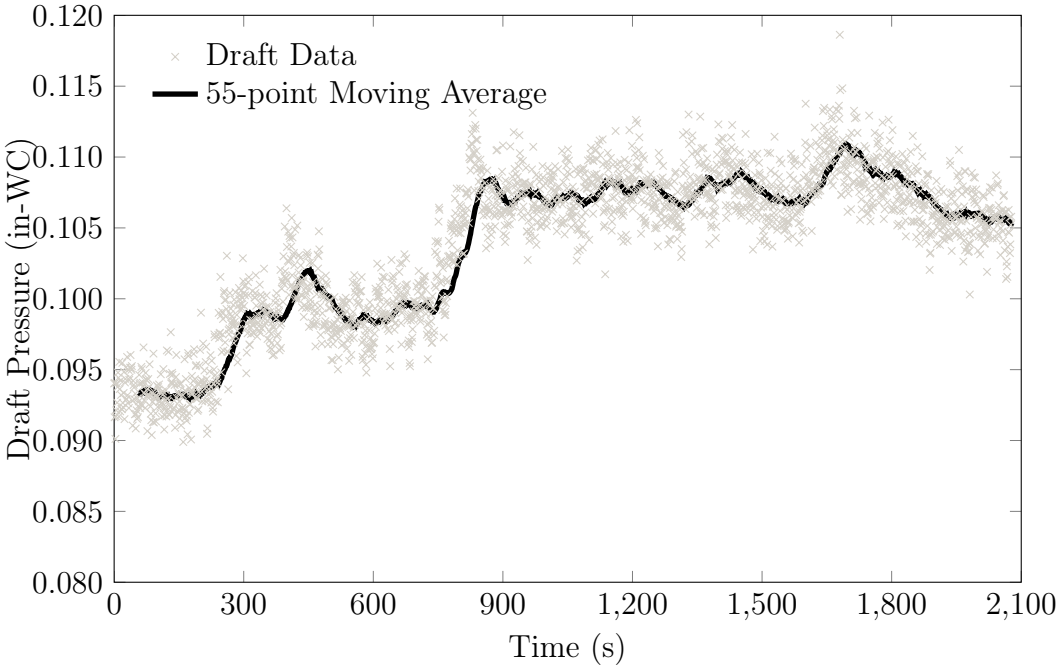

Figure 4.16: Cold-Draft pressure measurements at the air-inlet section of the tunnel

Table 4.6: Duration of steady draft for 'cold' draft pressure readings

Wind Speed	Total Test Length	Duration of Steady Draft
1.2 m/s	2600 s	331 s
2.5 m/s	2600 s	83 s
3.2 m/s	2600 s	79 s

Results in Table 4.6 suggest that instability of the draft pressure even during cold air purging of the tunnel prior to a test is significant. Even for tests at lower outside wind speeds, the draft is only stable for 331 s out of the total 2600 s, with this duration decreasing

to 79 in the case with a 3.2 m/s wind. Clearly stability of draft pressure in the tunnel is extremely sensitive to the level of ambient wind, suggesting that it may be necessary to define ambient conditions under which tunnel operation might need to be limited.

The next step in commissioning the tunnel is to analyze the impact of the outside wind on the temperatures developed in the tunnel during testing. This is of particular interest due to the sensitivity of the draft pressure to ambient winds discussed in the previous paragraphs. For reference, a typical time trace of temperatures measured along the mid-height of the tunnel on a day with low ambient wind velocities is presented in Figure 4.17. In this plot are shown measured values of temperature from thermocouples TC # 1-9, and the thermocouple located 1-in (25.4 mm) below the specimen, TC # 12. Time t=0 s is defined as the instant when gas is enabled to the burner ports. Each individual time trace of temperature is characterized by an initial sharp increase in temperature after the burner is ignited, followed by a more gradual increase in temperature lasting until t=150-200 s after ignition (Figure 4.17). Following this, temperatures level off to steadier values.

High temperatures (around 700^0C) are measured at the first thermocouple (TC # 1), at x = 1.0 ft (0.305 m), indicating the approximate location of the hot combustion zone of the fire. As expected, temperatures measured by thermocouples TC # 3 to TC # 9 decrease in value, indicating that the flow in the tunnel cools from the burner down the length of the tunnel as the flames and hot gases entrained additional air with distance downstream. The temperatures measured at TC # 12 are typically higher than the corresponding temperatures measured from TC # 3 through TC # 9 because TC # 12 is at a higher elevation into the bricks than the rest of the thermocouples (refer back to Figure 3.21) so it is much closer to the heated tunnel test section. Overall, these results suggest that the overall heat released from the fire into the tunnel is relatively steady, at least during this test, with little effect of the low outside wind velocities.

In contrast, it is evident that higher outside wind velocities did affect the steadiness of the flow inside the tunnel. For instance, in Figure 4.18, where the outside winds average 3.2 m/s, thermocouple TC # 3 experiences a sudden spike in temperature right before the middle of the test (200 s <t <300), followed by a subsequent decrease in temperature (300 s <t <350 s). This spike reoccurs once again near the end of the test around t=400 s. Although difficult to discern due to the legend on the plot, the subsequent decrease in temperature between 300 s <t <350 s is also observed in thermocouples situated downstream in the tunnel (TC # 6 - 8). These sudden spikes are not as evident at lower wind speeds (Figure 4.17). The temperature near the burner (TC # 1) remains relatively constant so can be ruled out as a potential source of the variation; as such, it is not included in the figures.

The sensitivity of the time-temperature fluctuations due to effects of the outside wind

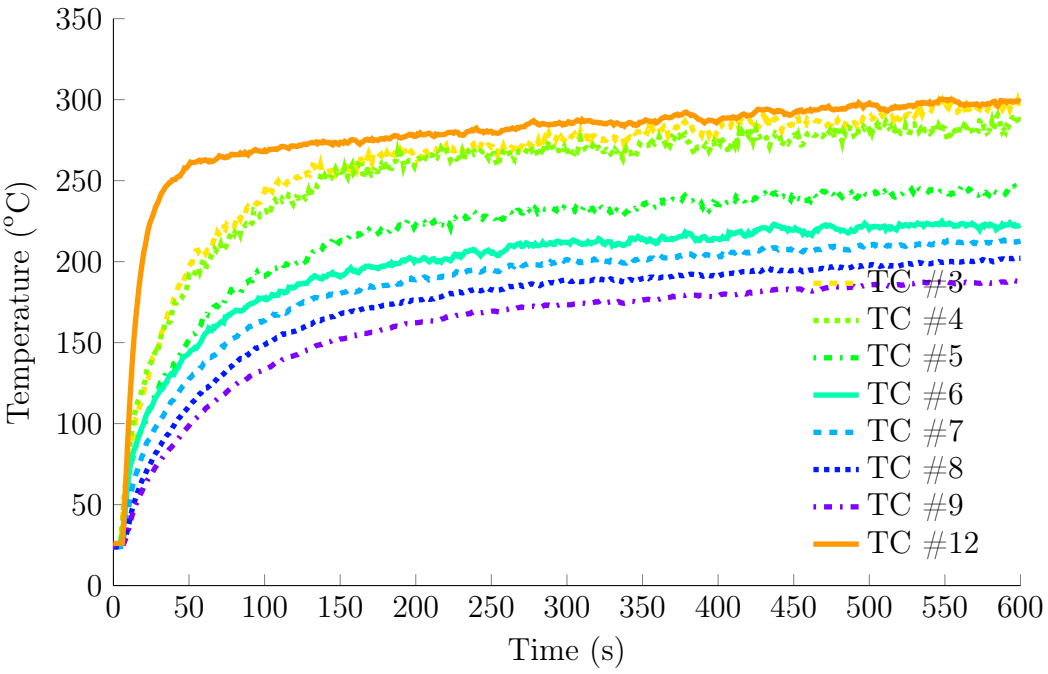

Figure 4.17: Typical time-temperature curves at steady conditions, outside wind 1.2 m/s

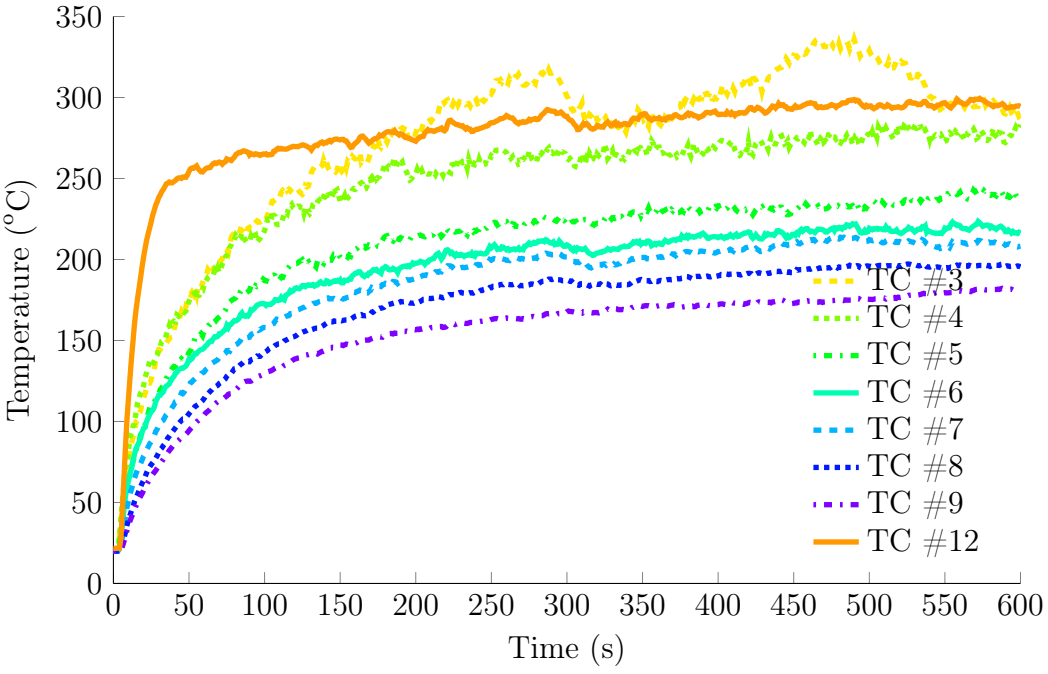

Figure 4.18: Typical time-temperature curves at unsteady conditions, outside wind 3.2 m/s

Table 4.7: Temperature variations in the tunnel at different wind speeds

	Wind 1.2 m/s	Wind 2.5 m/s	Wind 3.2 m/s
TC 1	1.2 %	2.1 %	2.2 %
TC 3	4.2 %	4.4 %	8.6 %
TC 4	4.1 %	5.4 %	5.8 %
TC 5	5.1 %	6.0 %	6.2 %
TC 6	5.3 %	5.7 %	6.2 %
TC 7	5.6 %	6.2 %	7.2 %
TC 8	6.2 %	7.4 %	7.7 %
TC 9	7.3 %	8.3 %	8.0 %
TC 12	2.8 %	2.7 %	3.2 %

is examined by calculating the relative standard deviation of the time averaged values of each thermocouple measurement under the 3 different wind conditions. The gas flow to the burner initially takes time to level out to its maximum adjusted flow. The time taken to reach this period is averaged across 43 'pre-heat' tests, and the average time is calculated to be 83 s. This is consistent with the time at which the temperatures start to approximately level off in Figures 4.17 and 4.18. For each time temperature trace, average temperature is calculated between 83 s <t <600 s.

Table 4.7 summarizes the relative standard deviation of each of the averaged thermocouple temperatures by varying the outside wind velocity between 1.2 and 3.2 m/s. The temperatures are found to fluctuate up to 8.6% for outside wind velocity of 3.2 m/s, with greater percent variations in general occurring for thermocouple positions further from the burner where the gas temperatures are lower. One exception is TC # 3, situated at x = 6.33 ft (1.93 m), which records the highest variation, from 4.2% to 8.6%. The thermocouple that is used for setting the time-temperature calibration curve for red oak and cement board (TC # 12) is within 5% across all wind speeds investigated. For most of the thermocouple measurements, the temperature fluctuations are the lowest at a wind speed of 1.2 m/s, with an average increase in variation of 0.71% between wind speeds of 1.2 m/s to 3.2 m/s.

The air velocity measurements are also affected by changes in the wind conditions outside the main test area. This is evident through the air velocity measurements at the end of the tunnel. One way to quantify this impact is to measure the average air velocity at the end of the tunnel for several trials in order to obtain a reasonable estimate of the variation caused by outside conditions. The average air velocity is measured by inserting the velocity probe through the tunnel cross section at 10 different instances. Figure 4.19

contains corresponding plots of average velocities measured at the end of the tunnel when outside wind speeds are recorded to be 1.2 m/s, 2.5 m/s and 3.2 m/s. For outside wind speeds of 3.2 m/s, the average air velocity at the end of the tunnel drifted up to 0.12 m/s from the required 1.2 m/s, a change of 10%.

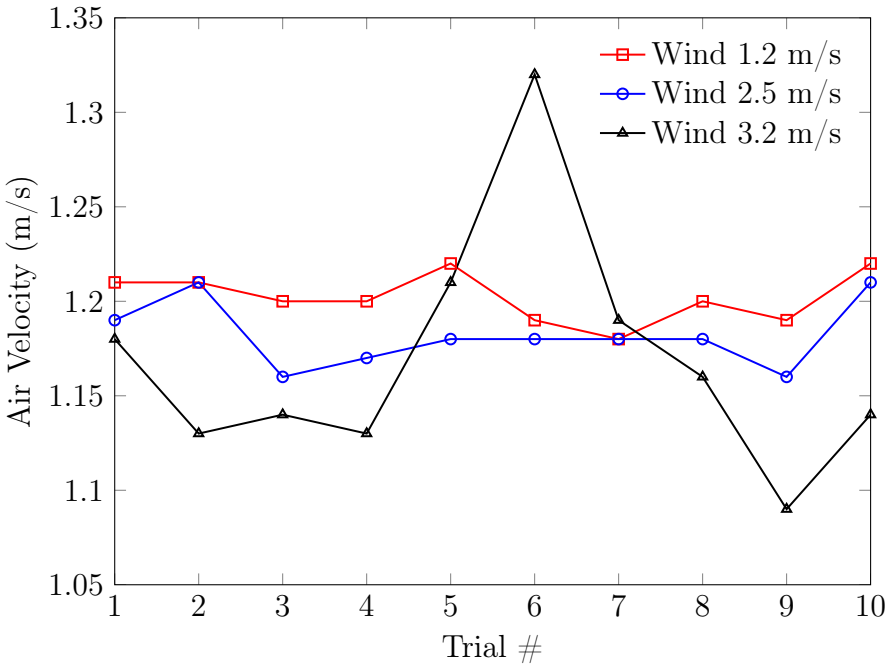

Figure 4.19: Air velocity averages at the end of the tunnel with different outside wind speeds

The temperature and tunnel velocity measurement fluctuations discussed above arise in part because there is no automatic inlet damper control on the Steiner tunnel. On the other hand, the main fan control in the small cone lab can be manually controlled during a test to reduce the effect of outside wind. Therefore, a test is conducted on a day with 3.2 m/s winds. A long VGA extension cord is run from the data acquisition laptop to a monitor situated in the small cone lab. A second operator then monitors the running average value of draft pressure in the tunnel and adjusts the fan speed to maintain the draft at the value set prior to the test when airflow adjustments are made during pre-heat, throughout the duration of the test. The variations in average temperatures measured for all the thermocouples for the test with no manual fan control (Table 4.7) are reduced by 1.48% and 0.52% on average when the fan is controlled, for wind speeds of 3.2 m/s and 2.5 m/s respectively. These results suggest that fan control could be utilized for the Steiner tunnel to minimize the effect of outside winds on the tunnel operation.

Based on the results discussed above, a series of tests are conducted in which the main

exhaust fan is manually controlled to minimize or eliminate the influence of outside winds on draft pressures in the tunnel. Implementing such fan control throughout the duration of a test should stabilize the draft pressure within the tunnel. A typical time trace of draft pressure measurements for Steiner tunnel tests in which the fan is controlled and is non-controlled are shown in Figure 4.20. The plots clearly show that there are lower levels of fluctuation in the 55 point moving averaged values of draft pressure when fan control is utilized during a test. Given the similarity in shape of the moving average curves between these plots and the one in Figure 4.15 for the 'hot' draft measurements using cement board, the technique used earlier to measure the 'steady draft' pressure discussed is considered appropriate for the present tests as well. Table 4.8 lists the duration of steady draft for particle board tests conducted under test with controlled and non-controlled fan operation, as well as the measured FSI for each test. The table shows that the values of FSI determined during tests for which the fan is controlled are higher than those for situations in which the fan is not controlled. This is partly due to wind effects being minimized, which increased the duration of steady draft pressure for the cases with fan control. The results in Table 4.8 indicate that use of manual control of the fan can lead to increases in measured values of FSI of 9%, while the period of steady draft can also be increased by 18 seconds on average.

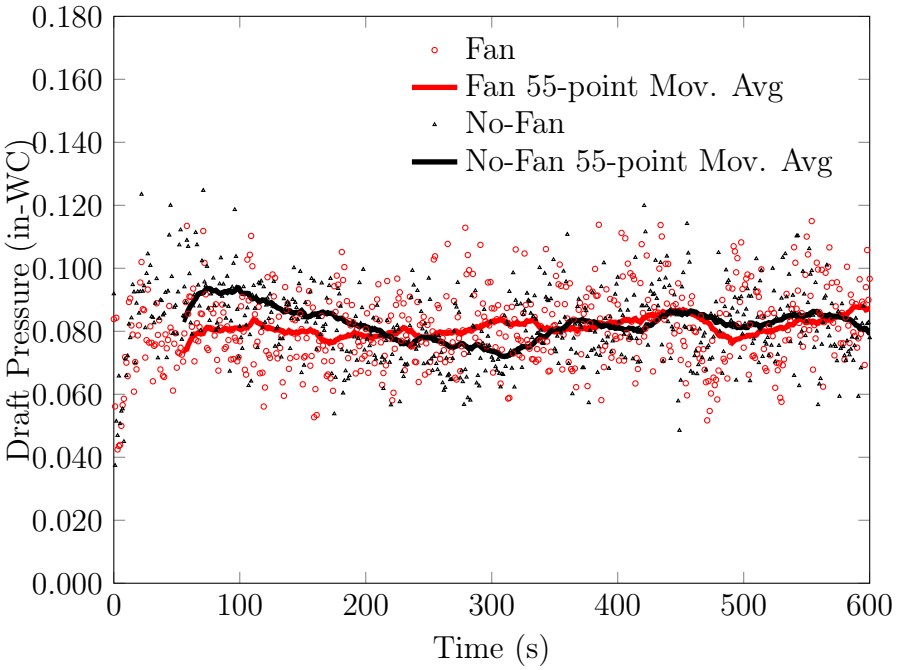

Figure 4.20: 'Fan' control versus 'No Fan' control test conducted on OSB

As a final step in determining the most appropriate draft pressure conditions to use

Table 4.8: Steady draft and flame spread when utilizing fan control

Tests	FSI	Duration of Steady Draft
0.090 in-WC (Particle Board)		
Fan Control	115.2	44 s
No-Fan Control	109.2	18 s
0.095 in-WC (Particle Board)		
Fan Control	130.0	38 s
No-Fan Control	124.6	17 s
0.105 in-WC (Particle Board)		
Fan Control	123.9	28 s
No-Fan Control	103.6	21 s

for testing particle board in the Steiner tunnel, the measured flame spread results are compared to values reported in the literature [63]. Since on average the literature suggests a FSI of 145, an average draft pressure of between 0.090 and 0.110 in-WC (22.4 - 27.4 Pa) would seem appropriate.

To further investigate whether this this value of draft pressure is appropriate for operation of the tunnel, measured FSI values for particle board and three other wood products are compared to flame spread indices reported in the literature as tabulated in Table 4.9 [67, 74, 63]. Measured flame spread indices from a total of 16 tests from Table 4.3 including 8 particle board tests are used. Although all of the tests are run with average gas flow rates within a 5% range, they exhibit a wide range of measured flame spread indices due to differences in tunnel draft pressure across the various tests. To assess the impact of the differing draft pressures, therefore, the measured values of FSI are divided by the values in Table 4.9 and are plotted against the average value of draft pressure for the corresponding test in Figure 4.21.

Table 4.9: FSI reported from literature for the tested wood products

Material	FSI from Literature
3/8 in DF Rough	90
1/4 in DF Sanded	150
13/64 in Luan Ply	120
Particle Board	145

It can be seen from the plot that for several of the tests chosen, the inlet draft pressure is significantly higher than the average draft pressure (0.099 in-WC), while in a few others

it is lower. In both cases, measured values of FSI are significantly lower than those reported in the literature. Therefore, the clustering of higher points on Figure 4.21 suggests that testing with the average draft pressure in the range between 0.090 - 0.110 in-WC (22.4 - 27.4 Pa) appears most appropriate for the present tunnel configuration.[1]

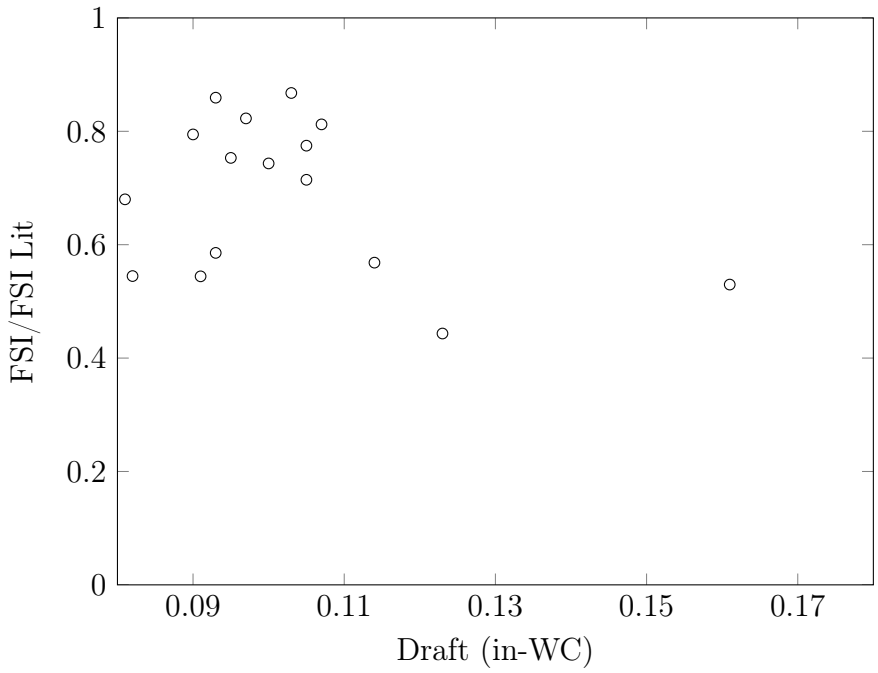

Figure 4.21: Influence of draft pressure on FSI

Even at these draft pressures, however, the highest measured FSI values in the Figure are still only 80-90% of the values reported in literature ($FSI/FSI_Lit<1$). Since the gas flow is held constant in these tests, this suggests that additional tunnel operating parameters are still impacting measured FSI values; however, due to the inherent variability in FSI across OSB and particle board seen in the literature, a series of red oak calibration tests are run to further troubleshoot the source of the inconsistency. These for the subject of the next section.

4.5.3 Initial Red Oak Calibration Tests

One of the final stages of testing the operation of any Steiner tunnel apparatus includes calibration tests utilizing red oak samples, following specific calibration procedures outlined in the ASTM E84 Standard Test Method [1]. To better troubleshoot the issues noted above

[1] 0.090 - 0.110 in-WC (22.4 - 27.4 Pa) will be referred to as the 'mid-point range' for the remaining sections.

Table 4.10: Summary of the 3 red oak calibration tests

	Test 39	Test 40	Test 41
Average Draft (in-WC)	0.110	0.102	0.103
Gas Flow Average (m^3/hr)	6.04	7.22	7.39
MC %	6.81	6.55	7.48
Ambient Temperature (^{0}C)	19.9	26.0	23.5
Relative Humidity (%)	64	57	50
FSI	59.0	68.9	63.5
TSO (%)	6.07	9.91	8.22

with present apparatus therefore, three red oak calibration tests are conducted using the near damper for flow control.

Table 4.10 summarizes the results for the 3 tests. The initial test utilizes the gas flow rate that is found to give good repeatable results in Section 4.4, but this is varied in subsequent tests in attempts to obtain better agreement with Steiner tunnel calibration curves reported in the ASTM E84 Standard[1] and the ULC fire testing lab [6]. The average draft pressure is held relatively constant across the tests. The flame spread recorded in the first test (Test 39) is fairly low and flames do not reach the end of the tunnel. In the next test (Test 40), the gas flow is increased, and the results are more promising, since the flame spreads closer to the end of the tunnel (FSI = 68.9). However the improvement in results does not continue with further increase in gas flow (Test 41), so there is clearly a point past which increasing gas flow no longer improves the results in the current tunnel.

To further understand the observed behaviour, the flame spread and smoke obscuration versus time curves for red oak are compared with the curves from ULC and ASTM E84 in Figures 4.22 and 4.23, respectively. The ULC curves are reproduced from a red oak calibration test conducted in 2013; provided by ULC fire testing engineers [6]. The ASTM E84 curve is reproduced from the standard representative plots provided in the ASTM E84 standard [1]. Curves from all these tests indicate the close relationship between the smoke measurements and flame spread that was noted earlier. Higher peaks of smoke are observed for tests having a higher flame spread, particularly in the early stages of the test (0 s $<$300 s).

Comparing the flame spread curves in Figure 4.22, the time evolution of flame propagation in the current tests closely follows that seen in the both ULC and ASTM results for the first 150 seconds, which corresponds to 10 - 11 ft of flame propagation down the tunnel. Early in the test, the rate of propagation is within 10% across all tests. After this time, the flame continues to propagate further down the tunnels in both the ULC

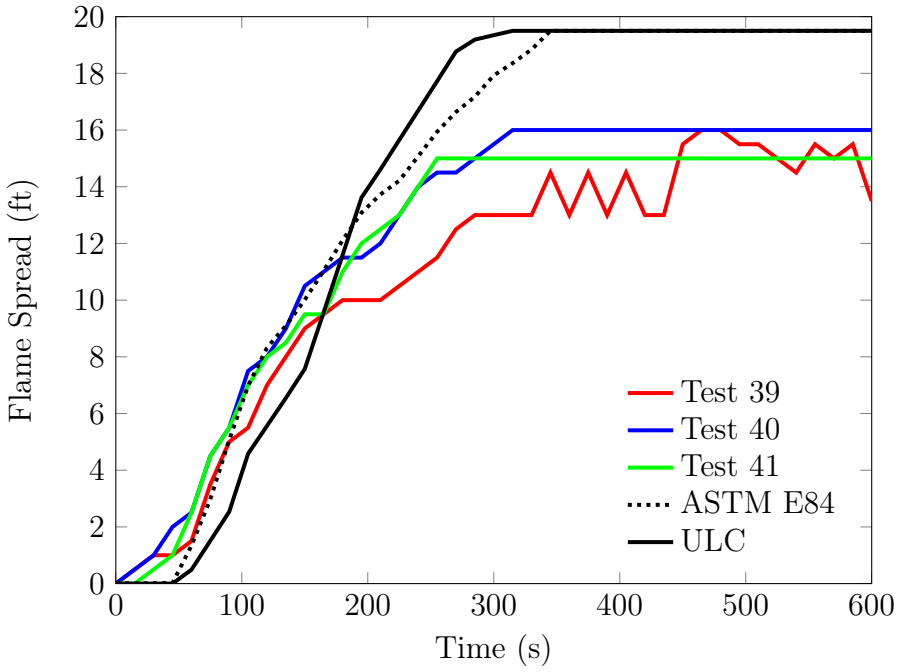

Figure 4.22: Comparison of red oak flame spread curves with those from certified testing labs when utilizing the near damper

and ASTM tests, with a slightly faster rate of propagation, 315 seconds to reach the end of the tunnel in contrast to 332 seconds for the ASTM test, in the ULC test results due to the higher average gas flow that is presented on the ULC test sheet [6]. In contrast for the present tests, the flame front appears to stall at a distance of approximately 16 ft down the tunnel. It is interesting to note that if, instead of stalling, the flame continues to propagate down the present tunnel at the same rate, it would reach the end of the tunnel in 322 seconds and the tunnel would satisfy the requirements of red oak calibration. Unfortunately, this is not the case in these tests so the cause for the truncated flame propagation have to be identified and corrected before the tunnel is deemed 'operational'.

In contrast to the differences in FSI between the ASTM and present red oak calibration test results, the smoke density results contained in Figure 4.23 suggest that the evolution of smoke obscuration with time in the current tests agrees fairly well with that shown in the ASTM E84 smoke curve. The average total area under the curve (TSO %) in the present tests only varied by 1.92 % with respect to the ASTM E84 curve. Neither the ASTM or present results agree well with the high smoke obscuration measured in the ULC tunnel test, but that can again be attributed to the higher average gas flow in that test [6].

From this series of FSI and smoke density tests, since the draft is constant and gas flow to the burner is not sufficient to correct the issues with flame propagation to the end of the

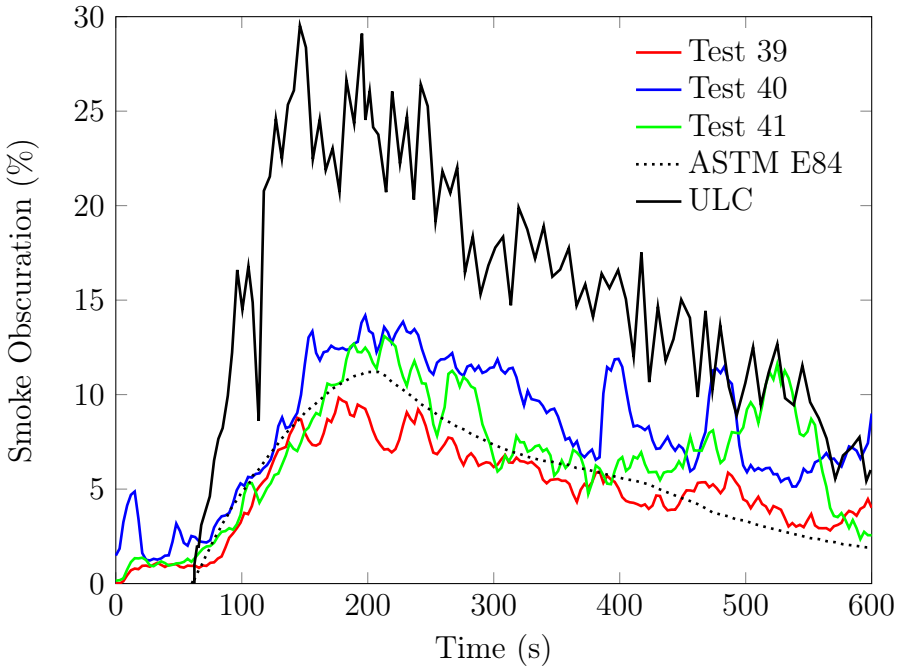

Figure 4.23: Comparison of red oak smoke obscuration curves with those from certified testing labs when utilizing the near damper

tunnel, it is evident that factors additional to those discussed in Sections 4.5.1 and 4.5.2 are preventing the flames from reaching the end of the current tunnel. One such potential contributing factor is moisture content of the samples under test. The oak used for both Tests 39 and 40 was conditioned for 6 months prior to testing, so the moisture content (MC% in Table 4.10) is slightly on the low side of the ASTM specified range.[1] Use of drier wood would normally increase the values of FSI, however, this is not thought to be a main reason for the differences seen here. For Test 41, the oak samples are assembled as soon as they are purchased and are only conditioned for 3 days prior to conducting the test. Thus, the MC of 7.48 % is on the high end of the range. In this case, FSI would decrease and may be at least part of the reason for the differences seen. However, this is not the case since the FSI for Test 41 is 63.5, having a higher MC than Test 39 (MC% - 6.81), and only recording an FSI of 59. Similarly then, the small differences in moisture content of the oak across these tests is not sufficient to explain the discrepancies in results. Therefore, it is deduced that the issues centered around the impact of the near damper on overall flow conditions within the tunnel testing chamber. Investigation of these effects is the subject of the next section.

[1]The red oak decks are to be conditioned at MC of 7% ±0.5% according to ASTM E84 [1].

4.5.4 Effect of Damper Position

In order to determine how the location of the damper and position of the damper plate are affecting the flame spread, tests are run to examine the measured values of FSI and SDI obtained when the tunnel flow conditions are adjusted using dampers located at two different positions in the duct. Since calculation of SDI requires a minimum of 5 red oak calibration tests to obtain a running average, the total smoke obscuration (TSO) is used here instead. The time-temperature curve at the end of the tunnel (TC # 12) is further used as an indicator of tunnel performance since TC # 12 is one of the main instruments used for calibrating the tunnel with red oak. The two situations that are investigated in this portion of the study are 1) control of tunnel flow using the near damper (briefly described in Section 3.1.1), and 2) control of tunnel flow using a new far damper, placed further downstream from the tunnel end (Section 3.1.2). For this, a set of four pre-calibration tests run with the damper inclined to achieve a draft pressure within the 'mid-point range' are selected as outlined in Table 4.11. In these, the average gas flow and draft pressures are within 5% in comparative tests involving the near and far dampers, thus isolating the effect of damper position on flame spread in the tunnel.[1] Based on previous discussions from Chapter 2, smoke development is highly interlinked with flame spread, therefore values of FSI and TSO are calculated for both OSB and particle board samples according to Equations 2.1a and 2.14) and summarized in Table 4.12 for all tests.

From Table 4.12, it can be seen in general that measured values of flame spread are higher for tests conducted with tunnel flow controlled via the far damper. Furthermore, values of FSI with the far damper system fall within the range of values reported in the literature for both OSB and particle board [63, 64, 65, 66]. As such, these values are taken as the reference in the following discussion of why the damper position and orientation has such an impact on measurement of fire performance characteristics in the present tunnel.

Table 4.11: Pre-calibration tests used for comparison

	Near Damper	Far Damper
OSB-A	Test 22	Test 26
OSB-B	Test 62	Test 28
OSB-C	Test 63	Test 29
PB	Test 54	Test 64

Decreases of 25% and 21% in FSI and TSO for OSB, and 11% and 61% for particle board, are seen when air flow is adjusted using the near damper instead of the far damper. This can be explained by combined effects of the location and opening position of the near

[1] Test 22 is slightly lower than the 'mid-point range' at 0.088 in-WC.

Table 4.12: FSI and TSO measured from pre-calibration tests conducted on OSB and particle board (PB)

Damper Position	OSB-A	OSB-B	OSB-C	PB
Near Damper:				
FSI	159.7	161.3	151.4	125.8
TSO	214.4	128.1	183.0	145.0
Far Damper:				
FSI	223.4	198.5	177.8	140.3
TSO	220.1	218.6	213.2	271.5

damper. First, because of space limitations and tunnel position in the large test enclosure, the near damper is situated only 3.45 pipe diameters (based on the transition piece duct diameter) from the exhaust end of the tunnel. Since flow components placed within 10 pipe diameters upstream of an inlet can affect overall pressure loss, and even longer lengths can be affected for laminar flows [75], the near damper appears to be located too close to the end of the tunnel with the result that pressure losses through the damper impact flow within the main chamber of the Steiner tunnel apparatus. Furthermore, the near damper itself is a thin flat plate that, due to exhaust fan limitations, has to be inclined to a position of approximately $\theta = 70^o$[1] in order to restrict the flow sufficiently that the tunnel draft pressure lies at approximately the mid-point of the recommended draft pressure range for tunnel operation. For a thin flat plate oriented at a $\theta = 70^o$ to the flow, the pressure loss coefficient, K, is reported from various sources to range between 62 and 750 [76, 77, 78]. The significant flow losses across the near damper serve to induce upstream pressure effects in the exhaust end of the tunnel, thus slowing down the spread of flame and even preventing the flames from reaching the end of the tunnel. As a result, when the near damper is used for flow control, measured values of FSI are rendered lower than for the case of unrestricted exhaust flow ducting.

Values of TSO% measured during OSB tests conducted with the near damper plate adjusted to various angles are shown in Figure 4.25. While there is significant scatter in the data, it is clear that closing the damper down (i.e., increasing the damper plate angle) results in a notable reduction in the value of averaged smoke obscuration as well. This is likely because the exit flow of smoke is physically restricted and held in the tunnel behind the damper, thereby never reaching the smoke analyzer. However, in the case of red oak from earlier, when utilizing the near damper, the smoke is less dense than OSB and the damper position does not impose a significant impact on the results.

[1] $\theta = 0$ designates the angle of the fully open damper plate.

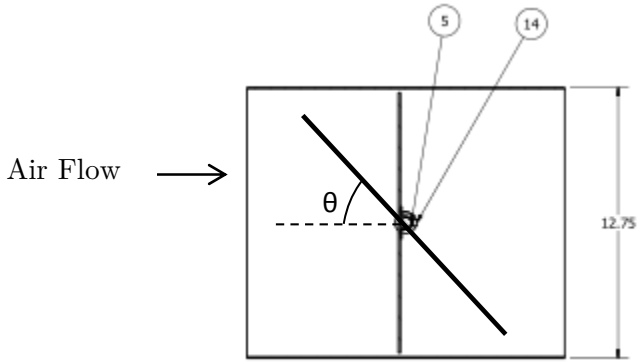

Figure 4.24: Incline of the damper plate to regulate draft pressure for the near damper

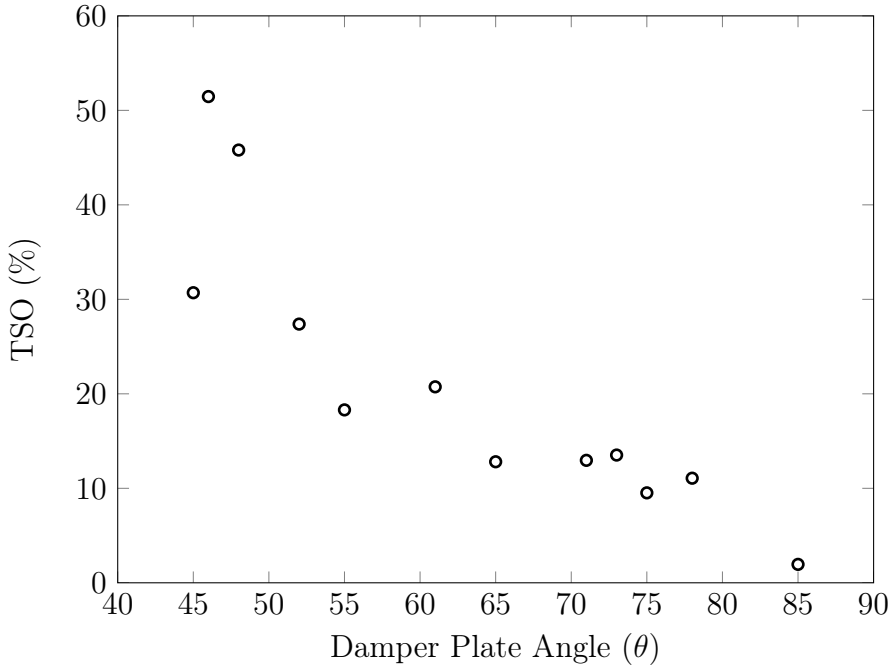

Figure 4.25: Effect of inclining damper plate angle on smoke measurements for the near damper

It is evident from the results that the removal of the flow restriction near the end of the tunnel associated with the near damper and instead utilizing the far damper for flow control during testing provides better flow conditions in the tunnel and allows the flames to progress freely along the full length of the sample under test. This is consistent with the fact that the far damper is situated 19 pipe diameters from the exhaust end of the

[1]The pressure loss coefficient, K, for such a perforated plate is 34 [75].

tunnel and uses a perforated damper plate (Section 3.1.2) with a significantly lower loss coefficient [1] than that for the near damper.

Figures 4.26 and 4.27 compare the measured temperatures at TC # 12 determined in tunnel tests that employ the near and far dampers in testing samples of OSB and particle board. As illustrated in the Figures, the results from Table 4.12 can be further validated through examination of the temperature readings at the end of the tunnel. The temperature measurements near the end of the tunnel are 19% to 23% higher for tests conducted for OSB and particle board, respectively, using the far damper for flow control. Higher temperatures are also recorded on the remainder of the thermocouples (TC # 1-9), confirming better flow conditions and flame spread characteristics when the far damper is used.

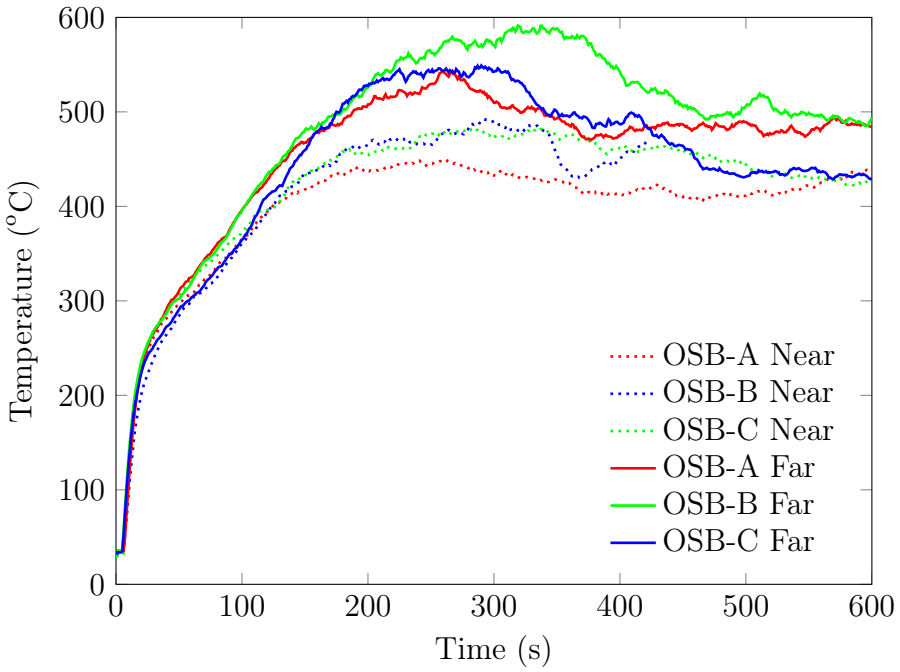

Figure 4.26: Comparison of temperature measurements at TC # 12 for near and far damper tests for OSB

Based on the combined results above, it is determined that the flow conditions in the UW Steiner tunnel apparatus should be controlled using the far damper that is installed in the exhaust duct well away from the tunnel exit. Also, noting the large variation among published values of FSI for OSB [2] and comparatively less variations reported for particle board, testing of the flame spread performance of particle board is deemed to be a good,

[2] these measured values depend on many factors, including moisture content, wood specie, surface type and adhesives used.

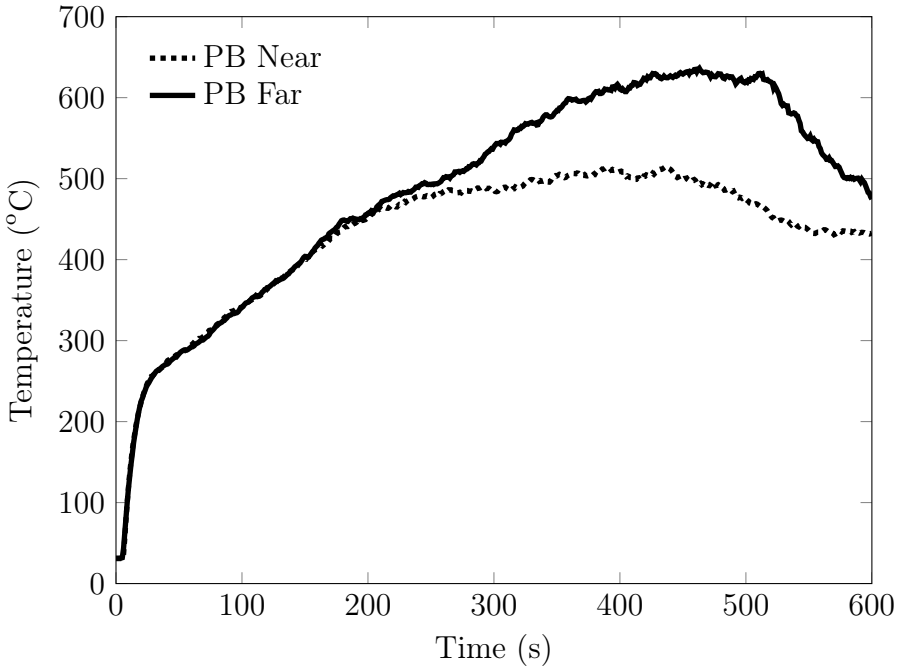

Figure 4.27: Comparison of temperature measurements at TC # 12 for near and far damper tests for particle board

and relatively inexpensive method, by which to repetitively determine any other calibration and operational details associated with the tunnel. The ASTM E84 standard does require at least periodic calibration using the much more expensive samples of red oak, however, so as a final experiment in this research, a full calibration test is run using red oak with results discussed in the section below.

4.6 Final Red Oak Test

Based on the above tests, it is evident that utilizing the far damper for control of the flow in the UW Steiner tunnel is the best configuration for testing in the tunnel. As a final step of testing in this research, therefore, the far damper is properly inserted in the exhaust duct and tunnel parameters are optimized for operation. Then, a full tunnel test is conducted using a red oak sample and following the tunnel calibration procedures outlined in the ASTM E84 Standard Test Method [1].

The time evolution of flame propagation with time is plotted in Figure 4.28 against previous tests conducted using the near damper for flow control. It is clear from these results that by controlling tunnel flow using the far damper, flames established on the red

oak sample are able to reach the end of the tunnel, although the time taken for them to reach the end of the tunnel is still considerably longer than that reported in the ASTM calibration test. Unfortunately, no additional oak is available to continue testing, however based on test experience accumulated above, only some small additional adjustments in draft pressure and gas flow are needed to bring the UW Steiner tunnel operation within acceptable agreement to the ASTM calibration results. Even without such adjustments, it is commissioned and ready to use to obtain (at least) relative rankings of candidate materials during research and development into flame spread characteristics of different formulations of lining materials.

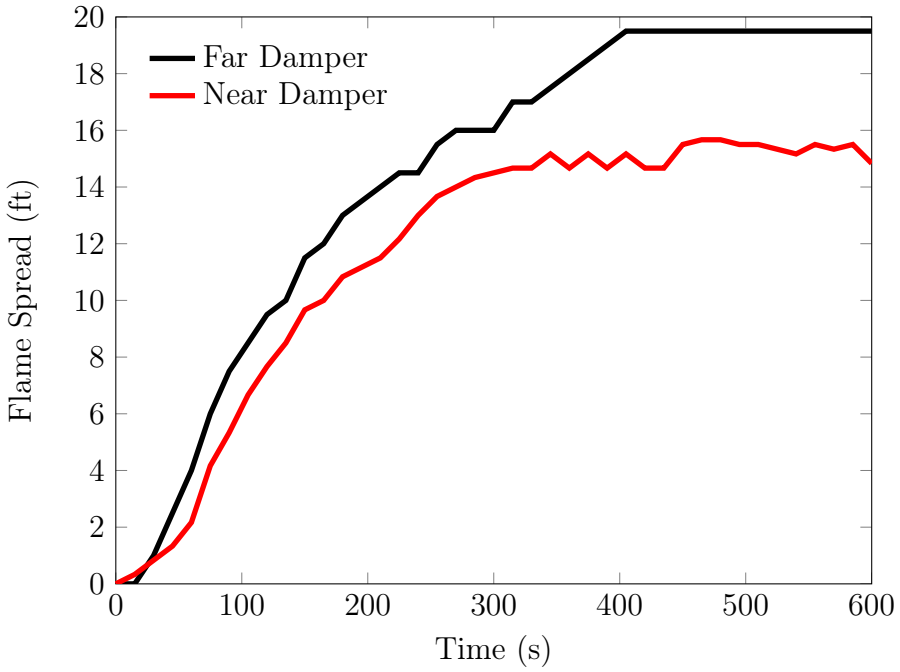

Figure 4.28: Flame spread reaching the end of the tunnel (19.5 ft) when utilizing the far damper for red oak test

Chapter 5

Closure

This thesis presents methods used for, and results from, tests conducted during the final installation and commissioning of a modular Steiner tunnel delivered to the UWFRL. Safety control systems were designed to meet the requirements stipulated in the appropriate TSSA and other safety regulations associated with operation of the tunnel apparatus. Tunnel exhaust ducting and instrumentation were also designed as necessary, installed and tested. Finally, the tunnel performance was evaluated through a series of tests conducted using calibration procedures specified in the ASTM E84 standard test method [1]. The calibration procedures included an air leak test, as well as flame spread tests using cement board and red oak. To supplement the calibration tests, additional experiments were conducted to determine a measure of the repeatability of the tests conducted in the tunnel, as well as to identify key operational parameters and rectify any issues encountered during calibration. Tests were conducted on various wood products including red oak, OSB, particle board, and plywood to evaluate the tunnel performance. The three specific parameters that were found to have significant influence on tunnel operation were gas flow to the burner, draft pressure within the main tunnel section, and the exhaust damper position. Draft pressure measurements, thermocouples, a gas flow meter and smoke measurements were used to characterize the effects of systematically changing each of these parameters. Results were evaluated and a consistent methodology was developed that would minimize time and cost of ongoing calibration of the tunnel.

5.1 Conclusions

The conclusions of this research are as follows:

1. The safety control systems were successfully designed and implemented for the tunnel

gas burners. The components in the gas supply train were assessed on an individual basis, and calculations were performed until the right combination of components were selected that was able to adhere to both the safety regulations and the gas burner requirements. The proposed design received field approval from TSSA and the gas burners were able to obtain the gas flow required to conduct calibration tests. Additional safety requirements for the tunnel were also met, such as the NFPA 86 ventilation, purge and explosion relief calculations to ensure that the tunnel apparatus is safe from explosions.

2. The Steiner tunnel has been successfully operated in accordance with the calibration procedures specified in ASTM E84. Specifically it should be noted that:

   (a) After performing major repairs on the tunnel seals, the tunnel satisfied the minimum requirement for the draft pressure reading.

   (b) Testing showed that the tunnel pre-heat should be limited to 34 minutes due to operational constraints arising from overheating of the as-designed glass windows.

   (c) With adjustment of gas supply to the burner system, the standard ASTM time temperature curve was obtained during calibration testing with cement board samples.

   (d) Tests conducted using OSB samples showed consistent results for smoke and flame spread measurements across 3 repeated tests. The standard deviation between FSI results in these tests was significantly less than those reported in the ASTM standard.

3. During calibration tests, it was found that of the three parameters that were studied (gas flow, tunnel draft, and damper position), the damper position had the most influence on FSI. Gas flow effects were found to be largely dependent on outside temperatures, and most likely is outside of lab facilities control. Therefore, it was determined that the tunnel should only be operated when the lab temperature is above 18^{o}C. Airflow through the tunnel as indicated by tunnel draft pressure was found to greatly impact measured flame spread characteristics for most samples tested. Since sudden changes in draft pressure were found to essentially obstruct flame progression, FSI results were improved when fan control measures were implemented to stabilize the draft pressure within the main tunnel enclosure. Design, installation and use of the far damper served to further greatly improve the FSI results from the tunnel.

4. Smoke obscuration values were found to be largely affected by flame spread. As a result if tunnel operating conditions are optimized for FSI measurement, they were also found to be adequate for smoke measurements of reasonable accuracy.

5. An appropriate operating range was defined for each major tunnel parameter in order to develop guidelines for a consistent methodology by which to calibrate the tunnel. These are as follows 1) For gas flow, flame spread results were most affected for flowrates below 7.0 m^3/hr which corresponded to maintaining inlet gas temperature above 18^oC. 2) The appropriate range for the tunnel draft pressure was determined to be between 0.090 - 0.110 in-WC (22.4 - 27.4 Pa) so that it would not have a significant effect on flame spread results. 3) The far damper should be utilized to control tunnel air flow. If this is not possible, the damper position should be kept 18 pipe diameters from the end of the tunnel. The near damper should be removed from the tunnel apparatus since the pressure losses created near the end of the tunnel have been shown to have significant impact on FSI results.

5.2 Recommendations for Future Work

Now that the important tunnel parameters have been studied and the proper ranges for each of the parameters have been identified, future tests on shortening the tunnel length can be conducted. First, the tunnel needs to be calibrated 5 times with red oak to obtain a running average for SDI, and final adjustments to gas flow or tunnel draft made to ensure that it meets the exact flame spread time of 5.5 minutes. Since OSB has demonstrated fairly consistent results when its testing parameters are controlled (Section 4.4), it would be considered as a good candidate material for performing scaling tests. Three more OSB tests should be conducted in the full length tunnel in order to achieve a good running average for the 'full-length' tunnel results.

5.2.1 Final Notes on Scaling of the UW Steiner Tunnel

Scaling tests should be conducted with the first and the last section of the tunnel kept unchanged (Module A and Module F), and the mid sections of the tunnel (Modules B to E) removed, gradually reducing the length of the tunnel for each scaling test to 20 ft, 16 ft, and 12 ft, as shown in Figure 5.1.[1] The gas flow and the tunnel draft will need to be adjusted for each new tunnel length since the time-temperature curve for TC # 12 will no longer be the same at the end of the tunnel, and cannot be used as a reference in determining the fuel contribution to the temperature of the tunnel. However, the 8

[1]The tunnel length should not be tested at 8-ft since there is only one thermocouple located in Module A that can be used as a reference thermocouple and it may be too close to the burner in a region where temperature fluctuations are significant.

upstream thermocouples (refer to Instrumentation Section 3.3) can be utilized to develop appropriate reference time-temperature curves for testing under shorter tunnel lengths.

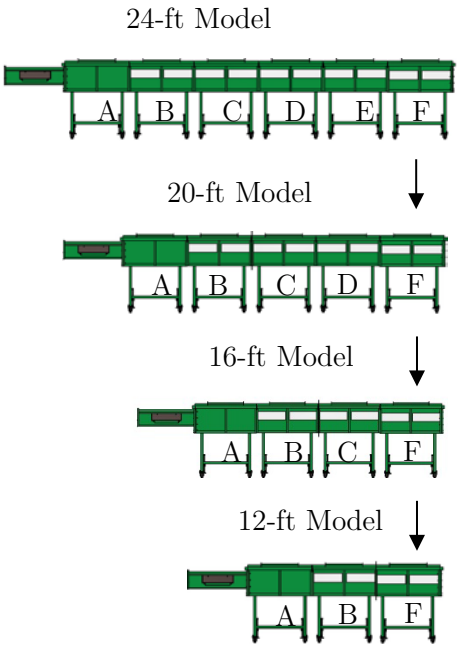

Figure 5.1: The proposed method for scaling tests

Unlike the 8-ft Tunnel Method, the present scaled tunnel test method will still use the same tunnel cross-section, with only the length of the tunnel shortened. In the 8-ft tunnel, a new flame spread time for red oak was evaluated to be 18.4 minutes due to the changes in tunnel dimensions, and a new method of calculating FSI (Equations 2.12 and 2.13) was also developed (Section 2.5.1). For the UW shortened tunnel, the gas flow and draft pressure in the tunnel will have to be adjusted so that the upstream thermocouples continue to meet the reference time-temperature curve from the 'full-length' tunnel.

Figure 5.2 shows an example of a potential flame spread measurement for OSB in a 12-ft tunnel test, compared to the full 24-ft tunnel test results for OSB. The flame spread index for the shortened tunnel can be still calculated using Equation 2.1a, however the newly calculated index will not be equivalent to the FSI calculated from a full length tunnel test since the equation was derived based on the 19.5 ft (5.94 m) flame spread length. A number of tests would have to be conducted at each new length in order to obtain a good correlation between the two indices. For example, if the calculated FSI from Figure 5.2 is 148 for the 24-ft tunnel, then the FSI for the 12-ft would be approximately 35 since the flames would hypothetically reach the end of the 12-ft tunnel in 1.25 min, if the tunnel

[1] 1.25 min is the same time flames reach 7.5-ft for OSB in the 24-ft tunnel.

parameters were adjusted appropriately.[1] In the above brief evaluation for the 12-ft tunnel, the flame spread is assumed to follow the same trend with time as that in the 24-ft tunnel test over the 7.5-ft length of sample.[2]

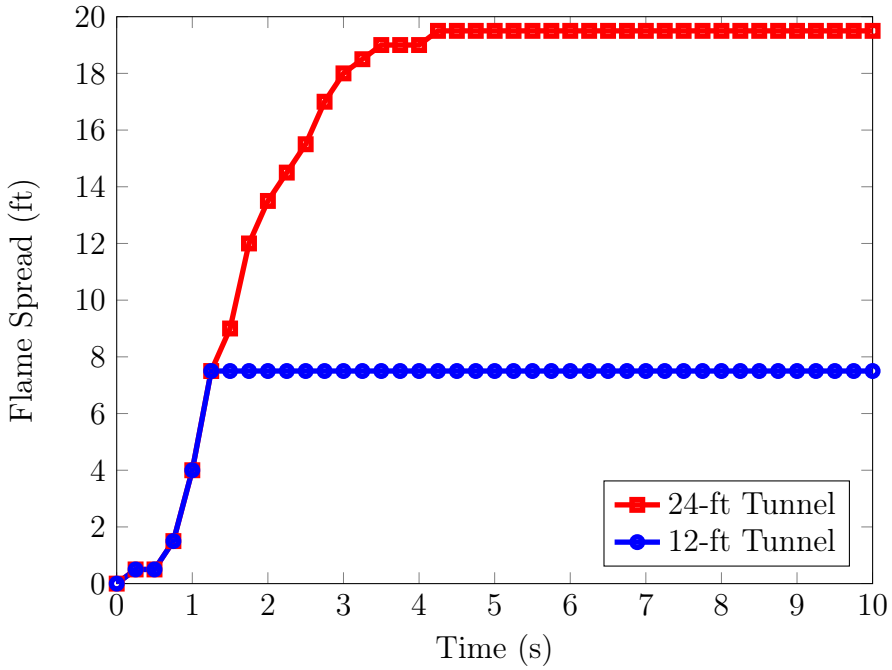

Figure 5.2: Potential flame spread comparison for a 24-ft tunnel and 12-ft tunnel

[2]It should be noted that for the 12-ft tunnel the burnable specimen length of OSB is only 7.5-ft because of the current 4.5-ft flame reference length; however, this reference flame length may also need to be varied as the tunnel is shortened as well in which case the burnable specimen length would also change.

References

[1] ASTM E84-13a Standard, 2013. *Standard Test Method for Surface Burning Characteristics of Building Materials*. ASTM International, West Conshohocken, PA.

[2] Laymon, R., 2004. Assessing the Burning Characteristics of Interior Finish Material. <http://magazine.sfpe.org/special-hazards/assessing-burning-characteristics-interior-finish-material>. Online magazine article; accessed 19-January-2014.

[3] Miniutti V.P., B. H., 1957. *Small Tunnel-Furnace Test for Measuring Surface Flammability*. US Department of Agriculture, Forest Products Laboratory in cooperation with University of Wisconsin. Report No. 2097.

[4] Babrauskas, V., White, A., and Urbas, J., 1997. "Testing for surface spread of flame : New tests to come into use". *Building Standards,* ***LXVI***(2), pp. 13–14.

[5] Rockler, 2013. Red Oak Lumber by the Lineal Inch. http://www.rockler.com/red-oak-lumber-by-the-lineal-inch?gclid=CJDd7eqMp7wCFQtgMgodORAAiQ. Rockler Companies Inc., Online; accessed 19-January-2014.

[6] Spiersi, B., 2014. ULC Steiner Tunnel Fire Testing Methods. Underwriters Laboratories of Canada, Toronto, ON. Personal Communication on 29-June-2014.

[7] NFPA 255 Standard, 2000. *Standard Method of Test of Surface Burning Characteristics of Building Materials*. National Fire Protection Association, Quincy, MA.

[8] UL Standard 723, 2008. *Standard for Test for Surface Burning Characteristics of Building Materials*. Underwriters Laboratories, Chicago, IL.

[9] CAN/ULC-S102-07, 2009. *Standard for Method of Test for Surface Burning Characteristics of Building Materials and Assemblies*. Underwriters Laboratories of Canada, Toronto, ON.

[10] Babrauskas, 2000. "Fire Test Methods for Evaluation of FR Efficacy". In *Fire*

Retardancy of Polymeric Materials, C. A. W. Arthur F. Grand, ed. Marcel Dekker, New York, NY, ch. 3, pp. 85–86.

[11] 2009 International Building Code, 2009. *International Building Code*, 2009 ed. International Code Council, Country Club Hills, IL. Chapter 8, pages 175–176.

[12] NRCC, 2010. *Flame Spread Ratings and Smoke Developed Classifications*, 2010 ed. Canadian Commission on Building and Fire Codes, Ottawa, Ontario. Section D-33.

[13] Janssens, M., Huczek, J., and Sauceda, A., 2008. "Development of a Model of the ASTM E 84 Steiner Tunnel Test". *Fire Safety Science - Proceedings of the Ninth International Symposium,* ***9***, pp. 279–289. International Association for Fire Safety Science.

[14] Resing, J. V., Gandhi, P. D., Sloan, D. E., and Laymon, R. K., 2013. "Measurement Uncertainty and Statistical Process Control for the Steiner Tunnel". *Journal of Testing and Evaluation,* ***39***(6), pp. 2–7.

[15] Laymon, R., 2004. Surface Burning Characteristics for Materials Used in Plenums - ASTM E84 (UL 723) vs. ULC S102.2: What's the difference? `http://ul.com/wp-content/uploads/2014/04/ASTME84_ULCS102.2.pdf`. Online; accessed 21-January-2014.

[16] NRCC, 2010. *Flame Spread and Smoke Developed Classifications*, 2010 ed. Canadian Commission on Building and Fire Codes, Ottawa, Ontario.

[17] Klein, G., 2011. "The Conflicting Roles of the Elevator Safety Code , LEED and ADA in Elevator Renovation". *Elevator World Continuing Education: Technology,* ***May 2011***, pp. 61–65.

[18] Babrauskas, V., Lucas, D., and Eisenberg, D., 2012. "Flame retardants in building insulation : a case for re-evaluating building codes". *Building Research and Information,* ***10***(1), pp. 1–28.

[19] Lawson, J. R., 2009. *A History of Fire Testing.* National Institute of Standards Technology (NIST), Gaithersburg, MD. NIST Tehnical Note 1628.

[20] Parker, W. J., 1977. An Investigation of the Fire Environment in the ASTM E 84 Tunnel Test. Tech. rep., (U.S. Department of Commerce, National Bureau of Standards) Center for Building Technology, Institue for Applied Technology, Washington, D.C. NBS Technical Note 945.

[21] Randall, J., 1979. An Interlaboratory Evaluation of the ASTM E 84-77a Tunnel

Test Modified By the Consumer Product Safety Commission for Cellulosic Loose Fill Insulation. Tech. Rep. NBSIR 79-1922, Center for Fire Research, National Engineering Laboratory, National Bureau of Standards, Washington, D.C.

[22] K.C., D., and E.F., F., 1994. "Predicting the Steiner Tunnel Test Performance of Rigid Polyurethane Foams using Cone Calorimeter". In *Utech'94: Groundwork for Growth*, D. Reed and C. Lee, eds. The International Polyurethane Industry Conference, Hague, Netherlands. Paper 55, pages 1-8.

[23] DiDomizio, M. J., 2013. "On the Potential Use of Small Scale Fire Tests for Screening Steiner Tunnel Results for Spray Foam Insulation". Master's thesis, University of Waterloo, Waterloo, ON.

[24] Holmes, G., 2011. Report of Surface Burning Characteristics Tests on Samples. Tech. Rep. SV17128/07CA57156, Underwriters Laboratories, Northbrook, IL. UL Test Report for Acoustiblok Inc.

[25] Abrams, M. S., Souza, V. D., Higginson, P., Metes, W. S., Quintiere, J. G., Parker, J., Robins, R. F., White, J. A., Abrams, R., and Souza, D., 1985. "Review of ASTM Test for Surface Burning Characteristics of Building Materials (E 84) (An ASTM White Paper)". *Journal of Testing and Evaluation,* ***13***(2), pp. 89–114.

[26] Banu, D., Feldman, D., Haghighat, F., and Paris, J., 1998. "Energy-Storing Wallboard: Flammability Tests". *Journal of Materials in Civil Engineering,* ***10***(05), pp. 98–105.

[27] Mehaffey, J., 1987. Archived Document - Flammability of Building Materials and Fire Growth. `http://archive.nrc-cnrc.gc.ca/eng/ibp/irc/bsi/87-flammability.html`. Online; accessed 23-January-2014.

[28] Sheppard D.T., and Gandhi P.D., 1991. "Estimatlng Smoke Hazard from Steiner Tunnel Smoke Data". *Fire Technology,* ***1***(1), p. 66.

[29] Hirschler, M., 2011. "Use of the Steiner Tunnel for Fire Testing in North America". In *12th International Conference and Exhibition*. Fire and Materials 2011, San Francisco, CA.

[30] ASTM E286-85 Standard, 1985. *Method of Test for Surface Flammability of Building Materials Using an 8-Ft.(2.44-m) Tunnel Furnace*. ASTM International, West Conshohocken, PA.

[31] Peters, C., and Eickner, H., 1962. "Surface Flammability as Determined by the FPL 8-FT Tunnel Method". In *Symposium on Fire Testing Methods*. ASTM International, Philadelphia, PA, pp. 18–30.

[32] ASTM E162 Standard, 1962. *Standard Test Method for Surface Flammability of Materials Using a Radiant Heat Energy Source*. ASTM International, West Conshohocken, PA.

[33] Teague, P. E., 2009. "Case Histories : Fires Influencing the Life Safety Code". In *2009 Life Safety Code Handbook - Supplemental Information*, R. R. Farr, ed., 2009 ed. National Fire Protection Association, Quincy, MA, ch. Supplement 1, pp. 1147–1160.

[34] White, R. H., 2010. "Ten decades of flame retardancy testing at the U.S. Forest Products Laboratory". In *21st Annual Conference on Recent Advances on Flame Retardancy of Polymeric Materials*. BCC Research, Wellesley, MA, pp. 445–454.

[35] Eickner, H., 1977. "Surface Flammability Measurements for Building Materials and Related Products". In *Treatise on Analytical Chemistry*, I. Kolthoff, J. Elving, and F. Stross, eds., 3 ed., Vol. 4. John Wiley & Sons, Inc, Madison, WI, ch. D-1, pp. 16–20.

[36] White, R., and Schaffer, E., 1981. Thermal characteristics of thick red oak flakeboard. Research Paper FPL 407, Forest Products Laboratory, Madison, WI.

[37] Le Van, S. L., 1985. "Flamespread Variability of Candidate Wood-Based Reference Materials". *Journal of Fire Sciences,* ***3***(3), Jan., pp. 208–223.

[38] Syska, A., 1969. Exploratory Investigation of Fire-Retardant Treatments for Particleboard. Research Note FPL-0201, Forest Products Laboratory, Forest Service U.S. Department of Agriculture, Madison, WI.

[39] Gardner, W., and Thomson, C., 1991. "Ignitability and Heat-Release Properties of Forest Products". *Fire and Materials,* ***15***(1), pp. 3–9.

[40] Hirschler, M., 2004. Fire Testing of Interior Finish. `http://magazine.sfpe.org/special-hazards/fire-testing-interior-finish`. Society of Fire Protection Engineers (SFPE), Online magazine article; accessed 23-February-2014.

[41] Zicherman, J. B., 2009. "SFPE Classic Paper Review: Fire Performance under Full-scale Test Conditions – A State Transition Model and Coupling Deterministic and Stochastic Modeling to Unwanted Fire by Robert Brady Williamson". *Journal of Fire Protection Engineering,* ***19***(1), Feb., pp. 73–80.

[42] Yuill, C. H., 1962. "Flame Spread Tests in a Large Tunnel Furnace". In *Symposium on Fire Test Methods*. ASTM International, Philadelphia, PA, pp. 1–15.

[43] Lee, T., and Huggett, C., 1975. "lnterlaboratory Evaluation of ASTM E 84-70 Tunnel Test Applied to Floor Coverings". *Journal of Testing and Evaluation,* ***3***(1), pp. 3–14.

[44] AWC, 2010. "Flame Spread Performance of Wood Products". In *Design for Code Acceptance*. American Wood Council Inc., Leesburg, VA, pp. 1–5.

[45] Groah, W. J., 1973. "A Study of Certain Operating and Material Variables of the 25-Foot Tunnel Flamespread Test". *Forest Products Journal,* ***23***(12), pp. 39–45.

[46] Endicott, L. E., and Bowhay, R. B., 1970. "A Statistical Evaluation of the Fire Hazard Classification Furnace (ASTM E84-68)". *Materials Research and Standards,* ***50***(1), pp. 19–21.

[47] Quintiere, J. G., and Raines, J. W., 1975. "Thermal and Flow Characterstics of the ASTM E84 Tunnel Test Method". In *Centre for Fire Research, Institute for Applied Technology*. National Bureau of Standards, Washington, DC, pp. 1–20. Report NBSIR 75-705.

[48] White, R. H., 2000. "Fire Performance of Hardwood Species". *Forest Products Journal,* ***1***(8), pp. 7–12.

[49] Grisack, H., Roberts, J., and White, J., 1994. "Interlaboratory Test Program to Validate ASTM E 84 Test Method for Surface Burning Characteristics of Buifding Materials (PCN 33-000014-31)". In *ASTM Institute for Standards Research*. ASTM International, pp. 3–15. Research Report ISR# E05-0001.

[50] Babrauskas, V., 1981. "Applications of Predictive Smoke Measurements.". *Journal of Fire and Flammability,* ***12***(1), pp. 51–64.

[51] Algonquin College Student Team, 2011. "Steiner Tunnel Assembly Report". In *Algonquin College - Final Project Report - Team #4*. Algonquin College and Elevator Cab Renovations (ECR), Ottawa, ON, pp. 3–13. Non-published Report.

[52] NFPA 86 Standard, 2011. *Standard for Ovens and Furnaces - 2011 Edition*. National Fire Protection Association (NFPA), Quincy, MA.

[53] TSSA-Field Approval Code, 2012. *TSSA Field Approval Code, TSSA-FA-2012, December 2012*. Technical Standards and Safety Authority (TSSA), Toronto, ON.

[54] CSA B149.1-10 Standard, 2010. *Natural Gas and Propane Installation Code*. Canadian Standards Association (CSA), Mississauga, ON.

[55] Obach, M., and Weckman, E., 2010. "Comparing the Heat Release Rate and Heat Flux of Uniformly Constructed Wood Cribs". In *Presentation at the Combustion Institute*. University of Waterloo, Ottawa, ON.

[56] Limited, U. G., 2014. Chemical Composition of Natural Gas. http://www.uniongas.com/about-us/about-natural-gas/chemical-composition-of-natural-gas. Online; accessed 04-May-2014.

[57] ASTM E1537 Standard, 2014. *Standard Test Method for Fire Testing of Upholstered Furniture*. ASTM International, West Conshohocken, PA.

[58] Ku, H. H., 1966. "Notes on the Use of Propagation of Error Formulas". *Journal of Research of the National Bureau of Standards,* ***79***(4), pp. 75–79.

[59] Taylor, J. R., 1997. "Precision error". In *An Introduction to Error Analysis: The Study of Uncertainties in Physical Measurements*, 2 ed. University Science Books, Sausalito, CA, p. 94.

[60] ASTM E691-14 Standard, 2014. *Standard Practice for Conducting an Interlaboratory Study to Determine the Precision of a Test Method*. ASTM International, West Conshohocken, PA.

[61] Lam, C. S., 2009. "Thermal Characterization of a Pool Fire in Crosswind With and Without a Large Downwind Blocking Object". Phd thesis, University of Waterloo, Waterloo, ON.

[62] (USG), D., 2012. *Cement Board Systems (SA932 09305)*. United States Gypsum Company, Chicago, IL. Technical Specification Sheet.

[63] APA - The Engineered Wood Association, 2009. *Oriented Strand Board*. APA Wood, Tacoma, WA. Technical Specification Sheet.

[64] SBA, 2005. "OSB Performance by Design - Fire Performance". In *OSB in Wood Frame Construction - US Edition 2005*. Structural Board Association (SBA), Markham, ON, p. 8.

[65] AWC, 2012. "Fire Performance of Wood Products". In *Fire Performance of Wood Products Awareness Guide*. American Wood Council (AWC) Inc., Leesburg, VA.

[66] Weyerhaeuser, 2014. "Fire-Rated Assemblies and Sprinkler Systems - Featuring Fire Assembly Details and Sprinkler Installation Guide". In *#1500 Design/Installation Guide*. Weyerhaeuser Installation Guide, Federal Way, WA, pp. 3–4.

[67] CANPLY, 2009. Plywood Design Fundamentals. CANPLY Brochure, Tolko Industries and The CertiWood Technical Centre, North Vancouver, BC.

[68] ASTM D4442 Standard, 2003. *Standard Test Methods for Direct Moisture Content*

Measurement of Wood and Wood Base Materials. ASTM International, West Conshohocken, PA.

[69] Australian Window Association, 2009. "Thermal Stress Glass Breakage". In *Key Message Guide*. Australian Window Association, Turramurra, NSW, Australia, p. 3.

[70] Skelly, M. J., and Richard, J., 1991. "An Experimental Investigation of Glass Breakage in Compartment Fires". *Journal of Fire Protection Engineering,* ***3***(1), pp. 29–32.

[71] Babrauskas, V., 2010. "Glass Breakage in Fires". In *Fire Science Publishers*. Fire Science and Technology Inc., Issaquah, WA, pp. 1–7.

[72] ASTM E177-14 Standard, 2014. *Standard Practice for Use of the Terms Precision and Bias in ASTM Test Methods*. ASTM International, West Conshohocken, PA.

[73] Noviyanto, I. D., 2014. "Thermal Efficiency Improvement Through Fuel Gas Rate and Excess Oxygen Control". In *The 4th International Conference on Technology and Operations Management*. Institute of Technology Bandung (ITB), Bandung, Indonesia, pp. 434–443.

[74] Bengelsdorf, M. F., 1997. "Fire-Hazard Classification of Construction Plywood Panels". In *APA Research Report 128*. APA - The Engineered Wood Association, Tacoma, WA, pp. 9–10.

[75] Blevins, R., 1984. "Pressure Loss Through Pipes". In *Applied Fluid Dynamics Handbook*, first ed. Van Nostrand Reinhold Company, New York, NY, pp. 65–316.

[76] Idelchick, I., 1960. "Flow Through Orifices with Sudden Changes in Velocity and Flow Area". In *Handbook of Hydraulic Resistance*. Hemisphere Publishing, New York, NY.

[77] Guins, V., 1968. "Flow Characteristics of Butterfly and Spherical Valves". *Journal of the Hydraulics Division,* ***94***(3), pp. 675–690.

[78] McPherson, M., Strausser, H., and Williams, J., 1957. "Butterfly Valve Flow Characteristics". *Journal of Hydraulics Division,* ***83***(1), pp. 1–28.

[79] Progressive Components Catalog, 2014. Pipe Thread Check. `http://www.procomps.com/products/Style.aspx?cat_id=13&style_id=293`. Online; accessed 28-August-2014.

[80] Jusoh, A., 2010. "Flow Equations in Commercial Gas Piping System". Undergraduate project paper, Universiti Malaysia Pahang, Pahang, Malaysia.

[81] Schroeder, D. W., 2001. "A Tutorial on Pipe Flow Equations". In *Flow Formula Tutorial*. Stoner Associates Inc., Carlisle, PA, pp. 8–9.

APPENDICES

Appendix A

Construction and Assembly of the UW Steiner Tunnel

This Appendix contains a step by step procedure of constructing and assembling the UW Steiner tunnel. Since the fume hood at the UW Fire Lab is a multi-use exhaust duct between the Steiner tunnel and the furniture calorimeter; modules and exhaust duct transition piece are assembled separately. Figures illustrated in this section are in the same order that the assembly procedure was performed. The assembly procedure starts from the exhaust duct transition piece connection to the exhaust end of the tunnel (Module F), and it ends at the last connection of Module A. Some of the procedures outlined in this Appendix are only performed during the initial construction of the tunnel. Procedures such as brick alignment, height adjustment, and section removal are always performed when shortening the tunnel length.

Measurements are taken for the alignment of the exhaust duct transition piece to the exhaust entrance of the fume hood. Figure A.1 shows a 34.5-in (0.88 m) by 15-in (0.38 m) exhaust opening underneath the fume hood, and in Figure A.2, a 17.5-in (0.44 m) by 12.75-in (0.32 m) exhaust end opening at the end of the tunnel. The exhaust duct transition piece is then aligned and installed between the two openings as illustrated in Figure A.3. During the alignment of the exhaust duct and the exhaust end of the tunnel, height adjustment rods on Module F (Figure A.4) are lifted accordingly. The rods are threaded through 3/4-in (19 mm) hex nuts which are welded to the supporting beams.

Fire bricks are measured and cut to line the floors and walls of the tunnel (Figure A.5). This procedure is only done once during the initial construction phase, however, if any of the bricks are damaged during testing, then the bricks are to be replaced. Tunnel sections (Modules A-F) are then joined and held together by assembly clamps and bolts as described in Chapter 3. Simultaneously, the height adjustment rods are lifted accordingly for every

Figure A.1: Exhaust entrance opening underneath the fume hood

module and employing levels to compensate for the uneven floor surface (Figure A.6). High temperature gaskets are sealed with silicon caulking along the joining edges to prevent air leaks within the tunnel (Figure A.7). Fire bricks are then straightened along the joints to provide a smooth cross section along the entire length of the tunnel (Figure A.8).

Once all the modules are connected, final height adjustments are made to even out the bricking surface of the tunnel, as illustrated in Figure A.9. Placement of lids on top completes the assembly of the tunnel (FigureA.10).

Figure A.2: Exhaust end opening for the UW Steiner tunnel

Figure A.3: Exhaust duct transition piece aligned and installed between the two openings

Figure A.4: Height adjustment rods are lifted to align the height between the exhaust and the tunnel opening

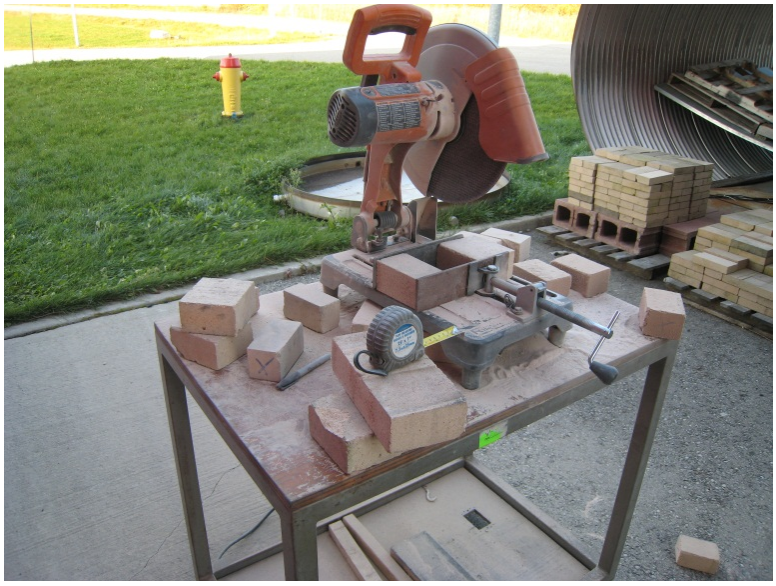

Figure A.5: Radial arm saw is used to cut fire bricks to size

Figure A.6: Final height adjustments are made to level the tunnel sections even

Figure A.7: Gaskets are placed between module assemblies to prevent air leaks

Figure A.8: Bricks are evenly aligned at the joints for a smooth transition between modules

Figure A.9: Proper alignment of bricks along the cross-section

Figure A.10: Every module is accommodated with a corresponding lid assembly to conceal the tunnel

A.1 Drawings

The assembly drawings in this section are not to scale. The original size of the drawings could not fit to the page size of this document and they were scaled down accordingly. The drawings were created to provide more detail of the UW tunnel assembly and its components.

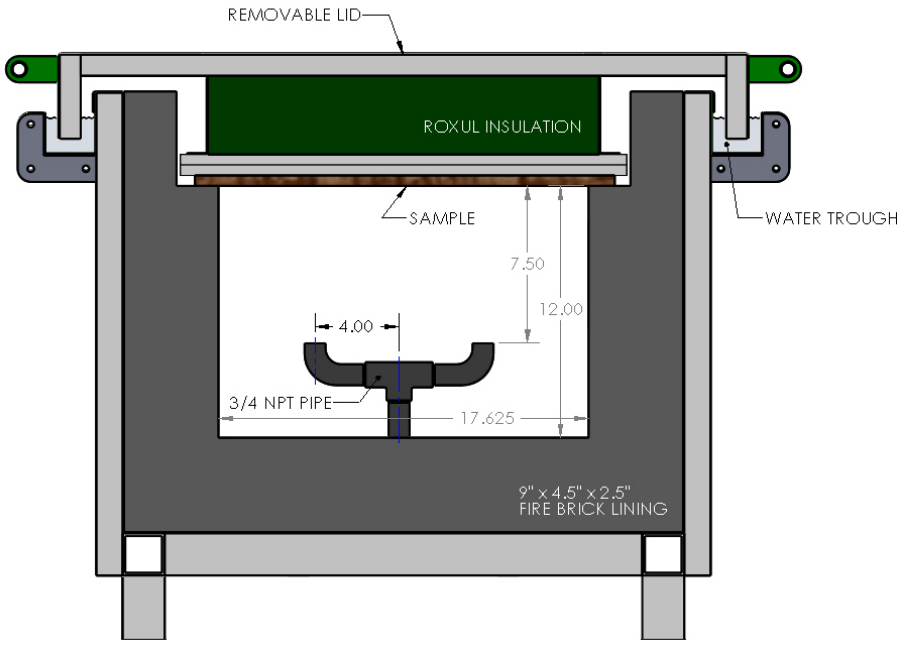

Figure A.11: Cross-sectional view of the burner from the air intake module with the sample mounted in place

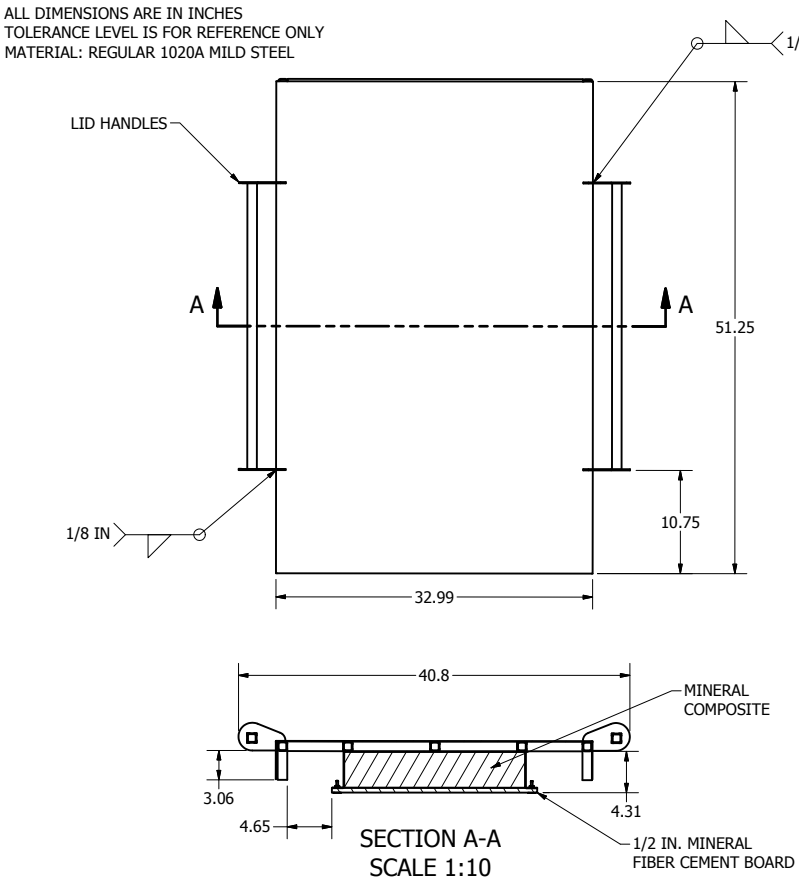

Figure A.12: Removable lid assembly for the modules

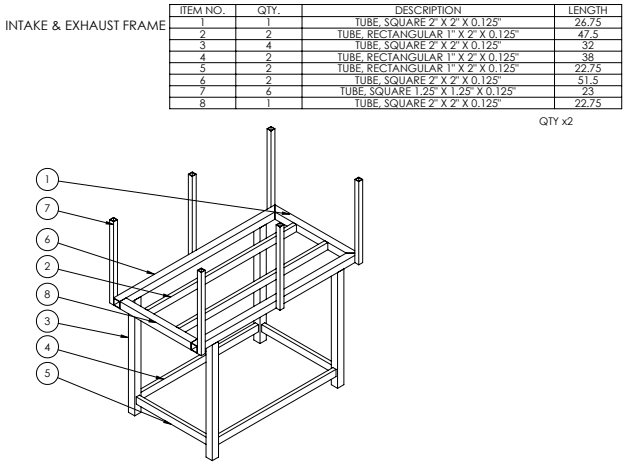

Figure A.13: A typical frame assembly of a single module

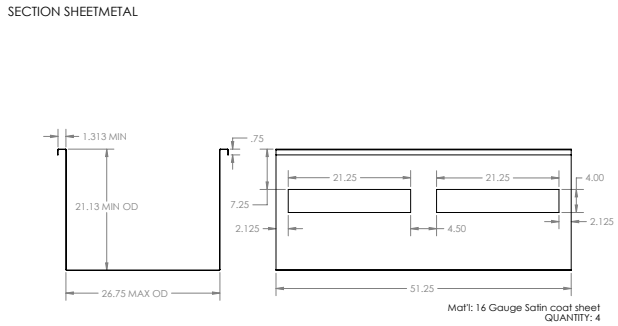

Figure A.14: Corrugated steel section for the tunnel windows

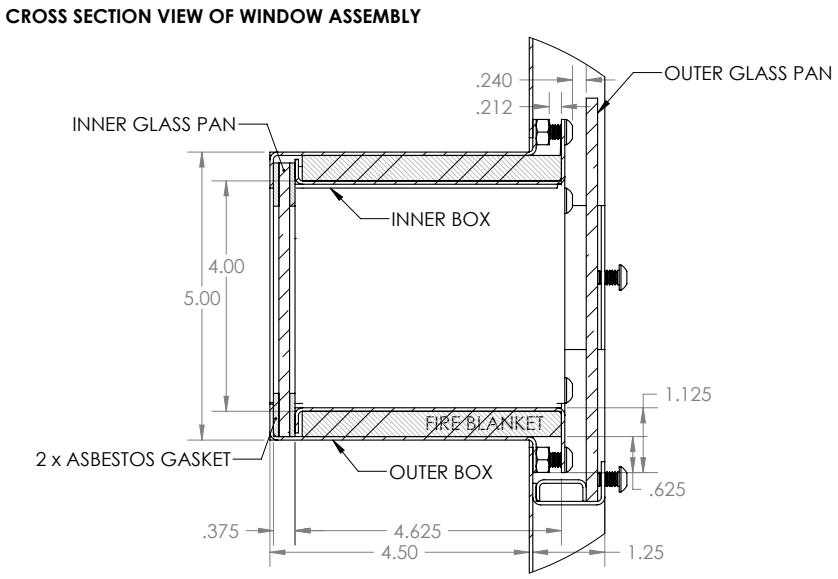

Figure A.15: Cross-sectional view of the window assembly

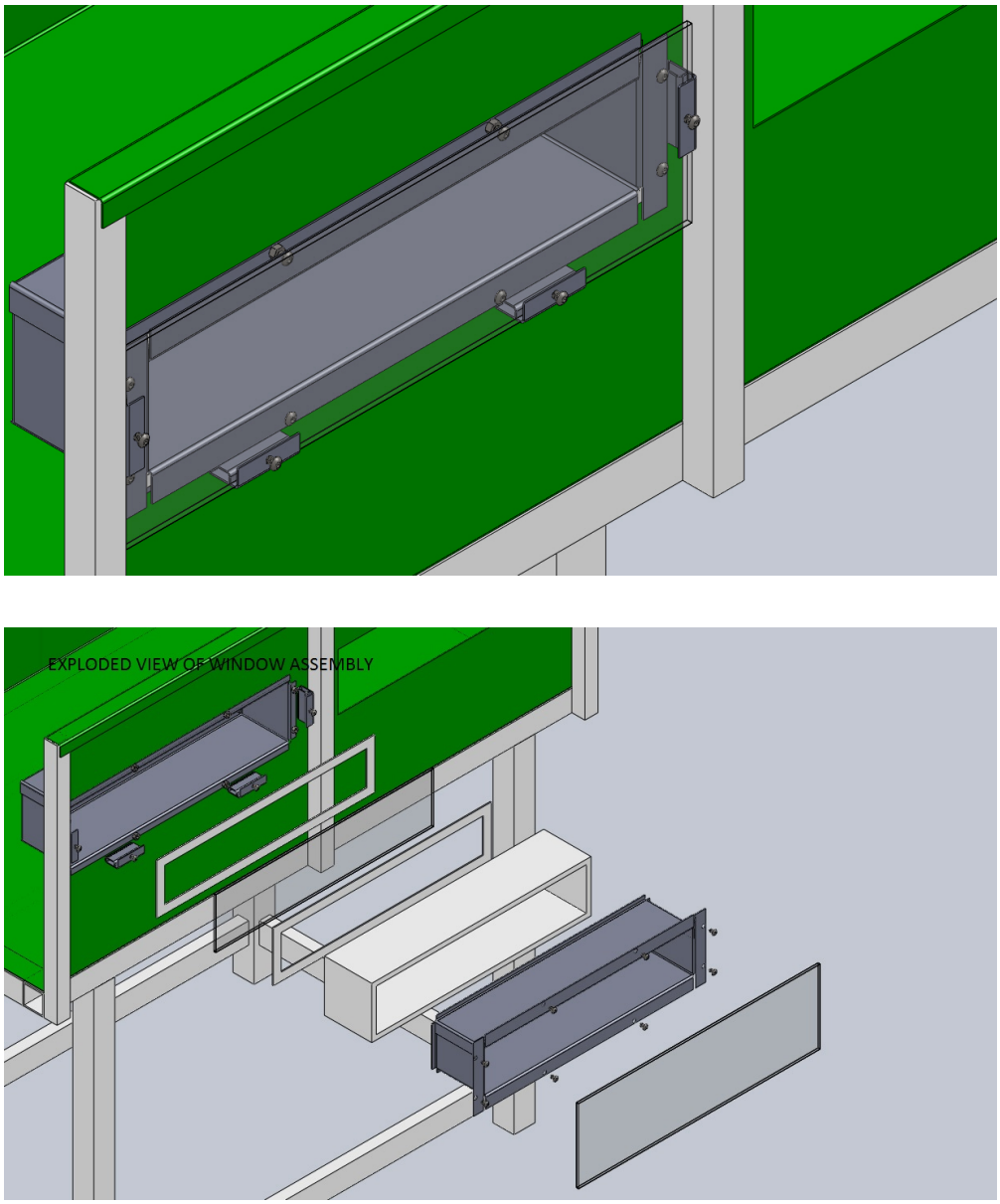

Figure A.16: Window assembly

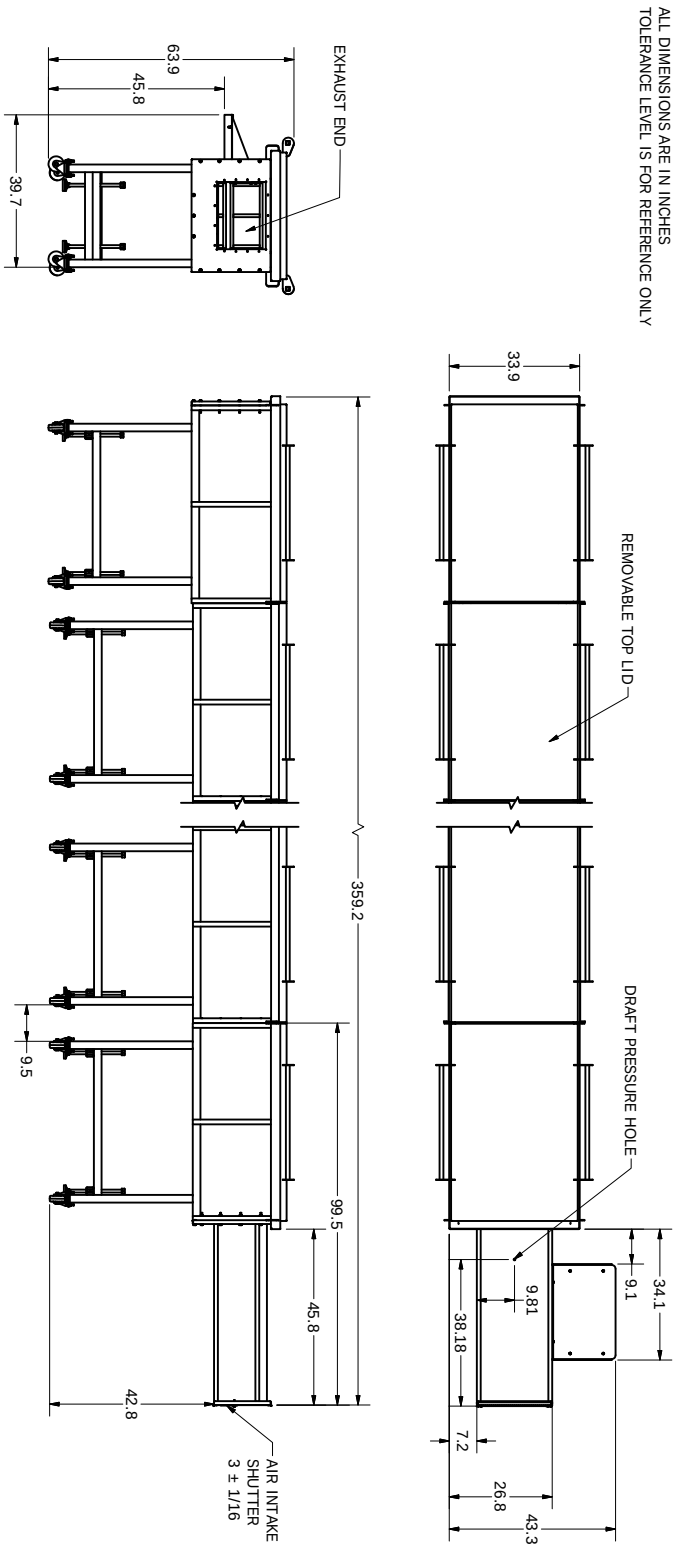

Figure A.17: Top and side view of the full tunnel assembly

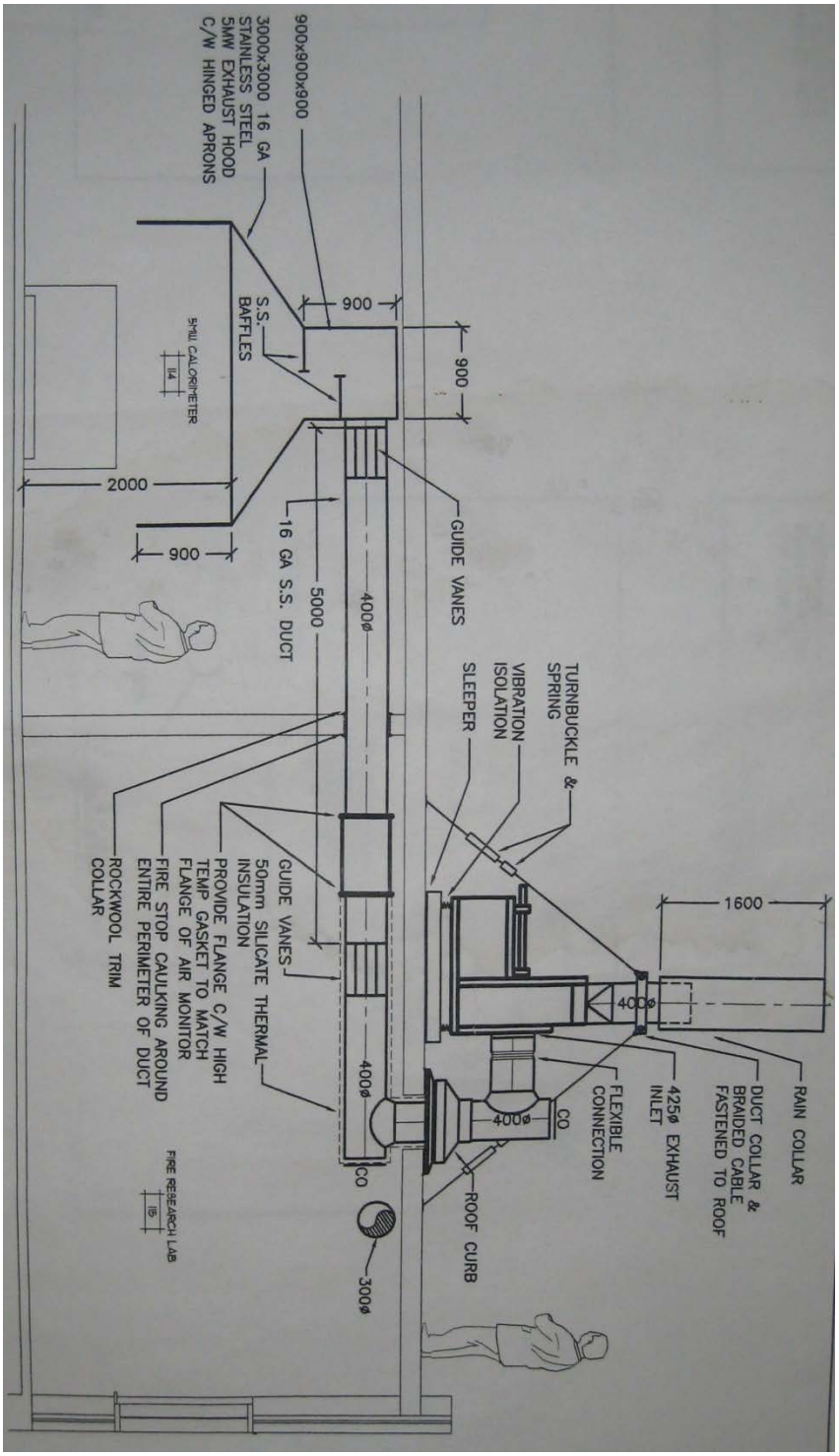

Figure A.18: The exhaust duct system for the furniture calorimeter

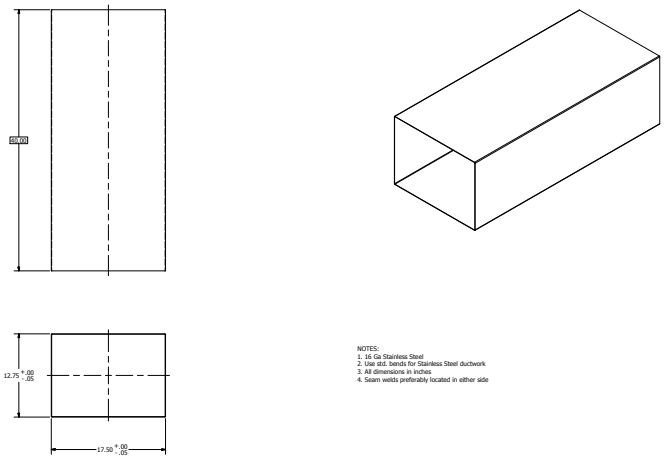

Figure A.19: Rectangular duct used for the exhaust duct assembly

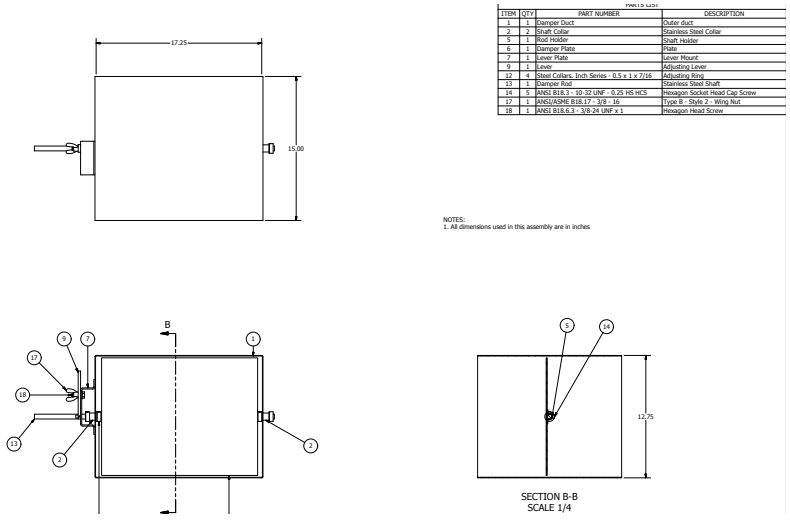

Figure A.20: Damper assembly of the exhaust duct transition piece

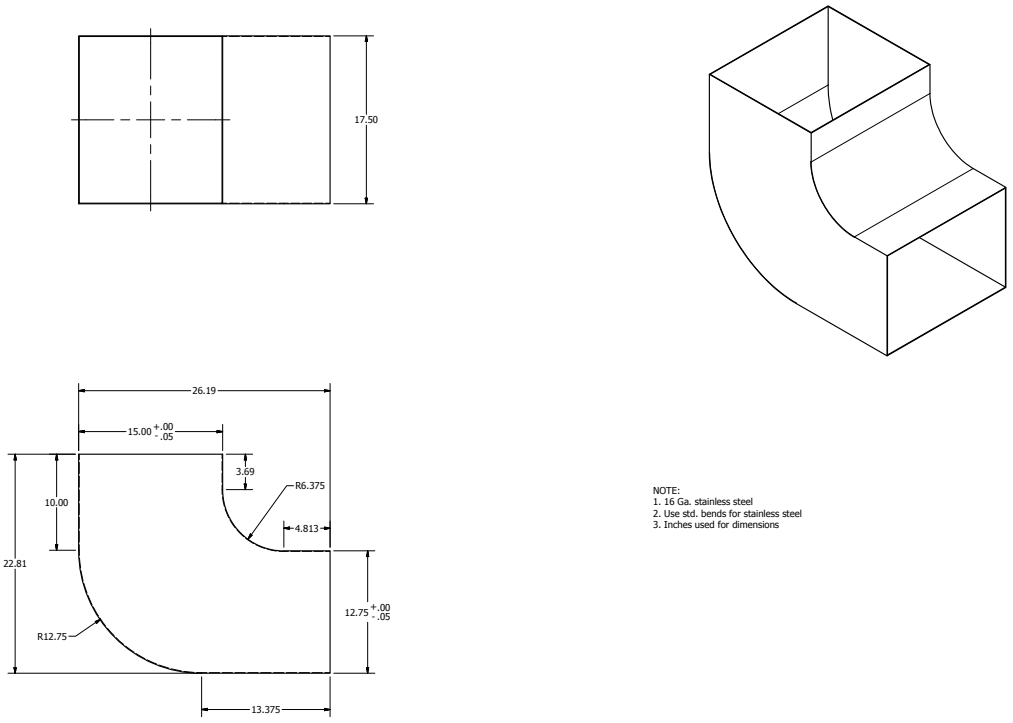

Figure A.21: 90^0 elbow connection

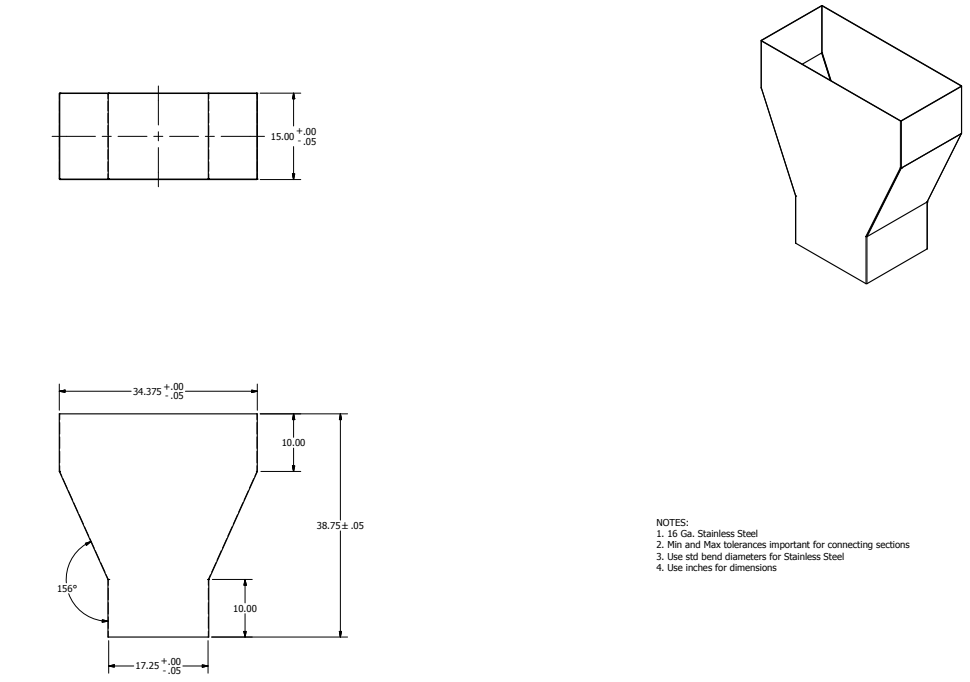

Figure A.22: Main transition piece

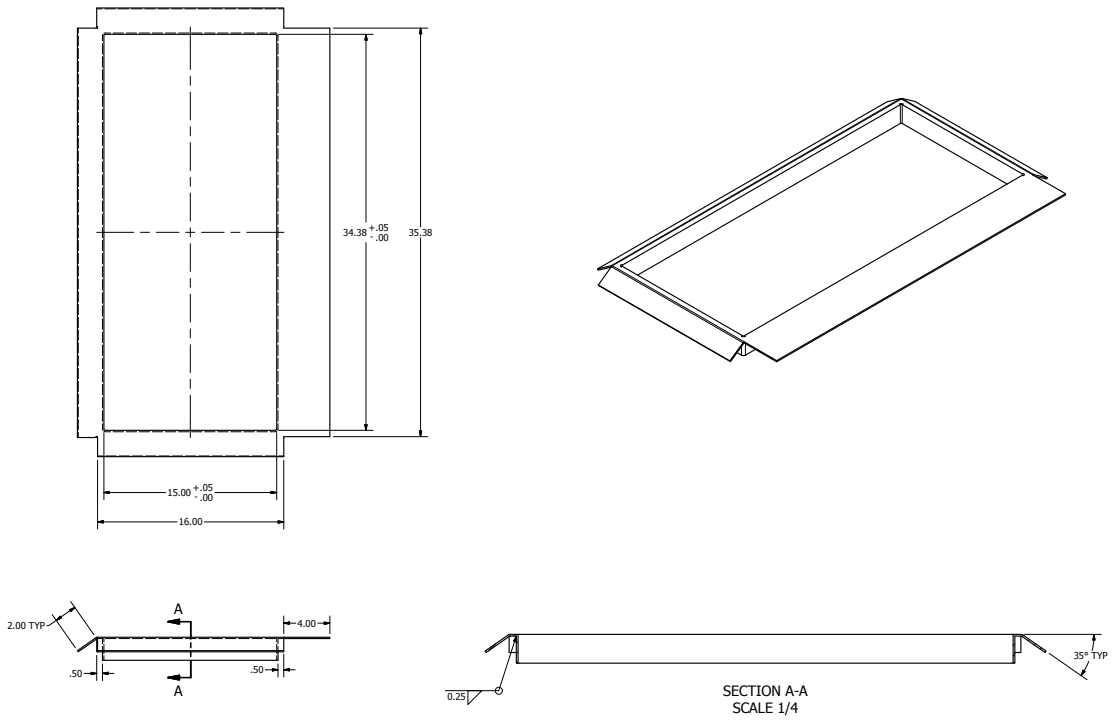

Figure A.23: Main transition piece flange

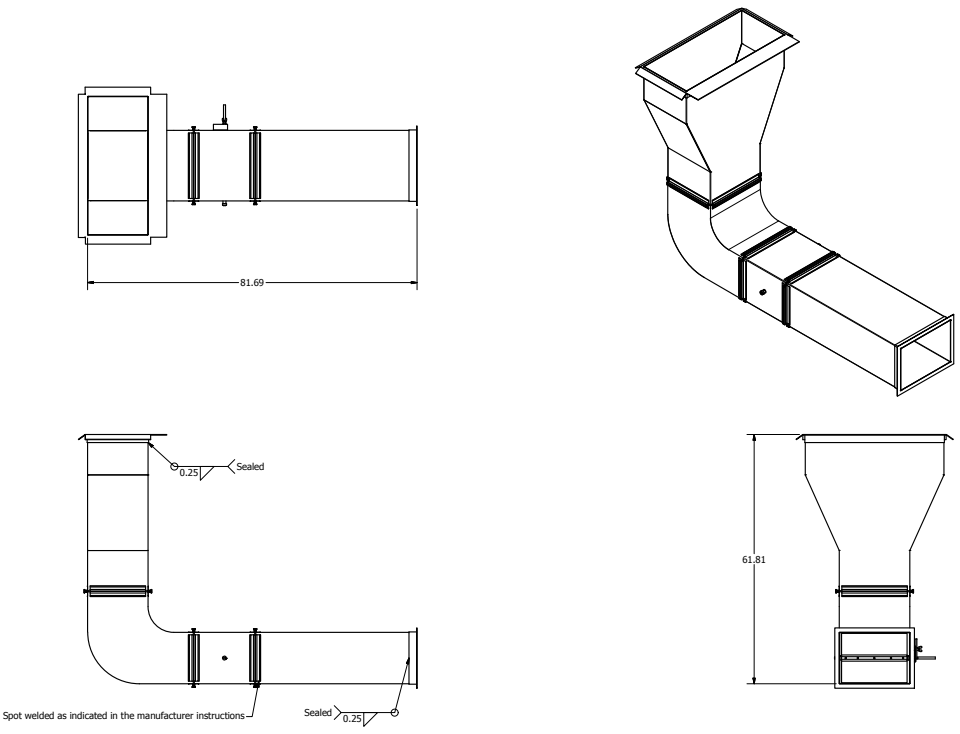

Figure A.24: Exhaust duct transition assembly

Appendix B

Additional Features of the Control Systems

The figures presented in this section will provide some additional illustrations of the Control Systems that were not included in Section 3.2. These features include initial design proposals of the Control Systems, electrical diagrams, S8702D flow chart, additional gas train and control panel box figures, and TSSA approval tag.

The overall design proposal of the Control Systems that was approved by the TSSA authorities is shown in Figure B.1. The initial design of the gas train that was proposed to TSSA required some changes (shown in Figure B.2).

The electrical schematics of the initially proposed Control Systems design is shown in Figures B.3 and B.4. ATMEGA 328 micro-controller was initially proposed with programmable input and output peripherals, and a flame detect board that would essentially act as ignition control device. However, after further consultation with the TSSA authorities, it was required that all TSSA recommended components be directly hard wired to the ignition controls. Therefore the ATMEGA 328 micro-controller and the flame detect board were removed from the design and the S8702D ignition control module was suggested instead. The wiring of the Control Systems was conducted in the electrical control panel box. The electrical control panel box (Figure B.5) was initially designed to collaborate with the flame detect board and the micro-controller by having two separate push-buttons for start and ignite. Although, there were no significant changes to the front panel of the control box when compared to Figure 3.17b.

The internal logic of S8702D ignition control is dictated by the TSSA safety components. The control module is directly wired to the two safety solenoid shut-off valves (ASCO and VR8345 valves) that enable gas flow to the burners. From Figure B.6 flow chart, the solenoid valves are disabled and the ignition cycle does not start until the safety

requirements are met. Once the gas valves are open and spark igniters (Q347) are generating spark ignition, the flame rod sensors (Q354) provide feedback to S8702D for flame detection. Flames must be detected within 5 seconds or else the S8702D will go into lockout. When S8702D is in lockout, the gas solenoid valves are shut-off and ignition cycle stops.

Some components that were not identified in Figure 3.15 of the gas train are shown in Figure B.7. The 1/4-in (6.35 mm) steel plate was used as electrical ground. The gas thermocouple is directly connected to the DAQ terminal,[1] and quick disconnect hose is the first component of the gas train. The elevation height from the gas train to the burner nozzles is approximately 2.5-ft (0.76 m). Figure B.8 shows the left side view of the gas train where the manual shut-off valve is located as the last component of the gas train.

The tunnel draft pressure hose was installed in-line with the airflow pressure switch (shown in Figure B.9), however their separation distances differ.[2] The USB cable that is connected to the DAQ module inside the control panel box is tie wrapped with the draft hose. On the left hand side of the control panel box (Figure B.10) are two 1/2-in (12.7 mm) taps that are protected with rubber grommets. They provide entrance for spark igniter cables and flame rod sensor wires to the control panel box. Inside the control panel box, the cable and the wires are connected to the S8702D ignition module.

TSSA field inspector visited the UW Fire Lab to perform site verification and testing of the UW Steiner tunnel Control Systems. The electrical wiring did not require Electrical Safety Authority (ESA) approval prior to the inspection since the power supply operated at a maximum of 24 V. An agreement was made that the purge time was to be performed manually before the test for 10 seconds. Each component of the Control Systems was tested on individual basis and the field approval tag was obtained in Figure B.11.

[1]The gas thermocouple was installed between the pressure switch and ASCO solenoid valve.

[2]The tunnel draft hose is 15-in (0.38 m) downstream of the air inlet section and the pressure switch hose is 38.2-in (0.97 m).

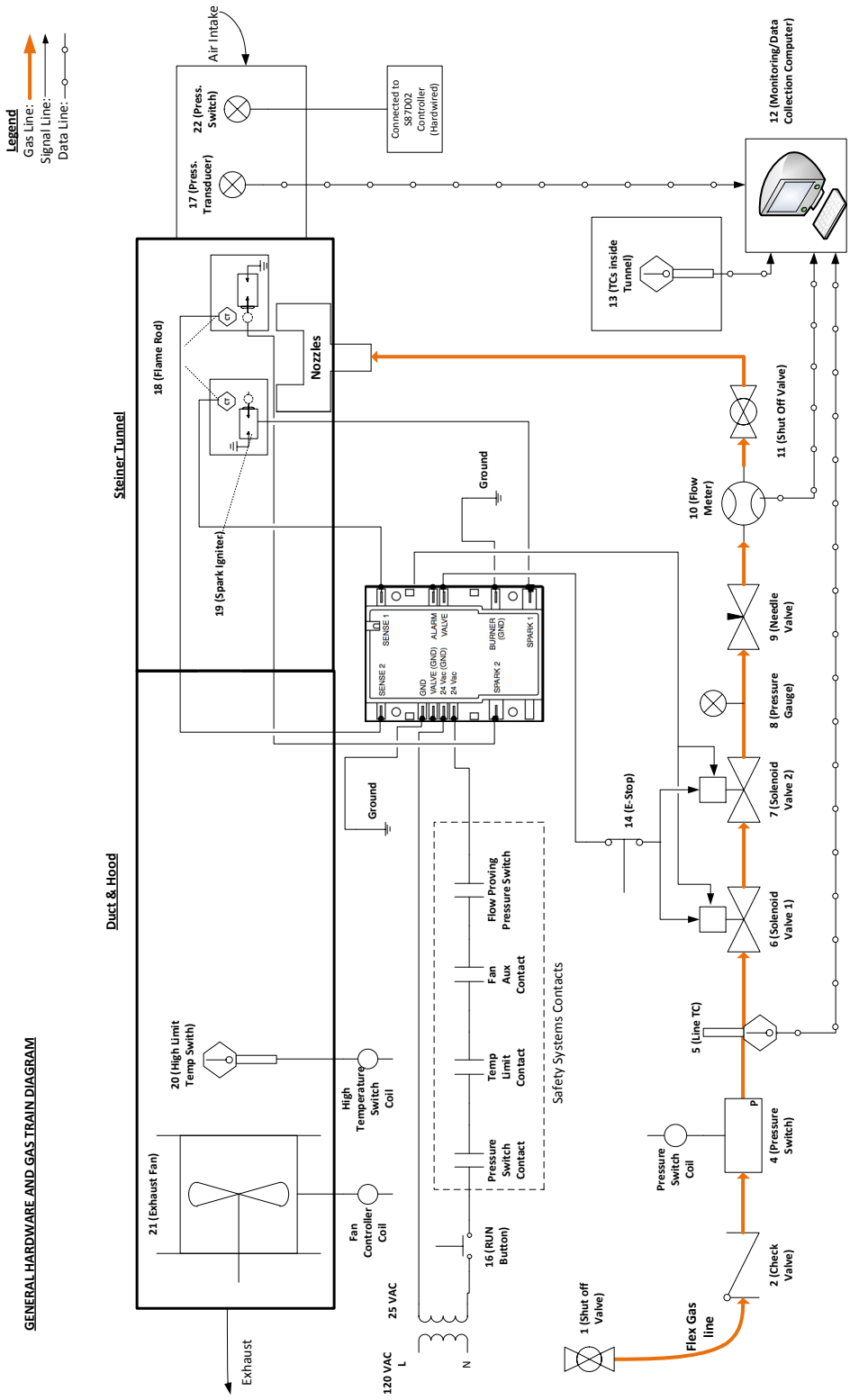

Figure B.1: Designed proposal of the UW Steiner tunnel Control Systems

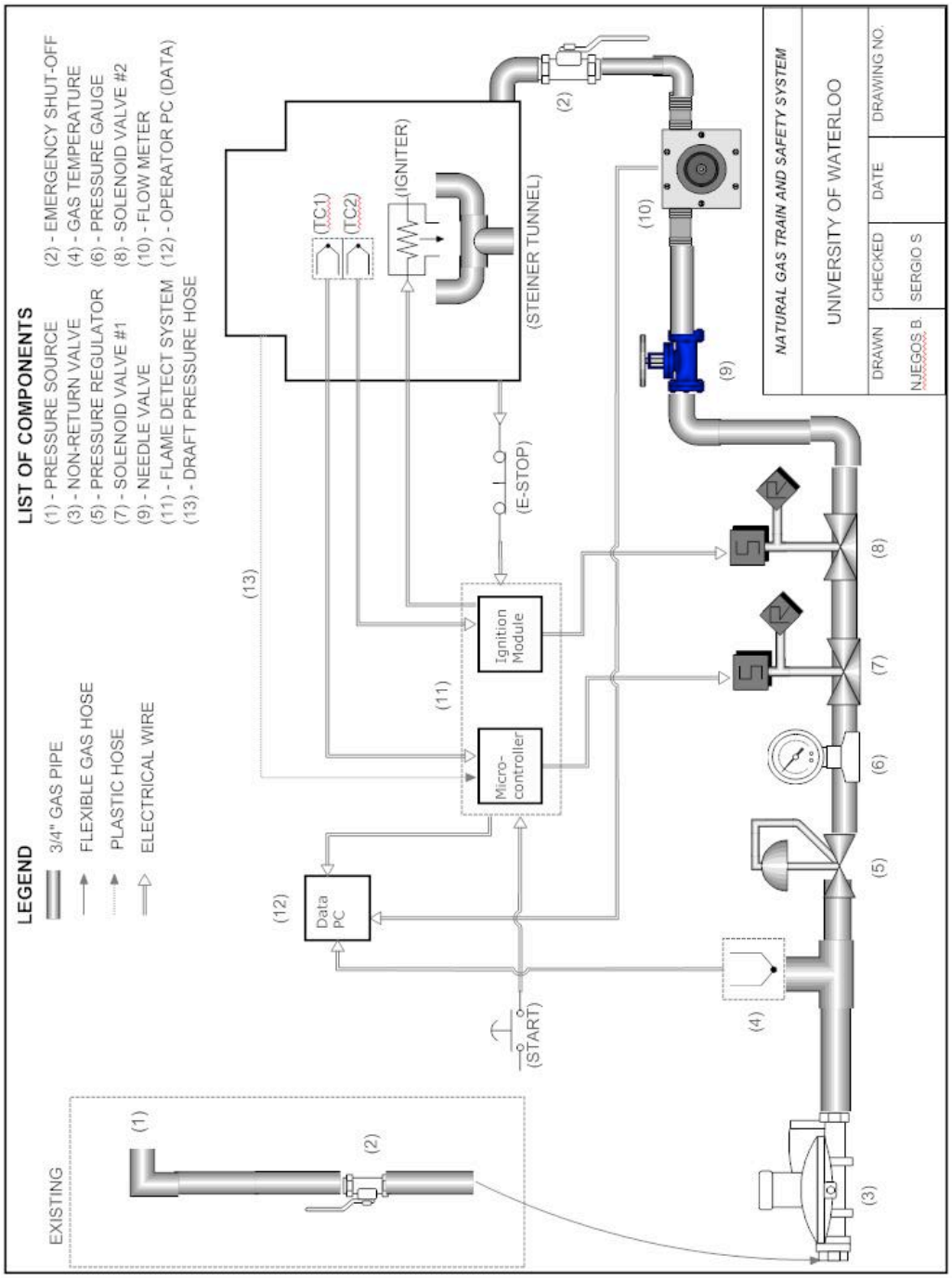

Figure B.2: Proposed design for the gas train

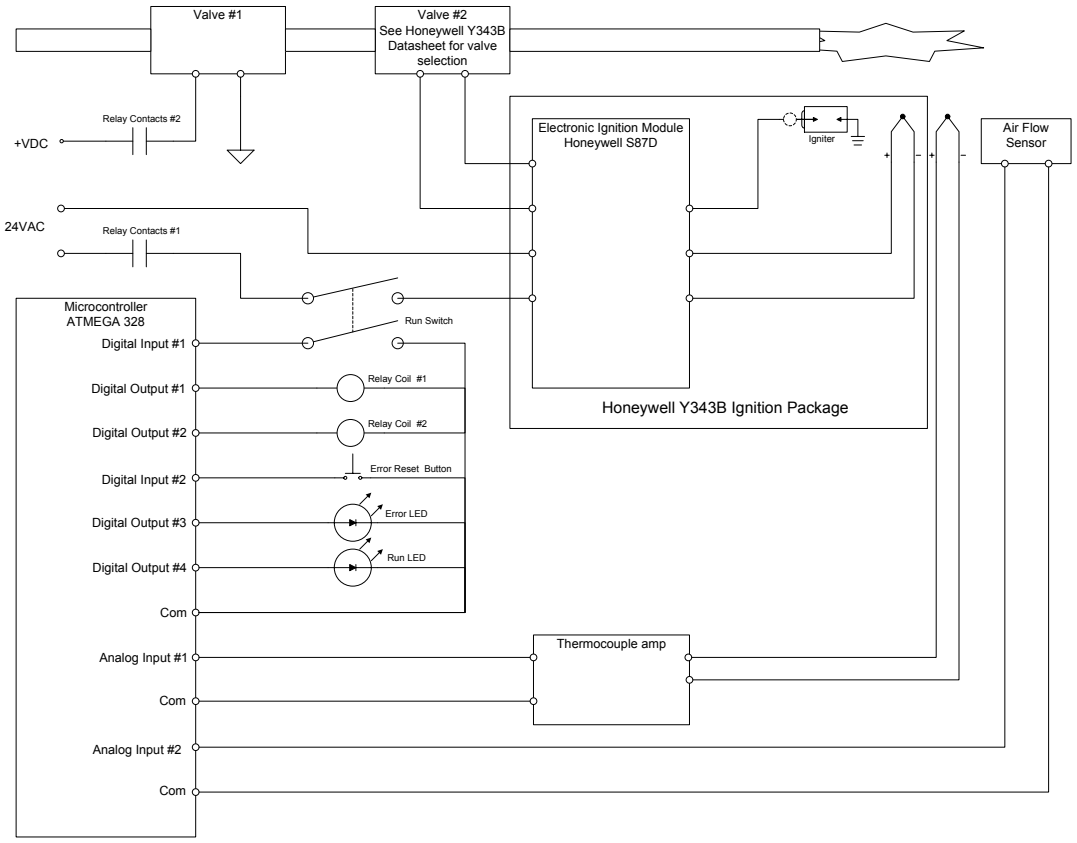

Figure B.3: Electrical schematic using the S8702D ignition control in the control systems

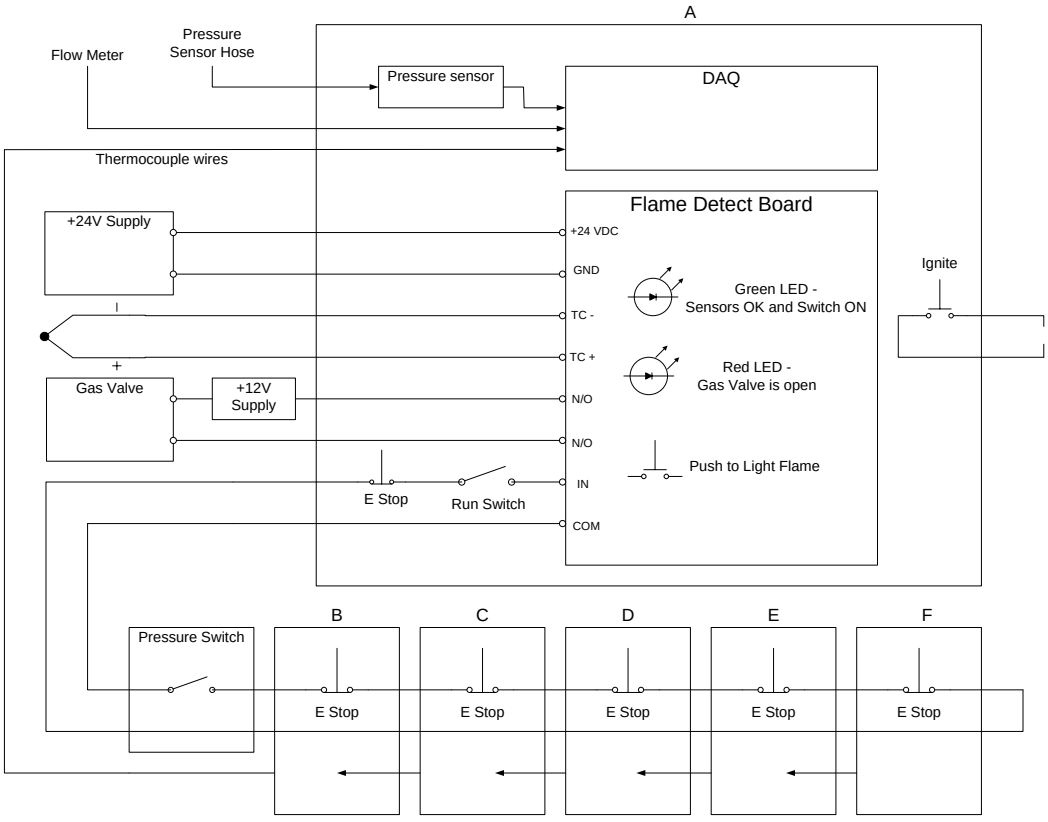

Figure B.4: Electrical schematic showing the wiring of E-Stops in the Control Systems

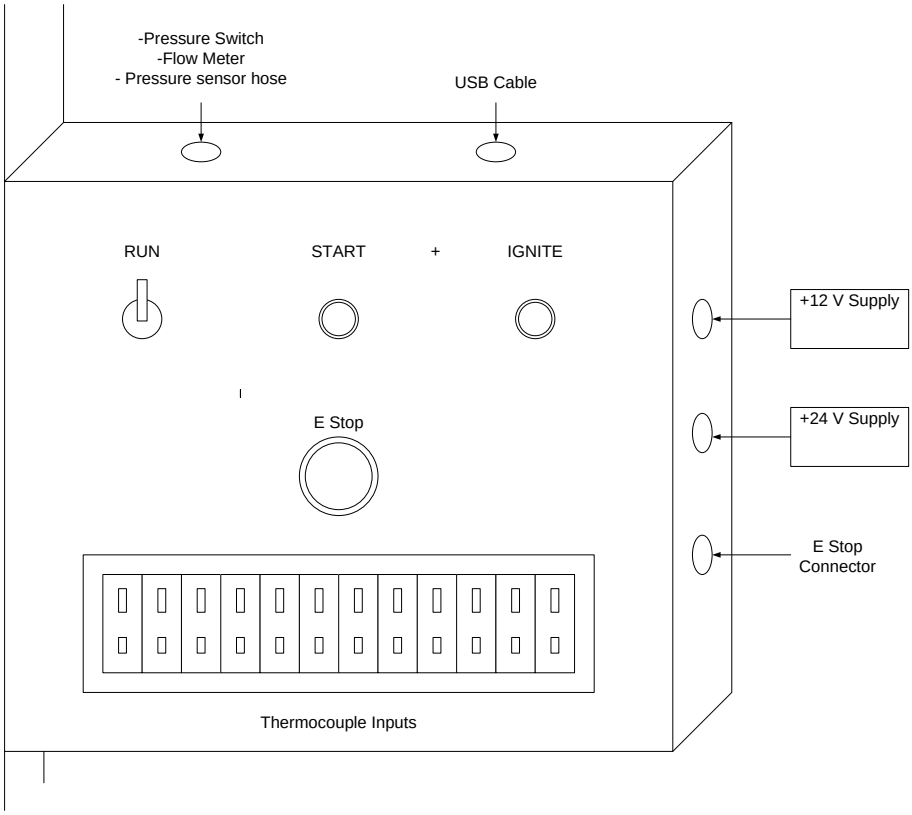

Figure B.5: Control panel box

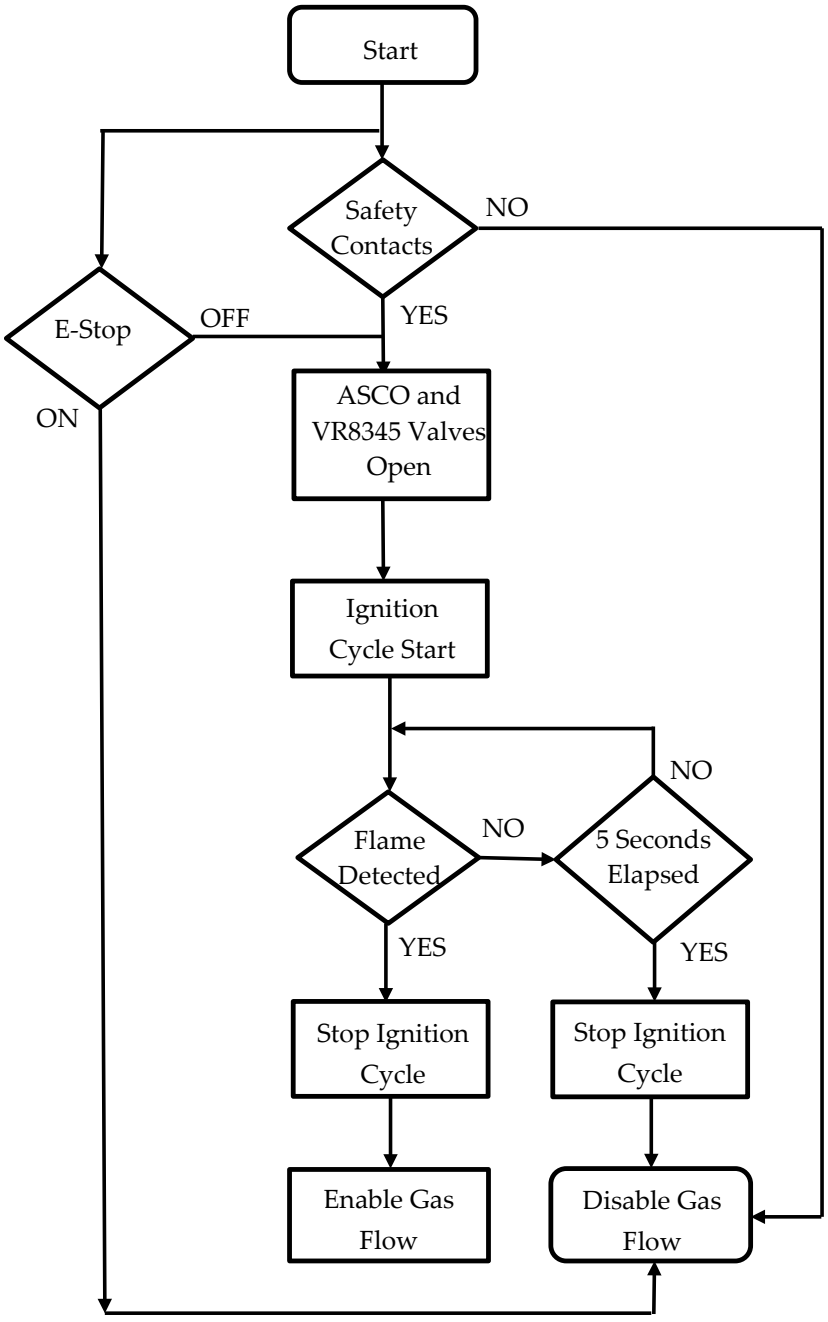

Figure B.6: S8702D ignition control internal logic flow chart

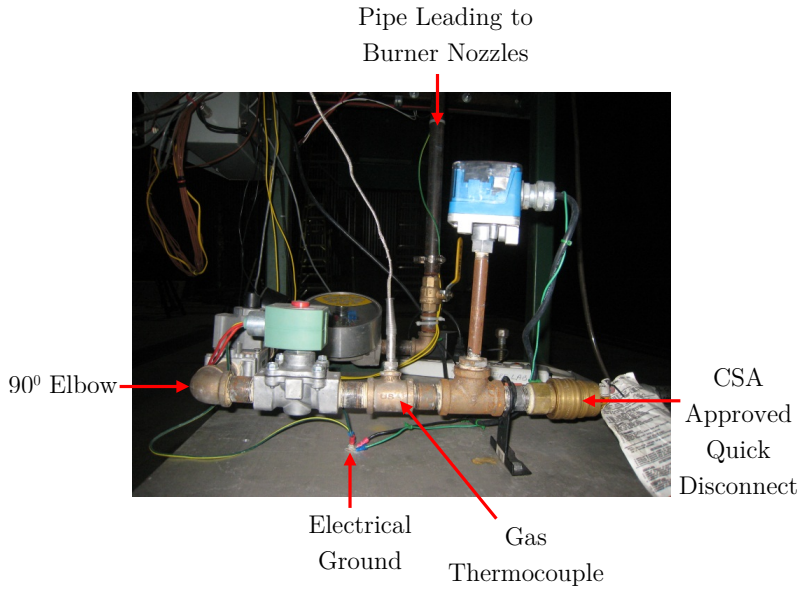

Figure B.7: Right-side view of the designed gas train

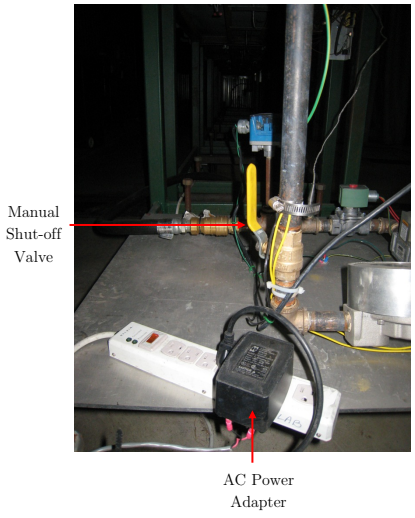

Figure B.8: Left-side view of the designed gas train

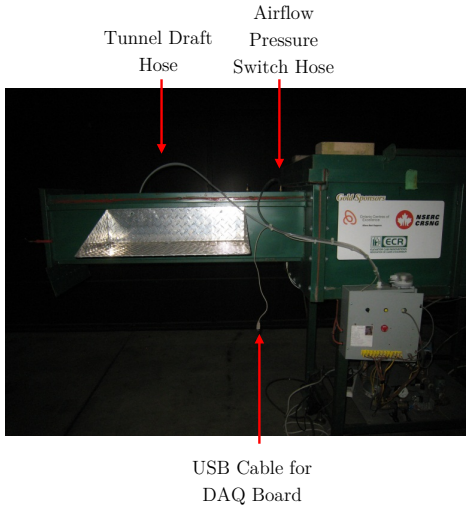

Figure B.9: Draft pressure hoses and USB cable for DAQ board leading to control panel box

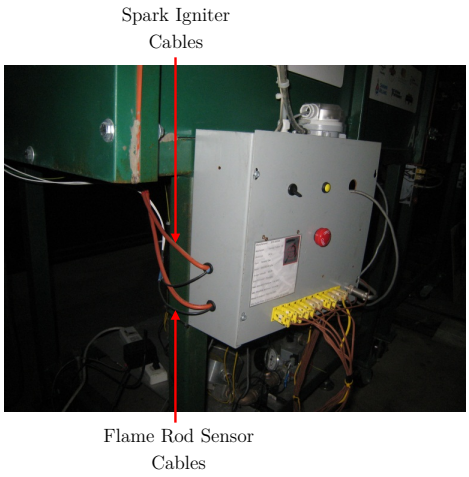

Figure B.10: Flame rod sensors and spark igniter cables leading to control panel box

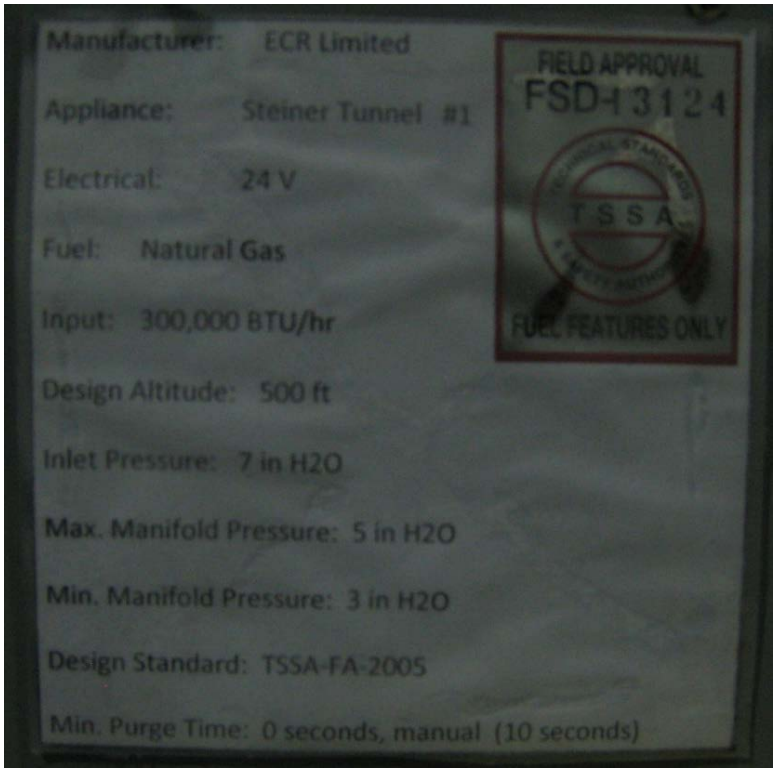

Figure B.11: TSSA field approval tag for the Control Systems design

Figure B.12: Protective housing for the ERDCO gas flow meter

B.1 Draft Pressure Calculations

Calculating the ideal gas flow rate using Equation 3.4, it is calculated to be 8.53 m^3/hr (301.2 ft^3/hr). A rough estimate of gas flow for the UW Steiner tunnel burners can be determined using Bernoulli principle from the gas train to the burner ports. However, the pressure at the burner nozzles induced by the air draft needs to be determined first. From Figure B.13, the Bernoulli principle can be applied at points 1, 2 and 3 to determine the pressure at point 3. Points 3 looks at the position of the burner nozzle tip with respect to the ground (z=0), while points 1 and 2 are located in line with the floor surface of the testing chamber. Point 1 is assumed to be at standard room conditions with an atmospheric pressure of 101 325 Pa and an initial air velocity of 0 m/s. The air inlet cross section length from point 1 to point 2 (L12) is assumed to be plain steel, with an absolute roughness of k = 0.5 x 10^{-3} m. The length from points 2 to 3 (L23) is fire brick with an estimated absolute roughness of k = 2.5 x 10^{-3} m.

The inlet section has a significantly smaller opening with the air shutter restricting the height to 0.076 m. This will slightly increase the air velocity from point 1 to 2. The air velocity is assumed to average out to 1.2 m/s by the time it reaches points 2 and 3.[1] With the air inlet cross sectional areas defined in Appendix B, Section B.1 Draft Pressure Calculations, using the absolute roughness factor k for steel and fire brick, the Reynolds number of the air flow can be determined. The Bernoulli principle will be used to calculate the pressure at point 2 (P2) and pressure at point 3 (P3) using the distance between points 1 and 2, and points 2 and 3, respectively. As two equations are derived, each with pressure as the unknown variable, EquationB.1 is used to calculate P3. The full derivation of Equation B.1 is shown in Section B.1, with all of its parameters being defined and P3 being evaluated at 101 317 Pa. With $P1$ being the atmospheric pressure at point 1, and hL_{12} and hL_{23} is the head loss between points 1-2, 2-3, ρ is the density of air and v_{12} is the velocity between point 1 and 2; g is defined as gravity.

$$P3 = P1 - hL_{12} - hL_{23} - \frac{\rho \cdot v_{12}^2}{2} + g \cdot \rho \cdot z_2 \ - g \cdot \rho \cdot z_3 \tag{B.1}$$

[1]The average mid-cross section air velocity of the Steiner tunnel is calibrated to 1.2 m/s [1]

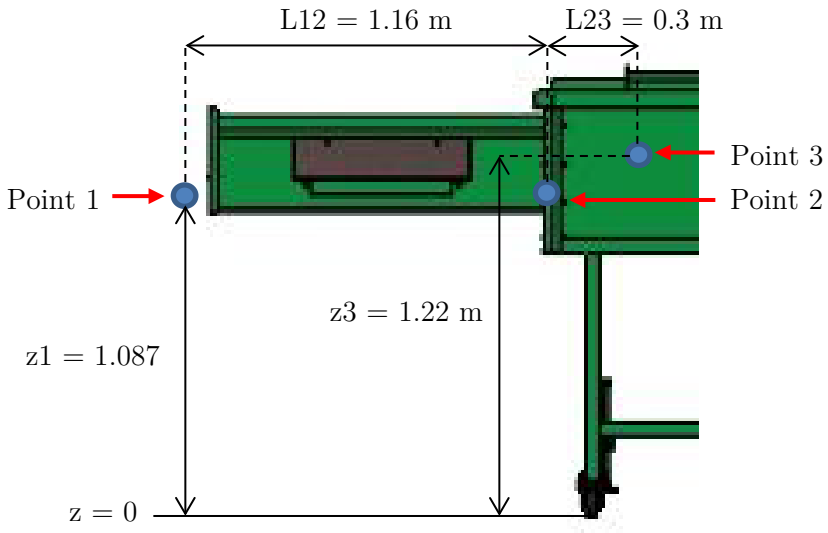

Figure B.13: Location of the 3 points selected using Bernoulli equation for draft pressure calculation

B.2 MATLAB Calculations for Draft

```
format long
% Density of air (kg/m^3)
p = 1.205
% Kinematic viscosity of air at room temperature (Pa*s)
mu = 1.983*10^-5

% Average air velocity inside the tunnel (m/s)
v2 = 1.2

% Width of the tunnel section (m)
w = 0.45

% Air inlet height with the shutter closed (m)
h1 = 0.076
% Height of the tunnel section (m)
h2 = 0.32

% Hydraulic diameter of the rectangular cross section (m)
dh = (2*w*h2)/(w+h2)

% Area of the inlet section (m^2)
A1 = h1*w
% Area of the tunnel section (m^2)
A2 = h2*w

% Air velocity starts from zero outside of the tunnel section
v1 = 0
% Air velocity at inlet section (m/s)
v1_f = (v2*A2)/A1
% Rough estimate of average velocity from point 1 to point 2 (m/s)
v12 = (v1_f+v2)/2

% Determine the Reynolds number inside the air inlet section
Re = (p*v12*dh)/mu

% Absolute roughness for cast iron steel (m)
k = 0.5*10^-3
% The relative roughness ratio
rough = k/dh

% Friction factor selected from Moody chart
f = 0.025

% K losses from the air inlet entrance reduction
K_sum = (1+0.8*f)*(1-(h1/h2)^2)^2

% Length of the air inlet section (m)
L12 = 1.16

% Gravity (m/s^2)
g = 9.81
```

```
% Losses in the air inlet section (m)
hL12 = (f*L12/dh+K_sum)*((v12^2)/(2*g))

% Height to the air inlet section (m)
z1 = 1.087

% Atmospheric pressure (Pa)
P1 = 101325

% Height at point 1 and 2 are equal
z2 = z1


syms P2

% Bernoulli equation from point 1 to point 2, isolate for P2 pressure
Eq1 = solve(0.5*p*v1^2+p*g*z1+P1 == 0.5*p*v12^2+p*g*z2+P2+hL12, P2)


% Similar analysis from point 2 to point 3, except now there is fire b
% lining that acts as resistance to air flow

% Assuming velocity is regulated to average velocity by the time it re
% the entrance of the tunnel section
v23 = v2

v3 = v2

% Same procedure for finding Reynolds number
Re23 = p*v23*dh/mu


k23 = 2.5*10^-3

rough23 = k23/dh

L23 = 0.3


f23 = 0.038


hL12 = ((f*L12)/(dh)+K_sum)*((v12^2)/(2*g))


hL23 = ((f23*L23)/(dh))*((v23^2)/(2*g))


syms P3

z3 = z2+0.1

% Bernoulli equation from Point 2 to Point 3, isolate for P2 pressure
Eq2 = solve(0.5*p*v23^2 + p*g*z2 + P2 == 0.5*p*v23^2 + p*g*z3 + P3 + h
```

```
% Set P2 = P2 and isolate for P3 pressure (Pa)
P3 = solve(Eq1 == Eq2, P3)
```

```
p =

   1.205000000000000


mu =

     1.983000000000000e-05


v2 =

   1.200000000000000


w =

   0.450000000000000


h1 =

   0.076000000000000


h2 =

   0.320000000000000


dh =

   0.374025974025974


A1 =

   0.034200000000000


A2 =

   0.144000000000000


v1 =

     0
```

```
v1_f =

   5.052631578947368

v12 =

   3.126315789473684

Re =

     7.105570279708349e+04

k =

     5.000000000000000e-04

rough =

   0.001336805555556

f =

   0.025000000000000

K_sum =

   0.908176548339844

L12 =

   1.160000000000000

g =

   9.810000000000001

hL12 =

   0.491039475604402

z1 =

   1.087000000000000
```

```
P1 =

      101325

z2 =

   1.087000000000000

Eq1 =

1825194000995559449101/18014398509481984

v23 =

   1.200000000000000

v3 =

   1.200000000000000

Re23 =

     2.727390612413306e+04

k23 =

   0.002500000000000

rough23 =

   0.006684027777778

L23 =

   0.300000000000000

f23 =

   0.038000000000000

hL12 =
```

```
   0.491039475604402

hL23 =

   0.002237003058104

z3 =

   1.187000000000000

Eq2 =

P3 + 2730906728269676401/2305843009213693952

P3 =

2336221012207033398085 27/2305843009213693952
```

Published with MATLAB® R2013b

B.3 Gas Flow Calculations

Similarly, volume gas flow at the burner nozzles is calculated using Bernoulli principle with 3 selected points. From Figure B.14, the first point is located at the pressure gauge where the gas pressure would be known. The components in front of the pressure gauge will be first analyzed to determine if there is sufficient amount of gas flow to the burners. Point 2 is located 1.12 m above the ground as depicted in Figure B.14.[1] Point 3 is located right at the tip of the burner outlets where the igniters are located. Since gas flow is split-off into two burner outlets at point 2 (refer back to Figure 2.2 of the burner), then the flow going from point 2 to point 3 would be defined as (2 x Q_{23}) = Q_{12}.

Once gas train components were installed according to the gas train diagram (Figure 3.14), and approved by TSSA authorities, the gas flow was enabled through the Control Systems and the initial pressure reading at gauge was 0.60 in-WC (150 Pa). Therefore assuming that the atmospheric pressure is 101 325 Pa, the pressure at point 1 is $P1 = 101325 + 150 = 101475\ Pa$. The burner port outlets are situated 1.22 m from the ground. The calculated draft pressure at the burner nozzles is 101 317 Pa, and it will be used as the pressure at point 3 (P_3). As previously mentioned, the pipe used for the gas train is 3/4-in NPT pipe, and the internal diameter of the pipe is 0.824-in (20.9 mm) [79].

To determine gas flow in pipes, certain 'practical' equations have been adopted from the industry. One approach is to use the Spitzglass equation (Equation B.2) to determine the gas flow of low gas pressure pipes [80]. Spitzglass equation has been used in the industry since 1912 [81]. However, this equation is only practical for straight pipes that do not contain valves that restrain the flow. Since the gas train in the Control Systems contains multiple valves (refer to Figure 3.14), it would be impractical to apply Spitzglass formula for the UW Steiner tunnel gas train. Although, each screwed fitting within the gas train can be compensated with an equivalent length factor (L/D). The total sum of the equivalent length can be used as the total pipe length in Equation B.2. Thus, a rough estimate of the gas flow (Q_s) can be determined in ft^3/hr.

$$Q_s = \ 3550 \cdot K\sqrt{\frac{h}{L}} \tag{B.2}$$

For the simplified Spitzglass equation only 3 variables are needed; K parameter from Equation B.3, frictional head loss along the pipe length (h) measured in in-WC, and the

[1]Point 2 contains a Tee with flow through sides that lead to the two burner outlets

[1]Spitzglass formula comes in two versions, one for low and one for high gas pressure. Equation B.2 is

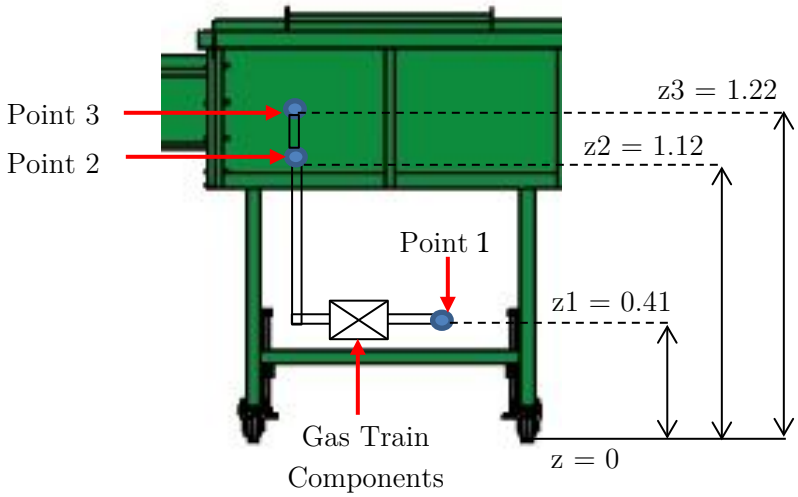

Figure B.14: Location of the 3 points selected using Bernoulli equation for gas flow calculation

overall pipe length L measured in feet. A simplified Spitzglass Equation B.2 can be used to determine the flow with K parameter that is a function of pipe diameter D and friction f; Equation B.3. D is the internal pipe diameter measured in inches. Spitzglass Equation B.2 is derived from the fundamental flow equation and simplified by making several assumptions [81]. As previously mentioned, the equivalent length of each fitting in the gas train can be used as the total pipe length in Equation B.2. This however would provide highly inaccurate estimate for gas flow. Although, the friction factor from the Spitzglass equation is a function of pipe diameter D and it is calculated using Equation B.4 [80]. Equation B.4 was developed based on empirical correlations using the Moody diagram, and the friction factor decreases with increasing pipe size until 10.95-in (27.9 cm) [81]. Therefore that same friction factor can be used in the Bernoulli equation to calculate the major loss.

$$K = \sqrt{\frac{D^5}{1 + \frac{3.6}{D} + 0.03 \cdot D}} \tag{B.3}$$

$$f = 0.0112 \cdot \left(1 + \frac{3.6}{D} + 0.03 \cdot D\right) \tag{B.4}$$

Flow moving from point 1 to point 2 in Figure B.14 is also restricted with gas train components, and minor losses in the pipes are to be expected. The K loss of each component from point 1 to point 2 are summarized in Table B.1. The flow from point 2 to 3 contains

for low gas pressures less than 1 psig (6.89 kPa)[80].

Table B.1: K loss factors for all the fittings and components located between point 1 and point 2 in Figure B.14

Fitting/Valve Component	K
2 90^0 elbows	3.62
Needle valve	60.4
Gas flow meter	6.95
Standard tee	3.62
Shut-off valve	1.09
K_{total}	75.7

additional two 90^0 elbows that divide into two separate burner ports, and the total K loss there will be 3.62. The total head loss is then calculated using Equation B.5, the calculations are shown in Section B.3. Where h_L is the total head loss, f is the friction factor calculated using Equation B.4, L is the total pipe length in meters, D is the pipe diameter in meters, v is the velocity of the gas in m/s, and g is gravity assumed at 9.81 m/s^2. Velocity of the gas can be calculated with the assumptions stated earlier, using conservation of mass, where flow at point 1 is the same at point 2, and flow from point 2 to 3 is reduced by half due to burner symmetry, (2 x Q_{23}) = Q_{12}.

$$h_L = \left(f \cdot \frac{L}{D} \; + \; K_{total} \cdot \left(\frac{v^2}{2 * g} \right) \right) \tag{B.5}$$

All the variables of the Bernoulli equation are defined in Section B.3, except the unknown variables P_2 and Q_{23}. Similarly to the draft pressure calculation, the equation is applied two times, from point 1 to point 2, and point 2 to point 3. Two equations for pressure at point 2 (P_2) is solved in terms of the unknown variable Q_{23}. From two equations and two unknowns, the flow at the burner ports was calculated to be 3.78 m^3/hr. This clearly demonstrates that with the current fittings and valves placed between points 1 and 3 the gas flow is insufficient to meet the required gas flow rate of 8.53 m^3/hr.

Needle valve is used to adjust the correct flow to the burners, but it creates a high resistance to the gas flow compared to other components in Table B.1. The shut-off valve can also be employed to regulate the gas flow to the burners by adjusting the handle between the open and closed position. Therefore it was decided to remove the needle valve from the gas train. When the needle valve is removed from the gas train, the new K_{total} loss between point 1 and 2 was educed to 15.3, and the calculated flow at Q_{23} is 7.66 m^3/hr. This Calculated value was significantly closer to the required gas flow rate of 8.53 m^3/hr. The gas flow was further increased by regulating the pressure through the second solenoid

valve.

B.4 MATLAB Calculations for Gas Flow

```
% Assumptions: Atmospheric pressure Patm = 101325 Pa

% Density of Natural Gas (kg/m^3)
p = 0.7

% Gravit (m/s^2)
g = 9.81

% Height at point 1 of the gas pressure gauge (m)
z1 = 0.41

% Gas pressure reading from the gauge converted to absolute pressure (
P1 = 101325 + 150

% Height at point 2 (m)
z2 = 1.12

% Height at burner point 3 (m)
z3 = 1.22

% Calculated draft pressure at burner nozzle (Pa)
P3 = 101317

% Length of pipe from point 1 to 2; and point 2 to 3 (m)
L12 = 1.07


L23 = 0.3

% Pipe diameter (m)
D = 0.0209

% Friction from Spitzglass
f = 0.06049

% Sum of K losses
K_sum12 = 75.7

K_sum23 = 3.6

% Cross sectional area of the pipe (m^2)
A = (pi*D^2)/4


syms Q23 P2

% Flow defined
Q12 = 2*Q23

v12 = Q12/A

v23 = Q23/A
```

```
% Equation for total head loss
hL12 = (f*L12/D + K_sum12)*((v12^2)/(2*g))


hL23 = (f*L23/D + K_sum23)*((v23^2)/(2*g))



% Bernoulli Equation from Point 1 to Point 2, isolate for P2 pressure
Eq1 = solve(0.5*p*v12^2 +p*g*z1 + P1 == 0.5*p*v12^2 +p*g*z2 + P2 + hL1

% Bernoulli Equation from Point 2 to Point 3, isolate for P2 pressure
Eq2 = solve(0.5*p*v23^2 +p*g*z2 + P2 == 0.5*p*v23^2 +p*g*z3 + P3 + hL2

syms Flow
% Set P2 = P2 and isolate for flow from point 2 to point 3
Q23 = solve(Eq1 == Eq2, Q23)

% Flow is defined in (m^3/hr)
Flow = Q23*3600
```

```
p =

    0.7000


g =

    9.8100


z1 =

    0.4100


P1 =

      101475


z2 =

    1.1200


z3 =

    1.2200


P3 =
```

```
      101317

L12 =

    1.0700

L23 =

    0.3000

D =

    0.0209

f =

    0.0605

K_sum12 =

   75.7000

K_sum23 =

    3.6000

A =

   3.4307e-04

Q12 =

2*Q23

v12 =

(36893488147419103232*Q23)/6328520278965335

v23 =

(18446744073709551616*Q23)/6328520278965335
```

```
hL12 =

(21450544657528239991342833581874232478924 8*Q23^2)/157156862847084989523944

hL23 =

(52963248999409467145756940773717563272069 12*Q23^2)/27371486945867302342088

Eq1 =

714032522769040410672569/7036874417766400000 - (21450544657528239991342833

Eq2 =

(52963248999409467145756940773717563272069 12*Q23^2)/27371486945867302342088

Q23 =

  (165*304202354134570912111149124027702438313730097179249342644298062883
 -(165*304202354134570912111149124027702438313730097179249342644298062883

Flow =

  (37125*3042023541345709121111491240277024383137300971792493426442980628
 -(37125*3042023541345709121111491240277024383137300971792493426442980628
```

Published with MATLAB® R2013b

B.5 Ventilation and Explosion Relief Calculations

The temperature correction factor (K_T) is first calculated using the following equation from NFPA 86 [52]:

$$K_T = \frac{T_{Ex} + 273}{21 + 273} \tag{B.6}$$

Where T_{Ex} is the exhaust temperature in ^{o}C. Previous experience with crib fires and diesel fires conducted in the large cone calorimeter at UWFRL have shown that in general the exhaust temperature did not exceed 288^{o}C. It is expected that due to the length of the tunnel (24-ft from the burner) plus the entire duct length (35-ft), the exhaust temperature would not exceed 288^{0}C. Using 288^{0}C as the exhaust temperature in Equation B.6, the K_T factor calculated to be 1.91. The altitude correction factor stipulated in 11.6.6 of NFPA 86 - 2011 is disregarded since the local altitude of the testing facility is less than 305 m.

Determining the products of combustion value, V_{CT}, is then derived from the following ratio:

$$\frac{V_C}{Q_A} = \frac{5.18\ m^3/min}{293.1\ KW} \tag{B.7}$$

Where V_C is the required flow (uncorrected for temperature), and Q_A being the actual energy input. Ratio derived in Equation B.7 is based on the required values used for products of combustion in NFPA 86. Since the UW Steiner tunnel follows the guidelines stipulated in ASTM E84, the actual burner output is suggested to be 87.9 KW [1]. In addition, the sample under test will be burning along its surface as described in Section 2.3. Based on previous test results conducted in the furniture calorimeter at the UWFRL, the maximum heat release rate allowed without causing damage to the instrumentation was 800 KW. Therefore using the worse case scenario of Q_A = 800 KW, Equation B.7 determines the required flow of the exhaust to be V_C = 15.7 m^3/min. After applying the temperature correction factor, K_T = 1.91, V_{CT} = 29.9 m^3/min. The minimum required flow in the tunnel is therefore 29.9 m^3/min. From Section 3.1.3, the exhaust fan can generate flows up to 120 m^3/min, which is more than enough to extract the combustion products.

For the explosion relief calculations, the Steiner tunnel was designed to have two open ends. The inlet section is the air intake area of the tunnel, as described in Section 3.1.1, and the exhaust end of the tunnel is connected to the exhaust fan via the exhaust transition piece (described in Section 3.1.2). In the event of an explosion, the two open ends would act as the safety relief areas, illustrated in Figure B.15.

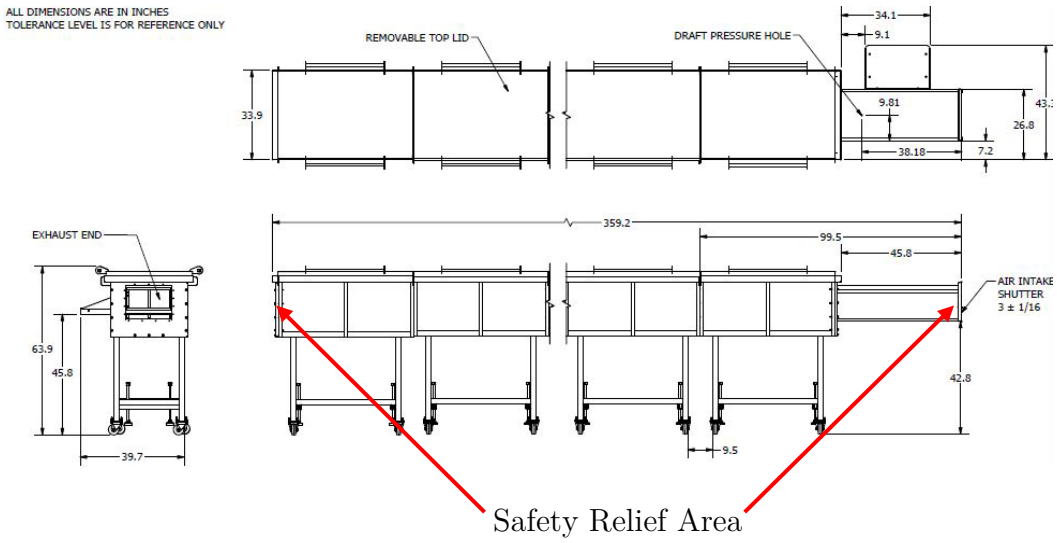

Figure B.15: Safety relief area for the UW Steiner tunnel

Table B.2: Safety relief area calculated results

UW Tunnel Volume	Safety Relief Area	(Relief Area/Volume Ratio)
Length - 29.9 ft	Width - 1.45 ft	Area/Volume Ratio 3/44
Width - 1.45 ft	Height of Inlet - 1.0 ft	
Height - 1.0 ft	Height of Exit - 1.0 ft	
Total Volume - 43.4 ft^3	Total Area - 2.9 ft^2	

NFPA 86 - 2011 presents a fairly simple formula for explosion relief in an oven or furnace. The explosion relief is designed as a ratio of relief area to oven volume [52]. The design ratio requires a minimum of 1 ft^2 (0.093 m^2) of relief area for every 15 ft^3 (0.425 m^3) of oven volume (1/15). Table B.2 results demonstrate that the two openings in the UW tunnel will satisfy NFPA 86 requirements for explosion relief. The overall length of the tunnel also includes the air intake section of the tunnel, adding a total length of the tunnel to be 29.9 ft (9.11 m). The overall relief area to volume of tunnel ratio is approximately 3/44, which satisfies the minimum requirement of 1/15.

Appendix C

Pre-Calibration Tests

The tables listed in this section provide some of the major parameters recorded for each of the conducted tests. Unfortunately, for some of the tests there was missing data from the acquisition system, or the flame spread was not recorded on that day for demonstration purposes, those missing data sets are marked 'N/A'.

Test 1	Aug 15/13	Units	Test 2	Aug 19/13	Units
Material	Plywood		Material	Plywood	
FSI	35		FSI	35	
Fan Speed	10	Hz	Fan Speed	10	Hz
Draft Pressure	0.073	in-WC	Draft Pressure	0.068	in-WC
Gas Flow	5.95	m^3/hr	Gas Flow	6.04	m^3/hr
Damper Position	90% Closed		Damper Position	75% Closed	
Room Temp.	21	C	Room Temp.	25	C
R.Humidity	N/A	%	R.Humidity	N/A	%

Test 3	Aug 22/13	Units	Test 4	Aug 30/13	Units
Material	OSB		Material	OSB	
FSI	65		FSI	65	
Fan Speed	10	Hz	Fan Speed	10	Hz
Draft Pressure	0.064	in-WC	Draft Pressure	0.086	in-WC
Gas Flow	6.03	m^3/hr	Gas Flow	7.19	m^3/hr
Damper Position	80% Closed		Damper Position	60% Closed	
Room Temp.	25	C	Room Temp.	26	C
R.Humidity	N/A	%	R.Humidity	74	%

Test 5	Sep 05/13	Units	Test 6	Sep 10/13	Units
Material	Plywood		Material	Plywood	
FSI	45		FSI	45	
Fan Speed	10	Hz	Fan Speed	10	Hz
Draft Pressure	0.09	in-WC	Draft Pressure	0.084	in-WC
Gas Flow	6.75	m^3/hr	Gas Flow	7.88	m^3/hr
Damper Position	80% Stuffed		Damper Position	Hardyboard (80%)	
Room Temp.	18	C	Room Temp.	32	C
R.Humidity	45	%	R.Humidity	68	%

Test 7	Sep 12/13	Units	Test 8	Sep 19/13	Units
Material	PVC-Stainless Steel		Material	PVC-Laminate	
FSI	20		FSI	N/A	
Fan Speed	10	Hz	Fan Speed	10	Hz
Draft Pressure	0.082	in-WC	Draft Pressure	0.056	in-WC
Gas Flow	7.42	m^3/hr	Gas Flow	7.26	m^3/hr
Damper Position	Hardyboard (80%)		Damper Position	Hardyboard (80%)	
Room Temp.	21	C	Room Temp.	22	C
R.Humidity	61	%	R.Humidity	74	%

Test 9	Sep 25/13	Units	Test 10	Oct 09/13	Units
Material	Particle Board		Material	OSB	
FSI	N/A		FSI	115	
Fan Speed	10	Hz	Fan Speed	11	Hz
Draft Pressure	0.067	in-WC	Draft Pressure	0.18	in-WC
Gas Flow	7.58	m^3/hr	Gas Flow	7.53	m^3/hr
Damper Position	N/A		Damper Position	Fully Open	
Room Temp.	22	C	Room Temp.	19.5	C
R.Humidity	N/A	%	R.Humidity	55	%

Test 11	Oct 09/13	Units	Test 12	Oct 11/13	Units
Material	OSB		Material	Particle Board	
FSI	135		FSI	75	
Fan Speed	10	Hz	Fan Speed	10	Hz
Draft Pressure	0.16	in-WC	Draft Pressure	0.16	in-WC
Gas Flow	7.51	m^3/hr	Gas Flow	7.56	m^3/hr
Damper Position	Fully Open		Damper Position	Fully Open	
Room Temp.	19.6	C	Room Temp.	19.5	C
R.Humidity	50	%	R.Humidity	44	%

Test 13	Oct 12/13	Units	Test 14	Oct 17/13	Units
Material	Particle Board		Material	OSB	
FSI	75		FSI	140	
Fan Speed	10	Hz	Fan Speed	10	Hz
Draft Pressure	0.16	in-WC	Draft Pressure	0.126	in-WC
Gas Flow	7.61	m^3/hr	Gas Flow	7.12	m^3/hr
Damper Position	Fully Open		Damper Position	Stuffed Blanket	
Room Temp.	20.8	C	Room Temp.	15.2	C
R.Humidity	65	%	R.Humidity	73	%

Test 15	Oct 18/13	Units	Test 16	Oct 18/13	Units
Material	OSB		Material	OSB	
FSI	125		FSI	125	
Fan Speed	10	Hz	Fan Speed	11	Hz
Draft Pressure	0.114	in-WC	Draft Pressure	0.118	in-WC
Gas Flow	6.18	m^3/hr	Gas Flow	6.3	m^3/hr
Damper Position	Stuffed Blanket		Damper Position	Stuffed Blanket	
Room Temp.	12.7	C	Room Temp.	13.6	C
R.Humidity	69	%	R.Humidity	63	%

Test 17	Oct 18/13	Units	Test 18	Nov 05/13	Units
Material	OSB		Material	OSB	
FSI	145		FSI	135	
Fan Speed	11	Hz	Fan Speed	10	Hz
Draft Pressure	0.111	in-WC	Draft Pressure	0.091	in-WC
Gas Flow	7.01	m^3/hr	Gas Flow	6.7	m^3/hr
Damper Position	Stuffed (6/8)		Damper Position	Hardyboard (80%)	
Room Temp.	15.4	C	Room Temp.	11	C
R.Humidity	55	%	R.Humidity	72	%

Test 19	Dec 05/13	Units	Test 20	Dec 05/13	Units
Material	OSB		Material	OSB	
FSI	120		FSI	100	
Fan Speed	10	Hz	Fan Speed	10	Hz
Draft Pressure	0.104	in-WC	Draft Pressure	0.104	in-WC
Gas Flow	N/A	m^3/hr	Gas Flow	5.71	m^3/hr
Damper Position	Hardyboard (80%)		Damper Position	Hardyboard (80%)	
Room Temp.	7.5	C	Room Temp.	6	C
R.Humidity	74	%	R.Humidity	71	%

Test 21	May 12 /14	Units	Test 22	May 12 /14	Units
Material	OSB		Material	OSB	
FSI	90		FSI	160	
Fan Speed	13	Hz	Fan Speed	13	Hz
Draft Pressure	0.083	in-WC	Draft Pressure	0.088	in-WC
Gas Flow	6.94	m^3/hr	Gas Flow	7.76	m^3/hr
Damper Position	Hardyboard (80%)		Damper Position	Hardyboard (80%)	
Room Temp.	22	C	Room Temp.	22	C
R.Humidity	73	%	R.Humidity	71	%

Test 23	May 13 /14	Units	Test 24	May 13 /14	Units
Material	OSB		Material	DF Plywood - Sanded	
FSI	170		FSI	80	
Fan Speed	13	Hz	Fan Speed	13	Hz
Draft Pressure	0.079	in-WC	Draft Pressure	0.082	in-WC
Gas Flow	7.73	m^3/hr	Gas Flow	7.94	m^3/hr
Damper Position	Hardyboard (80%)		Damper Position	Hardyboard (80%)	
Room Temp.	22	C	Room Temp.	26	C
R.Humidity	83	%	R.Humidity	70	%

Test 25	May 14 /14	Units	Test 26	May 29 /14	Units
Material	DF Plywood - Sanded		Material	OSB	
FSI	115		FSI	225	
Fan Speed	15	Hz	Fan Speed	13	Hz
Draft Pressure	0.105	in-WC	Draft Pressure	0.09	in-WC
Gas Flow	7.59	m^3/hr	Gas Flow	7.4	m^3/hr
Damper Position	Hardyboard (80%)		Damper Position	Hardyboard (80%)	
Room Temp.	18	C	Room Temp.	21	C
R.Humidity	79	%	R.Humidity	51	%

Test 27	May 29 /14	Units	Test 28	May 30 /14	Units
Material	OSB		Material	OSB	
FSI	185		FSI	200	
Fan Speed	14	Hz	Fan Speed	14	Hz
Draft Pressure	0.092	in-WC	Draft Pressure	0.096	in-WC
Gas Flow	7.29	m^3/hr	Gas Flow	7.62	m^3/hr
Damper Position	Hardyboard (80%)		Damper Position	Hardyboard (80%)	
Room Temp.	20.5	C	Room Temp.	23.5	C
R.Humidity	57	%	R.Humidity	48	%

Test 29	May 30 /14	Units	Test 30	June 03/14	Units
Material	OSB		Material	OSB	
FSI	180		FSI	132	
Fan Speed	14	Hz	Fan Speed	14	Hz
Draft Pressure	0.098	in-WC	Draft Pressure	0.097	in-WC
Gas Flow	7.52	m^3/hr	Gas Flow	6.78	m^3/hr
Damper Position	Hardyboard (80%)		Damper Position	Hardyboard (80%)	
Room Temp.	23.5	C	Room Temp.	24.7	C
R.Humidity	48	%	R.Humidity	73	%

Test 31	June 03/14	Units	Test 32	June 03/14	Units
Material	OSB		Material	OSB	
FSI	179		FSI	180	
Fan Speed	14	Hz	Fan Speed	14	Hz
Draft Pressure	0.096	in-WC	Draft Pressure	0.102	in-WC
Gas Flow	6.78	m^3/hr	Gas Flow	6.7	m^3/hr
Damper Position	Hardyboard (80%)		Damper Position	Hardyboard (80%)	
Room Temp.	26	C	Room Temp.	24.7	C
R.Humidity	65	%	R.Humidity	52	%

Test 33	June 05/14	Units	Test 34	June 09/14	Units
Material	OSB		Material	OSB	
FSI	170		FSI	129	
Fan Speed	14	Hz	Fan Speed	10	Hz
Draft Pressure	0.093	in-WC	Draft Pressure	0.086	in-WC
Gas Flow	6.46	m^3/hr	Gas Flow	6.61	m^3/hr
Damper Position	Hardyboard (80%)		Damper Position	Baffle	
Room Temp.	19	C	Room Temp.	24.6	C
R.Humidity	55	%	R.Humidity	51	%

Test 35	June 10/14	Units	Test 36	June 10/14	Units
Material	OSB		Material	OSB	
FSI	205		FSI	150	
Fan Speed	10	Hz	Fan Speed	10	Hz
Draft Pressure	0.095	in-WC	Draft Pressure	0.109	in-WC
Gas Flow	7.2	m^3/hr	Gas Flow	6.27	m^3/hr
Damper Position	Baffle		Damper Position	Baffle	
Room Temp.	24.4	C	Room Temp.	20	C
R.Humidity	53	%	R.Humidity	65	%

Test 37	June 11/14	Units	Test 38	June 11/14	Units
Material	OSB		Material	OSB	
FSI	138		FSI	148	
Fan Speed	10	Hz	Fan Speed	10	Hz
Draft Pressure	0.105	in-WC	Draft Pressure	0.102	in-WC
Gas Flow	6.3	m^3/hr	Gas Flow	6.3	m^3/hr
Damper Position	Baffle		Damper Position	Baffle	
Room Temp.	22.7	C	Room Temp.	24	C
R.Humidity	76	%	R.Humidity	69	%

Test 39	June 15/14	Units	Test 40	June 16/14	Units
Material	Red Oak		Material	Red Oak 2	
FSI	60		FSI	70	
Fan Speed	10	Hz	Fan Speed	10	Hz
Draft Pressure	0.11	in-WC	Draft Pressure	0.102	in-WC
Gas Flow	6.04	m^3/hr	Gas Flow	7.22	m^3/hr
Damper Position	Baffle		Damper Position	Baffle	
Room Temp.	19.9	C	Room Temp.	26	C
R.Humidity	64	%	R.Humidity	57	%

Test 41	June 19/14	Units	Test 42	June 19/14	Units
Material	Red Oak 3		Material	DF Ply - Sanded	
FSI	65		FSI		
Fan Speed	10	Hz	Fan Speed		Hz
Draft Pressure	0.103	in-WC	Draft Pressure	0.153	in-WC
Gas Flow	7.39	m^3/hr	Gas Flow	7.54	m^3/hr
Damper Position	Baffle		Damper Position	Baffle	
Room Temp.	23.5	C	Room Temp.	23.6	C
R.Humidity	50	%	R.Humidity		%

Test 43	June 19/14	Units	Test 44	June 21/14	Units
Material	DF Ply - Sanded		Material	DF Ply - Rough	
FSI			FSI	81.2	
Fan Speed		Hz	Fan Speed		Hz
Draft Pressure	0.126	in-WC	Draft Pressure	0.091	in-WC
Gas Flow	7.52	m^3/hr	Gas Flow	7.94	m^3/hr
Damper Position	Baffle		Damper Position	Baffle	
Room Temp.	24.5	C	Room Temp.	24	C
R.Humidity		%	R.Humidity		%

Test 45	June 23/14	Units	Test 46	June 24/14	Units
Material	DF Ply - Rough		Material	DF Ply - Rough	
FSI	40.2		FSI	52.7	
Fan Speed		Hz	Fan Speed		Hz
Draft Pressure	0.123	in-WC	Draft Pressure	0.093	in-WC
Gas Flow	8.02	m^3/hr	Gas Flow	8.07	m^3/hr
Damper Position	Baffle		Damper Position	Baffle	
Room Temp.	21.6	C	Room Temp.	25.5	C
R.Humidity		%	R.Humidity		%

Test 47	June 24/14	Units	Test 48	June 25/14	Units
Material	DF Ply - Rough		Material	Luan Ply	
FSI	73.1		FSI	68.2	
Fan Speed		Hz	Fan Speed		Hz
Draft Pressure	0.107	in-WC	Draft Pressure	0.114	in-WC
Gas Flow	8.10	m^3/hr	Gas Flow	8.00	m^3/hr
Damper Position	Baffle		Damper Position	Baffle	
Room Temp.	24.3	C	Room Temp.	21.9	C
R.Humidity		%	R.Humidity		%

Test 49	June 25/14	Units	Test 50	June 25/14	Units
Material	Luan Ply		Material	Luan Ply	
FSI	89.2		FSI	65.3	
Fan Speed		Hz	Fan Speed		Hz
Draft Pressure	0.100	in-WC	Draft Pressure	0.091	in-WC
Gas Flow	8.02	m^3/hr	Gas Flow	8.02	m^3/hr
Damper Position	Baffle		Damper Position	Baffle	
Room Temp.	22.6	C	Room Temp.	23.9	C
R.Humidity		%	R.Humidity		%

Test 51	Jun 26/14	Units	Test 52	Jun 27/14	Units
Material	Particle B.		Material	Particle B.	
FSI	103.6		FSI	119.3	
Fan Speed		Hz	Fan Speed		Hz
Draft Pressure	0.105	in-WC	Draft Pressure	0.097	in-WC
Gas Flow	8.09	m^3/hr	Gas Flow	8.14	m^3/hr
Damper Position	Baffle		Damper Position	Baffle	
Room Temp.	25.4	C	Room Temp.	27	C
R.Humidity		%	R.Humidity		%

Test 53	Jun 27/14	Units	Test 54	Jul 3/14	Units
Material	Particle B.		Material	Particle B.	
FSI	124.6		FSI	125.8	
Fan Speed		Hz	Fan Speed		Hz
Draft Pressure	0.093	in-WC	Draft Pressure	0.103	in-WC
Gas Flow	8.08	m^3/hr	Gas Flow	7.61	m^3/hr
Damper Position	Baffle		Damper Position	Baffle	
Room Temp.	27.2	C	Room Temp.	20.8	C
R.Humidity		%	R.Humidity		%

Test 55	Jul 3/14	Units	Test 56	Jul 6/14	Units
Material	Particle B.		Material	Particle B.	
FSI	109.2		FSI	115.2	
Fan Speed		Hz	Fan Speed	Hand Control	Hz
Draft Pressure	0.095	in-WC	Draft Pressure	0.090	in-WC
Gas Flow	7.57	m^3/hr	Gas Flow	7.87	m^3/hr
Damper Position	Baffle		Damper Position	Baffle	
Room Temp.	19.3	C	Room Temp.	25.9	C
R.Humidity		%	R.Humidity		%

Test 57	Jul 6/14	Units	Test 58	Jul 6/14	Units
Material	Particle B.		Material	Particle B.	
FSI	113.8		FSI	98.6	
Fan Speed	Hand Control	Hz	Fan Speed	Hand Control	Hz
Draft Pressure	0.084	in-WC	Draft Pressure	0.081	in-WC
Gas Flow	7.94	m^3/hr	Gas Flow	7.79	m^3/hr
Damper Position	Baffle		Damper Position	Baffle	
Room Temp.	24.8	C	Room Temp.	23.2	C
R.Humidity		%	R.Humidity		%

Test 59	Jul 7/14	Units	Test 60	Jul 7/14	Units
Material	Particle B.		Material	Particle B.	
FSI	123.9		FSI	130.0	
Fan Speed	Hand Control	Hz	Fan Speed	Hand Control	Hz
Draft Pressure	0.101	in-WC	Draft Pressure	0.094	in-WC
Gas Flow	7.95	m^3/hr	Gas Flow	7.98	m^3/hr
Damper Position	Baffle		Damper Position	Baffle	
Room Temp.	25.2	C	Room Temp.	25.7	C
R.Humidity		%	R.Humidity		%

Test 61	Jul 7/14	Units
Material	Particle B. (No Brick)	
FSI	100.8	
Fan Speed	Hand Control	Hz
Draft Pressure	0.099	in-WC
Gas Flow	7.62	m^3/hr
Damper Position	Baffle	
Room Temp.	24.9	C
R.Humidity		%

Test 62	Jul 10/14	Units
Material	OSB	
FSI	161.3	
Fan Speed	Hand Control	Hz
Draft Pressure	0.093	in-WC
Gas Flow	7.86	m^3/hr
Damper Position	Baffle	
Room Temp.	22.6	C
R.Humidity		%

Test 63	Jul 10/14	Units
Material	(19/32 in) OSB	
FSI	151.4	
Fan Speed	Hand Control	Hz
Draft Pressure	0.094	in-WC
Gas Flow	7.63	m^3/hr
Damper Position	Baffle	
Room Temp.	20.4	C
R.Humidity		%

Test 64	Jun 10/14	Units
Material	Cement Board	
FSI	0	
Fan Speed	10	Hz
Draft Pressure	0.108	in-WC
Gas Flow	7.63	m^3/hr
Damper Position	Near Damper	
Room Temp.	22.3	C
R.Humidity	62	%

Test 65	Jun 19/14	Units
Material	Cement Board	
FSI	0	
Fan Speed	10	Hz
Draft Pressure	0.104	in-WC
Gas Flow	7.78	m^3/hr
Damper Position	Near Damper	
Room Temp.	21.7	C
R.Humidity	68	%

Test 66	Jun 27/14	Units
Material	Cement Board	
FSI	0	
Fan Speed	10	Hz
Draft Pressure	0.107	in-WC
Gas Flow	8.19	m^3/hr
Damper Position	Near Damper	
Room Temp.	21.7	C
R.Humidity	68	%

Test 67	Sep 8/14	Units
Material	Particle B.	
FSI	140.3	
Fan Speed	Hand Control	Hz
Draft Pressure	0.094	in-WC
Gas Flow	7.34	m^3/hr
Damper Position	Far damper	
Room Temp.	21.9	C
R.Humidity	56	%

Test 68	Sep 09/14	Units
Material	Red Oak	
FSI	96.7	
Fan Speed	10	Hz
Draft Pressure	0.096	in-WC
Gas Flow	7.63	m^3/hr
Damper Position	Far damper	
Room Temp.	22.2	C
R.Humidity	54	%

Test 69	Sep 10/14	Units
Material	PVC Stainless	
FSI	18.4	
Fan Speed	11.5	Hz
Draft Pressure	0.096	in-WC
Gas Flow	7.71	m^3/hr
Damper Position	Far damper	
Room Temp.	21.5	C
R.Humidity	38	%

Test 70	Sep 10/14	Units
Material	PVC Laminate	
FSI	45.3	
Fan Speed	11.5	Hz
Draft Pressure	0.09	in-WC
Gas Flow	7.27	m^3/hr
Damper Position	Far damper	
Room Temp.	21.3	C
R.Humidity	57	%

Test 71	Sep 12/14	Units
Material	PVC Glass	
FSI	10.4	
Fan Speed	11.5	Hz
Draft Pressure	0.097	in-WC
Gas Flow	7.71	m^3/hr
Damper Position	Far damper	
Room Temp.	22.2	C
R.Humidity	43	%